ALFRED-WEGENER-INSTITUT
HELMHOLTZ-ZENTRUM FÜR POLAR- UND MEERESFORSCHUNG

705
2017

Berichte
zur Polar- und Meeresforschung

Reports on Polar and Marine Research

The Expedition PS100 of the Research Vessel POLARSTERN to the Fram Strait in 2016

Edited by
Torsten Kanzow
with contributions of the participants

HELMHOLTZ GEMEINSCHAFT

Die Berichte zur Polar- und Meeresforschung werden vom Alfred-Wegener-Institut, Helmholtz-Zentrum für Polar- und Meeresforschung (AWI) in Bremerhaven, Deutschland, in Fortsetzung der vormaligen Berichte zur Polarforschung herausgegeben. Sie erscheinen in unregelmäßiger Abfolge.

Die Berichte zur Polar- und Meeresforschung enthalten Darstellungen und Ergebnisse der vom AWI selbst oder mit seiner Unterstützung durchgeführten Forschungsarbeiten in den Polargebieten und in den Meeren.

Die Publikationen umfassen Expeditionsberichte der vom AWI betriebenen Schiffe, Flugzeuge und Stationen, Forschungsergebnisse (inkl. Dissertationen) des Instituts und des Archivs für deutsche Polarforschung, sowie Abstracts und Proceedings von nationalen und internationalen Tagungen und Workshops des AWI.

Die Beiträge geben nicht notwendigerweise die Auffassung des AWI wider.

Herausgeber
Dr. Horst Bornemann

Redaktionelle Bearbeitung und Layout
Birgit Reimann

Alfred-Wegener-Institut
Helmholtz-Zentrum für Polar- und Meeresforschung
Am Handelshafen 12
27570 Bremerhaven
Germany

www.awi.de
www.reports.awi.de

The Reports on Polar and Marine Research are issued by the Alfred Wegener Institute, Helmholtz Centre for Polar and Marine Research (AWI) in Bremerhaven, Germany, succeeding the former Reports on Polar Research. They are published at irregular intervals.

The Reports on Polar and Marine Research contain presentations and results of research activities in polar regions and in the seas either carried out by the AWI or with its support.

Publications comprise expedition reports of the ships, aircrafts, and stations operated by the AWI, research results (incl. dissertations) of the Institute and the Archiv für deutsche Polarforschung, as well as abstracts and proceedings of national and international conferences and workshops of the AWI.

The papers contained in the Reports do not necessarily reflect the opinion of the AWI.

Editor
Dr. Horst Bornemann

Editorial editing and layout
Birgit Reimann

Alfred-Wegener-Institut
Helmholtz-Zentrum für Polar- und Meeresforschung
Am Handelshafen 12
27570 Bremerhaven
Germany

www.awi.de
www.reports.awi.de

Titel: Blick aus einem Schlauchboot auf Polarstern in der Bucht vor dem 79N Gletscher (Foto: Wilken-Jon von Appen, AWI)

Cover: Polarstern in the bay in front of 79N glacier as seen from a zodiac (Photo: Wilken-Jon von Appen, AWI)

The Expeditions PS100 of the Research Vessel POLARSTERN to the Fram Strait in 2016

Edited by

Torsten Kanzow

with contributions of the participants

Please cite or link this publication using the identifiers
hdl:10013/epic.50192 or http://hdl.handle.net/10013/epic.50192 and
doi:10.2312/BzPM_0705_2017 or http://doi.org/10.2312/BzPM_0705_2017

ISSN 1866-3192

PS100

18 July 2016 - 6 September 2016

Tromsø - Tromsø

Chief Scientist

Torsten Kanzow

Coordinator

Rainer Knust

Contents

1. ZUSAMMENFASSUNG UND FAHRTVERLAUF

Torsten Kanzow AWI

Am 18. Juli verließ FS *Polarstern* den Hafen von Tromsø zu ihrer 100sten Reise. Auf der Expedition “Greenland ice sheet/ocean interaction and Fram Strait fluxes” (GRIFF) wurden Untersuchungen des physikalischen, biochemischen und biologischen Austausches zwischen dem Nordpolarmeer und dem europäischen Nordmeer durch die Framstraße durchgeführt und mit Beobachtungen der Wechselwirkung zwischen dem grönländischen Eisschild und dem europäischen Nordmeer kombiniert. Mit an Bord waren Wissenschaftlerinnen und Wissenschaftler aus dreizehn Nationen, die das Spektrum von physikalischer Ozeanographie, Geochemie, Geodäsie, Geologie, Geophysik, Seismologie, marine Biologie, Biochemie und Ingenieurswesen abdeckten.

Ein Schwerpunkt gleich zu Beginn der Reise stellte ein seismologisches Experiment am Knipovich Rücken dar. Um besser zu verstehen, wie neuer Ozeanboden an diesen ultralangsamen Rücken entsteht, werden kleinste Erdbeben aufgezeichnet, die diesen Prozess begleiten. Dazu wurden insgesamt 23 Ozeanbodenseismometer entlang 180 km der Rückenachse ausgebracht.

Hiernach führte uns der Weg in die Framstraße, wo wir nach einem kurzen Hafenanlauf in Longyearbyen intensive Stationsarbeiten durchführten. Es standen sowohl der nordwärtige Warmwassertransport des Westspitzbergenstroms als auch die Rezirkulation des Atlantikwassers im Fokus der Forschung. Hierbei wechselten sich schiffsgebundene hydrographische Messungen kombiniert mit Wasserprobennahmen zwecks Spurenstoffbestimmungen im Rahmen des GEOTRACES Programms, biologische Probennahme mittels Fangnetzen und das Bergen sowie Auslegen von Verankerungen ab. Die seit vielen Jahren betriebene Kette von Verankerungen im Westspitzbergenstrom konnte erfolgreich aufgenommen und wieder ausgelegt werden. Hiernach ging es entlang des Greenwich Meridians nach Norden, wo neben schiffgestützten Messungen auch 5 Verankerungen zur kontinuierlichen Beobachtung der Rezirkulation in der Framstraße ausgelegt wurden. Am Ende der zweiten Expeditionswoche erreichten wir den nördlichsten Punkt der Reise bei 80°10’N auf dem Greenwich Meridian.

Hiernach bewegten wir uns zunächst in südwestlicher Richtung über den Ostgrönlandstrom hinweg hin zum grönländischen Schelf, den wir auf der Höhe des Westwind Trogs erreichten. Dieser tiefe Einschnitt in den Schelf ist unterhalb des kalten Polarwassers mit relativ warmem Atlantikwasser gefüllt, das bis zur Küste Grönlands hin verfolgt werden kann. Wir folgten der Trogachse in östlicher Richtung weit auf besonders breiten Schelf hinauf bis ca. 13°W. Anschließend ging es in südlicher Richtung über die flache Belgica Bank hinweg, bis wir dann entlang der Breitengrades des traditionellen zonalen Hydrographieschnitts über die Framstraße bei 78°50’N in östlicher Richtung gen Schelfkante zurückfuhren.

Am Ende der dritten Expeditionswoche befanden wir uns wieder im tiefen Abschnitt der Framstraße im Bereich des Ostgrönlandstroms. Die Arbeitsschwerpunkte entlang der in dieser Woche absolvierten boxförmigen Fahrtroute umfassten die Vermessung der Zirkulation, der Hydrographie und der turbulenten Vermischung im Westwind Trog und nahe der Schelfkante, die geo- und biochemischen Kartierung dieser Region und Hubschrauber gestützte geodätische Arbeiten an der Küste Grönlands. Ein besonderer Fokus lag auf biologischen Arbeiten, die

sich mit der Frage beschäftigen, wie sich der Rückgang des arktischen Meereises und der Einstrom wärmerer atlantischer Wassermassen in das Nordpolarmeer auf das Zooplankton und auf die Nahrungsketten im Nordpolarmeer auswirken. So wurden intensive Beprobungen mit dem Multi- und dem Bongonetz vorgenommen.

Nach dem vorläufigen Abschluss der Arbeiten am 78°50'N Schnitt hatten wir dann bereits den größten Teil der meeresbiologischen Arbeiten und auch der geochemischen Spurenstoffbeprobungen im Rahmen von GEOTRACES absolviert. GEOTRACES ist ein weltweites Programm, das die Kreisläufe von Elementen und deren Isotopen im Weltozean erforscht. Wir legten dann unseren Weg zum Ausgang des Norske Trogs an der grönländischen Schelfkante fort. Diese Vertiefung im Schelf führt unterhalb des kalten Polarwassers das warme, salzreiche Wasser aus dem Atlantischen Ozean von der Schelfkante in der Framstraße bis hinauf zur Kalbungsfront des 79°N Gletschers an der grönländischen Küste. Wir untersuchten zunächst die Hydrographie, Zirkulation, Vermischung und biogeochemische Eigenschaften, die mit dem Transport von Atlantikwasser von der Framstraße auf den Schelf verbunden sind.

Bis zum Ende der fünften Woche hatten wir uns auf den inneren Schelf von Nordostgrönland zum Übergang zwischen dem Norsketrog und dem Westwindtrog vorgearbeitet, in den auch der 79°N Gletscher mündet. Einer unserer Arbeitsschwerpunkte bildete die Aufnahme der Hydrographie und Zirkulation des Atlantikwassers und die damit verbundene biochemische und geochemische Wasserprobennahme entlang des Pfades. Wir konnten zusätzlich alle sieben im Jahre 2014 auf dem mittleren Schelf ausgelegten Verankerungen erfolgreich bergen. Diese waren mit Sensoren zur kontinuierlichen Erfassung der Zirkulation des Atlantikwassers bestückt worden. Im Gegenzug wurden dort vier neue Verankerungen ausgelegt. Zudem nahmen wir die Helikopter basierten Operationen zur Ausbringung und Bergung von geodätischen Stationen auf dem grönländischen Festland wieder auf. Die Wetterbedingungen waren hierfür günstig.

Einen weiteren Schwerpunkt bildeten die geologischen Arbeiten im Norske Trog - bestehend aus einer Kombination von Parasound und Hydrosweep Echolotaufnahmen des Meeresbodens sowie Sedimentprobennnahme - deren Hauptziel es war, die seewärtige Ausdehnung des grönländischen Eisschildes während der letzten Eiszeit festzustellen und dessen nachfolgenden Rückzug zu kartieren.

In der sechsten Woche der Expedition standen vielfältige Forschungstätigkeiten nahe der Kalbungsfront des 79°N Gletschers an. Westliche Winde hatten das zuvor in der Bucht vor dem Gletscher gelegene Meereis und die Eisberge nach Osten vertrieben. So konnten wir über mehrere Tage hinweg den Meeresboden kartieren, Sedimentproben gewinnen, hydrographische Verteilungen und die Zirkulation und die turbulente Vermischung des Atlantikwassers ermitteln sowie Wasserproben erlangen. Zusätzlich waren durch das sehr freundliche Wetter viele Helikopter gestützte Einsätze möglich, so dass wir alle geodätischen und seismologischen Stationen vom grönländischen Festland erfolgreich bergen und zusätzlich noch zwei Eisradarsysteme auf dem 79°N Gletscher installieren konnten. Letztere werden im Verlauf eines Jahres die Stärke des Abschmelzens an der mit Meerwasser in Kontakt stehenden Eisunterseite des Gletschers kontinuierlich aufzeichnen, bevor sie in einem Jahr wieder geborgen werden sollen.

Am Anfang der siebten Expeditionswoche befanden wir uns noch auf dem inneren grönländischen Schelf am Übergang vom 79°N Gletscher zum Westwindtrog. Hier standen Messungen zur Zirkulation, Hydrographie und Turbulenz sowie biochemische und geologische Probennahmen auf dem Programm. Zusätzlich wurden drei Verankerungen ausgelegt, die die Zirkulation des Atlantikwassers kontinuierlich vermessen sollen. Hiernach besuchten wir den von einer mit Eisfeldern verzierten Felsenküste gesäumten Djimphnasund, an dessen Ende der 79°N Gletscher mit in einer zweiten, kleinen Kalbungsfront mündet. An der Schwelle am Eingang des Fjords wurden eine weitere Verankerung ausgelegt sowie Sedimentproben gewonnen.

Hiernach folgte ein Transit in südwestlicher Richtung über den weiten, eisbedeckten Schelf hin zur Schelfkante bei 79°36'N. Wir absolvierten an dieser Breite einen hydrographischen Schnitt über den Ostgrönlandstrom hinweg. Insgesamt haben wir hiermit vier Schnitte an verschiedenen Breitengraden über diesen Strom vollendet, was uns Aussagen über die räumliche Struktur der Rezirkulation und die seitliche Einmischung des Atlantikwassers erlauben wird. Wir kehrten dann erneut in den Ostgrönlandstrom bei 78°50'N zurück, wo wir die auf dieser Reise zu Testzwecken ausgelegte Windenverankerung bergen und zusätzlich zwei für das GEOTRACES Programm noch ausstehende Stationen absolvieren konnten. Hiernach verließen wir das von Meereis bedeckten Gebiet des Ostgrönlandstroms in südwestlicher Richtung zum Knipovich Rücken. Dort wurden als letztes großes Arbeitspaket der Expedition in kurzer Folge 13 Ozeanbodenseismometer ausgelegt, die die bereits in der ersten Expeditionswoche abgesetzten Geräte komplettieren.

Ein großer Dank gebührt Kapitän Schwarze, der gesamten Besatzung der *Polarstern*, dem Heliservice International und dem Deutschen Wetterdienst

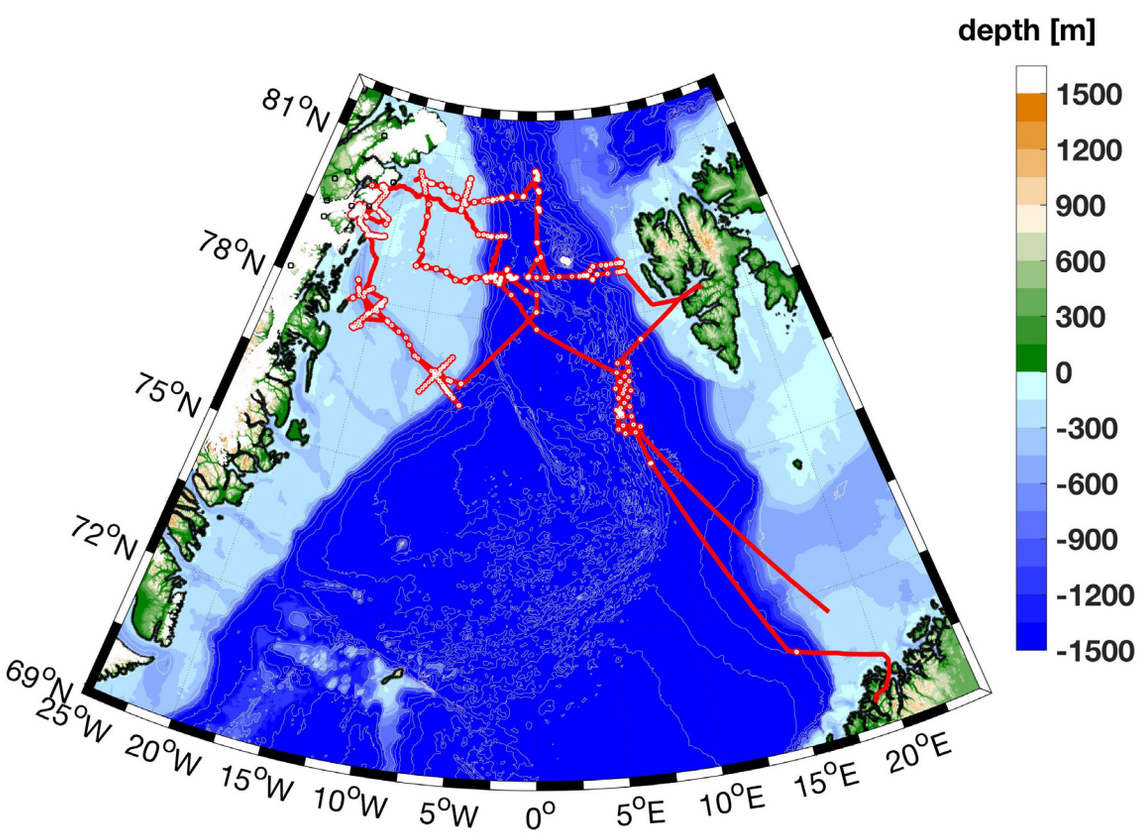

Abb. 1: Fahrverlauf (rote Linien) und Stationen (weiße Punkte) der Expedition PS100 (see https://doi.pangaea.de/10.1594/PANGAEA.869478).

Fig. 1: Cruise track (red lines) and stations (white dots) during expedition PS100 (see https://doi.pangaea.de/10.1594/PANGAEA.869478).

SUMMARY AND ITINERARY

On 18 July the research icebreaker *Polarstern* left the port of Tromsø (Norway) to start her 100th expedition. The aim of the "Greenland ice sheet/ocean interaction and Fram Strait fluxes" (GRIFF) expedition was to conduct investigations regarding the physical, biochemical and biological exchanges between the Arctic Ocean and the Nordic Seas through Fram Strait and to combine them with observations of the interaction between the Greenland ice sheet and the Nordic Seas. On board there were scientists from thirteen nations who cover the range from physical oceanography, geochemistry, geodesy, geology, geophysics, seismology, marine biology, biochemistry and mechanical engineering.

We started the expedition with a seismological experiment at Knipovich Ridge. To better understand how new ocean floor is created at these so-called ultra slow spreading ridges, we small earthquakes can be that accompany this process. For this purpose a total of 23 ocean bottom seismometers along 180 km of the ridge axis were deployed.

Polarstern then headed toward Fram Stait. After a short port call in Longyearbyen intense station work was conducted. Both the northward transport of warm water within the West Spitsbergen Current and the recirculation occurring in Fram Strait represent research foci of the expedition. During nighttime both hydrographic measurements combined with water sampling targeting trace element analyses in the framework of the GEOTRACES programme and biological sampling using nets were carried out, while the recovery and deployments moorings took place during daytime.

The array of moorings in the West Spitsbergen Current operated by AWI for many years was successfully recovered and subsequently redeployed. After completion of the work in the West Spitsbergen Current, RV *Polarstern* worked her way along the Greenwich meridian toward the north. Besides vessel-based lowered measurements five moorings were deployed along the south – north transect in order to make continuous observations recirculating branch of Atlantic water for the first time. By the end of week two, the northernmost of the expedition had been reached at 80°10'N.

We then moved southeastward across the East Greenland Current toward the continental shelf of Northeast Greenland, that we reached at the outlet of Westwind Trough. Underneath the surface layer of cold polar water, this deep shelf depression is filled with relatively warm water of Atlantic Ocean origin that can be traced up to the coast of Greenland. Subsequently we followed the trough axis far inshore up to 13°W, then turned toward the south across the shallow Belgica Bank until reaching the latitude of the traditional zonal hydrographic section across Fram Strait at 78°50'N and finally headed back westward toward the shelf edge. At the end of the third week of the expedition we found ourselves once more the East Greenland Current in the deep part of Fram Strait. The foci in that week had been to observe the circulation, hydrographic properties and turbulent mixing both in Westwind Trough and close to the shelf edge, the geochemical and biochemical mapping of this region, and helicopter-based geodetic work on the Greenland coast. A special focus was on marine biology, addressing the question how climate change, the retreat of the Arctic sea ice and the inflow of warmer Atlantic water masses into the Arctic affect zooplankton and marine food chains. Thus numerous zooplankton net hauls were carried out along the path.

After preliminarily finishing the work along the 78°50'N section we had already accomplished the largest part of the work programmes in marine biology and GEOTRACES. GEOTRACES is a world-wide programme for the investigation of cycles of trace elements and their isotopes in the world ocean. We then continued our way to Norske Trough. This depression acts as a conduit for inflow of warm Atlantic water from Fram Strait all the way to the inner shelf of Greenland up to the 79°N glacier. We started by investigating the hydrographic properties,

circulation, turbulent mixing and biogeochemical properties that are associated with the transport of Atlantic water from Fram Strait onto the shelf.

By the end of week 5, RV *Polarstern* had worked her way toward the inner shelf of Northeast Greenland and had reached the transition from Norske Trough to Westwind Trough, which is where the 79°N glacier meets the sea. One of our work foci were hydrographic measurements combined with biochemical and geochemical water sampling along the pathway of the Atlantic water. In addition, we were able to recover all of the seven moorings deployed on the mid-shelf in 2014. They had been equipped with sensors in order to measure the circulation of Atlantic water in the trough. In turn, an array of four moorings was subsequently redeployed. We further resumed the helicopter-based operations for the recovery and redeployment of several geodetic and one seismological station on the mainland of Greenland. Fortunately the weather conditions allowed us to conduct at least two operations per day.

Geological observations represented another work focus in Norske Trough consisting of a combination of Hydrosweep and Parasound surveys of the sea floor with coring of sea floor sediments. The main aims of this program is establish the extent of the Greenland ice sheet offshore and to map its retreat following the last glacial cycle.

In week 6 of the expedition numerous research activities were performed close to the calving front of the 79°N glacier. Westerly winds had driven both the sea ice and the icebergs toward the east, that had only days before occupied the bay in front of the glacier. Thus, over several days we were able to survey the sea floor, collect sea floor sediment samples, observe the distribution, circulation and mixing of Atlantic waters and collect water samples in this area. In addition the friendly weather allowed us to run a large number of helicopter-based operations. Therefore all geodetic and seismological stations could be recovered from the mainland of Greenland and two ice radar systems were installed. Over the course of one year the latter will continuously record the amount of melting at the base of the glacier that is in contact with sea water. Next summer the radar system will be recovered again.

In the beginning of the 7th week of the expedition, we found ourselves on the inner shelf of Northeast Greenland at the transition from the 79°N glacier to Westwind Trough. Here we both conducted measurements of the hydrography, circulation and turbulence and carried biochemical and geological sampling. In addition three moorings were deployed for the continuous observation of the circulation of Atlantic water. We then steamed toward Djimphna Sound, which is framed by rocky coastlines decorated by ice fields. Also, the 79°N glacier terminates in the fjord comprising a minor calving front. At the sill near the fjord entrance we deployed another mooring and collected sediment samples. This was followed by a transit toward in a south-westerly direction across the sea ice covered shelf toward the shelf edge at 79°36'N. We were able to complete a hydrographic section across the East Greenland Current. In total four such sections have been completed at different latitudes, from which we will be able to derive the spatial structure of the recirculation and the lateral mixing of Atlantic waters. Subsequently we returned to the East Greenland Current at 78°50'N, where we recovered in heavy sea ice the winch mooring deployed for testing purposes earlier in the expedition, and additionally carried out two stations for the GEOTRACES programme still missing. Our subsequent attempts to recover two sound source mooring deployed in 2012 unfortunately failed. We then left the sea ice covered area of the East Greenland Current toward the southeast for Knipovich Ridge. As the last major work programme 13 ocean bottom seismometers were deployed in quick succession, complementing the instruments deployed in this area during the first week of the expedition.

We owe many thanks to Captain Schwarze, the entire *Polarstern* crew, the helicopter service and the weather service.

2. WEATHER CONDITIONS DURING PS100

Dipl.-Met. Max Miller[1], Hartmut Sonnabend[1] [1]DWD

On Monday evening, July 18, 2016, 19:20 pm, *Polarstern* left Tromsø for the campaign PS100. Light rain, 9° C and moderate to fresh southerly winds were observed.

A low south of Bear Island moved northeast via Svalbard. Therefore we sailed at the south side of this low. After leaving the fjords southwest to westerly winds appeared rapidly at force 6 to 7 including short phases of 8 Bft. The sea state rose near 4 m. Until Thursday (July 21) we steamed south of the low, but winds and waves decreased gradually.

Meanwhile a high had moved from southern Scandinavia towards Barents Sea. On Friday (July 22) we operated at its northwest side and reached Longyearbyen at westerly winds 4 Bft.

Until Thursday (July 28) weak troughs and ridges crossed Fram Strait eastwards. Therefore winds alternated between north and south and blew most of the time at force 4 to 5 Bft. But along the west coast of Svalbard a jet-like effect caused temporarily an acceleration up to 7 Bft.

On Friday (July 29) *Polarstern* reached the ice. The high over Greenland spread towards Fram Strait and we got at its northeast side while sailing along the Greenwich Meridian. Wind force 4 to 5 Bft was prevailing and fog became more frequent.

Afterwards a weak trough formed along the east coast of Greenland and got stationary for several days. Moderate winds veered south until Wednesday (Aug. 03). Due to warmer air blowing over icy surface the risk of fog grew. Until Friday (Aug. 05) further weak ridges and troughs alternated off Greenland.

On Saturday (Aug. 06) a final trough left Greenland's coast and melted with a low moving from North Pole towards Svalbard. Together with the high over Greenland they caused increasing northerly winds over Fram Strait at 5 to 6 and some peaks at force 7 Bft. Off the ice a sea state of 1 to 2 m was forced.

On Tuesday (Aug. 09) the high near the Azores built a ridge towards Fram Strait. Therefore northerly winds abated clearly during the night to Wednesday.

From Wednesday (Aug. 10) on a trough formed again along the east coast of Greenland with only light to moderate southerly winds. During the night to Saturday (Aug. 13) a small secondary low developed at the north-eastern end of Greenland and moved towards Svalbard. Winds veered temporarily northwest and freshened up. But already on Sunday (Aug. 14th) the weak trough at Greenland's coast was renewed. The upcoming week southerly winds with some peaks at 5 Bft and fog patches were prevailing.

On Saturday (Aug. 20) the trough started moving east. A low north of the Queen-Elizabeth-Islands together with the high over Greenland caused westerly winds over the northern parts of Greenland. Foehn on rather katabatic effects forced stronger winds in front of the 79° N – Glacier than could be expected due to the pressure gradient. Especially on Sunday (Aug. 21) we often measured wind force 7 (gusts 8) Bft together with +8° C and a relative humidity of only 35 %. On Monday winds abated as the low moved away towards North Pole.

From Tuesday (Aug. 23) on only weak pressure gradient and light winds were prevailing off Greenland. Nevertheless local circulations occurred sometimes at the glacier with wind peaks at Bft 6.

On Saturday (Aug. 27) a low over eastern Siberia started moving north. It deepened to a storm and headed towards the North Pole. Off Greenland we operated far away from the stormy part of the low. But in interaction with the high over Greenland a Foehn situation was forced again at the coast. Already weakening the low reached Franz-Josef-Land on Monday (Aug. 29) evening. Steaming east we got northerly winds at Bft 8 for short times. But during the night to Tuesday winds abated rapidly.

During the final part of the cruise several lows moved from the Iceland area towards Svalbard or Barents Sea. Especially on Saturday (Sept. 03) winds freshened temporarily up to force 7 Bft from southeast. On our way to Tromsø we had a sea state between 2 and 3 m.

On Monday (Sept. 05) the high over Central Europe built a ridge towards northern Scandinavia.

On Tuesday morning, September 06, 2016, *Polarstern* reached Tromsø at light and variable winds.

For further statistics see attached files (Fig. 2.1 – Fig. 2.4).

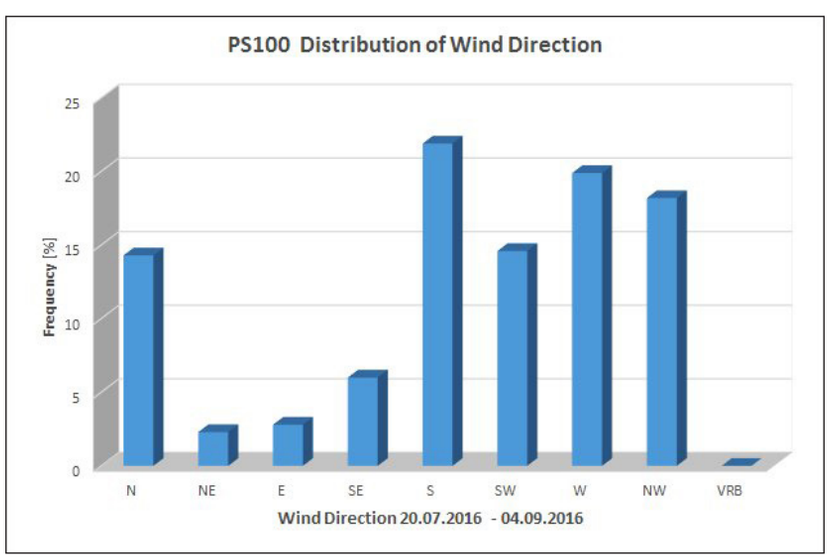

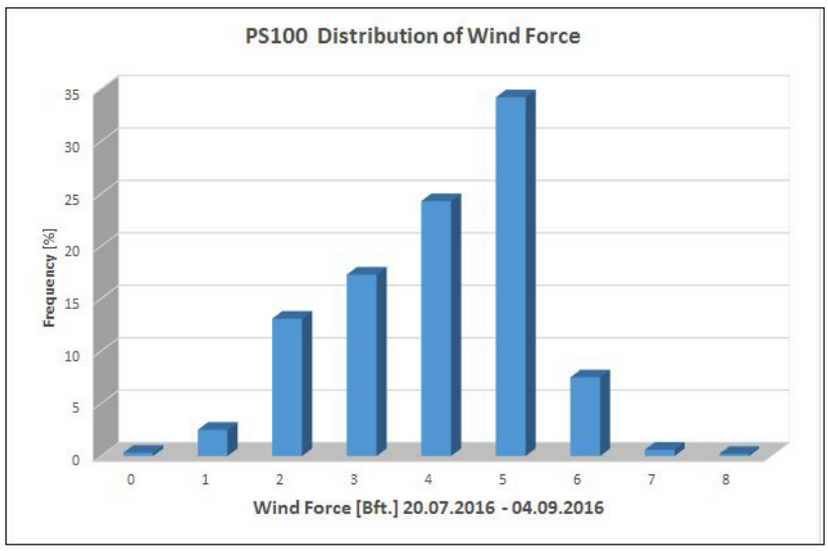
PS100 Distribution of Wind Force
Frequency [%]
35
30
25
20
15
10
5
0
0
1
2
3
4
5
6
7
8
Wind Force [Bft.] 20.07.2016 - 04.09.2016

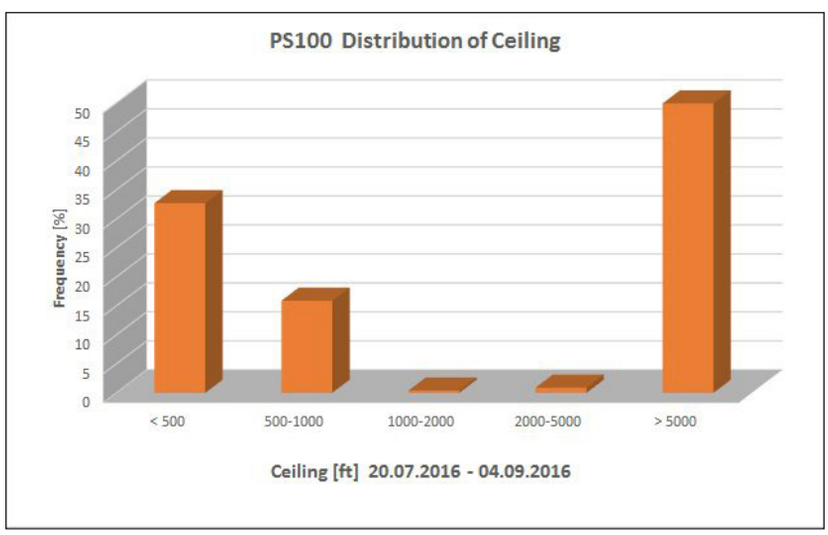
PS100 Distribution of Ceiling
Frequency [%]
50
45
40
35
30
25
20
15
10
5
0
< 500
500-1000
1000-2000
2000-5000
> 5000
Ceiling [ft] 20.07.2016 - 04.09.2016

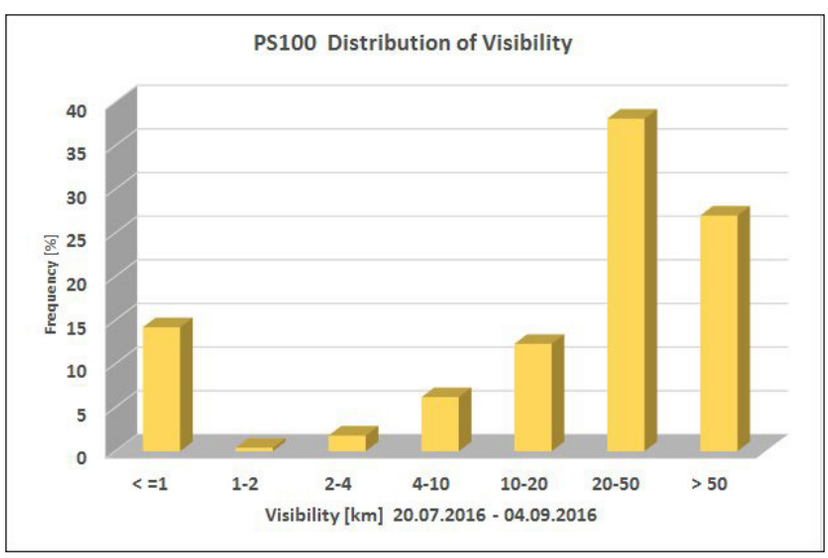
PS100 Distribution of Visibility
Frequency [%]
40
35
30
25
20
15
10
5
0
< =1
1-2
2-4
4-10
10-20
20-50
> 50
Visibility [km] 20.07.2016 - 04.09.2016

3. FLOW OF ATLANTIC WATER IN FRAM STRAIT AND ON THE EAST GREENLAND SHELF

Wilken-Jonn von Appen[1],Torsten Kanzow[1], Takamasa Tsubouchi[1], Janin Schaffer[1], Matthias Monsees[1], Carina Engicht[1], Eike Köhn[2] , Nat Wilson[3], Jonathan Poole[4]
not on board: A. Münchow (University of Delaware), Fiamma Straneo (WHOI), Malene Simon (Greenland Institute of Natural Resources)

[1]AWI,
[2]GEOMAR,
[3]MIT-WHOI,
[4]Squarewavemarine

Grant No. AWI-PS100_01

Background and objectives

West Spitsbergen Current

This cruise supports a long-term effort to monitor and quantify the variability of oceanic fluxes through the Fram Strait with a particular emphasis on the physical oceanography.

The Arctic Ocean is a semi-enclosed marginal sea with the Bering Strait, the Canadian Arctic Archipelago, and the Barents Sea being three shallow connections to the world oceans. The Fram Strait is the only deep strait (2,700 m), thereby allowing for the exchange of intermediate and deep waters between the Arctic Ocean and the Nordic Seas, which are in turn a marginal sea of the North Atlantic. Atlantic origin water is cooled throughout the cyclonic boundary current circulation in the Nordic Seas and enters the Arctic through the Barents Sea and the eastern Fram Strait. The temperature and other properties of the inflowing warm and salty Atlantic Water change in response to interannual variability (Beszczynska-Möller et al., 2012), to large scale-, multi-year climate patterns, such as the North Atlantic Oscillation, and to global climate change. The sum of these effects can be measured in the Fram Strait before it enters the Arctic Ocean, where it participates in the formation of the halocline north of Svalbard and forms a mid-depth cyclonic boundary current. Cooling, freezing, sea-ice melt, mixing with Pacific origin water, and the addition of large amounts of river runoff in the Arctic modifies the inflowing water (Rudels et al., 2005) before it exits through the western Fram Strait (de Steur et al., 2014). Thus observations of the outflow from the Arctic make it possible to monitor the effects of many processes in the Arctic Ocean.

The complicated topography in the Fram Strait leads to a horizontal splitting of the inflowing branches of Atlantic Water. Additionally, some of the Atlantic Water participates in a westward flow called the recirculation that then turns southward to exit the Fram Strait back to the Nordic Seas. The southward flowing cold and very fresh East Greenland Current is responsible for a large part of the liquid freshwater export from the Arctic and most of the solid freshwater export in the form of sea-ice. This freshwater has the potential to impact convection in the Nordic Seas and the northern North Atlantic and in turn the meridional overturning circulation.

Since 1997, AWI and the Norwegian Polar Institute have maintained a mooring array across the Fram Strait to monitor the fluxes of volume and heat, and, in the western part of the strait, freshwater into and out of the Arctic Ocean through this gateway.

Atlantic Water Recirculation

The recirculation of Atlantic Water (AW) in Fram Strait controls how much of the warm nutrient rich AW flowing northward in the West Spitsbergen Current enters the Arctic Ocean. This determines the oceanic heat input and therefore the extent of the partially ice-free halocline formation area north of Svalbard (Rudels et al., 2005). The inflow also impacts the light and nutrient distribution in the Arctic and therefore habitat distribution and biogeography in the Arctic Ocean (Metfies et al., 2016) as well as their future evolution.

The part of the AW, that does not enter the Arctic Ocean, follows distinct, but poorly understood, pathways in Fram Strait and is then exported southward in the East Greenland Current. Special to Fram Strait is also that the southward advection of sea-ice and the northward advection of AW balance such that the ice-edge location varies very little. Hence, the region where frontal dynamics associated with the meltwater front at the interface between the two can affect the physics and biology (e.g. Wulff et al., 2016 in review) is confined to a relatively small area. The Polar Water outflow is also located vertically above the AW. While it remains to be explained how that happens, it is clear that the large stratification associated with that transition leads to a similar situation to the halocline of the Arctic Ocean where the vertical nutrient supply to the shallow euphotic zone is inhibited and the primary production has to adapt accordingly. The meridional extent over which the recirculation takes place has not been constrained. A recent numerical model study (Hattermann et al., 2016 in review) has suggested that there are in fact two branches of the recirculation. A southern branch is thought to be comparatively steady, while a northern branch essentially can be considered as an extended region in which eddies are propagating westwards. The recirculation also likely has a baroclinic geostrophic and a barotropic wind-driven component, but it has only been possible to show that both contribute to the recirculation between 78°50'N and 79°0'N (de Steur et al., 2014). It also known that the West Spitsbergen Current is unstable at 78°50'N, especially in winter (von Appen et al., 2016), but it is not known whether there is even more eddy generation further north. The large seasonality in the region (e.g. de Steur et al., 2014, von Appen et al., 2016) also means that an understanding solely based on the summer time situation (calmest season) will inherently be incomplete. The dynamics that lead to the splitting of the AW inflow are essential to other regions of the ocean as well. For example, the Irminger Current splits at Denmark Strait and only some of the warm water flows northward through that strait. The lacking dynamical understanding of the present day recirculation also currently makes it impossible to predict how the recirculation and the processes influenced by it will evolve in the future under changing forcing conditions associated with e.g. climate change.

In order to improve the understanding of the recirculation in Fram Strait, it is crucial to measure several physical and biological parameters over the presumed meridional extension of the recirculation including during the winter months. The temperature and salinity distribution in space and time can be used to track the water of the recirculation and determine its modification and vertical motion reflected in the depth of the temperature maximum. The meridional gradient of the density can be used to elucidate the location of baroclinic geostrophic flows and combination with direct velocity measurements can reveal the full current structure. The short term variability of the currents gives information on the eddy field and its possible contribution to the flow. Vertical velocity shear can highlight the interface between the lighter Polar outflow water and the AW. The horizontal motion of those two layers is likely quite different in some regions and possibly also decoupled from the overlying ice motion. The vertical migration of the interface between the two water masses in response to external factors can be tracked even

in the absence of profiling temperature and salinity measurements. The oxygen distribution provides insights on the primary productivity while acoustic backscatter elucidates the presence and migration of zooplankton which possibly responds to the changes physical environment.

The ideal location to measure these properties is along the prime meridian (0°EW). This is outside of the West Spitsbergen Current and the East Greenland Current and what happens there is therefore not due to the boundary currents, but rather due to the recirculation. The prime meridian also avoids the 5,500 m deep Molloy Hole whose likely topographic steering would add an additional level of complexity to this already complex question. The prime meridian also cuts across the ice-edge (near 79°N at 0°EW) such that the influence of the recirculation on the ice-edge can be studied there. Additionally, the small amount of data that exist on the meridional structure of the recirculation is located along the prime meridian (Marnela et al., 2013) and it is hence valuable to collect new data at a comparable location. Mooring data will also be used for validation of and assimilation into a numerical model of the region around the Fram Strait.

For these reasons, five equally spaced moorings were deployed at the following locations along the prime meridian (0°EW): 78°10'N, 78°50'N, 79°30'N, 80°10'N, and 80°50'N which is in water depths between 2,000 m and 3,000 m. Velocity as well as temperature, salinity, and oxygen are measured in the upper 750 m on the moorings.

East Greenland Shelf Circulation

Mass loss from the Greenland Ice Sheet presently accounts for a third to a quarter of sea-level rise (Milne et al., 2009) and the rate of mass loss is increasing (Velicogna, 2009). The dominant mechanism is increased mass discharge along the marine margins where numerous major outlet glaciers have undergone a nearly simultaneous retreat, acceleration and thinning (Rignot and Kanagaratnam, 2006; Howat et al., 2008; Stearns and Hamilton, 2007; Dietrich et al., 2007). Both data and models indicate that this acceleration was triggered by a change at the tidewater margins of these glaciers (Thomas, 2004; Nick et al., 2009; Pritchard et al., 2009), suggesting that the ocean plays a key role in modulating the ice sheet's mass balance (Vieli and Nick, 2011; Straneo et al., 2012).

The proposed oceanic trigger is supported by recent studies showing that warm Atlantic waters are present and circulating in Greenland's glacial fjords (Holland et al., 2008; Straneo et al., 2010; Murray et al., 2010; Straneo et al., 2011) and by the observation that these waters were warming and accumulating in the subpolar North Atlantic at the same time as the glaciers started to retreat (e.g. Bersch et al., 2007).

Greenland's glacier acceleration has been concentrated along the southeastern and western margins terminating in the subpolar North Atlantic. Only recently, Helm et al. (2014) observed a general reduction in ice sheet elevation near the margins in the northeast of Greenland. Here, mainly two glaciers Nioghalvfjerdsfjorden glacier and Zachariae Isstrom drain the Northeast Greenland Ice Stream (NEGIS) whose drainage basin contains more than 15 % of the Greenland Ice Sheet area (Rignot and Kanagaratnam, 2006). Zachariae Isstrom lost about 5 Gt/yr of its mass since 2003 and was observed to retreat at an accelerated rate since fall 2012, whereas no mass loss but an increased bottom melting was found at Nioghalvfjerdsfjorden glacier (Mouginot et al., 2015). Khan et al. (2014) observed an acceleration of the ice flow of Nioghalvfjerdsfjorden glacier and a sustained dynamic thinning of NEGIS which they linked to a regional warming. The fact that a warming and thickening of the Atlantic layer has recently been observed in the Nordic Seas (e.g. in Fram Strait; Beszczynska-Möller et al., 2012) raises the question of whether the ocean changes may have triggered the fast retreat of

Zachariae Isstrom (as suggested by Mouginot et al., 2015) and will trigger unstable behavior of Nioghalvfjerdsfjorden glacier.

Warm Atlantic water is carried to the North by the North Atlantic Current - Norwegian Atlantic Current - West Spitsbergen Current system. In Fram Strait a sizable fraction of the Atlantic water recirculates to the south on the East Greenland continental slope. Studies on the eastern Greenland shelf in the 1980s and 1990s found this recirculating Atlantic water (RAW) to penetrate through sea bed troughs onto the East Greenland shelf (e.g. Bourke et al., 1987) below the fresh and cold polar waters (PW).

The Atlantic water mass found on the shelf was described by Bourke et al. (1987) as Atlantic Intermediate Water (AIW) with temperatures ranging between 0°C and 3°C and salinities between 34.5 and 34.9. Budeus et al. (1997) found two distinct types of Atlantic waters in the trough system. They found 1°C warm Atlantic waters with salinities of 34.9 to be present throughout the southern Norske Trough, which cooled and freshened towards 79N glacier, and 0.5°C warm Atlantic waters with salinities of 34.8 in the northern Westwind Trough. An anticyclonic surface circulation on the continental shelf following the trough axis was found based on hydrographic observations (Bourke et al., 1987; Schneider and Budeus, 1995), moored (Topp and Johnson, 1997) and ship based (Johnson and Niebauer, 1995) velocity measurements. In addition, Topp and Johnson (1997) proposed an anticyclonic subsurface circulation from moored measurements in Westwind Trough, in contrast to Budeus et al. (1997), who proposed that there is no one-directional flushing of the trough system. In the trough area east of the outlet glaciers, i.e. between Westwind and Norske Trough, Budeus and Schneider (1995) suggested a sill depth of 250 m causing the differences in water properties. This part of the shelf has rarely been studied due to a perennially fast sea ice cover (e.g. Schneider and Budeus, 1995; Schneider and Budeus, 1997), but is of strong interest when studying warm water pathways towards the outlet glaciers.

A survey of Nioghalvfjerdsfjorden glacier in the mid-1990s led to very high estimates of submarine melt rates (about 40 m/yr locally, with a mean basal melt rate of 8 m/yr), which account for the bulk of the ice shelf mass loss (Mayer et al., 2000). The melting was attributed to the presence of AIW in the 600 m to 800 m deep subglacial cavity as observed in several conductivity, temperature and depth (CTD) profiles collected at the glacier's margins (Thomsen et al., 1997; Mayer et al., 2000). A more recent survey conducted in the summer of 2009 (Straneo et al., 2012) confirmed that the AIW found under the floating ice tongue still contains large amounts of heat to drive melting. Based on three CTD sections taken north of the main glacier front, Wilson and Straneo (2015) discussed that warm AIW cannot enter the cavity through Dijmphna Sund due to a sill of 170 m depth but needs to pass the eastern pinned glacier front. They proposed that the exchange of warm Atlantic waters between the continental shelf and the cavity through Norske Trough occurs on timescales of less than a year.

Nonetheless these implications are not based on observations towards the east/southeast of Nioghalvfjerdsfjorden glacier, and a direct pathway of warm AIW from the shelf break, through Norske Trough towards Nioghalvfjerdsfjorden glacier is still missing.

Work at sea

Moorings

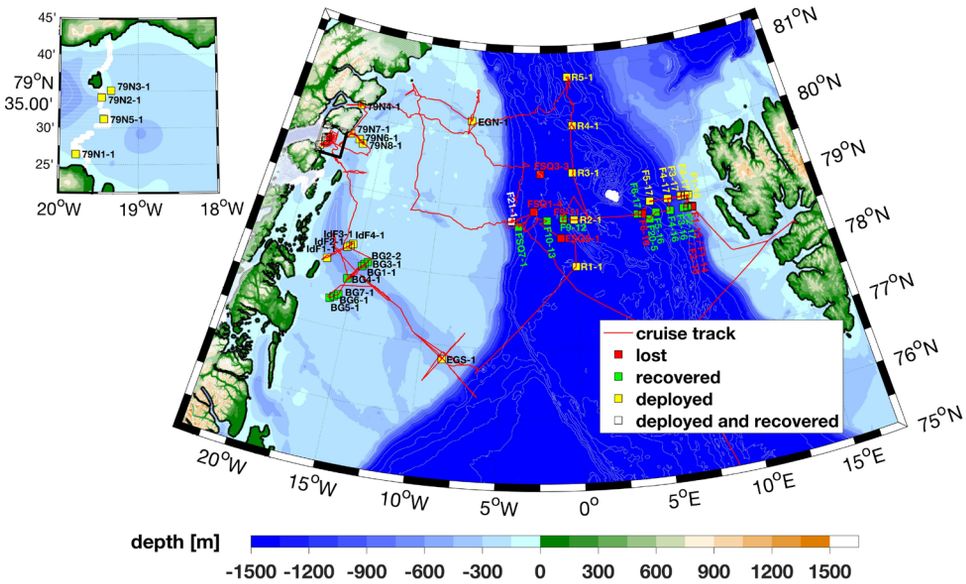

Fig. 3.1: Map of recovered and deployed moorings

Moorings have been deployed in the Fram Strait and on the East Greenland shelf by the Alfred Wegener Institute in 2012 (PS80), 2014 (PS85), and 2015 (PS93.1, HE451.2). Some of the moorings that were deployed in 2012 were recovered during the cruises in 2014 and 2015. The majority of the 28 moorings still in the water at the beginning of PS100 (Table 3.1) were recovered on PS100 or it was attempted to recover them (Fig. 3.1).

Another large part of the work of the physical oceanography group was to deploy 25 moorings (Table 3.1). The moorings in the West Spitsbergen Current and in the Atlantic Water recirculation are part of the FRAM infrastructure initiative. The moorings on the East Greenland shelf belong to the physical oceanography section of AWI with the exception of five of the moorings IdF2-1, IdF4-1, 79N5-1, 79N6-1, and 79N7-1 which belong to the University of Delaware.

The recovery of the remaining moorings deployed in 2012 was mostly unsuccessful. This was due to the fact that there had been attempts to recover the moorings in 2015 (PS93.1), but that those attempts already failed because the moorings were broken in some way. As such, FSQ7-1 was the only mooring from 2012 that could be recovered on PS100. The other moorings listed in Table 3.1 are declared finally lost though. Except for F1-15, which was lost, the recoveries of moorings deployed in 2014 and 2015 were successful. The data return of the instruments was good with most time series of the planned duration and instrument problems detected so far.

The deployment of the 25 moorings was mostly successful. During the night after the deployment of F3-17, a CTD cast was performed at the mooring site. Due to a communication error with the bridge, the location was exact and as a result the rosette became hooked into either an Aquadopp or a microcat and an Aquadopp during the upcast. This instrument(s) was/were dragged along the mooring line for 200 m until the termination of that mooring section. Then the mooring was lifted up before the top flotation reached the surface. At that point, the instrument(s) became unhooked and the mooring fell back to the ground. As a result, the mooring was moved about 180 m to the north. Also, the instrument(s) is/are now located 550 m

below the surface instead of the planned 750 m. The mooring was subsequently acoustically interrogated and appeared to be in order. Thus it was decided to leave the mooring in the water without recovering and redeploying it. During the deployment of F4-17, a 40 m mooring line (production December 2009 by Gleistein 29) overheated on the spill and subsequently broke. Thus the mooring was prematurely deployed. At the time, a sufficient amount of buoyancy had already been attached such that the mooring could be released and recovered. It was then redeployed as planned with the faulty mooring line replaced. During the later deployment of R2-1, a 500 m line of the same production line overheated, but this line could be recovered before it broke. This production line was subsequently eliminated from any use and will not be used in the future.

Tab. 3.1: Overview of the mooring actions on PS100 with the latitude, longitude, water depth in meters, station number, and mooring number as well as the action taken

Latitude	Longitude	Depth	Station	Mooring	Status
78 ° 50.24 ' N	8 ° 40.55 ' E	211.0	PS100/0014-2	F1-14	lost
78 ° 50.09 ' N	8 ° 20.24 ' E	0.0	PS100/0025-1	F2-16	lost
78 ° 50.16 ' N	5 ° 0.33 ' E	2701.2	PS100/0036-1	F6-16	lost; after Tucken
78 ° 50.04 ' N	0 ° 47.70 ' W	2618.8	PS100/0041-1	F9-11	lost
78 ° 44.12 ' N	4 ° 3.16 ' W	1755.9	PS100/0100-1	FSQ7-1	recovered
78 ° 34.79 ' N	1 ° 0.19 ' W	2803.9	PS100/0104-1	FSQ5-1	lost
77 ° 57.93 ' N	14 ° 29.97 ' W	403.7	PS100/0158-1	BG3-1	recovered
77 ° 55.61 ' N	14 ° 38.59 ' W	454.2	PS100/0164-1	BG1-1	recovered
77 ° 42.85 ' N	15 ° 26.42 ' W	372.5	PS100/0157-1	BG4-1	recovered
77 ° 23.42 ' N	16 ° 17.39 ' W	181.0	PS100/0154-1	BG5-1	recovered
77 ° 25.52 ' N	16 ° 2.52 ' W	277.6	PS100/0155-1	BG6-1	recovered
77 ° 27.93 ' N	15 ° 46.72 ' W	306.9	PS100/0156-1	BG7-1	recovered
78 ° 51.34 ' N	0 ° 48.33 ' W	2640.8	PS100/0040-1	F9-12	recovered
78 ° 49.56 ' N	1 ° 58.81 ' W	2671.8	PS100/0103-1	F10-13	recovered
78 ° 49.60 ' N	8 ° 40.90 ' E	244.2	PS100/0014-1	F1-15	lost
78 ° 44.90 ' N	5 ° 29.89 ' E	0.0	PS100/0031-1	F20-5	recovered mooring but profiler lost
77 ° 59.91 ' N	14 ° 18.43 ' W	241.7	PS100/0163-1	BG2-2	recovered
78 ° 49.63 ' N	8 ° 19.13 ' E	788.3	PS100/0024-1	F2-17	recovered
78 ° 49.97 ' N	8 ° 1.77 ' E	994.0	PS100/0026-1	F3-16	recovered
78 ° 49.67 ' N	7 ° 3.29 ' E	1397.5	PS100/0029-1	F4-16	recovered
78 ° 49.94 ' N	6 ° 0.62 ' E	2417.0	PS100/0030-1	F5-16	recovered
78 ° 50.46 ' N	4 ° 39.00 ' E	2725.7	PS100/0032-1	F6-17	recovered
79 ° 0.02 ' N	8 ° 19.84 ' E	785.2	PS100/0016-1	F2-18	deployed
79 ° 0.12 ' N	7 ° 59.84 ' E	1075.3	PS100/0017-1	F3-17	deployed; picked up and moved by CTD
79 ° 0.01 ' N	7 ° 0.03 ' E	1218.5	PS100/0018-1	F4-17	deployed; line broken during deployment
79 ° 0.02 ' N	5 ° 40.12 ' E	2100.4	PS100/0019-1	F5-17	deployed
79 ° 0.01 ' N	8 ° 32.51 ' E	345.9	PS100/0023-1	F1-16	deployed
78 ° 50.01 ' N	0 ° 0.09 ' E	2596.5	PS100/0039-2	R2-1	deployed
79 ° 30.00 ' N	0 ° 0.03 ' W	2778.0	PS100/0045-1	R3-1	deployed
80 ° 9.75 ' N	0 ° 10.19 ' E	3034.1	PS100/0047-1	R4-1	deployed
80 ° 51.18 ' N	0 ° 7.23 ' W	3139.5	PS100/0053-1	R5-1	deployed
80 ° 11.49 ' N	8 ° 8.96 ' W	306.8	PS100/0073-1	EGN-1	deployed
78 ° 48.77 ' N	4 ° 34.45 ' W	1380.6	PS100/0099-1	F21-1	deployed and recovered 24 days later
78 ° 10.21 ' N	0 ° 0.04 ' E	3012.9	PS100/0106-1	R1-1	deployed
76 ° 48.09 ' N	8 ° 36.93 ' W	352.6	PS100/0142-1	EGS-1	deployed
78 ° 12.45 ' N	15 ° 33.68 ' W	265.8	PS100/0180-2	IdF4-1	deployed
78 ° 10.59 ' N	15 ° 43.26 ' W	350.9	PS100/0181-1	IdF3-1	deployed
78 ° 9.02 ' N	15 ° 54.00 ' W	416.0	PS100/0182-1	IdF2-1	deployed
77 ° 55.62 ' N	17 ° 5.22 ' W	364.6	PS100/0183-1	IdF1-1	deployed
79 ° 34.13 ' N	19 ° 27.58 ' W	475.0	PS100/0238-1	79N2-1	deployed
79 ° 31.17 ' N	19 ° 25.83 ' W	296.9	PS100/0239-1	79N5-1	deployed
79 ° 26.40 ' N	19 ° 46.64 ' W	326.2	PS100/0240-1	79N1-1	deployed
79 ° 35.06 ' N	19 ° 20.56 ' W	358.7	PS100/0257-1	79N3-1	deployed
79 ° 40.15 ' N	16 ° 53.36 ' W	256.6	PS100/0263-3	79N6-1	deployed
79 ° 43.23 ' N	17 ° 40.40 ' W	404.1	PS100/0272-1	79N7-1	deployed
79 ° 37.15 ' N	16 ° 32.61 ' W	287.0	PS100/0273-1	79N8-1	deployed
80 ° 8.92 ' N	17 ° 24.56 ' W	155.1	PS100/0274-1	79N4-1	deployed
79 ° 29.16 ' N	2 ° 28.52 ' W	2711.0	PS100/0287-1	FSQ3-3	lost
78 ° 57.12 ' N	2 ° 57.53 ' W	2455.0	PS100/0289-1	FSQ1-4	lost

The settings of the data recording instruments deployed on PS100 is documented in Tables 3.5 to 3.14. The RCM11 were set to sample every 2 hours, but no further settings are possible.

F20-5 was a mooring with a winch and a profiler intended to sample the upper ocean stratification. Unfortunately, the profiler was lost and only the winch with the rest of the mooring underneath was recovered. Thus no data on the upper ocean stratification was collected. F21-1 with a winch and profiler was supposed to be deployed adjacent to F4-17. However, there were problems with the electronics of the profiler before deployment and after the recovery of F20-5, a decision against a year-long deployment was taken. Therefore, the mooring was only deployed for 24 days in the East Greenland Current. The recovery was successful including the profiler. However, problems with the programming of the winch were detected that also resulted in no data being collected.

Tab. 3.2: Overview of the instruments recovered from moorings on PS100. The type is identified in Tab. 3.4. Also given are the serial numbers of the instruments and their depths in meters from the surface according to the mooring drawings. Moorings listed without instruments are where the mooring recovery attempt failed (Tab. 3.1).

Mooring	Type	SN	Depth drawing
F1-14			
F2-16			
F6-16			
F9-11			
FSQ7-1	SQ	14	747
FSQ5-1			
BG2-1	SBE37	10941	40
	LRADCP	3813	240
	SBE37	10939	248
	SBE26	227	250
BG3-1	LRADCP	3194	400
	SBE37	2932	402
BG1-1	SBE37	10940	170
	LRADCP	6240	445
	SBE37	9832	452
	SBE26	257	456
BG4-1	LRADCP	3654	370
	SBE37	2921	372
BG5-1	LRADCP	3656	179
	SBE37	2917	181
BG6-1	LRADCP	3751	275
	SBE37	2927	277
BG7-1	LRADCP	3655	304
	SBE37	2925	306
F9-12	SBE37	10949	74
	QMADCP	15082	244
	RCM8	11890	245
	SBE37	10950	246
	RCM8	9763	401
F10-13	SBE37	10951	68
	QMADCP	15083	249
	RCM11	20	250
	SBE37	10952	252

Mooring	Type	SN	Depth drawing
	RCM11	458	402
	SBE37	7690	742
	AQD	11333	2702
	SBE37	218	2703
F1-15			
F20-5	Winch	2	92
BG2-2	SBE37	2383	65
	SBE37	2087	85
	SBE37	233	185
	QMADCP	14971	235
	SBE37	235	242
F2-17	SBE37	246	64
	QMADCP	23548	253
	SBE37	247	255
	AQD	11330	778
	SBE37	214	779
F3-16	SBE37	249	62
	SBE37	10934	151
	QMADCP	14951	151
	SBE37	1232	253
	SBE37	1233	503
	Sonovault	1095	751
	AQD	11328	752
	SBE37	10938	753
	AQD	11348	996
	SBE37	215	997
F4-16	SBE37	1234	72
	SBE37	1606	151
	QMADCP	14088	251
	SBE37	1564	254
	SBE37	1603	254
	AQD	11342	748
	SBE37	10936	749
	AQD	11337	1411
	SBE37	10937	1412
F5-16	SBE37	2395	77
	QMADCP	14087	256
	SBE37	2611	257
	Sonovault	1096	755
	AQD	9936	756
	SBE37	10935	757
F6-17	SBE37	10942	72
	QMADCP	14086	251
	SBE37	10933	253
	Holgiphone	1477	503
	Sonovault	1101	752
	RCM11	314	753
	AQD	11350	754
	AQD	11324	2697
	SBE37	216	2698

Tab. 3.3: Overview of the instruments deployed on moorings on PS100. The type is identified in Tab. 3.4. Also given are the serial numbers of the instruments and their depths in meters from the surface according to the mooring drawings.

Mooring	Type	SN	Depth drawing
F1-16	AQD	12677	244
F2-18	SBE37 ODO	13900	43
	SBE37 ODO	13920	250
	LRADCP	23612	400
	AQD	12687	780
	SBE37 ODO	13902	781
F3-17	SBE37 ODO	13903	54
	SBE37 ODO	13905	256
	LRADCP	23043	405
	AQD	11329	756
	SBE37 ODO	13906	757
	AQD	12696	1067
F4-17	RAS	ML14128-06	52
	SBE37 ODO	13908	52
	SBE37	243	150
	SBE37 ODO	13968	250
	LRADCP	23978	385
	SBE37	245	500
	AQD	12658	750
	SBE37 ODO	13966	751
	AQD	12654	1207
F5-17	SBE37 ODO	13967	74
	Sonovault	1054	94
	AZFP	55112	146
	SBE37 ODO	13901	223
	LRADCP	24014	405
	AQD	12679	732
	SBE37	232	733
	Sonovault	1088	808
	Sonovault	1025	2091
F21-1	SBE19 Profiler	7687	139
	Winch	3	140
	SBE37 ODO	13983	140
R1-1	SBE37 ODO	13973	64
	SBE56	6363	100
	SBE56	6364	150
	QMADCP	24069	247
	SBE37 ODO	13974	252
	SBE56	6365	349
	SBE56	6366	499
	AQD	12685	751
	SBE37 ODO	13985	752
	Sonovault	1097	799
	SBE53	436	3012
R2-1	SBE37 ODO	13979	52
	SBE56	6567	109
	SBE56	6368	148

Mooring	Type	SN	Depth drawing
	AZFP	55114	149
	QMADCP	23806	253
	SBE37 ODO	13980	254
	SBE56	6369	355
	SBE56	6370	505
	AQD	12718	754
	SBE37 ODO	13981	755
	Sonovault	1091	806
	SBE37 ODO	13969	2500
R3-1	SBE37 ODO	13982	65
	SBE56	6371	109
	SBE56	6372	173
F4-16	AZFP	55113	174
	QMADCP	23673	278
	SBE37 ODO	13986	285
	SBE56	6394	367
	SBE56	6395	517
	AQD	12745	771
	SBE37 ODO	13984	772
	Holgiphone	1477	836
	SBE53	437	2778
R4-1	SBE37 ODO	13978	63
	SBE56	6396	101
	SBE56	6397	149
	QMADCP	23976	251
	SBE37 ODO	13907	253
	SBE56	6398	353
	SBE56	6399	503
	AQD	12680	752
	SBE37 ODO	13987	753
R5-1	SBE37 ODO	14015	78
	SBE56	6400	57
	SBE56	6401	107
	QMADCP	24071	279
	SBE37 ODO	14005	281
	SBE56	6402	358
	SBE56	6403	508
	AQD	12667	707
	SBE37 ODO	14006	708
	SBE53	438	3141
EGN-1	SBE37	1237	110
	SBE56	6222	139
	SBE56	6257	169
	SBE56	6235	199
	SBE56	6300	229
	SBE56	6335	259
	SBE37	437	299
	QMADCP	24070	300
EGS-1	AuralM2	179LF	127
	SBE37	2100	127
	SBE56	6358	160

Mooring	Type	SN	Depth drawing
	SBE56	6359	190
	SBE37	2393	220
	SBE56	6360	240
	SBE56	6361	260
	SBE56	6362	290
	SBE56	6373	319
	LRADCP	24013	320
	RCM8	11890	321
	SBE37	438	348
IdF1-1	AuralM2	251LF	192
	SBE37	2396	192
	SBE56	6374	214
	SBE56	6375	244
	SBE56	6376	274
	SBE56	6377	304
	SBE37	439	334
	QMADCP	24068	354
	SBE56	6378	360
	SBE26	227	365
IdF2-1	LRADCP	3194	409
	SBE37	2932	414
IdF3-1	AuralM2	252LF	178
	SBE37	2392	178
	SBE56	6379	200
	SBE56	6380	230
	SBE56	6381	260
	SBE56	6382	290
	SBE37	447	320
	QMADCP	24052	340
	SBE56	6383	346
	SBE53	439	351
IdF4-1	LRADCP	3655	258
	SBE37	2925	263
79N1-1	SBE37	10937	206
	SBE56	6384	236
	SBE56	6385	266
	SBE56	6386	296
	QMADCP	24053	320
	SBE37	2386	322
79N2-1	SBE37	10934	204
	SBE56	6387	240
	SBE56	6388	264
	SBE56	6390	294
	SBE56	6391	324
	SBE56	6392	354
	SBE56	6393	384
	SBE56	6404	414
	SBE56	6405	434
	LRADCP	23613	454
	AQD	12665	464
	SBE37	2382	467

Mooring	Type	SN	Depth drawing
79N3-1	SBE37	3813	186
	600ADCP	19316	187
	SBE37	2385	227
	SBE56	6406	272
	SBE56	6407	317
	300ADCP	1368	359
	SBE37	10950	360
79N4-1	300ADCP	951	168
	SBE37	236	169
79N5-1	LRADCP	3656	293
	SBE37	2917	298
79N6-1	LRADCP	3751	249
	SBE37	2927	254
79N7-1	LRADCP	3654	394
	SBE37	2921	399
79N8-1	RCM11	458	191
	SBE56	6408	202
	SBE56	6409	242
	RCM11	314	262
	SBE37	7727	282

Tab. 3.4: Abbreviations of the instrument types used in Tab. 3.2 and Tab. 3.3 along with the long names and the parameters measured by those instruments

Abbreviation	Long name	Parameters measured
300ADCP	RDI 300kHz ADCP	velocity profiles, temperature, pressure
600ADCP	RDI 600kHz ADCP	velocity profiles, temperature, pressure
AQD	Nortek Aquadopp Deep Water	point velocity, temperature
AuralM2	ASL AuralM2 sound recorder	sound
AZFP	ASL Acoustic Zooplankton and Fish Profiler	particle concentration profiles
Holgiphone	Hc12 sound recorder	sound
LRADCP	RDI 75kHz ADCP	velocity profiles, temperature, pressure
QMADCP	RDI 150kHz ADCP	velocity profiles, temperature, pressure
RCM11	Aanderaa acoustic current meter	point velocity, temperature, pressure
RCM8	Aanderaa mechanical current meter	point velocity, temperature, pressure
SBE19 Profiler	Seabird SBE19 CTD in profiling mode	temperature, conductivity, pressure, oxygen
SBE26	Seabird SBE26 bottom pressure recorder	pressure, temperature
SBE37	Seabird SBE37 CTD	temperature, conductivity, pressure
SBE37 ODO	Seabird SBE37 CTD with oxygen	temperature, conductivity, pressure, oxygen
SBE53	Seabird SBE53 bottom pressure recorder	pressure, temperature

Abbreviation	Long name	Parameters measured
SBE56	Seabird SBE56 temperature logger	temperature
Sonovault	Develogic Sonovault sound recorder	sound
SQ	Develogic Sound Source	-
Winch	NGK profiling winch	rope distance

Tab. 3.5: Example command file for 75kHz ADCPs belonging to AWI

CR1
CQ255
CF11101
EA0
EB0
ED01700
ES35
EX10111
EZ1111101
WB1
WD111100000
WF704
WN50
WP00120
WS800
WV175
TP00:13.00
TE00:30:00.00
TF16/08/22 10:00:00
CK
CS

Tab. 3.6: Example command file for 75kHz ADCPs belonging to the University of Delaware

CR1
CQ255
CF11101
EA0
EB0
ED0
ES35
EX00111
EZ1111101
WA50

WB1
WD111100000
WF704
WN70
WP1
WS800
WV175
TP00:07.00
TE00:00:07.00
TC20
TB01:00:00.00
TF16/07/22 14:00:00
CK
CS

Tab. 3.7: Example command file for 150kHz ADCPs

CR1
CF11101
EA0
EB0
ED0
ES35
EX00111
EZ1111101
WA50
WB1
WD111100000
WF352
WN70
WP1
WS400
WV175
TP00:04.00
TE00:00:04.00
TC50
TB01:00:00.00
TF16/07/26 20:00:00
CK
CS

Tab. 3.8: Command file for 300kHz ADCP not used to measure turbulence parameters

CR1
CF11101
EA0
EB0
ED0
ES35
EX00111
EZ1111101
WA50
WB0
WD111100000
WF176
WN54
WP1
WS200
WV175
TB02:00:00.00
TC240
TE00:00:01.00
TP00:01.00
TF16/08/26 08:00:00
CK
CS

Tab. 3.9: Command file for 300kHz ADCP used to measure turbulence parameters

CR1
CF11101
EA0
EB0
ED0
ES35
EX00111
EZ1111101
WA50
WB0
WD111100000
WF176
WN54
WP1
WS200
WV175

TB02:00:00.00
TC240
TE00:00:01.00
TP00:01.00
TF16/08/26 08:00:00
CK
CS

Tab. 3.10: Command file for 600kHz ADCP used to measure turbulence parameters

CR1
CF11101
EA0
EB0
ED0
ES35
EX00111
EZ1111101
RN 19316
WA50
WB0
WD111100000
WF88
WN70
WS50
WV175
WP1
TP00:00.50
TE00:00:00.50
TB02:00:00.00
TC1200
TF16/08/25 14:00:00
CK
CS

Tab. 3.11: Example summary of programmed settings for Aquadopps

```
============================================================
Deployment   :                12687
Current time :                22.07.2016 10:58:31
Start at     :                22.07.2016 12:00:00
Comment:
SN 12687 for deployment at F2-18
------------------------------------------------------------
Measurement interval       (s) :          1200
```

```
Average interval          (s) :      60
Blanking distance         (m) :      0.50
Measurement load          (%) :      4
Power level :                        HIGH
Diagnostics interval      (min) :    720:00
Diagnostics samples :     20
Compass upd. rate         (s) :      600
Coordinate System :       ENU
Speed of sound            (m/s) :    MEASURED
Salinity                  (ppt) :    35
Analog input 1 :                     NONE
Analog input 2 :                     NONE
Analog input power out :             DISABLED
Raw magnetometer out :               OFF
File wrapping :                      OFF
TellTale :                           OFF
AcousticModem :                      OFF
Serial output :                      OFF
Baud rate :                          9600
-----------------------------------------------------------

Assumed duration          (days) :   820.0
Battery utilization       (%) :      94.0
Battery level             (V) :      11.4
Recorder size             (MB) :     9
Recorder free space       (MB) :     8.970
Memory required           (MB) :     3.7
Vertical vel. prec        (cm/s) :   1.4
Horizon. vel. prec        (cm/s) :   0.9
-----------------------------------------------------------
Instrument ID          :             AQD12687
Head ID                :             A6L 7654
Firmware version       :             3.39
-----------------------------------------------------------
Aquadopp Deep Water Version 1.40.14
Copyright (C) Nortek AS
===========================================================
```

Tab. 3.12: Example start protocol of microcats with oxygen sensor.

```
ds
SBE37SMP-ODO-RS232 v2.3.1  SERIAL NO. 13900  22 Jul 2016 16:00:21
vMain = 13.50, vLith =  3.18
samplenumber = 317, free = 399140
```

not logging, stop command
sample interval = 10 seconds
data format = converted engineering
output temperature, Celsius
output conductivity, S/m
output pressure, Decibar
output oxygen, ml/L
transmit real time data = no
sync mode = no
minimum conductivity frequency = 3267.0
adaptive pump control enabled
<Executed/>
AdaptivePumpControl=0
<Executed/>
OxNTau=14
<Executed/>
DateTime=07222016160111
<Executed/>
AdaptivePumpControl=0
<Executed/>
OxNTau=14
<Executed/>
OutputFormat=1
<Executed/>
TxRealTime=0
<Executed/>
SampleInterval=3600
<Executed/>
SampleNumber=0
memory pointers will be modified
repeat command to confirm:
SampleNumber=0
<Executed/>
StartDateTime=07252016000000
<start dateTime = 25 Jul 2016 00:00:00/>
<Executed/>
StartLater
<!--start logging at = 25 Jul 2016 00:00:00, sample interval = 3600 seconds-->
<Executed/>
ds
SBE37SMP-ODO-RS232 v2.3.1 SERIAL NO. 13900 22 Jul 2016 16:04:03
vMain = 13.39, vLith = 3.18
samplenumber = 0, free = 399457

not logging, start at 25 Jul 2016 00:00:00
sample interval = 3600 seconds
data format = converted engineering
output temperature, Celsius
output conductivity, S/m
output pressure, Decibar
output oxygen, ml/L
transmit real time data = no
sync mode = no
minimum conductivity frequency = 3267.0
adaptive pump control disabled, pump on time 14.0 * 5.5 = 77.0 sec
<Executed/>

Tab. 3.13: Example start protocol of microcats without oxygen sensor.

ds
SBE37SM-RS232 v4.1 SERIAL NO. 10937 23 Aug 2016 02:59:27
vMain = 13.53, vLith = 3.01
samplenumber = 2081, free = 557159
not logging, stop command
sample interval = 10 seconds
data format = converted engineering
transmit real-time = no
sync mode = no
pump installed = yes, minimum conductivity frequency = 3153.5
<Executed/>
DateTime=08232016030000
<Executed/>
TxRealTime=0
<Executed/>
OutputFormat=1
<Executed/>
SampleInterval=600
<Executed/>
SampleNumber=0
this command will modify memory pointers
repeat the command to confirm
<Executed/>
SampleNumber=0
<Executed/>
StartDateTime=08242016000000
<start dateTime = 24 Aug 2016 00:00:00/>
<Executed/>

StartLater
<!--start logging at = 24 Aug 2016 00:00:00, sample interval = 600 seconds-->
<Executed/>
ds
SBE37SM-RS232 v4.1 SERIAL NO. 10937 23 Aug 2016 03:01:50
vMain = 13.43, vLith = 3.01
samplenumber = 0, free = 559240
not logging, waiting to start at 24 Aug 2016 00:00:00
sample interval = 600 seconds
data format = converted engineering
transmit real-time = no
sync mode = no
pump installed = yes, minimum conductivity frequency = 3153.5
<Executed/>

Tab. 3.14: Example start protocol of SBE53 bottom pressure recorders.

S>DS
SBE 53 BPR V 1.1e SN 436 28 Jul 2016 14:43:45
user info=
quartz pressure sensor: serial number = 134952, range = 10000 psia
internal temperature sensor
conductivity = NO
iop = 6.4 ma vmain = 22.0 V vlith = 8.9 V
last sample: p = -99.0000, t = -99.0000

tide measurement: interval = 15 minutes, duration = 1 minutes, power pressure sensor continuously
measure reference frequency every 672 tide samples
logging start time = 29 Jul 2016 00:00:00
logging stop time = do not use stop time

tide samples/day = 96.000
memory endurance = 20560.3 days
nominal battery endurance = 523 days alkaline, 1521 days lithium
total recorded tide measurements = 0
total recorded reference frequency measurements = 0
tide measurements since last start = 0
transmit real-time tide data = NO

status = stopped by user
logging = NO, send start command to begin logging
S>datetime=07282016144349
S>TE_XTide=N

S>SetSampling
continuously power pressure sensor (y/n) = y, new value = y
tide interval (integer minutes) = 15, new value = 15
tide measurement duration (integer minutes) = 1, new value = 1
measure reference frequency every N tide samples: N = 672, new value = 7_667__72
use start time (y/n) = y, new value = y
use stop time (y/n) = n, new value = n
S>SetStartTime
set time to start logging:
month (1 - 12) = 7
day (1 - 31) = 28
year (4 digits) = 2016
hour (0 - 23) = 15
minute (0 - 59) = 0
second (0 - 59) = 0
S>InitLogging
S>start
logging will start at 28 Jul 2016 15:00:00
SBE 53 BPR
S>
S>ds
SBE 53 BPR V 1.1e SN 436   28 Jul 2016 14:45:09
user info=
quartz pressure sensor: serial number = 134952, range = 10000 psia
internal temperature sensor
conductivity = NO
iop = 6.4 ma vmain = 22.0 V vlith = 8.9 V
last sample: p = -99.0000, t = -99.0000

tide measurement: interval = 15 minutes, duration = 1 minutes, power pressure sensor continuously
measure reference frequency every 672 tide samples
logging start time = 28 Jul 2016 15:00:00
logging stop time = do not use stop time

tide samples/day = 96.000
memory endurance = 20560.3 days
nominal battery endurance = 523 days alkaline, 1521 days lithium
total recorded tide measurements = 0
total recorded reference frequency measurements = 0
tide measurements since last start = 0
transmit real-time tide data = NO

status = waiting to start at 28 Jul 2016 15:00:00
logging = YES, waiting to start
S>

CTD and salinometer

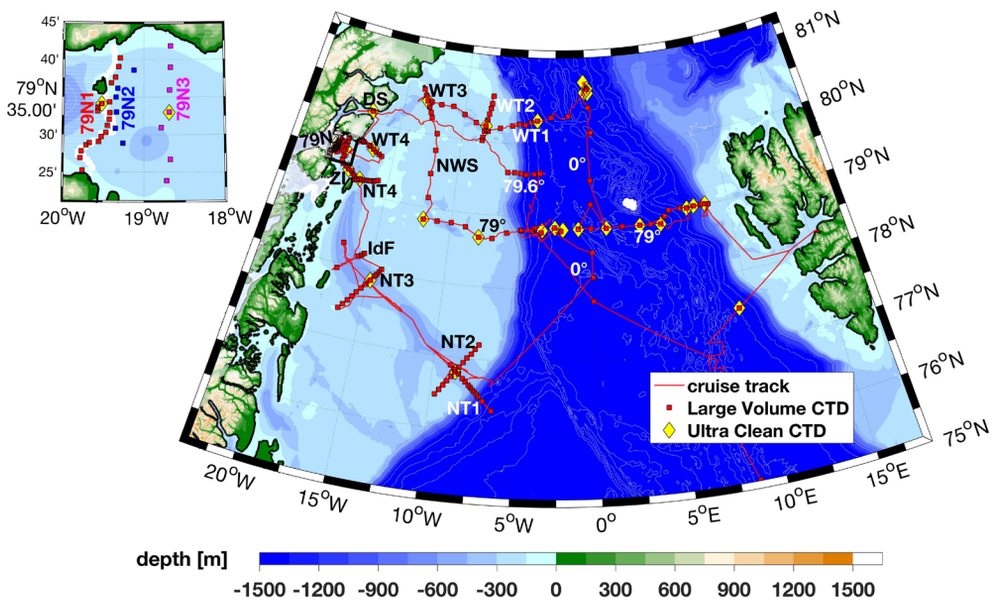

Fig. 3.2: Map of CTD stations during PS100. By default the large volume CTD was used on every cast. Stations where the ultra clean CTD was used in addition are marked.

The CTD measurements during the PS100 cruise were conducted by two CTDs, a large volume CTD and a clean CTD from GEOMAR (Fig. 3.2). Large volume CTD's sensors and main unit were provided AWI, and bottles and rosette were provided by NIOZ. Altogether 193 CTD profiles were taken by large volume CTD and 31 CTD profiles were taken by clean CTD. Water samplings from large volume CTDs were mainly used for biogeochemical and GEOTRACER measurements (see detail for section 6). Water samplings from clean CTDs were mainly used for tracer metal measurements (for details see Geotraces section).

Large volume CTD sonde was mounted in a rosette with 22 bottles (24 liter each) for water sampling (bottles #1-22 were mounted). The CTD contained dual sensors for temperature and conductivity, one sensor for pressure and one for oxygen. A fluorometer for chl a fluorescence, a beam transmissometer, a downward looking altimeter were also attached to the frame and connected to the coaxial cable. Details of the sensors can be found in Table 3.15. Altimeter was changed at station 056-02. Upward and downward looking LADCP was in serve from station 42-02. There were few events to notice. At the station 022-02, CTD sonde picked up near by mooring F3-17 during upward cast, from 600 m to 350 m. During this time, rope tension increased from 9kN to 16kN. Since then, CTD casts were conducted away from a nearby mooring site. Bottle #9 did not close for station from 082-02 to 088-01. Bottle #6 and #8 were out service for station 178-01 and 180-01. This was because release pin on top of the rosette was stuck. All sensors provided reasonable values during the entire cruise. Behaviors of temperature and salinity sensors were monitored by taking difference between primary and secondary sensors (secondary minus primary). The difference in two temperature sensors stayed almost constant through the cruise of -0.001˚C. Noticeable event happened during station 055-01 to 057-01, when the temperature difference became c.a. +0.000˚C (Fig. 3.3a).

Regarding the conductivity sensors, the difference in conductivity sensors shifted at station 048-01, from c.a. 0.0002 [mS/cm] to c.a. 0.0004 [mS/cm]. These differences stayed constant before and after the shift (Fig. 3.3b).

Clean CTD sonde was mounted in a rosette with 24 bottles (12 liter each) for water sampling. The CTD contained dual temperature and conductivity sensors and one pressure sensor. Additionally one altimeter sensor, two dissolved oxygen sensors and one beam transmissometer sensor were mounted on the carousels. There were few events to notice. At the station of 050-01, bottom detecting alarm sounded during the down cast. Measurements were halted at station 050-01, 052-01. The bottom detecting alarm also sounded at station at 056-01 and 101-01, but measurements were carried out. At station 288-01, data transmission was stopped during the up cast at 250 m. A fuse in CTD deck unit was burst. This also happed at station 290-01. All sensors provided reasonable values during the entire cruise, apart from altimeter and NMEA. Altimeter did not work well for first 21 casts during station 013-03 to 103-01. At the station 033-01, CTD hit the bottom as altimeter only worked only 5 meters above the bottom. The altimeter sensor was physically disconnected during station 102-01 to 135-01. This resulted in stopping CTD at c.a. 30 meters above the hydrosweep bottom depth measurement. NMEA was not in serve at station 021-01 and 028-01. See detail for Table 3.17. The difference in two temperature, conductivity and oxygen sensors stayed constant through the cruise, within range of 0.001˚C, 0.0007 [mS/cm], -0.054 [ml/l] below 1000 [dbar], respectively.

In order to define offset and drift of conductivity sensors, 78 salt samples were taken at 16 stations (12 stations for large volume CTD and 4 stations for clean CTD). Conductivities were measured under temperature and pressure controlled environment using the Optimare Precision Salinometer on-board *Polarstern* (SN. 006) and standard seawater from Ocean Scientific International. The salinity measurement with salinometer was conducted following a guideline of Operational manual of Precision salinometer System issued on 1 May 2011. Preliminary result suggests that primary and secondary conductivity sensors from large volume CTD may have offset of -0.0045±0.0031 [psu] and +0.0009±0.0031 [psu], respectively (Fig. 3.4). Likewise, primary and secondary conductivity sensors from clean CTD may have offset of -0.0023±0.0024 [psu] and -0.0021±0.0023 [psu], respectively. Regarding the shift of conductivity difference in large volume CTD at station 048-01, it is not strait forward to determine which conductivity sensor was shifted. The temperature difference during station 055-01-057-01 and higher salinity reading by salinometer at station 081-01 and 098-01 makes difficult to come up with a conclusion. Precise calibration on the conductivity sensors will be carried out later on. Likewise, we collected 65 oxygen samples from 16 casts using a titration method for later calibration of the oxygen sensor.

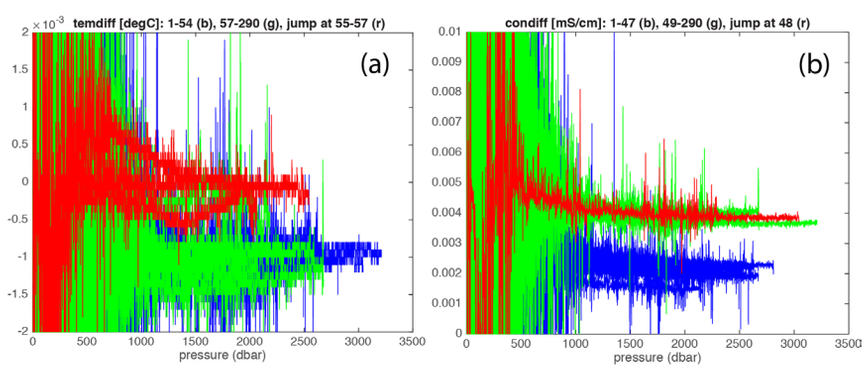

Fig. 3.3: (a) Difference in temperature sensors (secondary - primary) in large volume CTD. Station 1-54 in blue, station 55-57 in red, station 57-290 in green. (b) Difference in conductivity sensors (secondary - primary) in large volume CTD. Station 1-47 in blue, station 48 in red, station 49-290 in green.

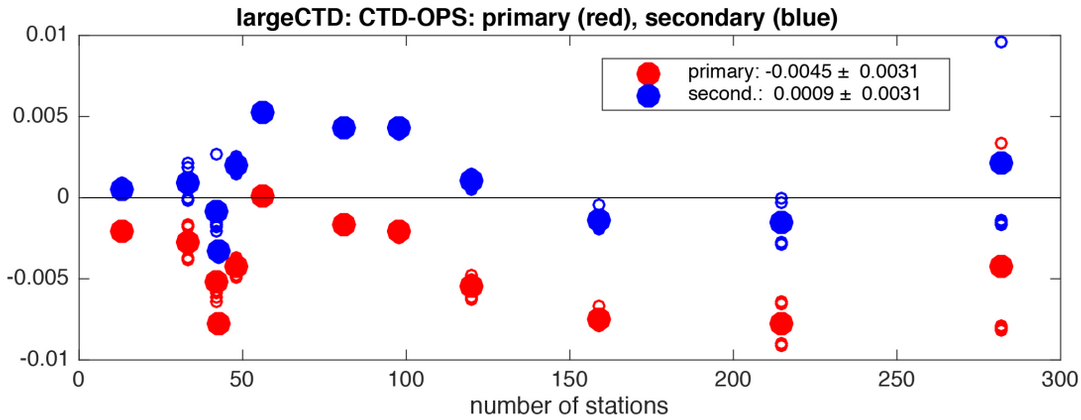

Fig. 3.4: Difference in salinity measurement (large volume CTD - salinometer) as a function of station number. Salinity derived from primary (secondary) sensors in red (blue).

Tab. 3.15: Large volume CTD/Rosette configuration through the entire cruise, except test station of 002-01

	Type	**SN and calibration date**
CTD	SBE911plus	
CTD-Sensors	SBE3 T0 (primary)	5101, cal.date 01-Dec-2015
	SBE4 C0 (primary)	3290, cal.date 22-Dec-2015
	SBE9plus pressure	0937, 20-Nov-2012
	SBE3 T1 (Secondary)	5112, cal.date 19-Dec-2015
	SBE4 C1 (secondary)	3570, cal.date 01-Dec-2015
Oxygen	SBE43	0467, cal.date 05-Dec-2015
Altimeter	Benthas PSA916	51533, until 055-01
	Benthas PSA916	1229, cal.date 01-Jan-2010 from 056-02
Transmissometer	WETLabs C-Star	1220, cal.date 02-Apr-2009
Fluorometer	WETLabs ECO-AFL/ FL	1853, cal.date 26-May-2010
Rosette	SBE Carousel	22 bottles á 24L
Winch	EL 32	

Tab. 3.16: Clean CTD/Rosette configuration through the entire cruise. Altimeter and NMEA were sometimes out of order. For detail see text and Tab. 3.17

	Type	**SN and calibration date**
CTD		
CTD-Sensors	Temperature (primary)	5562, 07-Apr-2016
	Conductivity (primary)	4064, 07-Apr-2016
	Pressure	1086, 11-Apr-2016
	Temperature (secondary)	5661, 07-Apr-2016
	Conductivity (secondary)	4084, 07-Apr-2016
Oxygen	SBE 43 (primary)	2336, 20-Apr-2016

	Type	SN and calibration date
	SBE 43 (secondary)	53899, 30-Apr-2016
Altimeter		1520, 30-Apr-2016
Transmissometer	WETLab C-Star	2337, N/A
Aux. Sensor		
Rosette	SBE Carousel	24 bottles
Winch		

Tab. 3.17: Clean CTD stations

	Date	Station-cast	Latitude	Longitude	Depth [m]	CTD	Salinity	NMEA	Alti-meter
1	20/07	002-2	75° 06.89' N	008° 36.16' E	2666	X		X	/
2	21/07	013-1	77° 29.94' N	009° 16.62' E	1965	X		X	/
3	21/07	013-3	77° 29.83' N	009° 17.09' E	1967	X		X	/
5	22/07	015-1	79° 00.07' N	008° 19.70' E	793	X		X	/
6	24/07	021-1	79° 00.02' N	007° 29.90' E	1224	X			/
7	24/07	028-1	78° 59.16' N	006° 59.66' E	1200	X			/
8	25/07	033-1	78° 49.16' N	004° 59.84' E	2688	X		X	/
9	26/07	037-1	78° 50.00' N	003° 30.15' E	2301	X	X	X	/
10	27/07	042-1	78° 50.02' N	000° 53.96' W	2601	X		X	/
11	28/07	044-1	78° 49.83' N	001° 05.67' E	2475	X		X	/
12	30/07	050-1	80° 42.83' N	000° 07.68' W	3204	X		X	/
13	30/07	052-1	80° 45.67' N	000° 07.66' E	3159	X		X	/
14	31/07	052-5	80° 42.08' N	000° 09.97' E	3208	X		X	/
15	31/07	053-2	80° 51.19' N	000° 12.35' W	3171	X		X	/
16	01/08	056-1	80° 19.55' N	004° 00.56' W	2544	X	X	X	/
17	03/08	074-1	80° 13.11' N	008° 08.66' W	283	X		X	/
18	04/08	082-1	80° 26.90' N	013° 11.65' W	290	X		X	/
19	05/08	090-1	78° 49.85' N	011° 59.71' W	202	X		X	/
20	06/08	094-1	78° 40.67' N	007° 56.90' W	170	X		X	/
21	07/08	101-1	78° 48.26' N	003° 30.59' W	2222	X	X	X	/
22	08/08	102-1	78° 51.22' N	002° 34.01' W	2577	X		X	
23	08/08	103-2	78° 49.32' N	002° 02.51' W	2668	X		X	
24	13/08	135-1	76° 48.09' N	008° 36.88' W	351	X		X	
25	16/08	165-1	77° 52.00' N	014° 48.06' W	466	X		X	X
26	19/08	189-1	79° 11.73' N	017° 06.30' W	398	X		X	X
27	21/08	202-1	79° 17.24' N	018° 05.87' W	362	X		X	X
28	22/08	214-1	79° 32.97' N	018° 41.29' W	425	X		X	X
29	23/08	241-1	79° 34.13' N	019° 31.08' W	469	X	X	X	X
30	27/08	262-1	79° 38.30' N	016° 39.36' W	237	X		X	X
31	29/08	274-2	80° 08.96' N	017° 22.85' W	178	X		X	X
32	30/08	280-1	79° 35.34' N	004° 46.31' W	1336	X		X	X
33	01/09	288-1	78° 49.71' N	004° 11.31' W	1743	X		X	X
34	02/09	290-1	77° 49.98' N	000° 00.14' W	3049	X		X	X

Tab. 3.18: Clean CTD salinometer results. Suspicious salinity reading are marked with asterisk

Date	Station	cast	depth	OSA	standardi-zation	Remarks
26.07	37	01	2000	34.9157	2016-07-30 11:25	
26.07	37	01	2000	34.9154		
26.07	37	01	1500	34.9157		
26.07	37	01	1500	34.9166		
26.07	37	01	1250	34.9129		
26.07	37	01	1250	34.9133		
01.08	56	01	2430	34.9255	2016-08-07 11:09	Measured 1.5 days after the pressure release of salinity bottles.
01.08	56	01	2430	34.9261		
01.08	56	01	1750	34.9230		
01.08	56	01	1750	34.9166		
01.08	56	01	1500	34.9156		
01.08	56	01	1500	34.9166		
07.08	101	01	2130	34.9218*	2016-08-12 11:17	OSA reading is lower than expected.
07.08	101	01	2130	34.9216*		
07.08	101	01	1750	34.9147*		
07.08	101	01	1750	34.9152*		
07.08	101	01	1250	34.9077*		
07.08	101	01	1250	34.9078*		
23.08	241	01	464	34.8011*	2016-08-29 14:57	Sample from shallow depth, and reading value differs from CTD values.
23.08	241	01	464	34.8010*		
23.08	241	01	440	34.7761*		
23.08	241	01	440	34.7760*		
23.08	241	01	350	34.6672*		
23.08	241	01	350	34.6681*		

Tab. 3.19: Large volume CTD salinometer results. Suspicious salinity reading are marked with asterisk

Date	Station	cast	depth	OSA	standardization [UTC]	Remarks
21.07	13	02	1800	34.9132	2016-07-30 11:25	
21.07	13	02	1800	34.9127		
21.07	13	02	1200	34.0108		
25.07	33	02	2630	34.9243	2016-07-28 11:40	
25.07	33	02	2580	34.9227		
25.07	33	02	2000	34.9161		
25.07	33	02	1500	34.9158		
25.07	33	02	1000	34.9161		

Date	Station	cast	depth	OSA	standardization [UTC]	Remarks
27.07	42	02	2589	34.9235	2016-08-04 11:05	Measured 2.5 days after the pressure release of salinity bottles.
27.07	42	02	2589	34.9273		
27.07	42	02	2500	34.9240		
27.07	42	02	2500	34.9241		
27.07	42	02	1500	34.9186		
27.07	42	02	1500	34.9189		
28.07	43	01	1200	34.9184		
28.07	43	01	1200	34.9182		
28.07	43	01	1000	34.9127		
28.07	43	01	1000	34.9132		
29.07	48	01	2990	34.9287	2016-08-07 11:09	Measured 1.5 days after the pressure release of salinity bottles.
29.07	48	01	2900	34.9288		
29.07	48	01	1500	34.9188		
29.07	48	01	1500	34.9189		
01.08	56	02	2505	34.9240*	2016-08-12 11:17	OSA reading is lower than expected.
01.08	56	02	2505	34.9239*		
01.08	56	02	1750	34.9190*		
01.08	56	02	1750	34.9191*		
04.08	81	01	267	34.7788*		
04.08	81	01	267	34.7790*		
07.08	98	01	1830	34.9213*		
07.08	98	01	1830	34.9217*		
07.08	98	01	1500	34.9153*		
07.08	98	01	1500	34.9154*		
11.08	120	01	2296	34.9196	2016-08-16 13:58	
11.08	120	01	2296	34.9198		
11.08	120	01	2000	34.9173		
11.08	120	01	2000	34.9173		
11.08	120	01	1000	34.9162		
11.08	120	01	1000	34.9160		
15.08	159	01	431	34.9415	2016-08-25 03:07	Pressure release for 10 hours, instead of 1 hour.
15.08	159	01	431	34.9424		
15.08	159	01	400	34.9413		
15.08	159	01	400	34.9414		
22.08	215	01	443	34.9286		
22.08	215	01	443	34.9285		
22.08	215	01	400	34.9237		
22.08	215	01	400	34.9238		
22.08	215	01	350	34.9072		
22.08	215	01	350	34.9074		

Date	Station	cast	depth	OSA	standardization [UTC]	Remarks
30.08	282	01	2000	34.9137	2016-09-02 17:30	
30.08	282	01	2000	34.9137		
30.08	282	01	1500	34.9140		
30.08	282	01	1500	34.9141		
30.08	282	01	1000	34.8908		
30.08	282	01	1000	34.8909		

At station 82_02, the CTD was brought onto deck with bottle #9 not closed, despite firing signal. On first inspection the hook was a little stuck in the gate and not as freely movable as usual. In the following cast, bottle #9 was tested again, but came back on deck again with the open bottle, but unfortunately snapped on deck. Thus, the firing-signal is correctly transmitted to the CTD, but the hook is stuck in the gate and could fire any time after sending the release command.

The carousel was inspected further. The hook appeared to have a small section where it had widened. This part is located on the bottom part of the hook (thus facing upwards, when the hook is flipped open). The situation worsened in such a way, that the hook didn't fit into the gate anymore. As a result, bottle #9 was taken out for the time being. To solve the problem, the overarching titanium of the hook was fined down by the welder. After this, the hook could move freely again and all bottles could be applied in the following CTD casts.

At station 178_01 and 179_01 bottle #6 and #8, respectively did not fire. On first analysis the problem seems to be similar as with bottle #9. Thus the bottles were taken out one after the other.

The hypothesis as to how the hooks widen is as follows: After each CTD cast the cable with the large metal bolt, connecting the CTD to the winch cable is lowered onto the CTD. There, the bolt lands on the opened hooks, thus landing on the upward facing lower ends of the hooks. This impact might cause an initial scratch which could worsen over time. Another hypothesis is, that the metal ring on top of the carousel, which was removed after the CTD got caught in the mooring (causing it to be strongly bent afterwards), was there to protect the carousel from the impact of the cable lowering.

During the following CTD casts a wooden piece was always put onto the CTD frame when lowering the cable onto the carousel to prevent the metal block from hitting the hooks. At station 216_01 bottle #3 did not close. The hook wasn't even released, so that the cause for that problem seems different than previously. On the next casts bottle #3 closed normally again.

Lowered ADCP

Two 300kHz RDI Workhorse ADCPs were mounted on the large volume rosette to act as lowered ADCPs. Since the large volume rosette had been supplied by NIOZ only for PS100, the mounting could only take place during the cruise. Given other tasks at the beginning of the cruise, this was only accomplished after station PS100_041. The LADCP system belongs to AWI and consists of the two 300kHz ADCPs, a battery container, and a custom built logger. The logger is a development of SubCTech in collaboration with AWI. It contains an inertial navigation system with the goal to provide direction information for the orientation of the CTD rosette with the ADCPs that is independent of the Earth's magnetic field. Before and after each CTD cast, the absolute direction of the rosette is obtained from the ship's GPS and the

INS then integrates that direction at each time step. As part of this development effort it was also planned that the logger housing would contain a pressure sensor and a microprocessor that stores all the data obtained by the INS, the pressure sensor, the ADCPs, and the ship's GPS. It was also intended to simplify the communication with the LADCPs, which usually is accomplished via serial communication to a laptop. Since the system had been developed just in time to be delivered to *Polarstern* for PS100, there were a number of issues that produced problems in the handling. Therefore, the INS data was only stored during PS100, but not analyzed.

Table 3.20 documents the CTD casts during which LADCP data was collected. The Master (downward) and Slave (upward) ADCP data files do not have unique names, but are only unique in the combination between name of the folder in which the data is stored and file name in the respective folder. Due to a programming error, the internal real time clock of the logger was reset by the ship's GPS. However, the time (UTC) was always correct while the date was set incorrectly and delayed by one day at a time. This could happen multiple times such that the date of the real time clock was off by several days. The date offset was always such that the actual date (e.g. August 22, 2016) was later than what the real time clock was set to (e.g. August 20, 2016). This date offset is documented for each CTD cast in Table 3.20. The problem causing this date offset was then fixed after station PS100_124. The data collected by the logger (GPS and INS data) was saved in individual folders with the folder name structure according to YYMMDDXX where YY=year, MM=month, DD=day, XX=incrementally counted casts on that date (where the date of the real time clock is used that was wrong at times). The internal memory of the ADCPs was full after station PS100_095, but this was only detected later. Therefore the ADCPs did not record data during stations PS100_096 to S100_106. Then the internal memory was emptied and the ADCPs collected data until the end of the cruise. Sometimes the ADCPs were not turned off during consecutive CTD casts such that the respective ADCP data files contain data from two CTD casts.

In the beginning of the cruise, the settings documented in Tables 3.21 and 3.22 were used. These settings are similar to what is used at University of Bremen. Specifically, they use a bin size of 4 m, a maximum range of 108 m, instrument coordinates, blanking time after transmission, broad band processing, and a timing of the master and slave that sends out the acoustic energy of both instruments in close temporal proximity to each other. Since the results in the deep Fram Strait with these settings were bad, the command files were changed on August 14, 2016 to the settings documented in Tables 3.23 and 3.24. These settings are similar to what is used at GEOMAR and WHOI. Specifically, they use a bin size of 10 m, a maximum range of 250 m, beam coordinates, no blanking after transmission, narrow band processing, and a timing of the master and slave such that the acoustic energy of the master is separated by 0.5 seconds from the acoustic energy of the slave.

Onboard data processing was carried out with the processing package LDEO_IX_11. The LADCP data collected in water depths shallower than ~800 m was good. It agreed with and supported the scientific knowledge of the respective region. However, in greater water depths, the inversion often failed and the oceanic velocities could not properly be determined. This is likely due to low concentrations of acoustic scatterers in the high latitude ocean and/or the proximity to the magnetic pole.

Tab. 3.20: Overview of the stations and data files collected by the LADCP. The LADCP data is stored in separate folders depending on when during the cruise it was taken and the files are not strictly incrementally numbered. The logger data is stored in separate folders and has led to date offsets in the LADCP data as listed.

CTD cast	LADCP folder	Master file	Slave file	Date offset	Logger folder	Comment
PS100_042_02	Aug09	64	62	0	16072704	from here on beams 1 are aligned with each other
PS100_043_01	Aug09	67	65	0	16072802	
PS100_044_02	Aug09	68	66	0	16072803	
PS100_044_04	Aug09	71	69	0	16072806	
PS100_046_01	Aug09		70	0	16072901	Master did not record
PS100_048_01	Aug09	73	75	0	16072907	from here on beams 3 are aligned with each other
PS100_049_01	Aug09	74	76	0	16073001	
PS100_052_02	Aug09	75	77	0	16073002	
PS100_052_04	Aug09	76	78	0	16073101	
PS100_054_01	Aug09	78	80	0	16073103	
PS100_055_01	Aug09	79	81	0	16080101	
PS100_056_02	Aug09	80	82	0	16080102	LADCP battery changed after this cast
PS100_056_05	Aug09	86	88	0	16080108	
PS100_057_01	Aug09	87	89	0	16080109	
PS100_058_01	Aug09	88	90	0	16080201	
PS100_059_01	Aug09	89	91	0	16080202	
PS100_060_01	Aug09	90	92	0	16080203	from here on ship GPS
PS100_061_01	Aug09	91	93	0	16080204	
PS100_062_01	Aug09	92	94	0	16080205	
PS100_063_01	Aug09	94	96	0	16080207	processing fails in getinv.m line 669
PS100_064_01	Aug09	95	97	0	16080208	
PS100_065_01	Aug09	96	98	0	16080209	
PS100_066_01	Aug09	97	99	0	16080210	
PS100_067_01	Aug09	98	100	1	16080211	Logger GPS reset RTC date by 1 day
PS100_068_01	Aug09	99	101	1	16080212	
PS100_069_01	Aug09	101	103	1	16080214	
PS100_070_01	Aug09	102	104	1	16080215	
PS100_072_01	Aug09	103	105	1	16080216	
PS100_075_01	Aug09	104	106	1	16080217	
PS100_076_01	Aug09	105	107	1	16080301	
PS100_077_01	Aug09	106	108	1	16080302	
PS100_078_01	Aug09	107	109	1	16080303	

CTD cast	LADCP folder	Master file	Slave file	Date offset	Logger folder	Comment
PS100_079_01	Aug09	108	110	1	16080306	from here on alignment blocks on floorboard in place
PS100_080_01	Aug09	109	111	1	16080307	
PS100_081_01	Aug09	110	112	1	16080308	RTC date manually reset after this cast
PS100_082_02	Aug09	111	113	0	16080401	
PS100_083_01	Aug09	112	114	1	16080402	Logger GPS reset RTC date by 1 day
PS100_084_01	Aug09	113	115	1	16080403	
PS100_085_01	Aug09	114	116	1	16080404	
PS100_086_01	Aug09	115	117	1	16080405	
PS100_087_01	Aug09	116	118	1	16080406	
PS100_088_01	Aug09	117	119	1	16080407	
PS100_089_01	Aug09	118	120	1	16080408	
PS100_090_02	Aug09	119	121	1	16080409	
PS100_091_01	Aug09	120	122	2	16080410	Logger GPS reset RTC date by 1 day
PS100_092_01	Aug09	121	123	2	16080411	
PS100_093_01	Aug09	123	125	2	16080413	
PS100_094_02	Aug09	124	126	2	16080414	
PS100_095_01	Aug09	125	127	2	16080415	
PS100_096_01	n/a			2	16080416	LADCP did not record as recorder was full
PS100_097_01	n/a			2	16080417	
PS100_098_01	n/a			3	16080418	Logger GPS reset RTC date by 1 day
PS100_101_02	n/a			3	16080419	
PS100_101_04	n/a			4	16080420	Logger GPS reset RTC date by 1 day
PS100_102_02	n/a			4	16080421	
PS100_103_03	n/a			4	16080422	
PS100_103_05	n/a			5	16080423	Logger GPS reset RTC date by 1 day
PS100_105_01	n/a			5	16080424	
PS100_106_02	n/a			5	16080425	LADCP recorder emptied after this cast
PS100_109_01	Aug11	0	0	0	16081001	RTC date manually reset before this cast
PS100_110_01	Aug11	1	1	0	16081002	
PS100_111_01	Aug11	2	2	0	16081003	
PS100_112_01	Aug11	3	3	1	16081004	Logger GPS reset RTC date by 1 day
PS100_113_01	Aug11	4	4	1	16081005	
PS100_114_01	Aug11	5	5	1	16081006	

CTD cast	LADCP folder	Master file	Slave file	Date offset	Logger folder	Comment
PS100_115_01	Aug11	6	6	1	16081007	
PS100_116_01	Aug11	7	7	1	16081008	
PS100_117_01	Aug11	8	8	1	16081009	
PS100_118_01	Aug11	9	9	1	16081010	
PS100_119_01	Aug11	10	10	1	16081011	RTC date manually reset after this cast
PS100_120_01	Aug11	11	11	0	16081101	
PS100_124_01	Aug13	0	0	1	16081102	GPZDA problem fixed after this cast
PS100_130_01	Aug13	2	2	0	16081202	from here on RTC date correct
PS100_131_01	Aug13	3	3	0	16081203	
PS100_132_01	Aug13	4	4	0	16081204	
PS100_133_01	Aug13	5	5	0	16081205	
PS100_134_01	Aug13	6	6	0	16081206	
PS100_135_02	Aug13	7	7	0	16081301	
PS100_136_01	Aug13	8	8	0	16081302	
PS100_137_01	Aug13	9	9	0	16081303	
PS100_138_01	Aug13	10	10	0	16081304	
PS100_139_01	Aug13	11	11	0	16081305	
PS100_140_01	Aug13	12	12	0	16081306	
PS100_141_01	Aug13	13	13	0	16081307	
PS100_150_01	Aug20	5	5	0	16081501	from here on new command files
PS100_151_01	Aug20	6	6	0	16081502	processing fails in getinv.m line 669
PS100_152_01	Aug20	7	7	0	16081503	
PS100_153_01	Aug20	8	8	0	16081504	
PS100_159_01	Aug20	9	9	0	16081505	
PS100_160_01	Aug20	10	10	0	16081601	
PS100_161_01	Aug20	11	11	0	16081602	
PS100_162_01	Aug20	12	12	0	16081603	
PS100_165_02	Aug20	13	13	0	16081604	
PS100_166_01	Aug20	14	14	0	16081605	
PS100_167_01	Aug20	15	15	0	16081606	
PS100_168_01	Aug20	16	16	0	16081607	
PS100_170_01	Aug20	17	17	0	16081701	LADCP not turned off after cast; ran for 23 hours
PS100_178_01	Aug20	18	18	0	16081801	
PS100_179_01	Aug20	19	19	0	16081802	
PS100_180_01	Aug20	20	20	0	16081803	
PS100_183_02	Aug20	21	21	0	16081804	
PS100_186_01	Aug20	22	22	0	16081901	

CTD cast	LADCP folder	Master file	Slave file	Date offset	Logger folder	Comment
PS100_187_01	Aug20	23	23	0	16081902	
PS100_188_01	Aug20	24	24	0	16081903	
PS100_189_02	Aug20	26	26	0	16081905	
PS100_190_01	Aug20	27	27	0	16081906	
PS100_191_01	Aug20	28	28	0	16081907	
PS100_192_01	Aug20	29	29	0	16082001	
PS100_193_01	Aug20	31	31	0	16082003	31 contains data from two CTD casts: 193 and 194
PS100_194_01	Aug20	31	31	0	16082003	processing fails in getinv.m line 669
PS100_195_01	Aug20	32	32	0	16082004	
PS100_196_01	Aug20	33	33	0	16082005	
PS100_197_01	Aug20	34	34	0	16082006	
PS100_200_01	Aug23	1	1	0	16082007	
PS100_201_01	Aug23	2	2	0	16082008	
PS100_202_02	Aug23	3	3	0	16082101	
PS100_203_01	Aug23	4	4	0	16082102	processing fails in getinv.m line 669
PS100_204_01	Aug23	5	5	0	16082103	
PS100_205_01	Aug23	6	6	0	16082104	
PS100_211_01	Aug23	7	7	0	16082105	
PS100_212_01	Aug23	8	8	0	16082106	
PS100_213_01	Aug23	9	9	0	16082107	
PS100_214_02	Aug23	10	10	0	16082108	
PS100_215_01	Aug23	11	11	0	16082201	
PS100_216_01	Aug23	12	12	0	16082202	
PS100_217_01	Aug23	13	13	0	16082203	
PS100_219_01	Aug23	14	14	0	16082204	
PS100_220_01	Aug23	15	15	0	16082205	
PS100_221_01	Aug23	16	16	0	16082206	
PS100_222_01	Aug23	17	17	0	16082207	
PS100_223_01	Aug23	18	18	0	16082208	
PS100_224_01	Aug23	19	19	0	16082209	
PS100_225_01	Aug23	20	20	0	16082210	
PS100_226_01	Aug23	21	21	0	16082211	
PS100_227_01	Aug23	22	22	0	16082212	
PS100_228_01	Aug23	23	23	0	16082301	
PS100_229_01	Aug23	24	24	0	16082302	
PS100_230_01	Aug23	25	25	0	16082303	
PS100_231_01	Aug23	26	26	0	16082304	
PS100_232_01	Aug23	27	27	0	16082305	battery empty; LADCPs finished cast; logger terminated early

CTD cast	LADCP folder	Master file	Slave file	Date offset	Logger folder	Comment
PS100_233_01	Aug23	30	29	0	16082310	LADCP battery changed before this cast
PS100_234_01	Aug23	31	30	0	16082311	
PS100_235_01	Aug23	32	31	0	16082312	
PS100_236_01	Aug23	33	32	0	16082313	
PS100_237_01	Aug23	34	33	0	16082314	
PS100_241_02	Aug26	0	0	0	16082315	
PS100_250_01	Aug26	1	1	0	16082501	
PS100_251_01	Aug26	2	2	0	16082502	
PS100_252_01	Aug26	3	3	0	16082503	
PS100_253_01	Aug26	4	4	0	16082504	
PS100_254_01	Aug26	5	5	0	16082505	
PS100_255_01	Aug27	6	6	0	16082601	
PS100_259_01	Aug27	7	7	0	16082701	7 contains data from two CTD casts: 259 and 260
PS100_260_01	Aug27	7	7	0	16082701	
PS100_261_01	Aug27	8	8	0	16082702	
PS100_262_02	Aug27	9	9	0	16082703	
PS100_263_01	Aug27	10	10	0	16082704	
PS100_264_01	Aug27	11	11	0	16082705	
PS100_265_01	Aug27	13	13	0	16082707	
PS100_266_01	Aug27	14	14	0	16082708	removed super-ensembles 7-10, 20-21 in processing
PS100_267_01	Aug29	0	0	0	16082709	0 contains data from two CTD casts: 267 and 268
PS100_268_01	Aug29	0	0	0	16082709	
PS100_274_03	Aug29	1	1	0	16082901	
PS100_277_01	Aug31	0	0	0	16083001	
PS100_278_01	Aug31	1	1	0	16083002	
PS100_279_01	Aug31	2	2	0	16083003	
PS100_280_02	Aug31	3	3	0	16083004	
PS100_281_01	Aug31	4	4	0	16083005	
PS100_282_01	Aug31	5	5	0	16083006	
PS100_283_01	Aug31	6	6	0	16083101	
PS100_285_01	Sep02	0	0	0	16083102	
PS100_285_03	Sep02	1	1	0	16090101	
PS100_288_02	Sep02	2	2	0	16090102	
PS100_290_02	Sep02	3	3	0	16090201	

Tab. 3.21: Start protocol of the Master LADCP used until August 14, 2016.

CR1
WM15
CB411
RN MASTE
LZ030,220
CF11111
EA0
EB0
ED0
ES35
EX01011
EZ1111101
WB0
WD111100000
WF176
WN27
WP1
WS400
WV175
SM1
SA001
SI0
SW75
TE00:00:01.00
TP00:01.00
CK
CS

Tab. 3.22: Start protocol of the Slave LADCP used until August 14, 2016

CR1
WM15
CB411
RN SLAVE
LZ030,220
CF11111
EA0
EB0
ED0
ES35
EX01011
EZ1111101

WB0
WD111100000
WF176
WN27
WP1
WS400
WV175
SM2
SA001
SI0
ST0300
TE00:00:01.00
TP00:01.00
CK
CS

Tab. 3.23: Start protocol of the Master LADCP used from August 14, 2016 onwards

CR1	;	Set to factory defaults
WM15	;	LADCP water ping mode 15
CB411	;	Baud rate 9600
RN MASTE	;	File name
CF11111	;	Allow serial output
EA0	;	No heading alignment
EB0	;	No heading bias
ES35	;	Salinity
EZ0111101	;	Fixed speed of sound
EX00111	;	Beam coordinates, use pitch/roll, 3 beam solution, bin mapping
WV250	;	Ambiguity velocity
WN25	;	25 bins
WS1000	;	10 m bins
WF0	;	No blank after transmit
WB1	;	Narrow band
WP1	;	Single ping data
TE00:00:01.50	;	Ensemble length of 1.5 seconds
TP00:00.90	;	Ping length of 0.9 seconds
SM1	;	Master, SM2 for Slave
SI0	;	Sync pulse on every ping, n/a for Slave, but needs ST0300
SA011	;	Sync pulse before every ensemble
SW5500	;	Wait 0.55 seconds which is 550.0 milliseconds, n/a for Slave
SB0	;	Ignore RS-422 break
CK	;	Keep parameters as user default
CS	;	Start pinging

Tab. 3.24: Start protocol of the Slave LADCP used from August 14, 2016 onwards.

CR1	;	Set to factory defaults
WM15	;	LADCP water ping mode 15
CB411	;	Baud rate 9600
RN SLAVE	;	File name
CF11111	;	Allow serial output
EA0	;	No heading alignment
EB0	;	No heading bias
ES35	;	Salinity
EZ0111101	;	Fixed speed of sound
EX00111	;	Beam coordinates, use pitch/roll, 3 beam solution, bin mapping
WV250	;	Ambiguity velocity
WN25	;	25 bins
WS1000	;	10 m bins
WF0	;	No blank after transmit
WB1	;	Narrow band
WP1	;	Single ping data
TE00:00:01.50	;	Ensemble length of 1.5 seconds
TP00:00.90	;	Ping length of 0.9 seconds
SM2	;	Slave, SM1 for Master
ST0300	;	Slave timeout 300 seconds, n/a for Master, but needs SI0
SA011	;	Sync pulse before every ensemble
SB0	;	Ignore RS-422 break
CK	;	Keep parameters as user default
CS	;	Start pinging

Vessel mounted ADCP

We measured profiles of ocean current velocity in the upper 300 m while underway with a vessel-mounted Acoustic Doppler Current Profiler (VMADCP). The RDI Ocean Surveyor instrument (150 kHz) was mounted at an angle of 45 degree in the ‘Kastenkiel’ of RV *Polarstern*. The instrument was configured in narrowband mode and set up to use 4 m bin size (configuration file cmd_OS150NB_trigger_off.txt) covering a range from 15 m to about 200 - 300 m depending

on sea state, ice conditions, ship's speed and backscatter signals. On the continental shelf, i.e. in areas shallower 500 m water depth, the configuration was changed to narrowband mode with single-ping bottom track pings (data set numbers 018 to 043, configuration file cmd_ OS150NB_BT_trigger_off.txt). We used a maximum search depth of 500 m. The ping rate was reduced from 2 s to 3 s by using the bottom track mode.

The setup of navigational input was used from the vessel’s GPS system. It worked almost flawlessly, except for some short events, when the communication from the GPS was lost. Problems to resolve velocities occurred due to low backscatters, low water depths and / or sea ice in front of the beams. Furthermore interferences with other acoustic signals from the vessel’s Doppler log (79 kHz) and especially during periods when the sediment echolot PARASOUND (18 kHz) was switched on degraded the velocity data. The multibeam echosounder HYDROSWEEP (15.5 kHz) and acoustic signals to release moorings might also affect the velocity data.

For unknown reasons the ADCP stopped recording data for several hours four times throughout the cruise:

- July 31, 22:00 UTC to August, 01 6:10 UTC (data set number 15)

- August 15, 0:30 UTC to 6:00 UTC (data set umber 32)

- August 17, 23:00 UTC to 18, August 6:00 UTC (data set number 34)

- August 28, 9:15 UTC to 11:00 UTC (data set number 41).

The software VmDas (Teledyne RD Instruments) was used to set the ADCP's operating parameters and to record the data. Finally the Ocean Surveyor data conversion was done using Matlab routines last changed by Gerd Krahmann in January 2015 (osheader.m, osdatasip.m, osrefine.m, osbottom.m). Hereby the VMADCP data was corrected by using a misalignment angle of 1.12° and an amplitude factor of 1.0171.

Tab. 3.25: VMADCP command file cmd_OS150NB_trigger_off.txt

```
;---------------------------------------------------------------------\

; ADCP Command File for use with VmDas software.

;

; ADCP type:     150 Khz Ocean Surveyor
; Setup name:    for Polarstern in 6/2014
; Setup type:    Low resolution, long range profile (Narrowband)
;
; NOTE:  Any line beginning with a semicolon in the first
;        column is treated as a comment and is ignored by
;        the VmDas software.
;
; NOTE:  This file is best viewed with a fixed-point font (e.g. courier).
; Modified Last: 12Jun2014
;---------------------------------------------------------------------/

; Restore factory default settings in the ADCP
cr1
```

```
; set the data collection baud rate to 115200 bps,
; no parity, one stop bit, 8 data bits
; NOTE:  VmDas sends baud rate change command after all other commands in
; this file, so that it is not made permanent by a CK command.
cb611

; Set for narrowband single-ping profile mode (NP), 100 (NN) 4 meter bins (NS),
; 2 meter blanking distance (NF), 390 cm/s ambiguity vel (WV)
WP000
NP001
NN080
NS0400
NF0400
;WV390

; Disable single-ping bottom track (BP),
; Set maximum bottom search depth to 1200 meters (BX)
BP000
;BX05000

; output velocity, correlation, echo intensity, percent good
ND111100000

; Ping as fast as possible
TP000000

; Since VmDas uses manual pinging, TE is ignored by the ADCP
; and should not be set.
;TE0000000

; Set to calculate speed-of-sound, no depth sensor, external synchro heading
; sensor,  pitch or roll being used, no salinity sensor, use internal transducer
; temperature sensor
EZ1011101

; Output beam data (rotations are done in software)
EX00000

; Set transducer misalignment (hundredths of degrees).
; Ignored here but set in VmDAS options.
;EA00000
; Set transducer depth (decimeters)
ED00110
```

```
; Set Salinity (ppt)
ES35
;set external triggering and output trigger; no trigger
CX0,0

; save this setup to non-volatile memory in the ADCP
CK
```

Tab. 3.26: VMADCP command file cmd_OS150NB_BT_trigger_off.txt

```
;------------------------------------------------------------------------\
; ADCP Command File for use with VmDas software.
;
; ADCP type:     150 Khz Ocean Surveyor
; Setup name:    for Polarstern in 6/2014
; Setup type:    Low resolution, long range profile (Narrowband)
;
; NOTE:  Any line beginning with a semicolon in the first
;        column is treated as a comment and is ignored by
;        the VmDas software.
;
; NOTE:  This file is best viewed with a fixed-point font (e.g. courier).
; Modified Last: 12Jun2014
;------------------------------------------------------------------------/
; Restore factory default settings in the ADCP
cr1
; set the data collection baud rate to 115200 bps,
; no parity, one stop bit, 8 data bits
; NOTE:  VmDas sends baud rate change command after all other commands in
; this file, so that it is not made permanent by a CK command.
cb611
; Set for narrowband single-ping profile mode (NP), 100 (NN) 4 meter bins (NS),
; 2 meter blanking distance (NF), 390 cm/s ambiguity vel (WV)
WP000
NP001
NN080
NS0400
NF0400
;WV390

; Disable single-ping bottom track (BP),
; Set maximum bottom search depth to 1200 meters (BX)
BP001
BX05000
```

```
; output velocity, correlation, echo intensity, percent good
ND111100000

; Ping as fast as possible
TP000000

; Since VmDas uses manual pinging, TE is ignored by the ADCP
; and should not be set.
;TE0000000

; Set to calculate speed-of-sound, no depth sensor, external synchro heading
; sensor,  pitch or roll being used, no salinity sensor, use internal transducer
; temperature sensor
EZ1011101

; Output beam data (rotations are done in software)
EX00000

; Set transducer misalignment (hundredths of degrees).
; Ignored here but set in VmDAS options.
;EA00000

; Set transducer depth (decimeters)
ED00110

; Set Salinity (ppt)
ES35

;set external triggering and output trigger; no trigger
CX0,0
; save this setup to non-volatile memory in the ADCP
CK
```

Temperature-depth logger

The RBRduet 3.01 serial number 85201 pressure and temperature logger by RBR is rated to more 1700 m depth and powered by a single AA lithium battery. It was set to record at 16Hz to the internal memory. Setting the instrument to 16Hz recording is not possible with the RBR software, but this setting remained active nonetheless. The time of the sensor was set to UTC via the time setting of a used laptop.

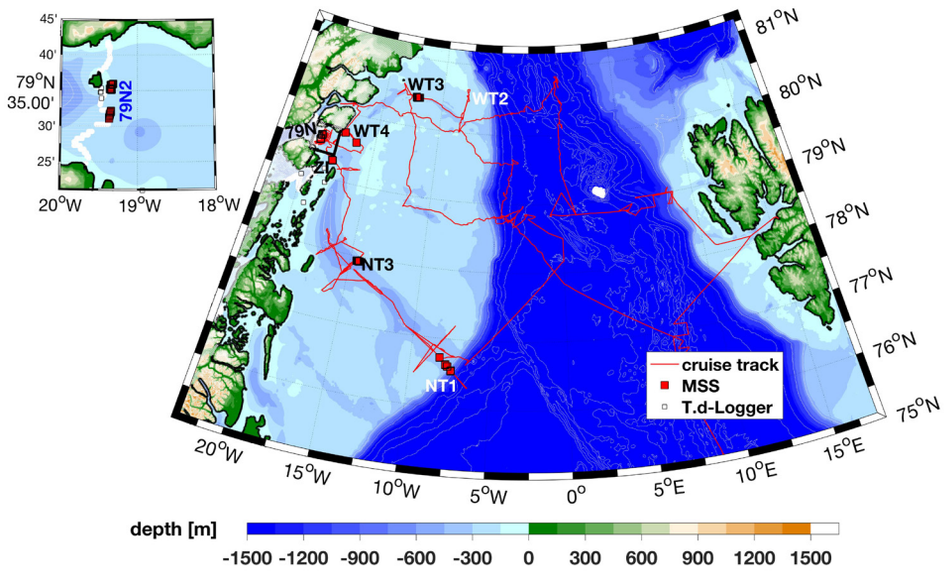

Fig. 3.5: Map of the temperature-depth logger and the microstructure sonde stations during PS100

This RBRduet was attached to a 800 m fishing line together with an electronic high seas fishing pole (Fig. 3.6) in order to achieve a system with maximum flexibility and light weight handling requirements. The system was first tested from *Polarstern* (Table 3.27), then it was tested from zodiac, and finally multiple helicopter borne deployments were carried out. During the ship and zodiac deployments, one 100g lead weight was attached to the line, while three 100g lead weights (total weight of 300g) were attached during the helicopter borne deployments. A target downcast speed of 1m/s was hard to achieve, as the brake of the fishing pole was hard to adjust manually. A target constant upcast speed of 1m/s was achieved more easily as the motor speed can be set digitally. The fishing pole's electrical motor was powered by rechargeable batteries located in a water-tight box.

The instrument was started at least an hour before each cast such that the deployment in the field get underway right away after arriving on station. The data was read out within minutes after the end of a cast to check the data quality. In all cases was it deemed good. Significant differences were detected between the wire out readings of the fishing pole and the depth calculated from the pressure sensor. The wire out reading was up to 10% smaller than the depth calculated from the pressure sensor. The time when the weights had reached the bottom could be clearly detected as the tension on the fishing line vanished. This was confirmed from the pressure time series which showed constant values near the bottom for at least a minute in each case. During the testing phase, the maximum pressure readings (when the system was on the bottom) were compared with *Polarstern's* hydrosweep multibeam system as well as with zodiac's fishfinder echosounder. The agreement was good to within meters. During the deep helicopter borne casts, the weights also hit very fine grained and sticky mud on the ground. After being brought back to the surface, the lower side of the lead weights was still covered in mud (Fig. 3.6c). Pressure time series showed constant value near bottom for at least a minute in each case.

During the field deployments, a Panasonic toughbook was also brought along. It contains an internal GPS and dumps that data to a com-port. This data was captured with putty.exe. Hence, the position versus time was also logged during the casts. Upon landing of the helicopter, the position of the helicopter's GPS was also recorded manually.

With this setup, five stations in the ice covered area in front of Zachariæ Isstrøm were occupied which could not be reached by *Polarstern*. There was first and multi year sea-ice which was partially land fast and in the process of breaking up in addition to an ice mélange right in front of the glacier. From the helicopter reasonably intact sea-ice floes were selected that had open water or <5cm thick new ice next to them. The helicopter was landed on the ice floe. The operators were connected to the helicopter by a rope and then walked to the side of the ice floe. If necessary, the new ice was broken with a metal pole. Then the logger was deployed with the fishing line from the side of the floe (Fig. 3.6b). For the deep stations, the majority of the time was spent on the down- and upcasts and a typical station time between landing of the helicopter and subsequent take off was about an hour.

Fig. 3.6: Examples of usage of temperature-depth logger in the field. (a) Deployment from the zodiac. (b) Deployment from the side of an ice-floe. (c) After a deployment from the side of an ice-floe. The muddy lead weights are visible on the snow.

Tab. 3.27: Stations where the temperature-depth logger was deployed

Date/Time	Latitude	Longitude	Water depth	Platform
22-Aug-2016 12:13:00	79°33.91'N	19°27.69'W	472m	Ship
25-Aug-2016 14:20:00	79°34.74'N	19°28.76'W	263m	Zodiac
25-Aug-2016 14:35:00	79°34.79'N	19°28.19'W	76m	Zodiac
25-Aug-2016 14:50:00	79°35.33'N	19°28.00'W	28m	Zodiac
26-Aug-2016 12:49:00	79°07.76'N	18°26.81'W	566m	Heli 1

Date/Time	Latitude	Longitude	Water depth	Platform
26-Aug-2016 14:15:00	79°04.92'N	19°09.54'W	153m	Heli 1
26-Aug-2016 15:01:00	78°55.89'N	18°08.75'W	498m	Heli 1
27-Aug-2016 14:06:00	78°57.57'N	20°01.81'W	620m	Heli 2
27-Aug-2016 15:30:00	78°33.99'N	19°14.44'W	635m	Heli 2

Microstructure profiler

Microstructure measurements were carried out to estimate the strength of turbulent motion and the associated energy dissipation rates in the water column which in turn can be interpreted as an indicator for the mixing strength. The key question is to quantify the turbulent exchange of properties between the warm and salty layer of Atlantic water at depth and the cold and fresh polar water layer sitting on top.

In total, 143 profiles were measured at 12 different locations on the East-Greenland shelf and shelf break. The first and last two stations (078_04, 271_01 and 273_02) were located in the Westwind-Trough. While station 078_04 is situated in the northern part (close to WT3), the latter two stations are located in close proximity to the 79N glacier (WT4), the potential beginning of Westwind Trough. The next four stations (121_01, 122_01, 123_01 and 125_01) are located across the shelf break at the entrance of the Norske Trough (along NT1). Station 159_02 is also located in the Norske Trough but further to the west (NT3). Its position on the northern slope was chosen to potentially capture higher dissipation rates in the proximity of the northwestward flowing observed boundary current. While station 206_01 was carried out in front of the Zacharias Ice field (ZI), stations 256_01, 257_02 and 258_01 were located directly in front of the glacier front of the 79°N glacier. The bathymetric survey exposed two sills directly in front of the glacier which potentially act as barriers for the bottom inflow of warmer Atlantic water into the cavity underneath the glacier. To estimate the turbulent motion in the bottom layer on these sills, the probe was let down as close as possible to the ground without touching it.

The microstructure winch system was mounted onto *Polarstern's* starboard railing, as far away as possible from the propellers and thrusters. During the measurements, the ship slowly moved sideways to prevent the probe from moving under the ship. Most stations were carried out in polynyas, allowing for generally ice-free conditions during lowering and hoisting of the probe. However, the limited space for ship manoeuvring allowed for ice flows to come close to the cable, rarely leading to the abortion of casts, but requiring longer waiting times to reduce the stress on the cable. During cast #3 on station 273_02, the probe touched the ground, but did not seem to have caused any damage on the sensors.

The used microstructure probe is of the type MSS90L (SN: MSS063) and was equipped with a standard CTD sensor set (Pressure, Temperature, Conductivity) as well as a Turbidity sensor (SN 1433). Furthermore, the microstructure is resolved by a fast temperature sensor (SN 8006) and two high resolution current shear sensors (SHE1 and SHE2). A high noise level in the energy dissipation rate based on the shear measurements was observed throughout the voyage. As the real signal of energy dissipation are obscured by the elevated noise level, both shear sensors were replaced and exchanged numerous times. At the end of the cruise five different shear sensors were in use: C6098, C6100, C6101, C6102 and C6103, but all yielded the elevated noise level. Table 3.28 contains an overview over the used shear sensors and their position on the probe for every individual cast.

During the first cast at station 121_01 the shear sensor on position 1 (SHE1) did not function. An exchange of the shear sensor C6100 with another sensor (C6011) or sensor C6102 from position 2 (SHE2) did not change its behavior. Measurements on this station were subsequently carried out with just one shear sensor. At the end of the station, the preamplifiers from SHE1 and SHE2 were interchanged, which shifted the problem from SHE1 to SHE2 and thus pointed towards a problem regarding the preamplifier. Due to the limited time between stations and the lack of spare electronic components, the next three stations (122_01, 123_01 and 125_01) were also carried out with just one working shear sensor. Before reaching station 159_02 the preamplifier was fixed by the ship's electrician, making further measurements with two shear sensors possible. Table 3.28 contains also an overview over which preamplifier was positioned on SHE1 and SHE2, respectively. The preamplifier that was temporarily defect is indicated by a "b" while the one that continuously worked is indicated by "ok".

As the noise levels in the calculated energy dissipation rate remained high throughout all microstructure stations, the current shear sensors on SHE1 and SHE2 were interchanged for the last two casts on station 273_02. This allows for a direct comparison of the influence of the preamplifiers on the noise level in the calculated energy dissipation rate. However, the differences appear to be minor, raising confidence regarding the repaired preamplifier.

Tab. 3.28: Microstructure profile overview

Cast #	Latitude	Longitude	Depth (HS) in m	Time: Start Winch	Depth (End Lower) in dbar	Shear Sensor 1 (SN)	Shear Sensor 2 (SN)	Pre-ampli-fier 1	Pre-ampli-fier 2	Comments
Station PS100_078_04				Aug 4, 2016						
1	80° 25.77' N	012° 01.38'W	263	7:54	100	C6103	C6098	b	ok	
2	80° 25.74' N	012° 01.96'W	263	8:02	190	C6103	C6098	b	ok	
3	80° 25.71' N	012° 02.55'W	262	8:12	193	C6103	C6098	b	ok	
4	80° 25.68' N	012° 03.34'W	260	8:22	219	C6103	C6098	b	ok	
5	80° 25.65' N	012° 04.18'W	260	8:33	238	C6103	C6098	b	ok	
6	80° 25.60' N	012° 05.20'W	260	8:45	201	C6103	C6098	b	ok	
7	80° 25.54' N	012° 07.93'W	267	9:30	213	C6100	C6098	b	ok	exchanging shear sensor 1 before cast
8	80° 25.43'N	012° 11.54'W	266	10:36	213	C6100	C6102	b	ok	exchanging shear sensor 2 before cast
9	80° 25.40'N	012° 12.09'W	264	10:46	216	C6100	C6102	b	ok	
10	80° 25.41'N	012° 12.85'W	263	10:57	225	C6100	C6102	b	ok	
11	80° 25.44'N	012° 13.55'W	263	11:09	240	C6100	C6102	b	ok	
12	80° 25.44'N	012° 14.08'W	264	11:20	228	C6100	C6102	b	ok	
13	80° 25.45'N	012° 14.67'W	265	11:31	244	C6100	C6102	b	ok	
14	80° 25.48'N	012° 15.20'W	267	11:42	242	C6100	C6102	b	ok	
15	80° 25.50'N	012° 15.65'W	267	11:53	235	C6100	C6102	b	ok	
16	80° 25.52'N	012° 16.19'W	269	12:05	232	C6100	C6102	b	ok	
17	80° 25.54'N	012° 17.01'W		12:17	227	C6100	C6102	b	ok	

Cast #	Latitude	Longitude	Depth (HS) in m	Time: Start Winch	Depth (End Lower) in dbar	Shear Sensor 1 (SN)	Shear Sensor 2 (SN)	Pre-ampli-fier 1	Pre-ampli-fier 2	Comments
18	80° 25.58'N	012° 17.52'W	266	12:28	238	C6100	C6102	b	ok	
19	80° 25.65'N	012° 17.96'W	265	12:39	239	C6100	C6102	b	ok	
20	80° 25.72'N	012° 18.35'W	267	12:51	240	C6100	C6102	b	ok	
21	80° 25.80'N	012° 18.68'W	266	13:03	242	C6100	C6102	b	ok	
22	80° 25.86'N	012° 18.94'W	267	13:14	246	C6100	C6102	b	ok	
23	80° 25.95'N	012° 19.14'W	269	13:26	252	C6100	C6102	b	ok	
Station PS100_121_01				Aug 11, 2016						
1	76° 32.71' N	007° 22.41'W	782	17:41	204	C6100	C6102	b	ok	before cast: testing system shows not functioning SHE1. testing with different sensor (C6011) shows no change.
2	76° 32.46' N	007° 23.39'W	780	19:07	208	C6102	C6101	b	ok	only shear sensor 2 works
3	76° 32.33' N	007° 23.61'W	777	19:38	282	C6102	C6101	b	ok	only shear sensor 2 works
4	76° 32.26' N	007° 23.67'W	-	19:51	272	C6102	C6101	b	ok	only shear sensor 2 works
5	76° 32.22' N	007° 23.66'W	-	20:04	337	C6102	C6101	b	ok	only shear sensor 2 works
6	76° 32.17' N	007° 23.60'W	-	20:21	333	C6102	C6101	b	ok	only shear sensor 2 works
7	76° 32.12' N	007° 23.48'W	-	20:39	325	C6102	C6101	b	ok	only shear sensor 2 works
8	76° 32.05' N	007° 23.31'W	-	20:54	326	C6102	C6101	b	ok	only shear sensor 2 works after cast #8: interchanging preamplifiers from SHE1 and SHE2 transfers the problem from SHE1 to SHE2. Measuring shear only with SHE1 from now on. hypothesis that the preamplifier is defect seems to be correct

Cast #	Latitude	Longitude	Depth (HS) in m	Time: Start Winch	Depth (End Lower) in dbar	Shear Sensor 1 (SN)	Shear Sensor 2 (SN)	Pre-ampli-fier 1	Pre-ampli-fier 2	Comments
Station PS100_122_01				Aug 11, 2016						
1	76° 36.07’ N	007° 37.82’W	332	22:37	257	C6102	C6101	ok	b	only shear sensor 1 works
2	76° 35.99’ N	007° 37.62’W	334	23:00	289	C6102	C6101	ok	b	only shear sensor 1 works
3	76° 35.93’ N	007° 37.31’W	334	23:20	298	C6102	C6101	ok	b	only shear sensor 1 works
4	76° 35.92’ N	007° 37.08’W	333	23:36	289	C6102	C6101	ok	b	only shear sensor 1 works
5	76° 35.88’ N	007° 36.81’W	337	23:51	276	C6102	C6101	ok	b	only shear sensor 1 works
6	76° 35.84’ N	007° 36.56’W	338	0:04	265	C6102	C6101	ok	b	only shear sensor 1 works
Station PS100_123_01				Aug 12, 2016						
1	76° 37.77’ N	007° 45.36’W	329	1:12	261	C6102	C6101	ok	b	only shear sensor 1 works
2	76° 37.66’ N	007° 45.22’W	327	1:26	258	C6102	C6101	ok	b	only shear sensor 1 works
3	76° 37.57’ N	007° 45.07’W	324	1:38	275	C6102	C6101	ok	b	only shear sensor 1 works
4	76° 37.44’ N	007° 44.86’W	324	1:50	277	C6102	C6101	ok	b	only shear sensor 1 works
5	76° 37.32’ N	007° 44.72’W	324	2:03	285	C6102	C6101	ok	b	only shear sensor 1 works
6	76° 37.21’ N	007° 44.55’W	323	2:17	300	C6102	C6101	ok	b	only shear sensor 1 works
7	76° 37.13’ N	007° 44.41’W	329	2:31	275	C6102	C6101	ok	b	only shear sensor 1 works
8	76° 37.08’ N	007° 44.30’W	329	2:44	293	C6102	C6101	ok	b	only shear sensor 1 works
Station PS100_125_01				Aug 12, 2016						
1	76° 43.12’ N	008° 09.10’W	341	5:14	258	C6102	C6101	ok	b	only shear sensor 1 works
2	76° 43.20’ N	008° 09.12’W	341	5:26	281	C6102	C6101	ok	b	only shear sensor 1 works

Cast #	Latitude	Longitude	Depth (HS) in m	Time: Start Winch	Depth (End Lower) in dbar	Shear Sensor 1 (SN)	Shear Sensor 2 (SN)	Pre-ampli-fier 1	Pre-ampli-fier 2	Comments
3	76° 43.30' N	008° 09.10'W	340	5:39	255	C6102	C6101	ok	b	only shear sensor 1 works
4	76° 43.38' N	008° 09.08'W	339	5:50	250	C6102	C6101	ok	b	only shear sensor 1 works
5	76° 43.46' N	008° 09.02'W	338	6:02	245	C6102	C6101	ok	b	only shear sensor 1 works
6	76° 43.56' N	008° 08.97'W	339	6:14	253	C6102	C6101	ok	b	only shear sensor 1 works
Station PS100_159_02				Aug 15, 2016						
1	77° 55.87'N	14°33.61'W	442	18:34	308	C6102	C6100	ok	b	preamplifier 2 is fixed again and measurements continue with two shear sensors
2	77° 55.94'N	14°33.38'W		18:50	308	C6102	C6100	ok	b	
3	77° 56.01'N	14°32.86'W	440	19:07	308	C6102	C6100	ok	b	
4	77° 56.01'N	14°32.58'W		19:25	325	C6102	C6100	ok	b	
5	77° 56.05'N	14°32.49'W		19:39	324	C6102	C6100	ok	b	
6	77° 56.12'N	14°32.01'W		19:55	291	C6102	C6100	ok	b	
7	77° 56.18'N	14°31.62'W		20:10	321	C6102	C6100	ok	b	
8	77° 56.12'N	14°31.67'W		20:24	315	C6102	C6100	ok	b	
9	77° 56.09'N	14°31.58'W		20:39	325	C6102	C6100	ok	b	
10	77° 56.03'N	14°31.39'W		20:57	327	C6102	C6100	ok	b	
11	77° 55.97'N	14°31.30'W		21:12	294	C6102	C6100	ok	b	
12	77° 55.91'N	14°30.96'W		21:27	303	C6102	C6100	ok	b	
13	77° 55.86'N	14°30.66'W		21:41	281	C6102	C6100	ok	b	
14	77° 55.81'N	14°30.15'W		21:58	290	C6102	C6100	ok	b	
15	77° 55.80'N	14°29.68'W		22:13	275	C6102	C6100	ok	b	
16	77° 55.78'N	14°28.97'W		22:28	285	C6102	C6100	ok	b	
17	77° 55.73'N	14°28.33'W		22:43	254	C6102	C6100	ok	b	
18	77° 55.72'N	14°27.51'W		22:56	285	C6102	C6100	ok	b	
19	77° 55.68'N	14°26.63'W		23:18	282	C6102	C6100	ok	b	profile had to be redone after cable problems on winch and aborted data streaming. restarting SDA and MSS Power Supply
20	77° 55.72'N	14°25.86'W		23:33	280	C6102	C6100	ok	b	
21	77° 55.74'N	14°25.02'W		23:50	280	C6102	C6100	ok	b	
22	77° 55.68'N	14°24.57'W		0:04	295	C6102	C6100	ok	b	

Cast #	Latitude	Longitude	Depth (HS) in m	Time: Start Winch	Depth (End Lower) in dbar	Shear Sensor 1 (SN)	Shear Sensor 2 (SN)	Pre-ampli-fier 1	Pre-ampli-fier 2	Comments
23	77° 55.63'N	14°24.12'W		0:18	290	C6102	C6100	ok	b	
24	77° 55.62'N	14°23.50'W		0:33	313	C6102	C6100	ok	b	
25	77° 55.62'N	14°23.04'W		0:48	296	C6102	C6100	ok	b	
26	77° 55.63'N	14°22.59'W	409	1:03	295	C6102	C6100	ok	b	
27	77° 55.65'N	14°22.17'W		1:17	296	C6102	C6100	ok	b	
28	77° 55.67'N	14°21.74'W		1:32	304	C6102	C6100	ok	b	
29	77° 55.67'N	14°21.37'W		1:46	303	C6102	C6100	ok	b	
30	77° 55.65'N	14°21.03'W		1:59	322	C6102	C6100	ok	b	
31	77° 55.63'N	14°20.79'W		2:15	308	C6102	C6100	ok	b	
Station PS100_206_01				Aug 22, 2016						
1	79° 16.57'N	18° 02.82'W	368	10:38	226	C6102	C6100	ok	b	
2	79° 16.49'N	18° 02.77'W	370	10:50	286	C6102	C6100	ok	b	many ice floats (small) close to cable during hoisting
3	79° 16.43'N	18° 02.43'W	-	11:11	240	C6102	C6100	ok	b	
4	79° 16.35'N	18° 01.96'W	-	11:25	236	C6102	C6100	ok	b	strong head wind. a lot of cable spooled out
5	79° 16.26'N	18° 01.34'W	371	11:37	274	C6102	C6100	ok	b	verholen after cast #5
6	79° 16.17'N	18° 00.55'W	370	12:07	272	C6102	C6100	ok	b	
7	79° 16.10'N	18° 00.27'W	-	12:20	242	C6102	C6100	ok	b	
8	79° 16.14'N	17° 59.05'W	-	12:45	257	C6102	C6100	ok	b	cable touches ship-hull already during free-falling period
9	79° 16.06'N	17° 58.79'W	-	13:00	238	C6102	C6100	ok	b	cable touches ship-hull already during free-falling period
10	79° 15.98'N	17° 58.50'W	-	13:13	271	C6102	C6100	ok	b	
11	79° 15.95'N	17° 58.59'W	-	13:25	246	C6102	C6100	ok	b	
Station PS100_256_01				Aug 26, 2016						
1	79° 35.46'N	19° 20.65' W	332	2:17	273	C6102	C6100	ok	b	
2	79° 35.29'N	19° 20.86' W	352	2:48	303	C6102	C6100	ok	b	extensive manoeuvring and tangled cable on winch before #2

Cast #	Latitude	Longitude	Depth (HS) in m	Time: Start Winch	Depth (End Lower) in dbar	Shear Sensor 1 (SN)	Shear Sensor 2 (SN)	Pre-ampli-fier 1	Pre-ampli-fier 2	Comments
3	79° 35.18'N	19° 21.16' W	366	3:01	318	C6102	C6100	ok	b	At end of #3 already drifted to next waypoint. transition back to beginning position
4	79° 35.94'N	19° 18.85' W	325	3:41	306	C6102	C6100	ok	b	during hoisting, ice tangled in cable (at 260 dbar)
5	79° 35.88'N	19° 19.12' W	325	3:56	299	C6102	C6100	ok	b	
6	79° 35.85'N	19° 19.53' W	322	4:09	295	C6102	C6100	ok	b	
7	79° 35.81'N	19° 19.97' W	320	4:22	307	C6102	C6100	ok	b	
8	79° 35.80'N	19° 20.36' W	319	4:35	309	C6102	C6100	ok	b	
9	79° 35.79'N	19° 20.67' W	322	4:48	316	C6102	C6100	ok	b	
10	79° 35.78'N	19° 20.89' W	322	5:01	316	C6102	C6100	ok	b	
Station PS100_257_02				Aug 26, 2016						
1	79° 35.30'N	19° 20.71' W	348	13:57	316	C6102	C6100	ok	b	turn ship after cast #1
2	79° 35.30'N	19° 20.92' W	356	14:23	338	C6102	C6100	ok	b	
3	79° 35.28'N	19° 21.07' W	361	14:38	353	C6102	C6100	ok	b	
4	79° 35.27'N	19° 21.31' W	358	14:54	354	C6102	C6100	ok	b	
5	79° 35.24'N	19° 21.43' W	359	15:09	346	C6102	C6100	ok	b	go to old position after cast #5
6	79° 35.27'N	19° 20.73' W	347	15:41	330	C6102	C6100	ok	b	
7	79° 35.27'N	19° 20.96' W	356	16:01	342	C6102	C6100	ok	b	
8	79° 35.23'N	19° 20.95' W	357	16:17	324	C6102	C6100	ok	b	
9	79° 35.18'N	19° 20.58' W	358	16:33	275	C6102	C6100	ok	b	turn by 90° after #9
10	79° 35.19'N	19° 20.13' W	343	16:58	328	C6102	C6100	ok	b	extensive manoeuvring and tangled cable on winch
11	79° 35.14'N	19° 19.89' W	353	17:49	339	C6102	C6100	ok	b	
12	79° 35.13'N	19° 19.96' W	353	18:05	334	C6102	C6100	ok	b	
13	79° 35.09'N	19° 20.14' W	364	18:19	343	C6102	C6100	ok	b	
Station PS100_258_01				Aug 26, 2016						
1	79° 32.15' N	19° 20.40' W	340	19:19	300	C6102	C6100	ok	b	
2	79° 32.08' N	19° 20.42' W	338	19:32	315	C6102	C6100	ok	b	
3	79° 31.99' N	19° 20.56' W	340	19:46	318	C6102	C6100	ok	b	

Cast #	Latitude	Longitude	Depth (HS) in m	Time: Start Winch	Depth (End Lower) in dbar	Shear Sensor 1 (SN)	Shear Sensor 2 (SN)	Pre-ampli-fier 1	Pre-ampli-fier 2	Comments
4	79° 31.88’ N	19° 20.82’ W	338	19:59	317	C6102	C6100	ok	b	
5	79° 31.75’ N	19° 21.07’ W	335	20:13	322	C6102	C6100	ok	b	
6	79° 31.60’ N	19° 21.27’ W	332	20:28	323	C6102	C6100	ok	b	
7	79° 31.47’ N	19° 21.43’ W	327	20:42	315	C6102	C6100	ok	b	
8	79° 31.32’ N	19° 21.59’ W	324	20:56	310	C6102	C6100	ok	b	
9	79° 31.19’ N	19° 21.74’ W	321	21:11	310	C6102	C6100	ok	b	
10	79° 31.06’ N	19° 21.89’ W	304	21:24	294	C6102	C6100	ok	b	
Station PS100_271_01				Aug 28, 2016						
1	79° 42.59’ N	17° 33.12 ‘W	337	4:33	254	C6102	C6100	ok	b	
2	79° 42.59’N	17° 32.94 ‘W	334	4:43	314	C6102	C6100	ok	b	
3	79° 42.57’N	17° 32.64 ‘W	332	4:57	325	C6102	C6100	ok	b	
4	79° 42.55’N	17° 32.43 ‘W	328	5:11	289	C6102	C6100	ok	b	
5	79° 42.54’N	17° 32.28 ‘W	327	5:23	306	C6102	C6100	ok	b	
6	79° 42.53’N	17° 32.26 ‘W	326	5:37	300	C6102	C6100	ok	b	extensive manoeuvring after #6 because of ice flow
7	79° 42.56’N	17° 32.23 ‘W	330	5:58	290	C6102	C6100	ok	b	
8	79° 42.54’N	17° 32.02 ‘W	326	6:11	290	C6102	C6100	ok	b	
9	79° 42.49’N	17° 31.76 ‘W	323	6:24	300	C6102	C6100	ok	b	
Station PS100_273_02				Aug 28, 2016						
1	79° 36.36’ N	16° 31.28 ‘W	291	12:24	242	C6102	C6100	ok	b	
2	79° 36.35’N	16° 31.20 ‘W	290	12:37	255	C6102	C6100	ok	b	
3	79° 36.34’N	16° 31.12 ‘W	290	12:53	293	C6102	C6100	ok	b	touch bottom at cast #3, vision check at surface shows no signs of damage
4	79° 36.32’N	16° 31.06 ‘W	291	13:06	238	C6102	C6100	ok	b	bottom touch doesn’t seem to have affected sensors
5	79° 36.40’N	16° 30.69 ‘W	288	13:38	243	C6102	C6101	ok	b	change sensor C6100 to C6101 because of weird behaviour (even observed before bottom touching)
6	79° 36.38’N	16° 30.78 ‘W	289	13:49	260	C6102	C6101	ok	b	

Cast #	Latitude	Longitude	Depth (HS) in m	Time: Start Winch	Depth (End Lower) in dbar	Shear Sensor 1 (SN)	Shear Sensor 2 (SN)	Pre-ampli-fier 1	Pre-ampli-fier 2	Comments
7	79° 36.21'N	16° 30.08 'W	277	14:34	252	C6101	C6102	ok	b	taping of power cable connection before #7 , also change position of C6101 and C6102 to see effect of preamplifiers on noise level
8	79° 36.17'N	16° 29.89 'W	276	14:47	239	C6101	C6102	ok	b	

Ice tethered mooring

The objective was the installation of an ice-tethered mooring in a glacial rift formed at the point where Nioghalvfjerdsbræ abuts Hovgaard Island. This mooring will record temperature, salinity, and current data from the ice tongue cavity beneath Nioghalvfjerdsbræ, helping us to understand the contribution of ocean heat to the submarine melting of the floating ice tongue.

A suitable site for the ice-tethered mooring (ITM) was identified on August 22nd, using the ship's helicopter to fly over a candidate site previously identified from Landsat-8- and Worldview-1/2-derived imagery. Two XCTD casts and two XBT casts provided a picture of the temperature and salinity structure at the mooring site. The XBT casts were necessary because the XCTD probes used (Sippican XCTD-01) activate past a salinity threshold of 10, however the geometry of the rift results in a lens of fresh water for several meters below the surface ice.

Fig. 3.7: Installed mooring. Surface package and winch at the mooring site (left). Detail of surface package mounted in float (right).

The ITM, winch, deployment tripod, and instruments were flown to the site on August 23rd, and the ITM was installed on that day. The ITM consists of a surface electronics package, four Seabird Microcat temperature and salinity loggers and four Nortek Aquadopp current meters.

The instruments send data to the surface electronics package via an inductive link, and the surface electronics package transmits data via an Iridium satellite antenna. Measurements

are made at a 15 minute interval, and Iridium transmissions are attempted every 24 hours. Initial diagnostic tests found that the eight instruments were operating and responding to the surface electronics package after installation. Initial data transmissions were received by persons based in Woods Hole, MA, USA. All deployment gear, including an aluminium winch and tripod, were returned to *Polarstern*.

Preliminary (expected) results

During the cruise, the CTD, VMADCP, and LADCP measurements were preliminarily analyzed. The CTD section along 78°50'N/79°N (Fig. 3.8) confirmed the expected distribution of water masses. Warm Atlantic Water was found in the West Spitsbergen Current as well as throughout the central part of Fram Strait in the recirculation region. The outflow from the Arctic Ocean in the East Greenland Current was cold and fresh. Compared to previous years, the maximum salinity in the center of Fram Strait was slightly elevated. The CTD section along NT3 (Fig. 3.9) confirmed the presence of warm salty modified Atlantic Water in Norske Trough below the cold fresh Polar Surface Water. Additionally, a warmer core was found on the northern side of the trough. The velocity measurements are consistent with the presence of a boundary current there transporting warm water to the 79N glacier.

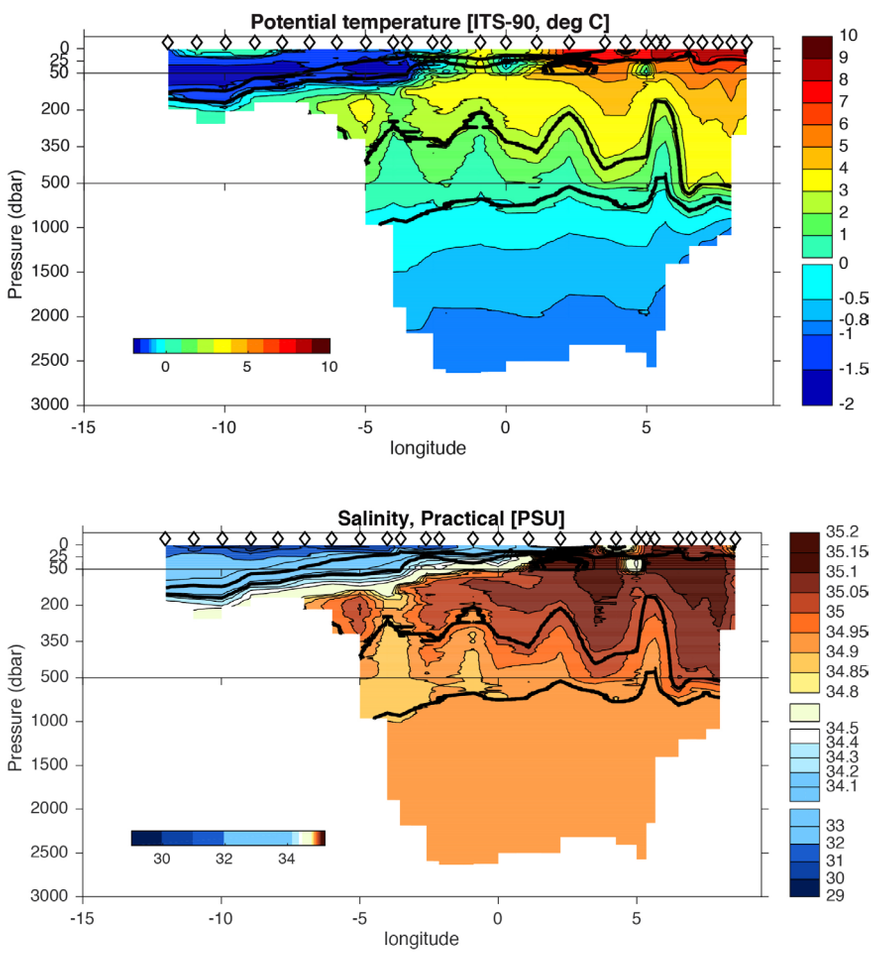

Fig. 3.8: Distribution of (a) potential temperature and (b) salinity along the 78°50'N/79°N CTD section. The black diamonds at the top indicate the station locations. Note the broken y-axis.

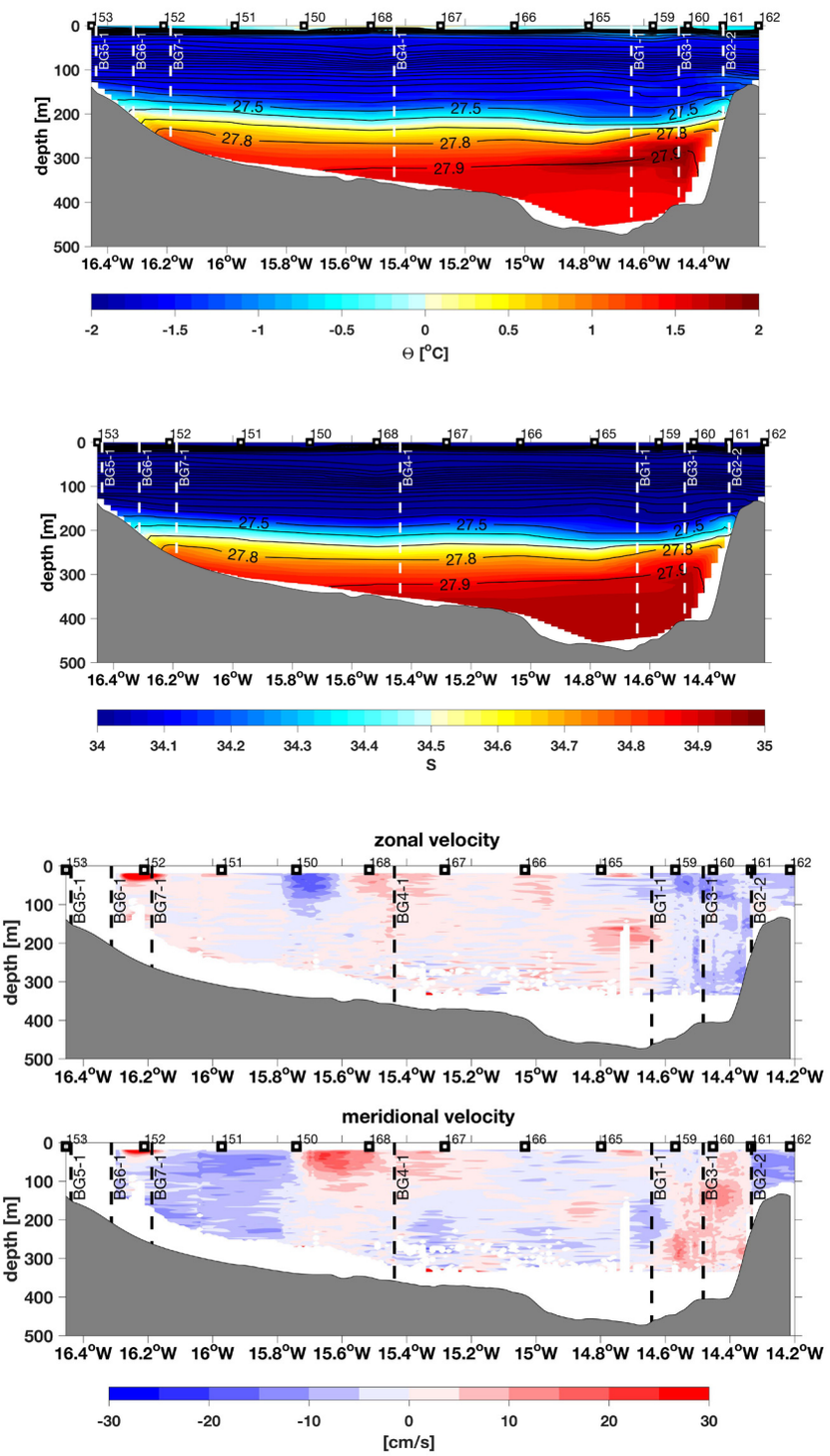

Fig. 3.9: Distribution of (a) potential temperature, (b) salinity, and (c) vessel mounted ADCP velocities along the NT3 CTD section. The black square at the top indicate the station locations. The vertical dashed lines indicate the location of the moorings recovered along this section on PS100.

The ice tethered mooring is expected to provide a direct measurements of temperature and circulation variability within the ice shelf cavity, which are critical for determining how much the shelf variability may influence melt rates beneath the floating glacier. Initial results from the XCTD casts (Fig. 3.10) and the transmitted mooring data reproduce the findings of Wilson and

Straneo (2015), who found warm Atlantic water in the ice tongue cavity, previously predicted by Mayer et al., (2000).

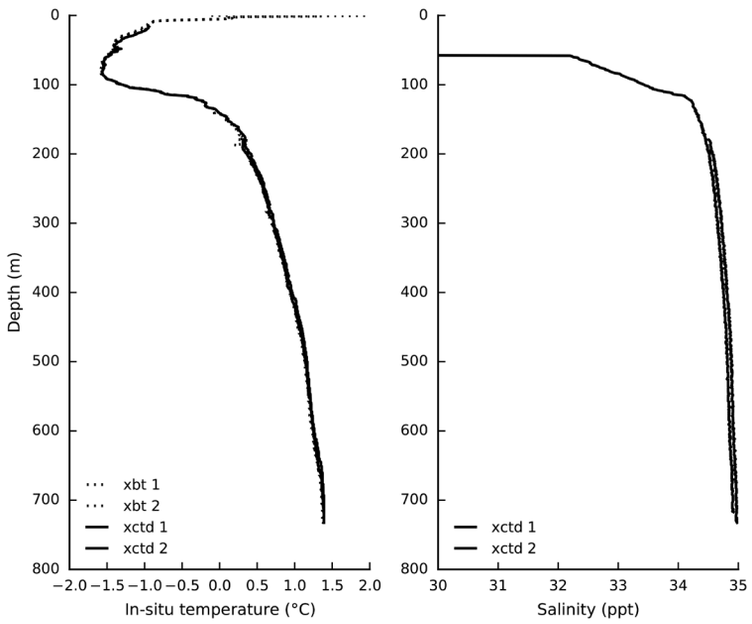

Fig. 3.10: Temperature (left) and salinity (right) profiles measured from XBT XCTD casts prior to deployment

Data management

The data recorded by the moored instruments recovered on PS100 will be processed after the cruise at AWI and submitted to the PANGAEA data publisher. Some of the moorings deployed on PS100 will be recovered in 2017 and the rest will be recovered in 2018. The data recorded on those instruments will accordingly be processed after recovery and submitted to the PANGAEA data publisher at that time. The data collected during PS100 from the different CTDs, the VMADCP, the LADCP, the temperature-depth logger, and the microstructure profiler will be processed at AWI and afterwards submitted to the PANGAEA data publisher.

Data from the ice-tethered mooring are transmitted via the Iridium satellite constellation to Woods Hole Oceanographic Institute in Woods Hole, MA, USA. This data is immediately posted on a public-facing website. Processed data products will be provided upon request as they are available.

References

Bersch M, I Yashayaev, and K P Koltermann (2007) Recent changes of the thermohaline circulation in the subpolar north Atlantic. Ocean Dynamics, 57(3), 223–235, doi:10.1007/s10236-007-0104-7.

Beszczynska-Möller A, E Fahrbach, U Schauer, and E Hansen (2012) Variability in Atlantic water temperature and transport at the entrance to the Arctic Ocean, 1997-2010, ICES Journal of Marine Science: Journal du Conseil. 69(5), 852–863, doi: 10.1093/icesjms/fss056.

Bourke R H , J L Newton, R G Paquette, and M D Tunnicliffe (1987) Circulation and water masses of the east Greenland shelf. Journal of Geophysical Research: Oceans, 92(C7), 6729–6740, doi:10.1029/JC092iC07p06729.

Budeus G, and W Schneider (1995) On the hydrography of the northeast water polynya. Journal of Geophysical Research: Oceans, 100 (C3), 4287–4299, doi:10.1029/94JC02024.

Budeus G, W Schneider, and G Kattner (1997) Distribution and exchange of water masses in the northeast water polynya (Greenland Sea). Journal of Marine Systems, 10(14), 123 – 138, doi:http://dx.doi.org/10.1016/S0924-7963(96)00074-7.

de Steur L, E Hansen, R Gerdes, M Karcher, E Fahrbach, and J Holfort (2009) Freshwater fluxes in the East Greenland Current: A decade of observations. Geophysical Research Letters, 36(23).

de Steur L , E Hansen, C Mauritzen, A Beszczynska-Möller, and E Fahrbach (2014) Impact of recirculation on the East Greenland Current in Fram Strait: Results from moored current meter measurements between 1997 and 2009. Deep Sea Research, 92, 26–40.

Dietrich R, H-G Maas, M Baessler, A Ru ̈lke, A Richter, E Schwalbe, and P Westfeld (2007) Jakobshavn isbræ, west Greenland: Flow velocities and tidal interaction of the front area from 2004 field observations. J Geophys. Res., 112(F03S21), doi: 10.1029/2006JF000601.

Hattermann T, P E Isachsen, W-J von Appen, J Albretsen, and A Sundfjord (2016) Eddy-driven recirculation of Atlantic Water in Fram Strait. Geophysical Research Letters, 43, 1-9.

Helm V, A Humbert, and H Miller 2014 Elevation and elevation change of Greenland and Antarctica derived from Cryosat-2. The Cryosphere, 8 (4), 1539–1559, doi:10.5194/tc- 8-1539-2014.

Holland D M , R H Thomas, B de Young, M H Ribergaard, and B Lyberth 2008 Acceleration of Jakobshavn Isbrae triggered by warm subsurface ocean waters. Nature Geosci, 1(10), 659–664.

Hopkins T S (1991) The GIN sea a synthesis of its physical oceanography and literature review 1972-1985. Earth-Science Reviews, 30(34), 175 – 318, doi: http://dx.doi.org/10.1016/0012-8252(91)90001-V

Howat I M, I Joughin, M Fahnestock, B E Smith, and T A Scambos (2008) Synchronous retreat and acceleration of southeast Greenland outlet glaciers 2000- 06: ice dynamics and coupling to climate. Journal of Glaciology, 54, 646–660, doi: 10.3189/002214308786570908.

Johnson M, and H J Niebauer (1995) The 1992 summer circulation in the northeast water polynya from acoustic Doppler current profiler measurements. Journal of Geophysical Research: Oceans, 100(C3), 4301–4307, doi:10.1029/94JC01981.

Khan S A, K H Kjær, M Bevis, J L Bamber, J Wahr, K K Kjeldsen, A A Bjørk, N J Korsgaard, L A Stearns, M R van den Broeke, L Liu, N K Larsen, and I S Muresan (2014) Sustained mass loss of the northeast Greenland ice sheet triggered by regional warming. Nature Clim. Change, 4 (4), 292–299.

Mayer C, N Reeh, F Jung-Rothenhusler, P Huybrechts, and H Oerter (2000) The sub-glacial cavity and implied dynamics under Nioghalvfjerdsfjorden Glacier, NE-Greenland. Geophysical Research Letters, 27(15), 2289–2292, doi:10.1029/2000GL011514.

Metfies K, W-J von Appen, E Kilias, A Nicolaus, and E-M Nöthig (2016), Biogeography and Photosynthetic Biomass of Arctic Marine Pico-Eukaroytes during Summer of the Record Sea Ice Minimum 2012. PLOS ONE, 11(2), doi: doi:10.1371/journal.pone.0148512.

Milne G A, W R Gehrels, C W Hughes, and M E Tamisiea (2009) Identifying the causes of sea-level change. Nature Geosci, 2 (7), 471–478.

Mouginot J, E Rignot, B Scheuchl, I Fenty, A Khazendar, M Morlighem, A Buzzi, and J Paden (2015) Fast retreat of Zachariæ Isstrøm, northeast Greenland. Science, doi:10.1126/science.aac7111.

Murray T, K Scharrer, T D James, S R Dye, E Hanna, A D Booth, N Selmes, A Luckman, A L C Hughes, S Cook, and P Huybrechts (2010) Ocean regulation hypothesis for glacier dynamics in southeast Greenland and implications for ice sheet mass changes. Journal of Geophysical Research: Earth Surface, 115 (F3), doi: 10.1029/2009JF001522, f03026.

Nick FM, A Vieli, I M Howat, and I Joughin (2009) Large-scale changes in Greenland outlet glacier dynamics triggered at the terminus. Nature Geosci, 2 (2), 110–114.

Pritchard H D, R J Arthern, D G Vaughan, and L A Edwards (2009) Extensive dynamic thinning on the margins of the Greenland and Antarctic ice sheets. Nature, 461(7266), 971–975.

Rignot E, and P Kanagaratnam (2006) Changes in the velocity structure of the Greenland ice sheet. Science, 311 (5763), 986–990, doi:10.1126/science.1121381.

Rudels B, G Björk, J Nilsson, P Winsor, I Lake, and C Nohr (2005) The interaction between waters from the Arctic Ocean and the Nordic Seas north of Fram Strait and along the East Greenland Current: results from the Arctic Ocean-02 Oden Expedition. Journal of Marine Systems, 55(1), 1–30.

Schneider W, and G Budeus (1997) A note on Norske ø Ice barrier (northeast Greenland), viewed by Landsat 5. Journal of Marine Systems, 10(14), 99 – 106, doi: http://dx.doi.org/10.1016/S0924-7963(96)00076-0.

Schneider W, and G Budeus (1995) On the generation of the northeast water polynya. Journal of Geophysical Research: Oceans, 100 (C3), 4269–4286, doi:10.1029/94JC02349.

Stearns L A, and G S Hamilton (2007) Rapid volume loss from two east Greenland outlet glaciers quantified using repeat stereo satellite imagery. Geophysical Research Letters, 34(5), n/a–n/a, doi:10.1029/2006GL028982, l05503.

Straneo F, G S Hamilton, D A Sutherland, L A Stearns, F Davidson, M O Hammill, G B Stenson, and A Rosing-Asvid (2010) Rapid circulation of warm subtropical waters in a major glacial fjord in east Greenland. Nature Geosci, 3(3), 182–186.

Straneo F, R G Curry, D A Sutherland, G S Hamilton, C Cenedese, K Vage, and L A Stearns (2011) Impact of fjord dynamics and glacial runoff on the circulation near Helheim Glacier, Nature Geosci, 4 (5), 322–327. Straneo, F., D A Sutherland, D Holland, C Gladish, G S Hamilton, H L Johnson, E Rignot, Y Xu, and M Koppes (2012), Characteristics of ocean waters reaching Greenland's glaciers. Annals of Glaciology, 53(60), 202–210, doi: doi:10.3189/2012AoG60A059.

Thomas HR (2004) Force-perturbation analysis of recent thinning and acceleration of Jakobshavn Isbrae, Greenland. Journal of Glaciology, 50, 57–66, doi: 10.3189/172756504781830321.

Thomsen H H, N Reeh, O B Olesen, C E Bøggild, W Starzer, A Weidick, and A K Higgins (1997) The Nioghalvfjerdsfjorden Glacier project, north-east Greenland: a study of ice sheet response to climatic change. Geology of Greenland Survey Bulletin, 176, 95–103.

Topp R, and M Johnson (1997) Winter intensification and water mass evolution from yearlong current meters in the northeast water polynya. Journal of Marine Systems, 10(14), 157 – 173, doi:http://dx.doi.org/10.1016/S0924-7963(96)00083-8.

Velicogna I (2009) Increasing rates of ice mass loss from the Greenland and Antarctic ice sheets revealed by grace. Geophysical Research Letters, 36(19), doi: 10.1029/2009GL040222, l19503.

Vieli A, and F M Nick (2011) Understanding and modelling rapid dynamic changes of tidewater outlet glaciers: Issues and implications. Surveys in Geophysics, 32(4), 437– 458, doi:10.1007/s10712-011-9132-4.

von Appen W-J, U Schauer, T Hattermann, and A Beszczynska-Möller (2016) Seasonal cycle of mesoscale instability of the West Spitsbergen Current. Journal of Physical Oceanography, 46 (4), 1231-1254.

Wilson N J, and F Straneo (2015) Water exchange between the continental shelf and the cavity beneath Nioghalvfjerdsbr (79 North Glacier). Geophysical Research Letters, 42(18), 7648–7654, doi:10.1002/2015GL064944, 2015GL064944.

Wulff T, E Bauerfeind, and W-J von Appen (2016) Physical and ecological processes at a moving ice edge in the Fram Strait as observed with an AUV. Deep-Sea Research I, 115, 253-264.

4. NEGIS: UNDERSTANDING THE MECHANISMS CONTROLLING THE LONG-TERM STABILITY OF THE NORTHEAST GREENLAND ICE STREAM

David Roberts[1], Jerry Lloyd[1], Colm Ó Cofaigh[1], Sarah Louise Callard[1], Henrik Grob[2], Maria Kappelsberger[2]

[1] DUR,
[2] AWI

Grant-No. AWI-PS100_02

Background

The NEGIS project is supported through the Alfred Wegener Institute (Project N405) via the GRIFF I project and the *Polarstern* programme (Cruise PS100) as well as through the UK Natural Environment Research Council (NERC Grant NE/N011228/1). The incursion of warm Atlantic Water (AW) over the last 15 years to many Greenland marine-terminating glaciers, as well as increased air temperatures and sea-ice loss, have all been linked to ice margin retreat and instability (Straneo et al., 2012; Mouginot et al., 2015; Wilson et al., 2015). However, despite our improved understanding of the forcing mechanisms that have driven recent glacier change in Greenland, the limited time-span of our observations provide only a short time series with which to understand the complex and non-linear response of ice streams to ocean and atmospheric forcing (Nick et al., 2010). This hinders our ability to understand and forecast how ice sheets will change over longer timescales (Seroussi et al., 2014). What we fundamentally lack is decadal to millennial scale input data with which to calibrate, validate and test the sensitivity of predictive models. One solution to this issue is to identify patterns of former rapid ice margin change during periods of warmer climate when the key forcing mechanisms that influence ice sheet stability can be simultaneously reconstructed so their relative importance can be determined.

This project will investigate the dynamics of the Northeast Greenland Ice Stream (NEGIS); the main artery for ice discharge from the NE sector of the Greenland Ice Sheet (GrIS) to the North Atlantic. Unlike other sectors of the GrIS, NEGIS and the ice shelves that front it, have exhibited little response to increased atmospheric and oceanic warming over the last 20 yrs. However, very recent ice shelf loss and grounding line retreat (~ 4 km) post 2010 suggest that this sector of the GrIS, and NEGIS in particular, is starting to respond to recent atmospheric/ oceanic change (Mouginot et al., 2015). Model projections suggest that ocean warming will double by 2100 (Yin et al., 2011) and air temperature will increase significantly in northeast Greenland (AMAP, 2011), so the future evolution of the NEGIS catchment is important not only for understanding changing dynamics in this sector of the GrIS, but also for predicting sea-level rise. The NEGIS catchment as a whole holds a significant sea-level equivalent (SLE) of 1.1 to 1.4 m, but it is the marine-terminating end of the NEGIS system that is particularly vulnerable to marine ice sheet instability because it sits within a series of interconnected, over-deepened, subglacial troughs; those troughs harbour a SLE of 0.12 - 0.35 m. A rapid retreat of this system would therefore have significant consequences for global sea-level rise.

A critical underlying component of this project is previous research that demonstrated that one of the NEGIS ice shelves (known as '79N') retreated 80 km during the mid-Holocene Thermal Maximum (HTM; 8.0 – 5.0 ka BP) (Bennike and Weidick, 2001). 79N is the only large-scale ice stream/shelf outlet system in Greenland that has a partially constrained Holocene retreat

and re-advance history (Bennike and Weidick, 2001). The HTM was a period when radiative forcing and summer temperatures were up to 2°C higher than present, and analogous to those predicted for the next 100 yrs and beyond. Hence, increased air temperature could have played a role in ice stream fluctuation and ice shelf collapse, but we presently lack the data to assess the role of different forcing mechanisms (e.g. ocean warming) on ice stream fluctuation. This limits our ability to predict the response of NEGIS to future change.

The overall aim of this project is to reconstruct the history of the NEGIS from the end of the last glacial maximum (LGM) and through the Holocene. Working both onshore and offshore the project will generate a series of tie points to reconstruct ice sheet thickness, grounding line position, and ice shelf presence/absence. It will also generate a time series of forcing data on ocean and atmospheric temperatures. These datasets will be used to test and model the sensitivity of the ice stream to different forcing mechanisms at 100 - 1,000 yr timescales.

Objectives

The project has three main objectives:

- Objective 1: To constrain ice stream/ice shelf extent and thickness in order to determine rates of retreat and re-advance between 15 – 0 ka BP.
- Objective 2: To constrain oceanographic and atmospheric conditions and sea-level change adjacent to NEGIS between 15 – 0 ka BP.
- Objective 3: To apply the 3D BISCICLES numerical ice sheet model to test the sensitivity of NEGIS to atmospheric/oceanic /sea-level forcing and to explore feedbacks over 1000 yr timescales.

Work at sea

During cruise PS100 the NEGIS project has concentrated on objectives 1 and 2. We have principally collected data from the Norske Trough and the area in front of the 79N ice shelf. However, bathymetric and sub-bottom profile data were also collected using the Hydrosweep and Parasound systems from areas in the Westwind Trough and across the Belgica Bank (Fig. 4.1). The bathymetric data was collected on the hull-mounted ATLAS Hydrosweep DS3 multibeam echo-sounding system. The instrument operated at a frequency between 13.6-16.4 kHz and was calibrated using sound velocity measurements of the water column collected from CTD stations. The data was processed and cleaned in CARIS Hips and Sips. The sub-bottom profiler data was collected using a hull-mounted Parasound DS III-P70 system operating at a pulse mode of between 4-20 kHz and a pulse length of 0.5 ms. The seismic profiles were visualized using PS3 file formats on SeNT v 2.02.

The main aim of using the Hydrosweep system has been to establish the bathymetry and seafloor geomorphology of key areas and to characterise the geomorphological imprint and extent of the ice sheet across the NE Greenland shelf. The Norske Trough has been a key focus because it is thought to have funneled ice offshore during the last glacial cycle and influenced ice flow pathways during ice sheet retreat at the start of the Holocene. The Parasound sub-bottom profiler system has enabled us to acquire sub-seafloor acoustic stratigraphic data. This provides not only an insight into the erosion and deposition of glacial and glaciomarine sediments across the seafloor, but has been critical in guiding the location of coring activity. Our coring strategy has been three-fold; 1) to sample different types of glacial, glaciomarine and marine sedimentary environments to establish ice sheet behaviour and postglacial marine conditions; 2) to sample material (e.g. marine molluscs; foraminifera) in order to date ice retreat and; 3) to extract proxies to establish palaeo-oceanographic conditions during deglaciation and the Holocene. In all, we collected 39 gravity cores and 4 box cores during the cruise (Table 4.1; Fig. 4.1)

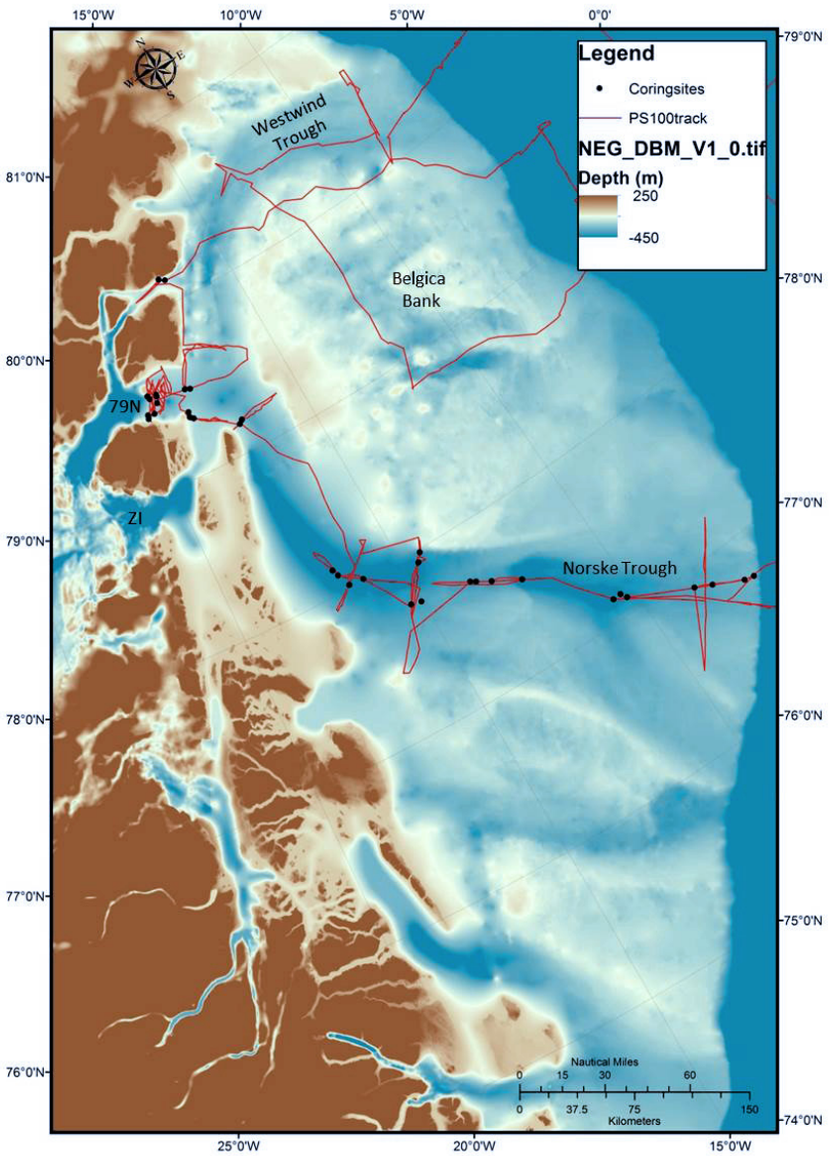

Fig. 4.1: An overview of the NE Greenland shelf showing the Norske Trough, Westwind Trough and Belgica Bank. The ice shelves, 79N and Zachariae Isstrom (ZI), can be seen to the west. Core locations from PS100 shown by black dot (offshore bathymetry compiled by Arndt et al., 2015).

Preliminary results

Norske Trough - Seafloor geomorphology and acoustic stratigraphy overview

The outer Norske Trough seafloor has several geomorphic and sedimentary features of note. Parasound data was particularly useful in revealing possible till units and grounding zone wedges marking ice advance to the outer shelf and its subsequent retreat (Fig. 4.2). In many instances these sediments have been heavily disturbed and dissected by iceberg scour which followed ice retreat to the northwest. Deeper basins over 400 m bsl on the outer shelf also revealed slightly thicker sedimentary records with over 20 m of sedimentary infill and four on-lapping units visible at core site PS100 146-01-GC (Fig. 4.3). Such deeper, un-scoured, areas suggest iceberg drafts did not exceed 400 m.

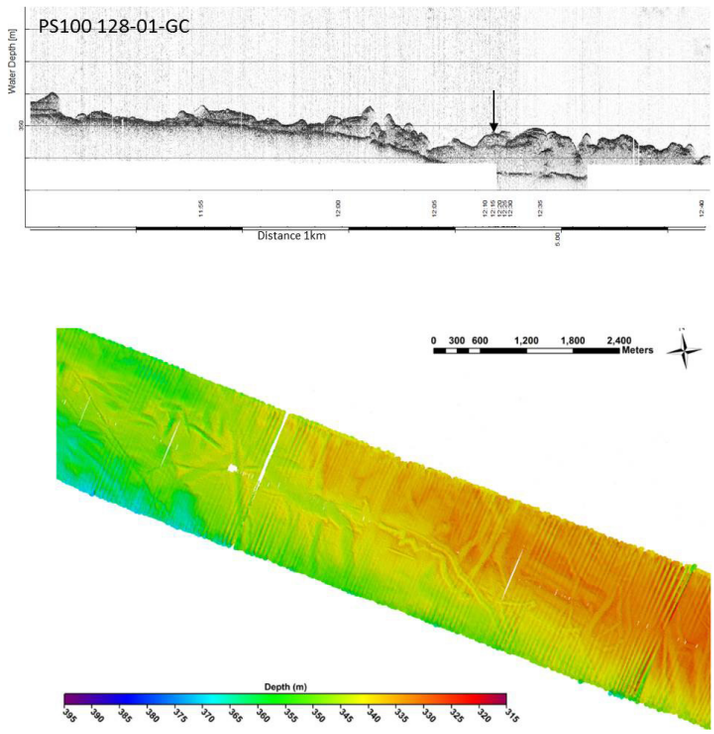

Fig. 4.2: A) Outer Norske Trough. A strong lower acoustic reflector representing the upper surface of a subglacial till overlain by two acoustic facies that are heavily iceberg turbated. B) Iceberg scour marks on the seafloor in the Outer Norske Trough.

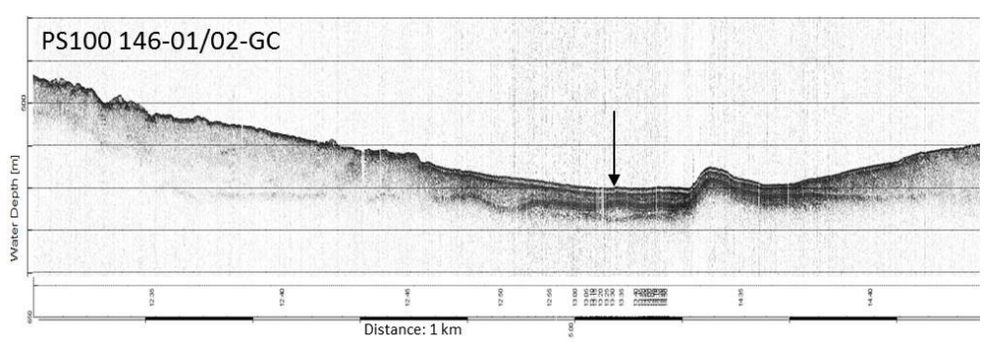

Fig. 4.3: A thicker sedimentary record with over 20m of sedimentary infill and four on-lapping units visible at core site PS 100 146-01-GC.

The mid-trough area is characterised by a series of grounding-zone wedges marking ice sheet retreat (Fig. 4.4) and in areas the seafloor is clearly streamlined with both drumlins and mega-scale glacial lineations formed across an area that appears to show an upper and lower till (Fig. 4.5). In places the streamlined terrain is draped by deglacial marine sediments that also infill some small basins.

The inner trough and embayment in front of the 79N margin display a marked transition in seafloor morphology and sedimentary environments with distinctive stratified basins separated by ice scoured bedrock highs in places shallower than 100mbsl (Fig. 4.6). In areas the sedimentary infills are over 75 m in thickness. They consist of stratified clays that most probably represent deglacial and Holocene glaciomarine sedimentation. Several cores from these basins are characterised by laminated/colour banded red and grey clays. Overlying the stratified sediments are acoustically massive sediments which most likely represent debris flow

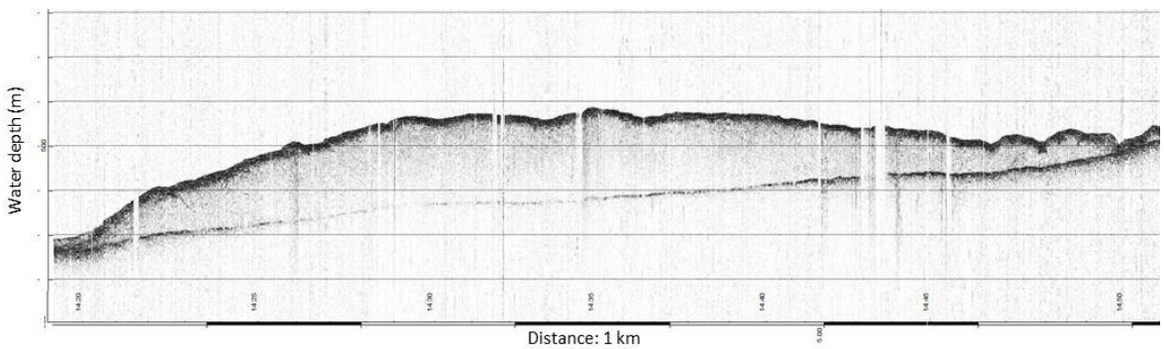

Fig. 4.4: Grounding zone wedge marking temporary ice stream stability during overall retreat along the mid Norske Trough. Palaeo-ice flow was from right to left.

activity fed from adjacent slopes, as well as sub-ice shelf sedimentation beneath areas formally covered by the ice shelf (Fig. 4.7). In areas east of the present ice shelf, the bedrock highs form classic knoc'n'lochan topography across the seafloor pointing to intensive subglacial abrasion and plucking prior to marine inundation (Fig. 4.8).

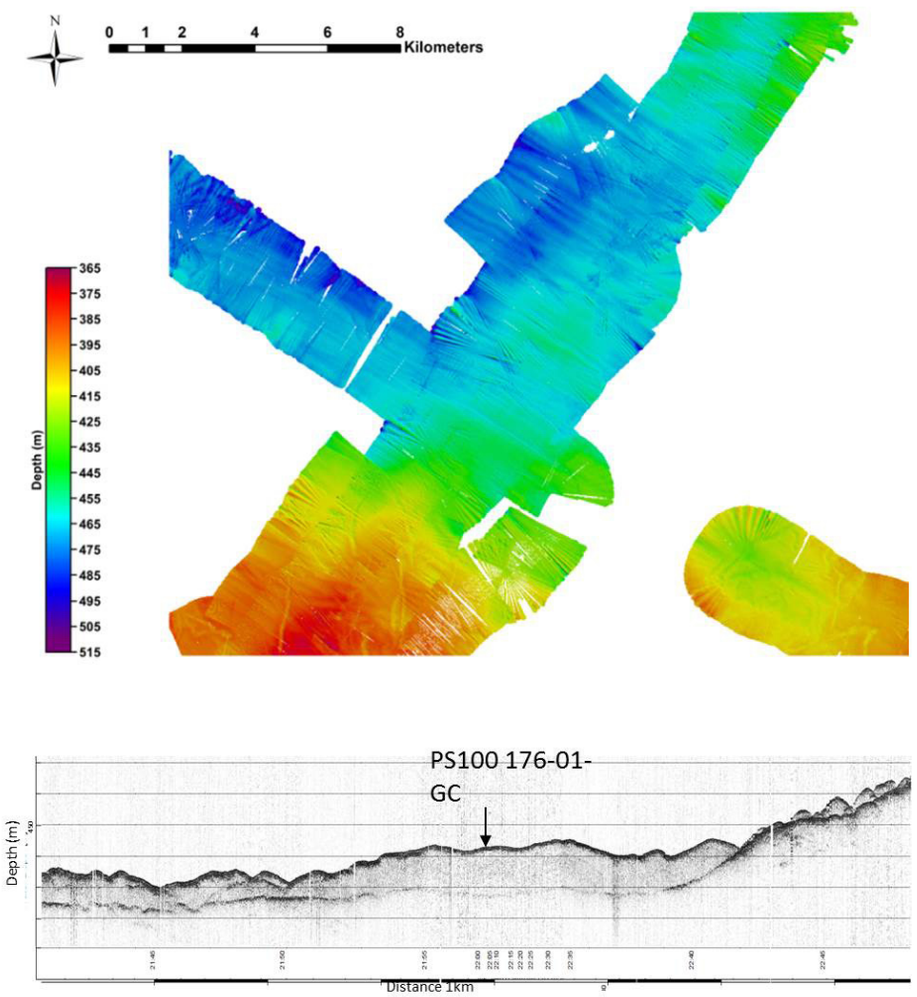

Fig. 4.5: A) Streamlined sediments in the mid Norske Trough with iceberg scour marks on shallower areas to the south. B) Parasound sub-bottom profile data through the streamlined area of the seabed displaying crude drumlinoid bedforms (palaeo-ice flow was out the page).

Westwind Trough - Seafloor geomorphology and acoustic stratigraphy overview

The Westwind Trough runs NE to E away from the coast towards the shelf break. It is generally shallower than the Norske Trough being less than 350m deep for most of its length. The seafloor geomorphology of this trough shares some similar characteristics to Norske Trough with streamlined bedforms (e.g. mega-scale lineations/drumlins) and iceberg scours being particularly prevalent (Fig. 4.9). Grounding-zone wedges are not as common, but moraines are clearly identifiable and have been previously reported by Winklemann et al., (2010) (Fig. 4.10). The glacial sediment cover on the outer- and mid-shelf is relatively thin (often less than 5m) and in many areas dipping bedrock strata can be clearly seen close to the seabed (Fig. 4.11). Only on the inner trough close to Dimphna Sund does the glacial sediment thickness increase with deep, deglacial sedimentary infills similar to those observed in the inner parts of the Norske Trough and close to the 79N glacier (Fig. 4.12).

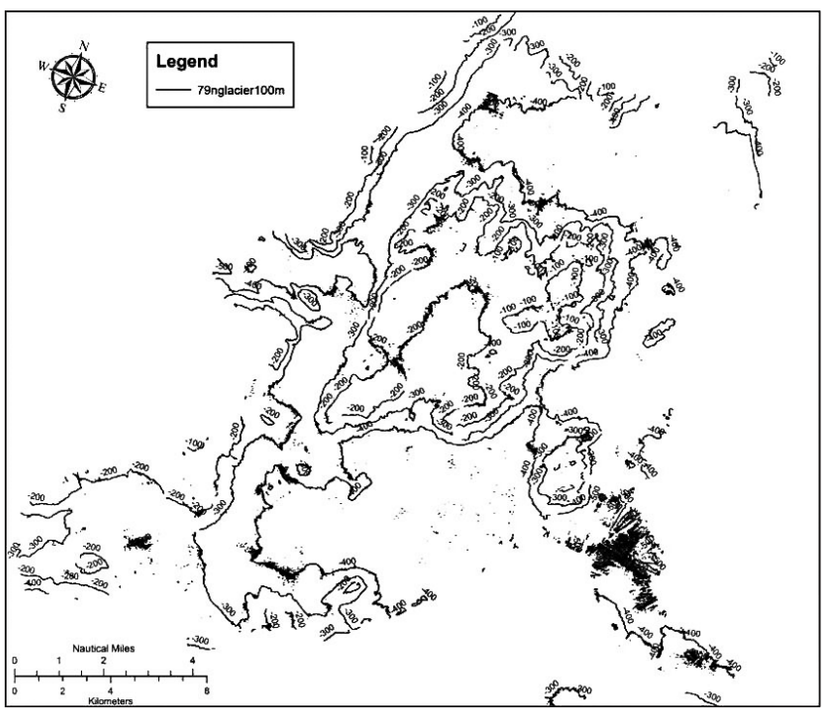

Fig. 4.6: A bathymetric overview of the seafloor to the east of the 79N ice shelf

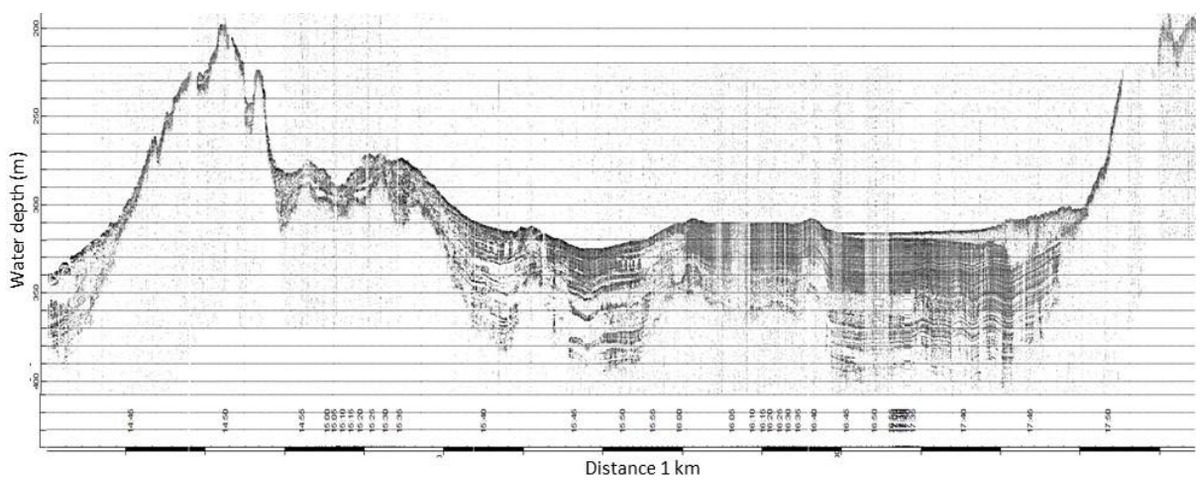

Fig. 4.7: A stratified basin infill typical of the inner Norske Trough. The stratified sediments are typically composed of alternating/banded red and grey clays. Overlying the stratified sediments are debris flows fed from the adjacent slopes (right hand side of image).

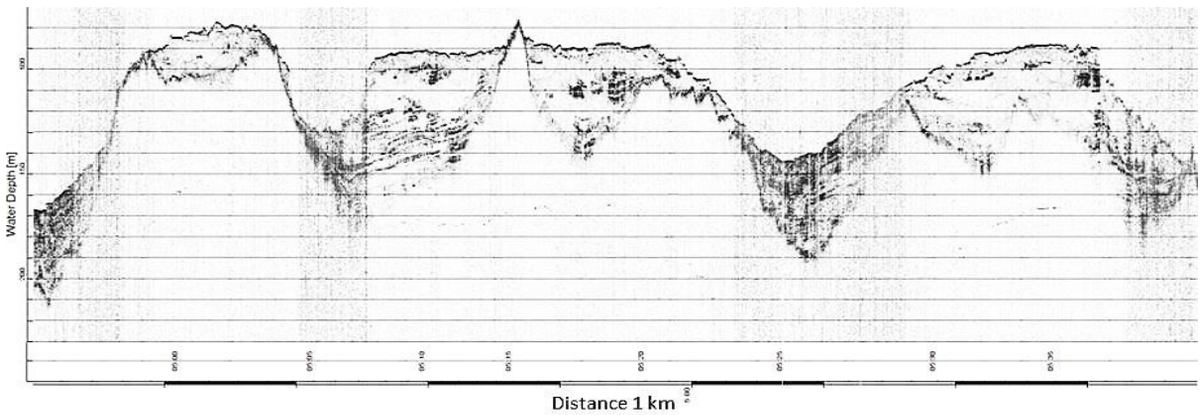

Fig. 4.8: Bedrock highs forming knoc'n'lochan-like topography across the seafloor. These bedrock hills form through subglacial abrasion and plucking (especially in areas underlain by crystalline, gneissic bedrock). Postglacial, marine inundation and high sedimentation rates have led to extensive draping of the subglacial terrain with stratified sediments. The stratified sediments are also overlain by opaque acoustic facies that may relate to sub-ice shelf sedimentation.

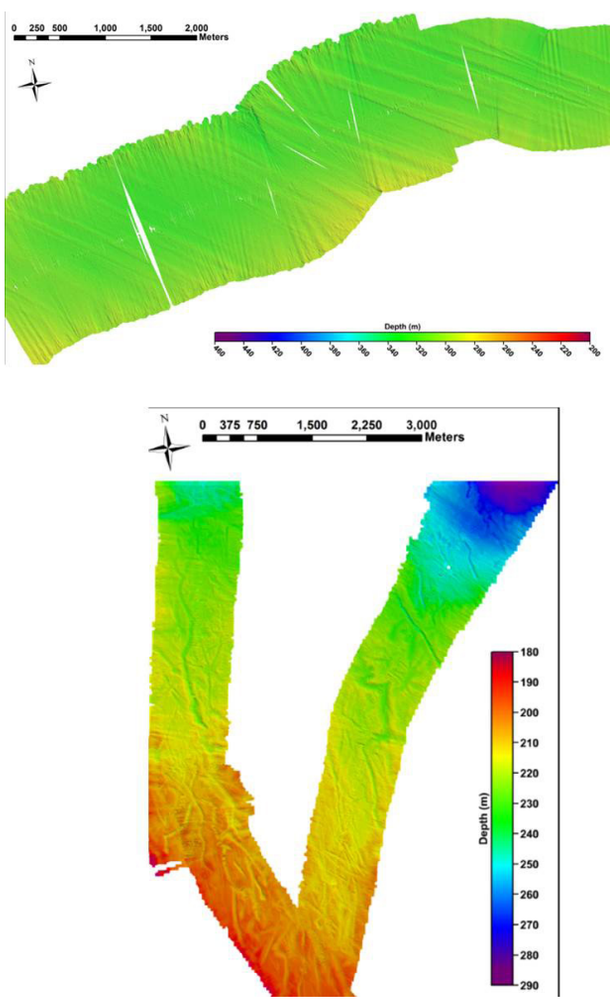

Fig. 4.9: A) Hydrosweep image of mega-scale glacial lineations in the mid Westwind Trough (Ice flow from left to right). B) Iceberg scours from mid Westwind Trough.

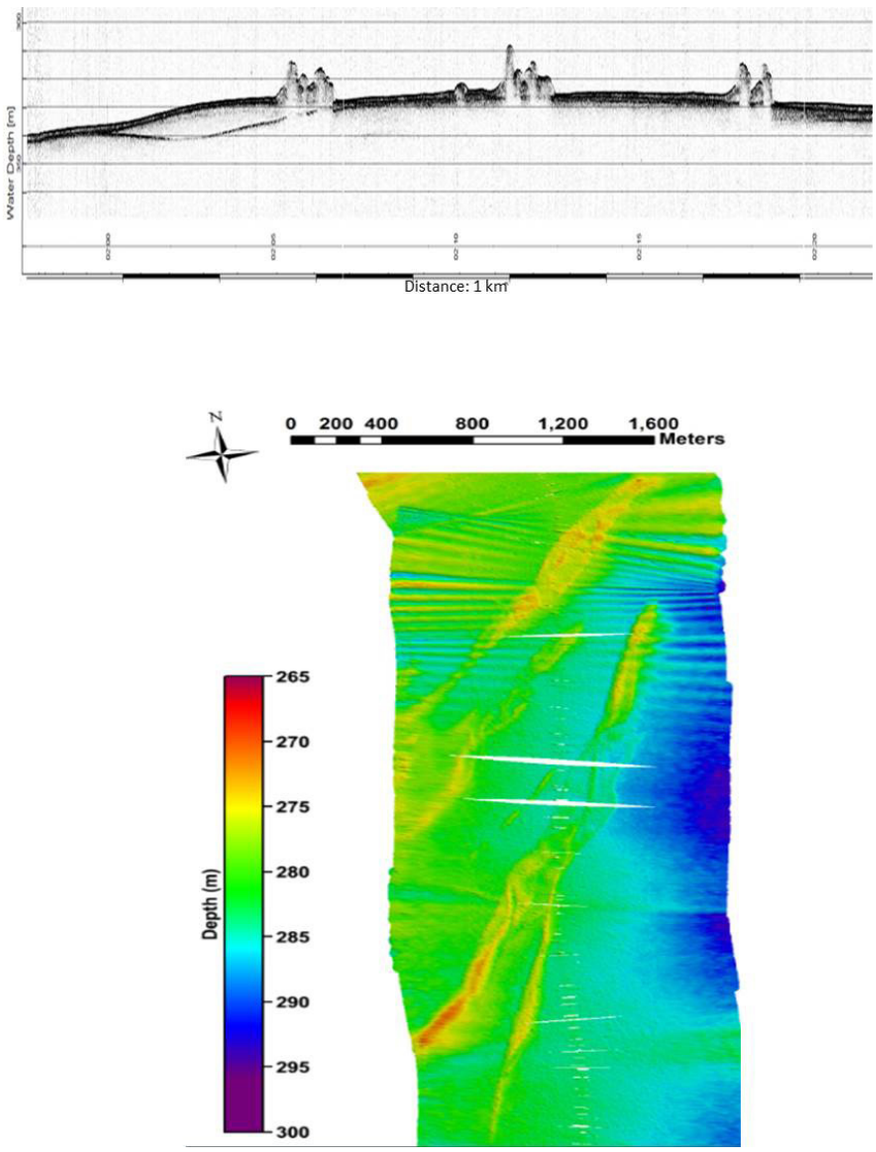

Fig. 4.10: A) Parasound image of distinctive moraines from the Westwind Trough. Ice flow from right to left. B) Hydrosweep image of the same moraines. Their steep slope angles and narrow width led Winklemann et al. (2010) to propose they were a form of De Geer moraine.

Sedimentary Environments

Based on the Parasound data a number of acoustic facies (AF) were identified and several core locations were deliberately chosen to establish the nature of these facies and the type of glacial and glaciomarine sediments below the seafloor.

Subglacial Tills (AF 1 + AF 2)

In several areas in the outer- and mid-Norske Trough the lowest acoustic reflector in the sequence (AF1) was accessible at the seabed. Cores PS100 126-01 and 174-01 sampled this reflector and recovered a grey/brown, stiff, massive diamict with shear strength over 100 kPa. This is typical of a subglacial till. In other areas in the mid Norske Trough area a second acoustic facies (AF2) above the lower till (AF1) formed a stratigraphic unit up to 15 m thick that was clearly streamlined (Fig. 4.5). This unit was sampled in core PS100 175-01-GC and was composed of dark, massive grey clay with low shear strength (~20kPa).

Glaciomarine stratified infills (AF3)

Across much of the outer- and mid-Norske Trough deglacial stratified sediments and drapes are difficult to map due to intense iceberg scour. However, on the inner shelf, deep basins below 400 m preserve well stratified sediments in depo-centres that escaped intensive scour during deglaciation and the Early Holocene. These sediments were sampled in several cores (e.g. PS100 198-01; 199-01; 207-01; 208-01; 248-01; 249-01) and contained laminated clays which often display alternating (occasionally rhythmic) red and grey colour bands, though there is no obvious change in grain size (Fig. 4.13). These sediments are interpreted as glaciomarine in origin and could relate to variations in source from the 79N and Zachariae Isstrom catchments or be related to variations in seasonal oceanic and sea-ice conditions. Further analysis will follow.

Debris Flows (AF4)

In many locations deeper basins are on-lapped from steep marginal areas by debris flows. These are clearly distinguishable in the Parasound data as wedges and lobes that are slope conformable, usually acoustically transparent or homogeneous and overlap older basin stratified sediments (Fig. 4.8). In core PS100-177-01-GC the upper part of a debris flow unit was composed of soft brown/grey, massive clay with dispersed pebbles and cobbles with low shear strength (2-4 kPa).

Sub-shelf facies (AF 5 and AF 6)

In several localities close to the present 79N ice shelf edge both transparent and opaque sedimentary facies conformably drape lower stratified basins. Where sampled they are composed of very soft, massive, red clays. These may represent sub-ice shelf facies but further analysis is required.

Foraminiferal analysis

Selected samples were chosen for qualitative foraminiferal analysis – principally from surface samples collected from box core sites, but also some subsurface samples. For each sample analysed, approximately 10 ml of sediment was added to a glass beaker with water and left to disaggregate for approximately 1 hour. Samples were then washed through a 500 µm and 63 µm mesh sieve. The residue coarser than 63 µm was collected and examined using a Leica binocular microscope. Samples were examined wet to reduce potential loss of fragile agglutinated specimens.

Samples were selected from a range of sites covering the coring transect from the outer part of the Norske Trough through the mid- and inner-trough to the embayment immediately in front of the modern ice shelf. All samples contained benthic foraminifera, often in high abundances. There was a mixture of agglutinated and calcareous species and also many samples contained planktic specimens (*Neogloboquadrina pachyderma*). A basic description of the faunas found will be presented below along with a brief environmental interpretation starting with the cores in the outer section of Norske Trough.

Core PS100-129-01-GC

This core was collected from outer Norske Trough. A surface sample investigated contained an abundant agglutinated fauna dominated by *Adercotryma glomerata, Saccammina diflugiformis, Saccammina subfusiformis,* and *Trochammina nana.* There were also some calcareous species present in low abundances (e.g. *Cassidulina neoteretis, Elphidium albiumbilicatum*). The planktic foraminifera, *Neogloboquadrina pachyderma*, was also present. The agglutinated fauna present is indicative of an Atlantic Water influence at the sea floor (relatively warm and saline conditions).

Core PS100-127-01-GC

This core was also collected from the outer section of the Norske Trough. A sample towards the base of the gravity core collected at this site was investigated (170 cm). The fauna was dominated by calcareous species with the following species particularly abundant: *Cassidulina neoteretis, Cassidulina reniforme, Cibicides lobatulus, Elphidium excavatum forma clavata* and *Melonis barleeanum*. The planktic foraminifera, *Neogloboquadrina pachyderma*, was also abundant in this sample. The benthic fauna present in this sample is rather mixed; the presence of *C. neoteretis* suggests the presence of Transformed or Chilled Atlantic Water at this time, while the presence of *E. excavatum f. clavata* and *C. reniforme* in particular are indicative of colder Arctic Water.

Core PS100-171-01-BC

This core was collected from the mid-trough and a surface sample from the box core was investigated. The sample is characterised by an abundant and diverse assemblage, with particularly abundant planktic foraminifera (*N. pachyderma*). The benthic foraminiferal assemblage is dominated by calcareous species, but with some agglutinated species also present. Common species include *C. neoteretis, Islandiella hellenae, M. barleeanum and E. albiumbilicatum*. The fauna suggests the influence of the Atlantic Water on bottom waters in this region.

Core PS100-249-01-BC

This core was collected from the embayment in front of the present day margin of the ice shelf of 79N glacier. The surface sample investigated from the box core recovered a rich and diverse benthic foraminiferal assemblage dominated by calcareous species, but with some agglutinated species also present. Common species include: *C. reniforme, C. neoteretis, E. excavatum, I. hellenae* and *Quinqueloculina* spp. This fauna is slightly more mixed with evidence of Atlantic Water influence (*C. neoterestis*) but also evidence of colder Arctic Water (*C. reniforme* and *E. excavatum*).

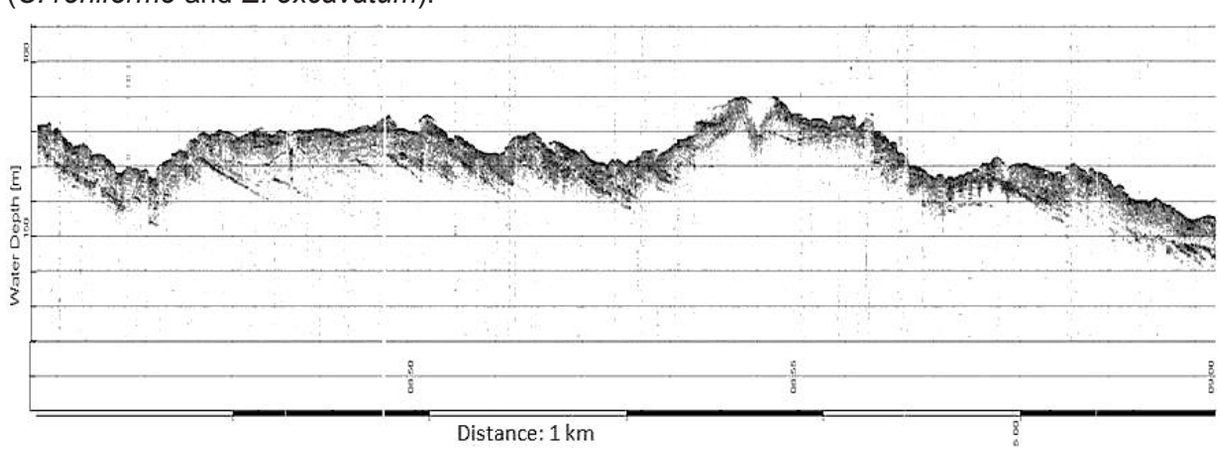

Fig. 4.11: Parasound image of distinctive dipping bedrock reflectors close to the seafloor. These are a common feature in the outer and mid sectors of the Westwind Trough and across parts of the Belgica Bank where the sediment cover is often very thin or removed by iceberg scour.

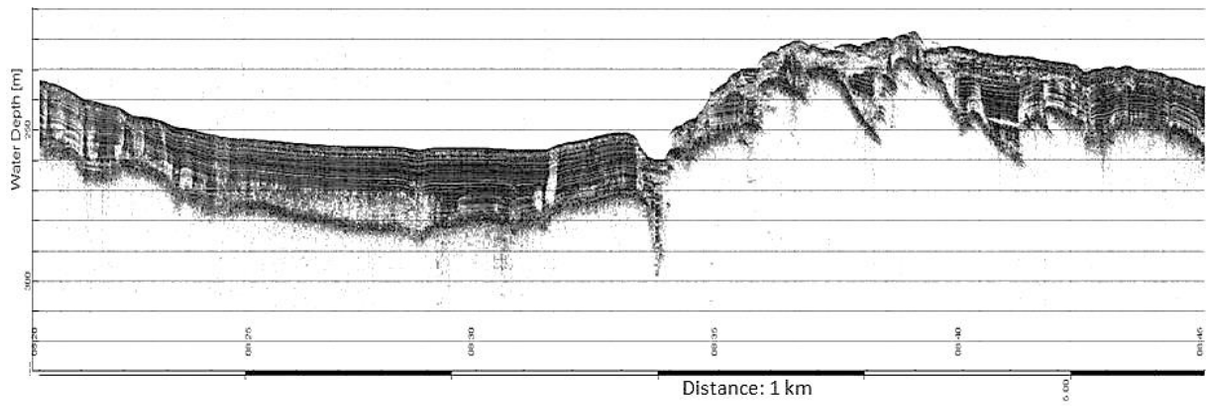

Fig. 4.12: Parasound image from the inner part of the Westwind Trough. Only on the inner shelf close to Dimphna Sund does the glacial sediment thickness increase with deep, deglacial sedimentary infills draped over the underlying bedrock.

Data management

A number of cores were split during cruise PS100, logged and described sedimentologically, but most cores remain unsplit. Samples were also taken from the cores for foraminiferal analysis. The cores will be shipped to Durham University for multi-sensor core logger (MSCL) measurements (e.g. bulk density, porosity, grainsize, P-wave velocities and water content), XRF and XCT 3D X-ray analysis. Foraminiferal, stable isotope analyses and sediment geochemistry (TOC, TN, C/N analysis) will also be conducted at Durham. The cores will be archived at AWI post analysis. Sample processing for radiocarbon dates (^{14}C) will be carried out at the NERC radiocarbon Laboratory, UK. All data will be uploaded to the PANGAEA database. Unrestricted access to the data will be granted after about three years from the end of the cruise, pending analysis and publication.

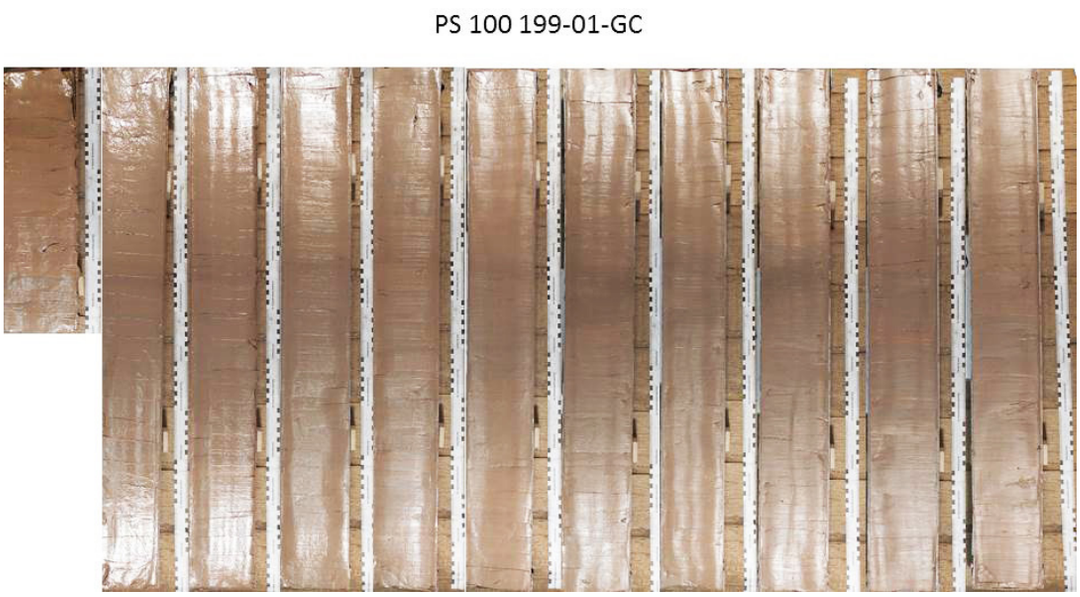

Fig. 4.13: Core PS100 199-01-GC displaying laminated clays with alternating red and grey colour bands.

Tab. 4.1: Core sample names and locational information details from PS100

Sample Name	Equipment	Latitude [N]	Longitude [W]	Water Depth [m]	Core recovery [cm]
PS100 126-01 GC	Gravity corer	76 44.637	7 13.250	312	22
PS100 127-01 GC	Gravity corer	76 45.549	7 28.353	312	183
PS100 128-01 GC	Gravity corer	76 51.081	8 13.080	344	141
PS100 129-01 GC	Gravity corer	76 54.15	8 38.64	362	286
PS100 143-01 GC	Gravity corer	77 5.309	10 14.304	449	197
PS100 144-01 GC	Gravity corer	77 7.495	10 34.239	496	217
PS100 144-02 BC	Giant box core	77 7.583	10.34.186	494	43
PS100 146-01 GC	Gravity corer	77 31.366	12 20.166	505	376
PS100 146-02 GC	Gravity corer	77 31.381	12 20.131	505	586
PS100 147-01 GC	Gravity corer	77 36.724	13 4.674	379	246
PS100 148-01 GC	Gravity corer	77 39.519	13 27.095	380	19
PS100 148-02 GC	Gravity corer	77 39.505	13 27.118	381	348
PS100 149-01 GC	Gravity corer	77 40.641	13 35.439	369	45
PS100 171-01-BC	Giant box core	78 8.449	16 50.139	542	51
PS100 171-02-GC	Gravity corer	78 8.482	16 49. 739	545	410
PS100 172-01-GC	Gravity corer	78 5.980	16 45.618	522	393
PS100 173-01-GC	Gravity corer	78 0.556	16 10.236	505	366
PS100 174-01-GC	Gravity corer	77 43.350	15 2.613	376	150
PS100 175-01-GC	Gravity corer	77 44.264	15 20.141	375	158
PS100 176-01-GC	Gravity corer	77 56.017	14 34.048	443	392
PS100 177-01-GC	Gravity corer	77 58.890	14 23.252	400	200
PS100 184-01-GC	Gravity corer	78 1.162	16 36.213	493	201
PS100 185-01-GC	Gravity corer	48 5.542	16 11.980	480	410
PS100 198-01-BC	Giant box core	79 11.333	17 6.950	393	44
PS100 198-02-GC	Gravity corer	79 11.474	17 6.430	398	960
PS100 199-01-GC	Gravity corer	79 10.390	17 14.023	400	1061
PS100 207-01-GC	Gravity corer	79 19.767	18 27.879	269	932
PS100 208-01-GC	Gravity corer	79 20.613	18 33.202	304	935
PS100 209-01-GC	Gravity corer	79 20.754	18 33.727	311	487
PS100 210-01-GC	Gravity corer	79 22.562	18 31.414	193	373
PS100 242-01-GC	Gravity corer	79 27.325	19 32.883	293	500
PS100 243-01-GC	Gravity corer	79 27.810	19 45.653	124	0
PS100 244-01-GC	Gravity corer	79 26.520	19 47.559	327	892

Sample Name	Equipment	Latitude [N]	Longitude [W]	Water Depth [m]	Core recovery [cm]
PS100 245-01-GC	Gravity corer	79 32.811	19 28.880	143	116
PS100 246-01-GC	Gravity corer	79 34.117	19 30.270	472	842
PS100 247-01-GC	Gravity corer	79 32.7	19 14.224	205	890
PS100 248-01-GC	Gravity corer	79 33.400	19 13.358	170	915
PS100 249-01-GC	Gravity corer	79 30.405	19 19.114	310	1000
PS100 249-02-BC	Gravity corer	79 30.411	19 19.202	310	0
PS100 269-01-GC	Gravity corer	79 30.429	18 18.108	470	886
PS100 270-01-GC	Gravity corer	79 29.824	18 8.399	424	944
PS100 275-01-GC	Gravity corer	80 9.748	17 23.960	166	782
PS100 276-01-GC	Gravity corer	80 8.502	17 13.049	170	671

References

AMAP (2011) Arctic Climate Issues 2011: Changes in Arctic Snow, Water, Ice and Permafrost. SWIPA 2011 Overview Report.

Bennike O, Weidick A (2001) Late Quaternary history around Nioghalvfjerdsfjorden and Jøkelbugten, North-East Greenland. Boreas, 30, 205-227.

Mouginot, J, Rignot E, Scheuchl B, Fenty I, Khazendar A, Morlighem M, Buzzi A, Paden J (2015) Fast retreat of Zachariæ Isstrøm, northeast Greenland. Science, DOI: 10.1126/science.aac7111

Nick F, van Der Veen CJ, , Vieli A, Benn D (2010) A physically based calving model applied to marine outlet glaciers and implications for the glacier dynamics. Journal of Glaciology, 56, 781–794.

Seroussi H, Morlighem M, Rignot E, Mouginot J, Larour E, Schodlok M, Khazendar A (2014) Sensitivity of the dynamics of Pine Island Glacier,West Antarctica to climate forcing for the next 50 years. The Cryosphere, 8, 1699–1710.

Straneo F, Sutherland D, Holland D, Gladish C, Hamilton GS, Johnson HL, Rignot E, Xu Y, Koppes M (2012) Characteristics of ocean waters reaching Greenland's glaciers. Ann. Glaciol., 53(60), 202–210.

Wilson NJ, Straneo F (2015) Water exchange between the continental shelf and the cavity beneath Nioghalvfjerdsbræ (79 North Glacier). Geophys. Res. Lett., 42, 7648–7654.

Winklemann D, Jokat W, Jensen, Schenkeb WK (2010) Submarine end moraines on the continental shelf off NE Greenland – Implications for Lateglacial dynamics. Quaternary Science Reviews, 29, 1069-1077.

Yin J, Overpeck JT, Griffies SM, Hu A, Russell JL, Stouffer RJ (2011) Different magnitudes of projected subsurface ocean warming around Greenland and Antarctica. Nature Geoscience, 4, 524-528.

5. OBSERVATION OF OCEANIC TRACE GASES: STABLE NOBLE GAS ISOTOPES (^{3}HE, ^{4}HE, NE) AND TRANSIENT TRACERS (CFCS)

Oliver Huhn[1], Jan Gerken[1], Timm Wegehaupt[1] [1]UHB-IUP

Grant-No. AWI-PS100_03

Objectives

Greenland Ice Sheet (GrIS) basal melting is one of the major contributors to GrIS ice mass loss and thus sea level rise, and accelerating melt rates are caused by intrusions of warm Atlantic Water into the sub-glacial cavity. However, estimates of submarine melt rates are usually based on indirect methods (difference between total mass loss from remote sensing methods and surface mass balance or estimated from measurements of ice velocities and ice thickness changes) and are still uncertain. So far, there are no sufficient data available that might allow to trace and to quantify the glacial melt water (GMW) in the ocean.

The major aims of our (first time) stable noble gas isotope and transient tracer observations in the vicinity of the 79° North Glacier (79NG, in northeast Greenland) are to investigate the interaction of the 79NG with ambient water masses (the warm Atlantic Water, AW) and to trace and quantify the (basal) GMW formed at the 79NG in its near and far field and in the East Greenland Current in Fram Strait.

Fram Strait is the most important gateway between the North Atlantic and the Arctic Ocean. Warm, saline AW is transported in the West Spitzbergen Current towards the North into the Arctic Ocean and partly recirculates, while cold Polar Water and fresh water from sea ice melting and glacial melting exits the Arctic Ocean in the East Greenland Current towards the North Atlantic.

We will also use the transient tracer data to investigate the transport and recirculation of water masses (AW, Polar Water, and GMW) in Fram Strait and on the east Greenland shelf, and the related oceanic transport and storage of (anthropogenic) carbon. Together with historic data we will assess the variability of the transfer of water masses and carbon.

Approach and methods

The oceanic measurement of the low-solubility and **stable noble gases** helium (^{3}He, ^{4}He) and neon (Ne) provide a useful tool to identify and to quantify (basal) GMW. Atmospheric air with a constant composition of these noble gases is trapped in the ice matrix during formation of the meteoric ice. Due to the enhanced hydrostatic pressure at the base of the shelf ice, these gases are completely dissolved in the water, when the ice is melting from below. This leads to an excess of Δ^4He = 1280 % and ΔNe = 890 % in pure GMW (Loose & Jenkins, 2015; the Δ stands for the noble gas excess over the air-water solubility equilibrium). Frontal or surface melt water would equilibrate quickly and not lead to any noble gas excess in the ocean water. With an accuracy of <0.5 % for He measurements performed at the IUP Bremen, basal GMW fractions of <0.05 % are detectable. The ^{3}He/^{4}He isotope ratio provides complementary information. Primordial helium (mantle helium with a far higher ^{3}He/^{4}He ratio, δ^3He ≈ 800 %)

enters the ocean from spreading regions of submarine ridge systems or other hydrothermal active sites like hydrothermal vents or submarine volcanoes.

The anthropogenic transient trace gases **chlorofluorocarbons** (CFC-11 and CFC-12) allow estimating the time scales of the renewal and ventilation of inner oceanic water mass transport. They enter the ocean by gas exchange with the atmosphere. Since the evolution of these transient tracers in the ocean interior is determined on first order by their temporal increase in the atmosphere and subsequently by advection in the ocean interior, they allow quantifying the time scales of subsurface water mass transport and formation. In a higher order approach, using the so called Transit Time Distribution (TTD) method (or water mass age spectra), they allow determining the integrated advection and mixing time scale of a water mass. These CFC and TTD method based time scales of ventilated water masses integrate residence, circulation, and transport and on the shelf, slope, and deep basin and allow determining water mass ventilation and formation rates. Combined CFC based time scales with noble gas and OMP based melt water inventories allow calculating basal glacial melting rates and the basal glacial melting induced WSBW formation rates.

Additionally, the CFCs and TTD method can be used to estimate the anthropogenic carbon content in deep water masses as in AW or PW by applying the CFC based TTDs to the well known atmospheric anthropogenic carbon history. That method is very reliable particularly in deep water masses and it is fully independent of carbon measurements and back calculating methods, which require additional geochemical observations or linear regression methods.

Work at sea

In total we took 650 water samples for stable noble gas isotopes (^{3}He, ^{4}He, Ne) in copper tubes from 69 stations in Fram Strait, on the north-eastern Greenland shelf and nearby 79NG (black circles in Fig. 5.1 and Fig. 5.2).

For the transient tracers (chlorofluorocarbons, CFC-11 and CFC-12), we took in total 740 samples on 61 stations in Fram Strait, on the north-eastern Greenland shelf and nearby 79NG (red dots in Fig. 5.1 and Fig. 5.2). Additional (SF_6, CFC-12) we took 190 samples on 19 stations on the north-eastern Greenland shelf and nearby 79NG (magenta dots in Fig. 5.1 and Fig. 5.2).

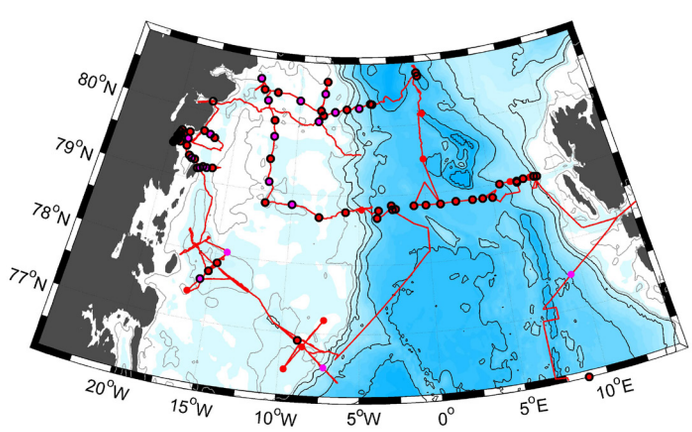

Fig. 5.1: Map of entire area of investigation indicating stations with noble-gas and transient tracer samples during PS100. Black circles are stations with noble-gas (He, Ne), red dots are stations with transient tracers (CFC-11, CFC1-12) and magenta dots with transient tracers (SF_6, CFC-12). The red line is the cruise track.

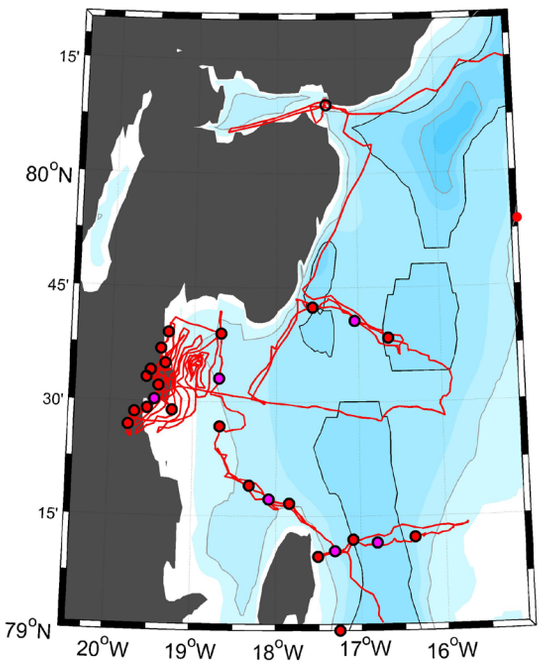

Fig. 5.2: Zoom into close vicinity of the 79NG indicating stations with noble-gas and transient tracer samples during PS100. Black circles are stations with noble-gas (He, Ne), red dots are stations with transient tracers (CFC-11, CFC1-12) and magenta dots with transient tracers (SF_6, CFC-12). The red line is the cruise track.

The water samples for helium isotopes and neon were stored from the CTD/water bottle system into gas tight copper tubes, which are clamped of at both sides. The noble gas samples are analyzed later in the IUP Bremen noble gas mass spectrometry lab. The copper tube water samples are processed in a first step with an ultra high vacuum gas extraction system. Sample gases are transferred via water vapor into a glass ampoule kept at liquid nitrogen temperature. For analysis of the noble gas isotopes the glass ampoules are connected to a fully automated ultra high vacuum mass spectrometric system equipped with a two-stage cryogenic trap system. The system is regularly calibrated with atmospheric air standards (reproducibility better ±0.2 %). Also measurement of blanks and linearity are done.

For the transient tracers (CFC) water samples from the CTD/water bottle system were collected into 100 ml glass ampoules and are flame sealed after a CFC free headspace of pure nitrogen had been applied. The CFC samples are later analysed in the CFC-laboratory at the IUP Bremen. The determination of CFC concentration will be accomplished by purge and trap sample pre-treatment followed by gas chromatographic (GC) separation on a capillary column and electron capture detection (ECD). The amount of CFC degassing into the headspace will be accounted for during the measurement procedure in the lab. The system will be calibrated by analyzing several different volumes of a known standard gas. Additionally the blank of the system will be analyzed regularly.

All samples will be shipped home after the expedition and will be analyzed in the UHB-IUP noble gas and CFC laboratories. The measurements are expected to be completed one year after arrival in our home lab in Bremen. A careful data quality check will be carried out then.

Expected results

As soon as the measured data are available, we will use the stable noble gas data (^{3}He, ^{4}He, Ne) to quantify the GMW inventories in the 79NG outflow region and its far field and to trace its pathways near the glacier and on the shelf and – if possible – even off the shelf.

We will use the transient tracer (CFC, SF_6) data to determine the time scales of circulation and residence to assess the formation rates of GMW (basal melting rates) of the 79NG.

We will use the transient tracer data from Fram Strait and the northeastern Greenland Shelf to trace the pathways, circulation and recirculation and the related time scales of AW and PW.

We will use the CFC and SF_6 data to estimate the anthropogenic carbon content in Polar Water and in AW and PW transferred through and recirculating in Fram Strait.

We will combine our new data set with available historic tracer data to assess possible temporal variability of transit times and carbon content and transfer in Fram Strait and on the northeastern Greenland Shelf.

Data management

All our data will be made public on the PANGAEA data base as soon as we have them available (approximately one year after the cruise), carefully quality controlled, and published in a peer reviewed journal. Our cooperation partners will receive the data as soon as the final data set is available.

Acknowledgements

We gratefully thank the master and crew of *Polarstern* for all support, maneuvering and running heavy gear, the oceanographic group of Torsten Kanzow et al. for providing water samples and hydrographic information, and AWI for the chance of participation.

6. GEOTRACES

Michiel Rutgers van der Loeff [1] and the GEOTRACES scientific party (the corresponding names of the participating party are listed under the respective articles)

[1]AWI

Grant-No. AWI-PS100_04

Objectives

GEOTRACES (www.geotraces.org) is an international programme that aims to determine global ocean distributions of selected trace elements and isotopes, including their concentration, chemical speciation and physical form, and to evaluate the sources, sinks and internal cycling of these species. This knowledge is needed to characterize more completely the physical, chemical and biological processes regulating their distributions so that the response of these cycles to global climate change can be predicted, and their impact on the carbon cycle and climate understood (Henderson et al., 2007).

Warming of Arctic terrestrial areas caused increased river discharge, which, combined with net loss of the Greenland ice cap and melting of sea ice, resulted in a freshening of surface waters and increased stratification. These climate-induced changes are expected to change the biogeochemical cycling and therefore the distribution of many Trace Elements and Isotopes (TEI's).

As part of a synoptic pan-Arctic GEOTRACES effort Polarstern had carried out a sampling program in 2015 (Expedition PS94) in coordination with Canadian and US initiated research cruises. The expedition PS100 in 2016 complements this pan-Arctic study with a detailed mapping of TEI distributions in the Fram strait. The objective is to constrain the TEI transport into and out of the Arctic through this major deep water opening between the Arctic and the World Ocean.

Work at sea

The sampling program of TEIs (Table 6.1) included all tracers considered as key TEIs by Henderson et al. (2007).

In total we have carried out 30 GEOTRACES stations (Tab. 6.2). At all but one of these stations we sampled with the Ultra Clean CTD while we collected ancillary parameters with the normal Rosette (Tab. 6.2). At 20 Large Stations (included in the GEOTRACES stations), large volume samples were collected for natural and artificial radionuclides and for rare earth elements and Nd isotope composition. At 12 Super Stations (a subset of the Large Stations) we additionally deployed in situ pumps to sample TEI in the particulate phase and to sample Radium isotopes.

Intercalibration and intercomparison are an essential part of the GEOTRACES program. Intercalibration samples were collected for intercalibration programs to be distributed among GEOTRACES partners.

Preliminary (expected) results

We will investigate for all GEOTRACES trace elements and isotopes whether a contrast exists between northward flowing Atlantic waters in the WSC and southward flowing waters of Arctic origin in the EGC. On board measurements of nutrients, CO_2 system, Hg, and radium isotopes already showed large differences in composition between these water masses.

From the concentration data observed in the northward and southward flowing water masses and in close cooperation with the physical oceanography team, we hope to be able to estimate import and export fluxes of trace elements across Fram strait.

From the composition of the southward flowing waters we hope to establish their origin, in terms of sources in the Siberian rivers and shelves through the Transpolar Drift, the Pacific Ocean through the Bering Strait inflow, or the Canadian and Greenland coast. The sampling right in front of the 79° Glacier (NEGIS) will allow us to investigate whether the circulation below the glacier tongue has an impact on trace element composition of the coastal water.

Data management

Intercalibration results from duplicate sampling will be submitted to the GEOTRACES Standards and Intercalibration Committee for evaluation and approval.

All data and metadata will be submitted to the international GEOTRACES data management office (BODC, www.bodc.ac.uk/geotraces) under the data management scheme agreed upon in the GEOTRACES programme available at http://www.geotraces.org. Most data and metadata will also be submitted to the PANGAEA database.

Reference

Henderson GM, Anderson RF et al. (2007) GEOTRACES - An international study of the global marine biogeochemical cycles of trace elements and their isotopes. Chem Erde-Geochem 67: 85-131.

Tab. 6.1: GEOTRACES and ancillary parameters sampled during PS100

GEOTRACES parameters	Name	Institute
Trace metals	Pablo Lodeiro, Stephan Krisch, Nicola Herzberg	GEOMAR
Particulate trace metals	Pablo Lodeiro, Stephan Krisch, Nicola Herzberg	GEOMAR
mercury	Lars-Eric Heimbürger	MIO Marseille
REE, Nd isotopes	Kirsten Meulenbroek	GEOMAR
Si, Ba isotopes	Kirsten Meulenbroek	GEOMAR
$^{230}Th/^{231}Pa$	Ole Valk	AWI
Radium isotopes, ^{228}Th	Michiel Rutgers van der Loeff, Dennis Koehler	AWI
Artificial radionuclides ^{129}I, ^{236}U	Núria Casacuberta	ETH, Zurich
Aerosols	Jaw Chuen Yong	GEOMAR
ancillary parameters		
Nutrients	Martin Graeve, Kai Uwe Ludwichowski	AWI

GEOTRACES parameters	Name	Institute
CO_2 and oxygen	Adam Ulfsbo	Uni Gothenburg/Duke University
	Elizabeth Jones	RuG/NIOZ
^{18}O	Dennis Koehler, Michiel Rutgers van der Loeff,	AWI
Dissolved and particulate organic matter	Martin Graeve	AWI
parameters collected for other groups	**name**	**contact person GRIFF**
Fe Ligands and TD Fe	Loes Gerringa, NIOZ	Pablo Lodeiro
Cu Ligands	Aridane González, LEMAR	Pablo Lodeiro
Pu-isotopes	Tim Kenna	Nuria Casacuberta
Pt	Jörg Schäfer, Univ. Bordaux	Lars Eric Heimbürger
Not-GEOTRACES related		
rubisco protein	Loes Gerringa, NIOZ	Pablo Lodeiro
Biomarker, ^{14}C	Gesine Mollenhauer	Dennis Koehler

Tab. 6.2: GEOTRACES Stations with Rosette types and cast numbers

Station	Station type	Ultra Clean cast	Large-Volume Rosette cast	ISP cast
PS100/0002	TEST		1	
PS100/0013	TEST	3		
PS100/0015	Super	1	2+5	3
PS100/0021		1		
PS100/0028	Super	1	2+4	3
PS100/0033	GT	1	2	
PS100/0037	Super	1	2+4	3
PS100/0042		1	2	
PS100/0044	Super	1	2+4	3
PS100/0050		1		
PS100/0052	Super	1+5	2+4	3
PS100/0053		2		
PS100/0056	Large	1	2+5	
PS100/0074 PS100/0075	Super	1	1	2
PS100/0082	Large	1	2	
PS100/0090	Large	1	2	
PS100/0094	Large	1	2	
PS100/0101	Super	1	2+4	3
PS100/0102	GT	1	2	

Station	Station type	Ultra Clean cast	Large-Volume Rosette cast	ISP cast
PS100/0103	Super	1	3+5	4
PS100/0135	Large	1	2	
PS100/0165	Super	1	2+4	3
PS100/0189	Super	1	2+4	3
PS100/0202	GT	1	2	
PS100/0214	GT	1	2	
PS100/0241	Super	1	2	3
PS100/0262	GT	1	2	
PS100/0274	Large	2	3	
PS100/0280	Large	1	2	
PS100/0285	Super	failed	1	2
PS100/0288	Large	1 (>250m)	2	
PS100/0290	GT	failed		
PS100/0291	Surface	1		

6.1 Nutrients, DOc and POc

Kai-Uwe Ludwichowski[1], Martin Graeve[1] [1]AWI

Objectives

The determination of nutrients and biogeochemical parameters is closely connected with the physical and planktological investigations. The development of phytoplankton blooms is especially dependent on the available nutrients. Nutrients are also well suited as tracers for the identification of water masses. Changes in nutrient concentrations will be followed in the Fram Strait region and across the Greenland shelf and slope. In comparison with similar transects in former years, the seasonal and interannual variability will be determined. In the 1980s and 1990s water masses of Pacific origin usually occurred in the shelf and slope regions of the Fram Strait and further south of the Greenland Sea. The nitrates *vs*. phosphate ratios in particular, but also silicate, are good tracers to follow the outflow of upper halocline Arctic surface water along the Greenland continental shelf and slope. Water masses may be especially rich in silicate compared to Atlantic waters. Providing baseline values for $\delta^{13}C$ and $\delta^{15}N$ isotopes of particulate organic matter (POM) is a further major aspect of this part of the GEOTRACES-project. Significantly higher ^{13}C enrichment in ice algae relative to pelagic phytoplankton allows for the tracking of carbon from ice algae and pelagic phytoplankton to higher trophic levels. The values are depending of various regional aspects of phytoplankton blooms and thus of the POM composition. The results will be used as baseline values for Bayesian multisource stable isotope mixing models (SIAR; Parnell et al., 2010).

Work at sea

Equipment and Methods

Nutrients were analysed with a SEAL QuAAtro 39, continuous flow auto analyser. CTD samples were measured unfiltered. Measurements were made simultaneously on five channels: phosphate, silicate, nitrate, nitrite, and ammonium. All measurements were calibrated with a five nutrient standard cocktail (All from Merck, traceable to SRM from NIST) diluted in artificial seawater (ASW), and ASW was used as wash-water between the samples. Each 20th run we checked our standards with Reference Material for Nutrients in Seawater (CRM 7602-a)

produced by NMIJ. Our standards and methods have been proven by inter calibration exercises like ICES and Quasimeme, and last year's RMNS exercise organised by Dr. Michio Aoyama National Meteorological Research Institute (NMIJ), Japan.

TOC samples were taken directly from the CTD Niskin bottles, filled in pre-cleaned HDPE bottles and immediately frozen at -20°C. At selected stations 8 L POC (2x2 L at Chl-a max and 2x2 L at 10 m) were taken from the Niskin bottles, filtered on Whatman GF/F filters (0.7 µm pore size) and stored at -80°C.

During this cruise we measured 2,510 samples: 300 samples from the ultra clean CTD (CTD-UC) and 2,210 from the large volume CTD. About 40 samples were measured for ammonia originating from on board excretion experiments with zooplankton organisms (H. Auel et al.). Additional nutrient samples, 300 from the CTD-UC and 350 from the large volume CTD, were frozen and will be analysed in the AWI home laboratory.

Preliminary (expected) results

The nutrients are important parameters allowing other parameters to be related to biological activity such as primary production and remineralization. Nutrients can also be used as tracers of water masses. Detailed analyses of TOC reveal its various terrigenous and marine sources throughout the Fram Strait and connected Fjord systems. Analysis of $\delta^{13}C$ and $\delta^{15}N$ of POM will highlight the interaction between sympagic and pelagic phytoplankton communities. This will be done by isotope ratio mass spectrometry in combination with an elemental analyser.

Data management

All nutrients data are available among all cruise participants. We plan that the full data set will be available as soon as possible, but about one and a half years after the cruise at the latest. After the cruise some re-analysis and quality management will be made before the data will be made available to the public via PANGAEA database. Data on total organic carbon and carbon and nitrogen isotope ratios of POC will be provided upon request by all cruise participants. The data for these specific parameters will be available at least within 1.5 years after the cruise. For additional information, please contact: Kai-Uwe Ludwichowski (kai-uwe.ludwichowski@awi.de) or Martin Graeve (martin.graeve@awi.de), Alfred Wegener Institute Helmholtz Centre for Polar and Marine Research, Am Handelshafen 12, 27570 Bremerhaven (+49 471 4831 -1419 or -1427).

References

Parnell A C, R Inger, S Bearhop and AL Jackson (2010) Source partitioning using stable isotopes: Coping with too much variation. PloS One 5: e9672.

The following references refer to methodological standards (not cited in text):

Grasshoff K, et al. (1983) Methods of seawater analysis. Verlag Chemie GmbH, Weinheim, 1983, 419 pp.

Murphy J, and Riley JP (1962) A modified single solution method for the determination of phosphate in natural waters. Analytica Chim. Acta, 27, p31-36.

Strickland JD, and Parsons TR (1968) A practical handbook of seawater analysis. First edition. Fisheries Research Board of Canada, Bulletin. No 167, p.65.

Pineault S, et al. (2013) The isotopic signature of particulate organic C and N in bottom ice: Key influencingfactors and applications for tracing the fate of ice-algae in the Arctic Ocean. Journal of Geophysical Research: Oceans, Vol 118, 1-14.

6.2 CO_2 System

Elizabeth Jones[1,2], Adam Ulfsbo[3], [1]NIOZ,
not on board: H.J.W. de Baar[1], L.G. Anderson[3] [2]RUG,
[3]UGOT/Duke

Objectives

The overarching objective of this study is to further improve our understanding of the carbon system in the rapidly changing Arctic Ocean and adjacent sub-regions. More specifically, we aim at improving our understanding of the feedbacks by physical and biogeochemical processes between the Arctic Ocean and the North Atlantic, across Fram Strait, and the Greenland-Iceland-Norwegian Seas with respect to the distribution of the seawater carbon dioxide (CO_2) system, air-sea CO_2 fluxes, transport of anthropogenic CO_2 and net community production. In addition, apart from hydrography, a thorough knowledge of the carbon system is essential for the understanding of the distribution of trace elements in the ocean in terms of their cycling, sources and sinks, supporting the onboard GEOTRACES programme.

In addition to the four core marine carbonate system parameters: dissolved inorganic carbon (DIC), total alkalinity (TA), pH, and the partial pressure of CO_2 (pCO_2), the on board participants were responsible for underway measurements of dissolved O_2/Ar (Section 6.2.1) and discrete samples for dissolved oxygen (Section 6.2.2.).

Work at sea

Seawater samples were taken from the Niskin bottles mounted to the large CTD rosette at depths throughout the water column, but with a bias towards the upper water column. Glacial ice was collected at 1 site from 79°N glacier and immediately sectioned into 4 and placed into individual 1 L PVF Tedlar bags and sealed with plastic clips. Excess air was removed with a Nalgene hand pump via Tedlar bag valve and sections were allowed to melt in the dark at laboratory temperature. Upon melting, usually within 20-24 hours, the bulk ice melt was carefully transferred to 250 ml borosilicate glass bottles using Tygon tubing for onboard CO_2 analyses. Samples for macronutrients were sampled directly from the Tedlar bag valve and frozen in 50 mL Nalgene bottles for analyses at AWI.

DIC and TA were determined on all seawater and glacial ice samples. Both DIC and TA are measured in parallel with a VINDTA 3C instrument (MARIANDA, Kiel). The accuracy is set by internationally recognized and widely used certified reference material (CRM), batches 127, 130, 154, obtained from Prof. A. Dickson at Scripps Institute of Oceanography (USA). DIC is the sum of all dissolved inorganic carbon species and is determined by a precise coulometric method (Dickson et al., 2007). For every coulometric cell that was used in the coulometer, at least two CRMs were measured in duplicate at the beginning and the end of the analyses, where differences in the measurements infer the precision of the instrument. The TA measurements were made by potentiometric titration with a strong acid (HCl) as a titrant. The acid consumption up to the second endpoint is equivalent to the titration/total alkalinity. The system uses a highly precise Metrohm Titrino for adding acid, a pH electrode and a reference electrode. The measurement temperature for both DIC and alkalinity was 25°C. Analyses were usually carried out immediately after sampling from the CTD and upon complete melt of the glacial ice sections. A total of 115 stations were sampled for DIC and TA (Table 6.2.1), totalling 2662 sample analyses. The precision for DIC and TA was determined from the in-bottle CRM duplicate analyses to be better than 2 µmol/kg. The accuracy was checked against frequent analysis of CRMs.

A total of 137 stations, comprising 1,614 sample analyses, were sampled for seawater pH (Table 6.2.1) using borosilicate bottles (250 mL), having tight plastic screw caps, and were

rinsed with at least one bottle volume and filled to the rim. All samples were thermostated to 25°C at least 30 min prior to analysis directly after sampling. Seawater pH was determined spectrophotometrically (Clayton and Byrne, 1993) using the sulfonephthalein indicator *m*-Cresol Purple (mCP). Purified mCP (Liu et al., 2011) was purchased from the laboratory of Robert H. Byrne, University of South Florida, USA. The indicator solution (0.2 mM) was prepared by dissolving pre-weighed mCP indicator in 0.5 L filtered seawater (0.20 µm) of about salinity 35. The indicator was adjusted to a pH in the same range as the samples, approximately ± 0.2 pH units, by adding a small volume of concentrated HCl or NaOH. Before running a set of samples, the pH of the indicator was measured using a 0.02 cm cuvette. The measurements were performed on board within hours of sampling. The shipboard setup is based on the absorption ratios of the indicator at wavelengths 434 nm, 578 nm, and 730 nm (background correction) using a 1-cm flow cuvette and a diode array spectrophotometer (Agilent 8,453). Each run consists of the three main steps; i) rinsing of tubing and cuvette with sample (15 mL) ii) sample blank (25 mL) and iii) sample run (20 mL) including indicator (0.5 mL). The sample is pumped and mixed using a Kloehn V6 syringe pump (Norgren) with a zero-dead volume syringe. Sample temperature is measured directly after the cuvette. The magnitude of the perturbation of seawater pH caused by the addition of indicator solution is calculated and corrected for using the method described in Chierici et al. (1999). The instrument setup is controlled by a PC running a LabView program (Fransson et al., 2013). The pH values are corrected to 25°C on the total scale. The overall precision from duplicate sample analysis was better than ±0.001 pH units. The accuracy is mainly set by the accuracy of the physico-chemical characterizations of the indicator with respect to temperature dependence and the determination of the equilibrium constants of the indicator, as well as the purity of the indicator (Liu et al., 2011). The accuracy was checked against Certified Reference Material for total alkalinity and total dissolved inorganic carbon, indicating that it should be well below 0.01 pH units.

Surface water partial pressure of CO_2 (pCO_2) was determined along the cruise track from the ship's underway seawater supply (Fig. 6.2.1). Sea surface pCO_2 is obtained with a General Oceanics (GO850) system with an infra-red analyser (LiCOR 7000), both for seawater using an water-air equilibrator and for the atmosphere, the air being pumped from the crow's nest.

Preliminary/Expected results

Across the Fram Strait, vertical profiles of DIC and alkalinity typically showed a high consistency below 500 m depth with increased values at intermediate depths in the northward flowing West Spitsbergen Current and in the warm Atlantic water that occupied the deepest layers across the survey region. Very low values for DIC and alkalinity occurred in the shallow surface layer near the 79°N glacier and near the sea ice edge and within other areas of recent sea ice melt, consistent with reduced salinity. Minima of sea surface pCO_2 of about 100 µatm occurred in these regions. As alkalinity is thought to be semi-conservative, the gradient within the deep water column was expected to be very low. This could be confirmed and revealed the high precision achieved with the analyses. The values of DIC and alkalinity in glacial ice had very low values compared to seawater samples and can be used to infer end-member values of the influence of glacial melt plumes of the seawater CO_2 system.

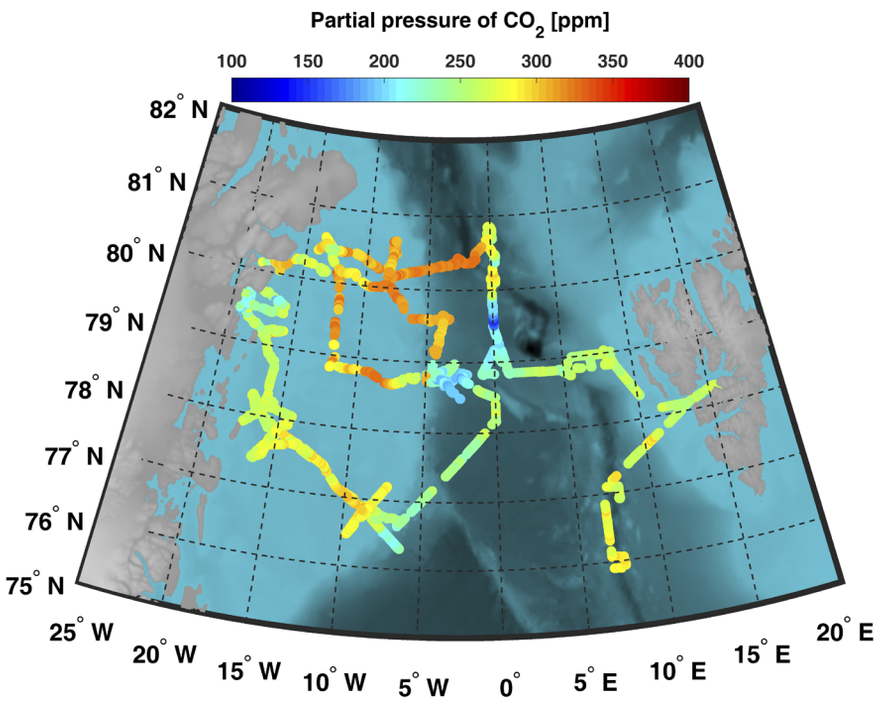

Fig. 6.2.1: Preliminary sea surface partial pressure of CO_2 (ppm) along the PS100 cruise track

6.2.1 Net community production using O_2/Ar ratios in surface waters

Adam Ulfsbo[1], Elizabeth Jones[2,3]

[1]UGOT/Duke,
[2]NIOZ,
[3]RUG

Objectives

The objective of this project is to estimate net community productivity in the Fram Strait using dissolved O_2/Ar measurements (Ulfsbo et al., 2014), investigate the physical and biological controls on oxygen saturation variability in the upper layers of Fram Strait, across the Greenland Shelf, and input of glacial melt water (Eveleth et al., 2014), as well as to constrain the biogeochemical controls on carbon fluxes. Oxygen in the mixed layer is influenced by biology, and by physical processes such as bubble injection, temperature and pressure changes. Because argon (Ar) has similar solubility properties as oxygen, the oxygen derived from physical processes can be estimated from the argon concentration relative to its saturation ($[Ar]_{sat}$). The oxygen derived from biology is equal to the total oxygen minus the oxygen derived from physical processes.

Work at sea

Biological oxygen supersaturation was measured continuously by Equilibrator Inlet Mass Spectrometry (EIMS, Fig. 6.2.2) provided by Nicolas Cassar, Duke University, USA, a method previously described (Cassar et al., 2009). Briefly, seawater from the ship's underway system was pumped through a gas equilibrator, the headspace of which was connected to a quadrupole mass spectrometer for continuous elemental O_2/Ar ratio measurements. The ion current ratio was calibrated by periodically sampling ambient air. From the O_2/Ar supersaturation, a gas exchange rate, and the oxygen concentration at saturation, the net biological oxygen flux across the ocean surface will be estimated. The oxygen optode (Aanderaa 4835) will be calibrated post-cruise against discrete Winkler samples from the ship's underway intake line.

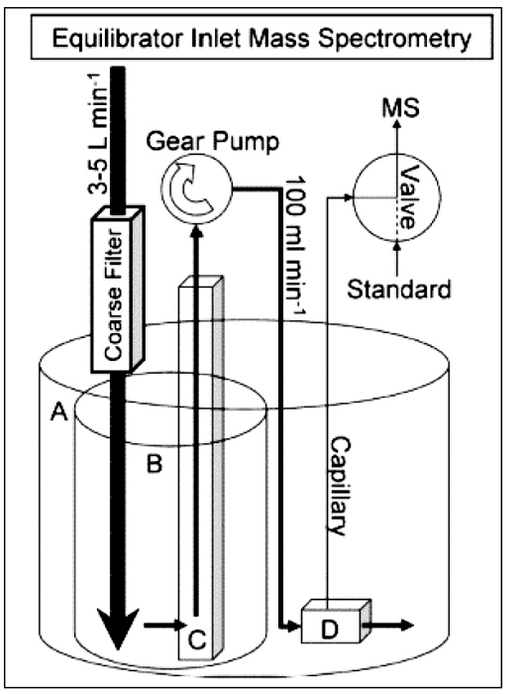

Fig. 6.2.2. Setup of the Equilibrator Inlet Mass Spectrometry. The large seawater reservoir (A) sits in a sink. After going through an inline coarse filter (500 µm pore size), seawater flows into the inner reservoir (B) at a rate of 3-5 L min^{-1} (large arrow). Most of the water running into B overflows into A, which is used as a water bath thermostated to the temperature of ambient seawater. A small fraction (100 mL min^{-1}) of the high flow rate is pulled with a gear pump through a filter sleeve (C), with 100 and 5 µm pore size on the outside and inside, respectively. From the gear pump, the seawater flows through the equilibrator (D). The equilibrator sits in reservoir A to keep its temperature identical to that of the incoming seawater. A capillary, attached to the headspace of the equilibrator, leads to a multiport Valco valve. This valve alternates between admitting gas from the equilibrator and ambient air to the quadrupole mass spectrometer. An optode (not shown) in container B measures total oxygen saturation. Also not shown is a water flow meter located downstream of the equilibrator and thermocouples monitoring temperatures through the system (from Cassar et al., 2009).

Preliminary/expected results

Our preliminary observations suggest net autotrophic conditions in the upper surface layer with largest biological activity in the West Spitsbergen Current and in the vicinity of the 79°N glacier.

6.2.2 Dissolved oxygen

Elizabeth Jones[1,2], Adam Ulfsbo[3]

[1]NIOZ,
[2]RUG,
[3]UGOT/Duke

Dissolved oxygen in seawater was determined by direct spectrophotometry of total iodine at 466 nm (Pai et al., 1993). The method is based on the classical Winkler method with respect to sampling and pickling reagents up to the point of titration with thiosulfate, according to the following redox-reactions:

$$2\ Mn^{2+} + 2\ OH^- \rightarrow 2\ Mn(OH)_2$$

$$2\ Mn(OH)_2 + O_2 \rightarrow 2\ MnO(OH)_2$$

$$2\ MnO(OH)_2 + 8\ H^+ + 6\ I^- \rightarrow 2\ Mn^{2+} + 2\ I_3^- + 6\ H_2O$$

First an excess of dissolved manganese and a strong base with an excess of iodide ions are added to the seawater sample, the Mn^{2+} is oxidized by the dissolved oxygen in the water to higher oxidation states and precipitates as $MnO(OH)_2$ to the bottom of the sample bottle. After a few hours, an excess of strong acid is added to the sample, to reduce the manganese back to the Mn^{2+} form. With the reduction of manganese the iodide ions become oxidized to iodine in the form of I_3^- ions, which has an intense yellow color, and was spectrophotometrically analysed using a flow-through cuvette (1 cm) and a peristaltic pump.

Work at sea

Samples for dissolved oxygen were collected from the specified Niskin bottle on the CTD rosette (Table 6.2.1). Samples for sensor calibration were typically taken below 400 m depth.

Samples were stored under water in the dark until analysis within one week of sampling. Standards for the calibration curve were prepared before each set of sample analyses using seawater from the ship‘s surface intake line. Pickling reagents and sulphuric acid were added in reverse order A pre-prepared potassium iodate standard solution (KIO_3, 70.16 mM) was added in a step-wise manner (0, 200, 300, 400, 500, 650, 750 µL). The calibration curve was fitted to a quadratic polynomial function since the spectrophotometer in use had a slightly non-linear response as determined pre-cruise. A total of 60 stations were sampled for dissolved oxygen.

Preliminary/expected results

The dissolved oxygen will be used for post-cruise calibration of the oxygen sensors mounted on the large (NIOZ) CTD-rosette and ultra-clean (GEOMAR) CTD-rosette.

Data management

The DIC, TA, pH, and pCO_2 data will undergo processing after the cruise. The final data will be submitted to data centers, as has been done with all data of previous cruises with *Polarstern*. The usual data center for carbon research is the Carbon Dioxide Information and Analysis Center (CDIAC; Boulder, USA). See chapter 6. for further details on data management.

References

Cassar N, Barnett BA, Bender ML, Kaiser J, Hamme RC, Tilbrook B (2009) Continuous High-Frequency Dissolved O_2/Ar Measurements by Equilibrator Inlet Mass Spectrometry. Analytical Chemistry, 81, 1855-1864, doi: 10.1021/ac802300u.

Chierici M, Fransson A, Anderson LG (1999) Influence of m-cresol purple indicator additions on the pH of seawater samples: correction factors evaluated from a chemical speciation model. Marine Chemistry, 65(3-4), 281–290, doi:10.1016/S0304-4203(99)00020-1.

Clayton TD, Byrne RH (1993) Spectrophotometric seawater pH measurements: total hydrogen ion concentration scale calibration of m-cresol purple and at-sea results. Deep Sea Research Part I, 40(10), 2115–2129, doi:10.1016/0967-0637(93)90048-8.

Dickson AG, Sabine CL, Christian JR (2007) Guide to best practices for ocean CO2 measurements, PICES Special Publication, 173 pp., North Pacific Marine Science Organization (PICES), Sidney, British Columbia.

Eveleth R, Timmermans M-L, Cassar N (2014) Physical and biological controls on oxygen saturation variability in the upper Arctic Ocean. J. Geophys. Res. Oceans, 119, 7420–7432, doi:10.1002/2014JC009816.

Fransson A, Engelbrektsson J, Chierici M (2013) Development and optimization of a Labview program for spectrophotometric pH measurements of seawater, pHspec ver 2.5, University of Gothenburg.

Liu X, Patsavas MC, Byrne RH (2011) Purification and characterization of meta-Cresol Purple for spectrophotometric seawater pH measurements. Environmental Science & Technology, 45(11), 4862–4868, doi:10.1021/es200665d.

Pai S-C, Gong G-C, Liu K-K (1993) Determination of dissolved oxygen in seawater by direct spectrophotometry of total iodine. Marine Chemistry, 41, 343-351.

Ulfsbo A, Cassar N, Korhone M, van Heuven S, Hoppema M, Kattner G, Anderson LG (2014) Late summer net community production in the central Arctic Ocean using multiple approaches. Global Biogeochemical Cycles, 28, doi:10.1002/2014GB004833.

Tab. 6.2.1: Stations and parameters sampled for DIC, TA, pH, and O_2.

Year	Month	Day	Station	Cast	DIC/TA	pH	O_2	Deployment
2016	7	22	15	1			x	UCC
2016	7	22	15	2	x	x	x	CTD
2016	7	23	15	5	x	x		CTD
2016	7	23	19	2	x	x		CTD
2016	7	23	20	1		x		CTD
2016	7	24	21	2	x	x		CTD
2016	7	24	22	1		x		CTD
2016	7	24	27	1	x	x		CTD
2016	7	24	28	1			x	UCC
2016	7	24	28	2	x	x	x	CTD
2016	7	25	28	4	x	x	x	CTD
2016	7	25	33	2	x	x		CTD
2016	7	26	35	1	x	x		CTD
2016	7	26	37	1			x	UCC
2016	7	26	37	2	x	x	x	CTD
2016	7	26	37	4	x	x		CTD
2016	7	27	38	1	x	x		CTD
2016	7	27	39	1	x	x		CTD
2016	7	27	42	2	x	x		CTD
2016	7	28	44	1			x	UCC
2016	7	28	44	2	x	x	x	CTD
2016	7	28	44	4	x	x		CTD
2016	7	29	46	1	x	x		CTD
2016	7	29	48	1	x	x		CTD
2016	7	30	52	2	x	x	x	CTD
2016	7	31	52	4	x	x		CTD
2016	7	31	54	1	x	x		CTD
2016	8	1	55	1	x	x		CTD
2016	8	1	56	1			x	UCC
2016	8	1	56	2	x	x	x	CTD
2016	8	1	56	5	x	x		CTD
2016	8	2	58	1	x	x		CTD
2016	8	2	60	1	x	x		CTD
2016	8	2	62	1	x	x		CTD
2016	8	2	64	1	x	x		CTD
2016	8	2	66	1	x	x		CTD
2016	8	3	68	1	x	x		CTD

Year	Month	Day	Station	Cast	DIC/TA	pH	O_2	Deployment
2016	8	3	69	1	x	x		CTD
2016	8	3	72	1	x	x		CTD
2016	8	4	75	1	x	x		CTD
2016	8	4	79	1	x	x		CTD
2016	8	4	80	1	x	x		CTD
2016	8	5	82	2	x	x		CTD
2016	8	5	84	1	x	x		CTD
2016	8	5	86	1	x	x		CTD
2016	8	5	87	1	x	x		CTD
2016	8	5	88	1	x	x		CTD
2016	8	5	89	1	x	x		CTD
2016	8	5	90	2	x	x		CTD
2016	8	6	92	1	x	x		CTD
2016	8	6	94	1	x	x		CTD
2016	8	6	96	1	x	x		CTD
2016	8	6	97	1	x	x		CTD
2016	8	7	98	1	x	x		CTD
2016	8	7	101	1			x	UCC
2016	8	7	101	2	x	x		CTD
2016	8	8	101	4	x	x		CTD
2016	8	8	102	2	x	x		CTD
2016	8	8	103	2			x	UCC
2016	8	8	103	3	x	x	x	CTD
2016	8	9	103	5	x	x		CTD
2016	8	10	109	1		x		CTD
2016	8	10	110	1		x		CTD
2016	8	11	111	1		x		CTD
2016	8	11	112	1		x		CTD
2016	8	11	113	1		x		CTD
2016	8	11	115	1		x		CTD
2016	8	11	117	1		x		CTD
2016	8	11	119	1		x		CTD
2016	8	11	120	1		x		CTD
2016	8	12	130	1	x	x		CTD
2016	8	12	132	1	x	x		CTD
2016	8	13	134	1	x	x		CTD
2016	8	13	135	2	x	x		CTD
2016	8	13	137	1	x	x		CTD

Year	Month	Day	Station	Cast	DIC/TA	pH	O_2	Deployment
2016	8	13	139	1	x	x		CTD
2016	8	13	141	1	x	x		CTD
2016	8	15	150	1	x	x		CTD
2016	8	15	151	1	x	x		CTD
2016	8	15	152	1	x	x		CTD
2016	8	15	153	1	x	x		CTD
2016	8	15	159	1	x	x		CTD
2016	8	16	160	1	x	x		CTD
2016	8	16	161	1	x	x		CTD
2016	8	16	162	1	x	x		CTD
2016	8	16	165	2	x	x		CTD
2016	8	16	166	1	x	x		CTD
2016	8	16	168	1	x	x		CTD
2016	8	18	186	1	x	x		CTD
2016	8	19	187	1		x		CTD
2016	8	19	188	1	x	x		CTD
2016	8	19	189	2	x	x		CTD
2016	8	19	190	1		x		CTD
2016	8	20	191	1	x	x		CTD
2016	8	20	192	1		x		CTD
2016	8	20	193	1	x	x		CTD
2016	8	20	194	1		x		CTD
2016	8	20	195	1	x	x		CTD
2016	8	20	196	1		x		CTD
2016	8	20	197	1	x	x		CTD
2016	8	21	200	1	x	x		CTD
2016	8	21	201	1	x	x		CTD
2016	8	21	202	1	x	x		CTD
2016	8	21	203	1	x	x		CTD
2016	8	21	204	1		x		CTD
2016	8	21	205	1	x	x		CTD
2016	8	21	211	1		x		CTD
2016	8	21	212	1	x	x		CTD
2016	8	21	213	1		x		CTD
2016	8	22	214	2	x	x		CTD
2016	8	22	215	1		x		CTD
2016	8	22	216	1	x	x		CTD
2016	8	22	217	1		x		CTD

Year	Month	Day	Station	Cast	DIC/TA	pH	O_2	Deployment
2016	8	22	219	1	x	x		CTD
2016	8	22	220	1	x	x		CTD
2016	8	22	222	1	x	x		CTD
2016	8	22	224	1	x	x		CTD
2016	8	22	226	1	x	x		CTD
2016	8	23	228	1	x	x		CTD
2016	8	23	230	1	x	x		CTD
2016	8	23	232	1	x	x		CTD
2016	8	23	234	1	x	x		CTD
2016	8	23	236	1	x	x		CTD
2016	8	23	237	1		x		CTD
2016	8	23	241	2	x	x		CTD
2016	8	25	250	1	x	x		CTD
2016	8	25	251	1	x	x		CTD
2016	8	25	252	1	x	x		CTD
2016	8	25	253	1	x	x		CTD
2016	8	26	254	1	x	x		CTD
2016	8	26	255	1	x	x		CTD
2016	8	27	260	1	x	x		CTD
2016	8	27	262	2	x	x		CTD
2016	8	27	264	1	x	x		CTD
2016	8	27	266	1	x	x		CTD
2016	8	27	268	1	x	x		CTD
2016	8	29	274	3	x	x		CTD
2016	8	30	278	1	x	x		CTD
2016	8	30	280	2	x	x		CTD
2016	8	31	282	1	x	x		CTD
2016	8	31	283	1	x	x		CTD
2016	8	31	285	1	x	x		CTD
2016	9	1	285	3	x	x		CTD
2016	9	1	288	2	x	x		CTD

6.3 Clean sampling systems for water column and aerosol samples

Pablo Lodeiro[1], Stephan Krisch[1], Nicola Herzberg[1], Jaw Chuen Yong[1], Florian Evers[1], E. Achterberg[1] (not on board)

[1]GEOMAR

Objectives

Working as part of the international GEOTRACES programme that aims to determine global ocean distributions and cycling of trace elements and isotopes with focus on concentration profiles including sources, sinks and chemical species, our work on the PS100 expedition is valuable for linking what is known for the arctic sea to the other world oceans. However, sampling for trace elements in oceanic waters requires specialized equipment. Only a handful of institutes in the world have the capacity to undertake trace metal clean water column sampling. During this cruise GEOMAR sampled for trace metal analysis in 30 stations operating a titanium conductivity, temperature, depth (CTD) rosette sampler (trace metal clean CTD) using a metal clean winch, with a dedicated Kevlar coated conducting wire. The winch (LEBUS UK) was placed on deck and operated by Florian Evers.

We also conducted sampling under trace metal clean conditions of aerosols and to characterise phytoplankton biomass, community structure and physiological status on cruise PS100. Atmospheric deposition is an important source of trace metals and nutrients source to the open ocean. The enrichment of these elements from the deposition could stimulate and enhance the biological community structure and function. Moreover, as phytoplankton are the primary driver of nutrient and carbon cycling in surface waters, and nutrient and carbon export to deeper waters, these measurements will also be valuable for interpreting chemical data collected on the cruise.

Work at sea

Seawater samples were obtained from the water column at 30 different sites using the GEOMAR trace metal clean CTD rosette (TM-CTD) equipped with 24 trace metal clean Go-Flo bottles. The TM-CTD water sampling rosette was attached to a conductive plastic coated Kevlar wire and was deployed over the side of the ship by a new trace metal winch. The TM-CTD was equipped with a Seabird temperature, conductivity, pressure, oxygen (two sensors of each) and turbidity sensor package. A Valeport altimeter was also attached to the the rosette. Due to the low water temperatures the closing mechanism of the Go-Flo bottles, based on the movement of an elastic rubber, was not working properly. The problem was solved changing all the original rubbers by a 10 mm stronger rubber.

Following the CTD casts, the 12L GoFlo bottles were immediately transferred to the GEOMAR clean container for processing of the samples. There, the samples were collected, and processed, if necessary, in a laminar flow hood.

Forty-eight hour duration on-deck incubation experiments were carried out in 1 L trace-metal-clean polycarbonate bottles. Seawater was collected at using the TM-CTD. Bottled seawater was spiked with the following combination of nutrients/trace metals: N, Fe, N+Fe, volcanic ash. Initial conditions were sampled in 1 L bottles for all experiments at 3 time points throughout the bottle filling procedure. Triplicate control bottles (1 L) with no nutrients added were also collected and alongside all treatment experiments. Bottles were placed in on-deck incubators connected to the ships underway flow-through system to continuously maintain temperatures at that of sea surface waters. After 48 hours incubation, experiments were taken down and measurements made for Chlorophyll-a concentrations (1 replicate per treatment bottle). Samples for flow cytometry and HPLC analysis were also collected and preserved frozen (-80ºC) to be analysed at GEOMAR.

Two high volume and one low volume aerosol collectors were placed on the A-deck for collection of trace element, and organic compounds. The units operated full time in an autonomous way. Both aerosol collectors were linked to an automatic control system to prevent the risk of contamination from the ship's diesel exhaust. The system monitored input from a digital wind vane and anemometer. The system was stopped to cut off the airflow when the wind direction and speed were outside specified limits. Overall, the low volume aerosol collector was collecting aerosol dust using polypropylene filters (0.45 µm nominal pore-size) and polycarbonate (0.4 µm nominal pore-size). These filters will be used to run dissolution experiments at GEOMAR after the cruise. The two high volume aerosol collectors constantly filtered air particles at the flow rate of approximately 1 m^3 min^{-1}. Due to air particles being relatively low abundant in FRAM strait, each filters were left to collect cumulative for 48 hours. Whatman 41 (W41) cellulose fiber filters and quartz microfiber filters were used to collect aerosol dust for trace elements determination and volatile analytes (Hg, water soluble organic carbon and nitrate).

Preliminary (expected) results

A total of 30 stations were sampled with success, resulting in more than 2,000 samples of trace metal clean seawater available for sampling for the different parameters. From the incubation experiments we will determine which nutrients are limiting phytoplankton growth in the Fram Strait. The high volume aerosol collectors have collected 15 samples for trace elements and volatile analytes respectively. There are another 52 samples which were collected from the low volume aerosol collector. These samples will be used for experiments and further determination analyses at GEOMAR.

Data management

See chapter 6. for details on data management.

References

The following references refer to methodological standards (not cited in text):

Browning TJ, Bouman HA and Moore CM (2014b) Satellite-detected fluorescence: decoupling non photochemical quenching from iron stress signals in the South Atlantic and Southern Ocean. Glob. Biogeochem. Cycles 28, 510–524.

Morton PL, Landing WM, Hsu S-C, Milne A, Aguilar-Islas AM, Baker AR, Bowie AR, Buck CS, Gao Y, Gichuki S, Hastings MG, Hatta M, Johansen AM, Losno R, Mead C, Patey MD, Swarr G, Vandermark A, and Zamora LM (2013) Methods for the sampling and analysis of marine aerosols: results from the 2008 GEOTRACES aerosol intercalibration experiment. Limnol. Oceanogr.: Methods 11, 62–78

6.4 Trace elements - dissolved Ag, Fe, Mn, Zn, Ni, Cu, Cd, Pb, Co

Pablo Lodeiro[1], Stephan Krisch[1], Nicola Herzberg[1], Jaw Chuen Yong[1], Florian Evers[1], E. Achterberg[1] (not on board)

[1]GEOMAR

Objectives

The objectives of this research cruise are to determine the processes (aeolian dust, re-suspension of continental shelf sediments and offshore transport processes) by which trace metals are supplied into and out of the Arctic Ocean through Fram Strait, and what mechanisms govern scavenge/uptake, solubility, mineralization or re-mineralization of dissolved trace metals. We will complete an overview of the distribution and key processes controlling biogeochemistry and mobilization of (co)-limiting nutrients for phytoplankton (Fe, Zn, Cd, Co, Mn, Cu and Ni) and toxic trace metals (Pb and Ag). The results together with our trace metal data collected in 2015 during TransARC II between Svalbard and Norway, as well as the PS94 Arctic expedition, will give us an estimate of the transport of trace metals between the Atlantic Ocean via the Greenland-Iceland-Norwegian Seas and the Arctic Ocean. The work will also extend our understanding of trace element cycling on Arctic shelf systems.

Work at sea

Along the different transects covering the full depth range from 150 down to 3,120 m seawater samples were obtained from the water column at 30 different sites using the GEOMAR trace metal clean CTD rosette.

After recovery the 12 L Go-Flo bottles were immediately carried to the trace metal clean sampling container. There, unfiltered seawater samples for total dissolvable trace metal analysis were transferred in acid washed 125 ml LDPE sample bottles. Another set of unfiltered samples for mercury, mercury-species, nutrients (filtered when not analyzed on board), salinity and oxygen analyses were collected in acid cleaned Teflon, LDPE, high density polyethylene bottles and glass bottles, respectively.

Filtered seawater samples for ligand (NIOZ (iron) and LEMAR (copper)), trace metal (GEOMAR and NIOZ), dissolved mercury and the protein Rubisco were obtained by applying a slight N2 overpressure (~0.2 bar) to the Go-Flo bottle and filtered the seawater through a 0.8/0.2 µm Acropak 500 cartridge filter (Pall). These samples were collected in acid cleaned 1000 mL, 125 mL LDPE, 60 mL Teflon and 15 mL HDPE bottles, respectively. In order to collect the soluble trace metal fraction, 125 mL of 0.2 µm filtered seawater were filtered through MQ washed 0.02 μm filters (Millipore). The filtrate was dispensed in acid washed 60 mL LDPE bottles. The particulate fraction of trace metals was collected over a 0.2 µm filter (Millipore) filtering ca. 4 L of seawater. The collected filters were rinsed with 10 mL of ultrapure water to remove the seawater matrix, and packed inside parafilm-sealed petri dishes.

Ligand and particulate samples were immediately transferred into a -20°C freezer and shipped frozen to be analyzed later on. The Rubisco samples were store at -80ºC. All trace metal seawater samples from the GEOMAR group were acidified to a pH<2 by ultra-pure grade hydrochloric acid (HCl, UpA Romil). The samples for TD-TM NIOZ were acidified adding 250 µL of HCl, Seastart UpA to each sample. Filtration and acidification of the samples were conducted in a laminar flow bench. The samples were stored in the dark and shipped for further analysis.

Preliminary (expected) results

We expect to be able to determine the fluxes of trace metals through Fram Strait into and out of the Arctic Ocean and to study shelf processes of trace metals. We plan to investigate the chemical speciation of Fe by investigating its organic complexation, its presence in colloids and its presence in the total dissolvable fraction. The trace metal content of soluble, dissolved, and total dissolvable seawater samples will be analyzed by the GEOMAR group by inline pre-concentration and isotope dilution inductively coupled plasma mass spectrometry (ID-ICP-MS, Element XR, Thermo).

Data management

See chapter 6. for details on data management.

References

The following references refer to methodological standards (not cited in text):

Johnson KS, Boyle E, Bruland K, Measures C, Moffett J, Aquilarislas A, Barbeau K, Cai Y, Chase Z, Cullen J, Doi T, Elrod V, Fitzwater S, Gordon M, King A, Laan P, Laglera-Baquer L, Landing W, Lohan M, Mendez J, Milne A, Obata H, Ossiander L, Plant J, Sarthou G, Sedwick P, Smith GJ, Sohst B, Tanner S, Van Den Berg S, Wu J (2007) Developing standards for dissolved iron in seawater. Eos Trans. 88, 131.

Klunder MB, Laan P, Middag R, De Baar HJW, van Ooijen JC (2011) Dissolved Fe in the Southern Ocean (Atlantic sector). Deep-Sea Res. II 58, 2678-2694.

Klunder MB, Bauch D, Laan P, De Baar HJW, van Heuven S, Ober S (2012a) Dissolved iron in the Arctic shelf seas and surface waters of the central Arctic Ocean: Impact of Arctic river water and ice-melt. J. Geophys Res. 117, C01027, doi:10.1029/2011JC007133.

Klunder MB, Laan P, Middag R, De Baar HJW, Bakker K (2012b) Dissolved iron in the Arctic Ocean: Important role of hydrothermal sources, shelf input and scavenging removal. J. Geophys Res. 117, C04014, doi:10.1029/2011JC007135.

Stoeven T, Tanhua T, Hoppema M, Appen W-Jv (2016) Transient tracer distributions in the Fram Strait in 2012 and inferred anthropogenic carbon content and transport. Ocean Science 12, 319-333.

6.5 Mercury

Lars-Eric Heimbürger[1] [1]MIO

Objectives

Mercury levels in Arctic biota are among the highest in aquatic ecosystems and impact the health of Arctic wildlife and human populations (AMAP, 2011). The idea has taken hold that the Arctic is a global mercury sink and that its main entry route is via the atmosphere (AMAP, 2011). A recent three-dimensional GEOS-Chem model run by Fisher et al. (2013) puts both ideas into question and argues that the Arctic Ocean is net source and boreal rivers to be the major input (Sonke and Heimbürger, 2012). Their findings shift current paradigms of the arctic mercury research that has focused for the past 20 years on atmospheric phenomena and cycling (e.g. atmospheric mercury depletion events). It has been shown for the Arctic (Beattie et al., 2014) and for Antarctica (Cossa et al., 2011) that sea ice, in particular brine formation is a major player in polar Hg budgets. Today, the relative contributions of sea ice dynamics, river inputs, transpolar drift and in/outflow at Fram Strait remain unclear. This is why the following key questions remain to be answered:

Is the Arctic Ocean a global sink or a source for mercury?

What is the cause for the high mercury concentrations in Arctic marine biota: anthropogenic Hg emissions or is that a “normal natural” phenomenon?

What is the impact of boreal rivers: how much of the dissolved and particulate mercury is transported to the central Arctic Ocean?

How much of the rapidly deposited mercury during atmospheric mercury depletion events is re-emitted to the atmosphere and which portion of it is bioavailable (bio-amplified along the marine food chain)?

What is the overall impact of warming climate to the arctic mercury cycle? Will warming climate shift mercury’s biogeochemical cycle and the functioning of the Arctic ecosystems is a way that we should expect even higher methylmercury levels in marine biota?

Our results from the 2011 Transarc (Heimbürger et al., 2015) and 2015 Transarc II cruises show that:

- Methylmercury levels in the Arctic Ocean are highest in the marginal sea ice zone and just below the halocline (~200 m-depth)
- Methylmercury concentrations are among the highest observed (together with the Mediterranean Sea (Heimbürger et al., 2010) and the Southern Ocean (Cossa et al., 2011)
- Contrary to the North Atlantic and other ocean basins, total mercury concentrations of the Central Arctic Ocean are surface enriched, and MeHg peaks much shallower (200 m compared to 1,000 m-depth in the North Atlantic)

Work at sea

Seawater

High resolution sampling for mercury species: Total dissolvable Hg (TD_Hg), Dissolved Hg (D_Hg), total methylated Hg (MeHg), MonomethylHg (MMHg), dissolved gaseous Hg (DGM; = Hg^0 + DMHg), with particular focus on in/outflow, halocline and gradient along the sea ice edge

- Analysis on board: TD_Hg, D_Hg and DGM
- Analysis at home lab: MeHg, MMHg and inorganic Hg

- Applications of new tracer: mercury stable isotopes to track sources and processes that govern Arctic Mercury cycling (sediments, suspended particulate matter)

We sampled for mercury species in seawater at all 27 GEOTRACES stations.

TD_Hg was determined on board on 525 samples (typically 24 depths resolution, with the exception of some of the shallow shelf stations) following a method that we had developed for the 2011 TransArc and the 2015 TransArC II cruises (Heimbürger et al., 2015).

D_Hg was sampled using Acropak filters (see section 6.3) and measured typically 8 depths spread in the upper part of the water column.

DGM was typically determined at 5 depths, including surface, chl-a maximum, 100 m, 200 m).

Unfiltered total MeHg was sampled at all stations (typically 20 depths) following also a method that we had developed for the 2011 Transarc cruise, and validated (Heimbürger et al., 2015). Acidification with double-distilled HCl (0.4 % v:v) rapidly converts dimethylmercury into monomethylmercury. We will therefore measure total methylmercury as the sum of both. On most stations we purged off dimethylmercury prior to acidification to determine, later on, MMHg alone. Methylmercury in seawater will be measured early 2017.

Zooplankton

The AMICA group provided a few samples. The samples consist in the selected material (copepods, Themisto, fecal pellets,…) from the multinet and bongo trawl sampling and incubation experiments. Excess water was removed and samples were frozen (-20°C). The samples will be freeze-dried and analyzed via CVAAS for total particulate mercury (USEPA, 2007), and if the quantity allows for particulate total methylmercury as well as mercury stable isotopic signatures.

Sediment

The glacial geology group provided 3 sediment cores that were subsampled from the box corer into multi-corer barrels, sliced on board into approximately 2.5 - 5 mm subsamples and stored in individual PE plastic bags. All samples were frozen (-20°C). If the results show consistent archives of Hg levels in the past, e.g. increases since the onset of the industrial revolution) then I would also request subsamples of the deeper gravity cores, likely covering a large part of the Holocene. The samples will be freeze-dried and analyzed via CVAAS for total particulate mercury (USEPA, 2007), and if the quantity allows for particulate total methylmercury as well as mercury stable isotopic signatures.

Suspended particles

The GEOTRACES natural radionucleide group provided QMA filters (142 mm) sampled at 50 and 100 m-depth (see section 6.7.1). The samples will be analyzed via CVAAS for total particulate mercury (USEPA, 2007). The large filtered volume should allow measuring particulate total methylmercury and mercury stable isotope signatures as well.

Aerosols

The GEOMAR group provided 15 subsamples of QMA filters for the determination of pHg. The samples will be freeze-dried and analyzed via CVAAS for total particulate mercury (USEPA, 2007).

Preliminary (expected) results

Alarming rise in Hg levels of Arctic marine biota has been attributed to increased anthropogenic Hg emissions. However, the Hg species that accumulates along the trophic chain is MMHg. MMHg (and DMHg) is produced in the oceanic water column during the remineralization of

organic matter. This process seems to be independent from atmospheric Hg deposition. The basis of the food web structure determines the amount of MMHg that is produced *in situ*. We will measure high resolution transect for Hg species at the Fram Strait passage. This is critical to understand the observed difference between the North Atlantic and the Arctic Ocean, the marine MeHg production as such and possibly to predict the impact of ongoing global warming on the Arctic Hg cycle.

- inorganic Hg and MeHg species were included in our Arctic Hg mass balance model (Soerensen et al., 2016), the new data in the central Arctic (PS94) and the in/outflow at Fram Strait (PS100) will allow to feed a coupled atmosphere-ocean 3D model
- Study possible temporal changes of North Atlantic inflow vs arctic outflow
- Exploring the role of the Arctic Ocean in the global mercury cycle

Our results will largely contribute to the understanding of mercury in the arctic, and we may say that the Arctic Ocean is not undersampled anymore. The shipboard TD_Hg and D_Hg indicate consistent surface enrichments, which is contrary to the global ocean. At a first glance the TD_Hg measurements also seem to confirm that the Hg outflow from the Arctic Ocean via the EGC exceeds the Hg inflow via the WSC. From our box model we had derived an outflow of about 50t and an inflow of 86t, but both and especially the outflow associated with a very large uncertainty (Soerensen et al., 2016). The new results from the PS100 cruise will allow narrowing that down.

Data management

See chapter 6. for details on data management.

References

AMAP (2011). AMAP Assessment 2011: Mercury in the Arctic. Oslo, Norway.

Beattie SA, Armstrong D, Chaulk A, Comte J, Gosselin M, Wang F (2014) Total and Methylated Mercury in Arctic Multiyear Sea Ice. Environmental Science & Technology 48(10): 5575-5582.

Cossa D, Heimbürger LE, Lannuzel D, Rintoul SR,. Butler ECV, Bowie AR, Averty B, Watson RJ,Remenyi T (2011) Mercury in the Southern Ocean, Geochimica Et Cosmochimica Acta 75(14): 4037-4052.

Fisher JA, Jacob DJ, Soerensen AL, Amos HM, Corbitt ES, Streets DG, Wang Q, Yantosca RM, Sunderland EM (2013) Factors driving mercury variability in the Arctic atmosphere and ocean over the past 30 years. Global Biogeochemical Cycles: 2013GB004689.

Heimbürger LE, Cossa D, Marty JC, Migon C, Averty B, Dufour A, Ras J (2010) Methylmercury distributions in relation to the presence of nano- and picophytoplankton in an oceanic water column (Ligurian Sea, North-western Mediterranean). Geochimica Et Cosmochimica Acta 74(19): 5549-5559.

Heimbürger, LE, Sonke JE, Cossa D, Point D, Lagane C, Laffont L, Galfond BT, Nicolaus M, Rabe B, Rutgers van der Loeff M (2015) Shallow methylmercury production in the marginal sea ice zone of the central Arctic Ocean. Scientific Reports 5.

Lamborg CH, Hammerschmidt CR, Bowman KL, Swarr GJ, Munson KM, Ohnemus DC, Lam PJ, Heimbürger LE, Rijkenberg MJA, Saito MA (2014) A global ocean inventory of anthropogenic mercury based on water column measurements. Nature 512(7512): 65-68.

Soerensen, AL, Jacob DJ, Schartup A, Fisher JA, Lehnherr I, St. Louis VL, Heimbürger LE, Sonke JE, Krabbenhoft DP, Sunderland EM (2016) A Mass Budget for Mercury and Methylmercury in the Arctic Ocean. Global Biogeochemical Cycles 30: 0.1002?2015GB005280.

Sonke JE, Heimbürger LE (2012) Environmental science: Mercury in flux. Nature Geosci 5(7): 447-448.

USEPA (2007) Method 7473.

6.6 Radiogenic isotopes and REE together with stable Ba and Si isotopes

Kirsten Meulenbroek[1], M. Frank[1] (not on board) [1]GEOMAR

Objectives

Tracing water mass mixing and continental inputs within the GEOTRACES programme is enabled through the application of radiogenic isotopes (neodymium, Nd) and Rare Earth Element distributions, which have residence times in seawater similar to the global ocean mixing time. Through weathering inputs, water masses are labeled with radiogenic isotope and REE signatures when they are in contact with the ocean's boundaries via dust, river inputs, or exchange with the particles of the shelf sediments. Continental rocks have distinctly lower $^{143}Nd/^{144}Nd$ than mantle rocks and young volcanic rocks (e.g. Frank, 2002) and together with REE patterns will allow the geochemical distinction of source waters in the Fram Strait and their mixing. This includes deep and shallow Atlantic and near surface Pacific Waters, as well as freshwaters originating from Siberian rivers and from meltwaters of glaciers supplied via the north-east Greenland Shelf, for which it is also planned to establish stable Ba isotopes as a new tracer. The new data will also serve to investigate the water mass variability in the upper 1,000 m via Nd isotope distributions based on results obtained during cruises in 2012 (Laukert et al, in prep.) and 2014.

Work at sea

99 large volume (20 liter) water samples were taken at several depths, mostly from the upper 1,000 m of the water column. 85 of these were subsequently filtered (at 0.45 µm), acidified, and $FeCl_3$ solution was added and all metals were coprecipitated at a pH of 8. The precipitate was separated for further treatment in the home laboratory (approximately 2 liters per sample). 2 liters of filtered and acidified water was separated before the iron solution was added and will be taken to the home laboratory for REE, Ba and Si isotope analyses. 14 samples were only filtered and acidified, the entire volume is taken home for further treatment. For 7 samples the precipitate was not separated, but the entire sample is taken to the home laboratory. At selected locations the entire water column was covered up to the bottom or 2,000 m water depth.

Expected results

We expect to find results leading to a better understanding of the annual variability of water masses and their mixing in the upper 1,000 m, in particular of the contributions from the Greenland shelf, the Pacific and the Siberian rivers, via the Nd isotope distribution. Therefore we will be comparing this year's results with those obtained in earlier cruises (2012 and 2014). Next to this we expect the Ba isotopic signal to be able to trace fresh water input with a terrestrial origin (glacial meltwater and river water in contrast to sea ice melting).

Data management

See chapter 6. for details on data management.

Reference

Frank M (2002) Radiogenic isotopes: Tracers of past ocean circulation and erosional input. Rev. Geophys. 40(1),1001, 10.1029/2000RG000094.

6.7 Natural radionuclides

Michiel Rutgers van der Loeff[1], Ole Valk[1], Dennis Köhler[1], Walter Geibert[1] (not on board) [1]AWI

Objectives

The unique conditions in the Arctic of input, removal, and exchange processes in relation to particle composition, particle fluxes, and circulation are acting on trace element and isotope distributions in the Arctic Ocean. These distributions are sensitive to the environmental changes already taking place in the Arctic. The simultaneous analysis of natural radionuclides with the other GEOTRACES key parameters on the same cruise and on the related expeditions in 2015 will provide a solid basis for the evaluation and modelling of biogeochemical processes in the Arctic.

Hypotheses:

1. Widespread ice melt and reducing ice cover allow terrigenous ice-rafted particles to settle out earlier in the central Arctic, enhancing the scavenging removal of ^{230}Th and ^{231}Pa within the Arctic and reducing their export through Fram Strait

2.^{228}Ra in Fram Strait can be related to its abundance in source waters on the Siberian shelf and used to estimate transit times

3.^{228}Th/^{228}Ra can be used as a tracer for export production with a long integration time

6.7.1 Long lived nuclides

Michiel Rutgers van der Loeff[1], Ole Valk[1], Dennis Köhler[1], Walter Geibert[1] (not on board) [1]AWI

Objectives

The study of Th isotopes and ^{231}Pa in the water column and particles in the Arctic will provide a baseline of their distributions for the evaluation of expected future changes in this rapidly changing environment.

Work at sea

Seawater samples for Th isotopes (^{230}Th, ^{234}Th, ^{232}Th) and ^{231}Pa were taken at 20 stations (5 to 15 depths per station) and directly filtered from Niskin bottles using AcroPak500 cartridges (0.45 µm pore size, Supor® pleated membrane). Dissolved isotope seawater samples were taken in volumes of 10-20 L per sample (20 L for 0-1,750 m, 10 L greater depths). All samples were acidified to pH 2 to 3.5 using ultra-clean concentrated (double distilled) hydrochloric acid. Suspended samples were taken at 12 stations at up to 14 depths using *in-situ* pumps (McLane and Challenger) equipped with pre cleaned (1N HCl and 18Ω MQ water) 0.45 µm pore size Supor® filters. Samples were cut in order to take subsamples under a laminar flow hood equipped with a HEPA filter. Subsequently the samples were stored at 0°C. At three stations samples for intercalibration studies between AWI, LDEO, NRM/LSCE and USM were taken.

Sediment samples for ^{231}Pa/^{230}Th analysis were taken at three stations from a box corer in an amount of ca. 100 g. At one station dirty ice samples (ice rafted sediments) were collected using a plastic bucket and then stored in sample bags at -20°C. The dirty ice will be melted under clean conditions and the particles will be collected by filtration over the same filter type used for suspended particles.

Expected results

We expect to quantify the import and export of ^{230}Th and ^{231}Pa from the Arctic Ocean through Fram Strait.

We hope to determine particle fluxes between the deep Fram Strait and shelves west off Svalbard and east of Greenland using ^{231}Pa and Th isotopes. A secondary goal will be to investigate particle transport from the 79°N Greenland glacier and the influence on radionuclide distributions.

Data management

See GEOTRACES introduction (section 6.) for details on data management.

6.7.2 Radium Isotopes and ^{228}Th

Michiel Rutgers van der Loeff[1], Ole Valk[1], Dennis Köhler[1], Walter Geibert[1] (not on board)

[1]AWI

Objectives

Four natural isotopes of radium (the radium quartet) occur in the ocean. ^{228}Ra (half life 5.8y) is a known tracer for shelf waters. It is strongly enriched in the Arctic shelves and in the Transpolar Drift waters that originate in the Siberian shelves (Rutgers van der Loeff et al., 1995). ^{223}Ra and ^{224}Ra are short lived (11.4 and 3.7 d half life, respectively). They can trace near-shore processes (Kadko et al., 2005) but can also be used as indirect tracer of the distribution of their parent nuclides, ^{228}Th (Rutgers van der Loeff et al., 2012) and ^{227}Ac (Geibert et al., 2008). The fourth isotope, ^{226}Ra (half life 1600yr), is stable on the time scale of mixing of the Arctic Ocean and can be used as yield tracer for the analysis of other isotopes. In previous expeditions we have studied the distribution of the radium quartet in surface waters and described the strong enrichment of ^{228}Ra in the Transpolar Drift derived from sources in the Siberian Shelf areas. Last year, during PS94, we have also studied depth profiles of these isotopes in the water column in the central Arctic and on the Bear Island Transect (Barents Sea Inflow) for the study of exchange rates between shelf/slope and open ocean. In the present expedition we wanted to measure the distribution of these isotopes in the water column in Fram Strait in order to follow the export of the ^{228}Ra-enriched waters of the Transpolar Drift towards the Norwegian Sea and Atlantic Ocean. We also investigated to what extent the particle-reactive intermediate nuclide ^{228}Th (1,9 y half-life) can be used to quantify particle settling and remineralization at depth.

FRAM - In the context of FRAM, we intend to take advantage of elevated production of ^{228}Th by ^{228}Ra released from the Siberian shelves. The ^{228}Th/^{228}Ra ratio integrates particle export and remineralization over timescales similar to the ^{228}Th half-life of 1.9 years. We will link this information to fluxes of main biogenic components and sediment trap fluxes, collected as part of FRAM. In order to achieve this goal, we have to address technological questions as well as questions of ^{228}Th distribution. The main goal of this contribution to the cruise program is therefore

(1) to evaluate the performance of the trace-element clean processing and detection of particulate ^{228}Th developed as part of FRAM to existing techniques for ^{228}Th measurement (collection and counting on acrylic fibre cartridges; alpha-counting of digested particles) and to ultra-clean trace element sampling performed as part of GEOTRACES.

(2) to establish the distribution of ^{228}Th/^{228}Ra ratios in the Fram strait as a background information for the interpretation of sediment trap data that will be collected as part of the previous cruise leg PS99.

Work at sea

Water column profiles – At 11 out of 12 deployments of the in-situ pumps (ISP, see section 6.7.1), we mounted 75-mm MnO_2-coated acrylic cartridges (Henderson et al., 2013) in the pumps at 8 to 13 depths to collect dissolved radium and thorium isotopes by adsorption on the MnO_2. Splits from the filters with suspended material collected with the in-situ pumps were analyzed for ^{228}Th with the newly developed trace-metal clean ^{228}Th detection system (modified RaDeCC developed as part of FRAM).

Surface water – Throughout the cruise, surface water samples were collected from the ship's seawater intake. During PS100, as during PS94, this intake was connected to the centrifugal pump with inlet close to the moon pool (Klaus Pumpe) at 11 m depth and was sampled close to this inlet to avoid possible ingrowth of ^{224}Ra from ^{228}Th adsorbed to the walls of the tubing. Seawater was prefiltered by passing over an uncoated cartridge and then passed over two MnO_2-cartridges (identical to the ones used in the in-situ pumps) connected in series for the collection of Radium. The absorption efficiency of the cartridges, derived from the activity ratio between the first and second cartridge, was 93±7%.

The activities of ^{223}Ra and ^{224}Ra were determined by alpha scintillation counting of the radon emanation in a delayed coincidence counting system (RaDeCC; Moore and Arnold, 1996). ^{228}Th was determined through a new generation of its daughter ^{224}Ra by a second RaDeCC count after a minimum of 20 days. This second count was completed on board for samples up to Sta 120 (Fig. 6.7.1) and will be continued in the home laboratory for the samples collected after 15 August. The ^{228}Ra/^{226}Ra ratio will be determined later in the home laboratory using gamma spectrometry or mass spectrometry.

At station 44 we collected 5-L samples for mass spectrometric analysis of ^{226}Ra.

Preliminary and expected results

As we found last year in the central Arctic, particulate material collected from the surface water with uncoated cartridges did not contain ^{224}Ra during sampling, but from the ingrowth of ^{224}Ra we could derive the distribution of particulate ^{228}Th.

The ^{228}Th distribution in the water column must be largely supported by parent ^{228}Ra and displays the sources of ^{228}Ra in surface water (especially from the shelf in the Trans Polar Drift) and at the seafloor. Most remarkable is the East-West contrast (Fig. 6.7.1). Whereas ^{228}Th activities are low in the West Spitsbergen Current, they increase sharply towards the West and reach activities in the East Greenland Current that are comparable to the activities we found in 2015 in the Transpolar Drift in the central Arctic.

The profiles we obtained on board of ^{228}Th activity in the West Spitsbergen Current show a clear reduction in the upper water layer. It is unlikely that this is due to reduced ^{228}Ra activities and we expect that this reduction is due to the sinking of organic matter by export production. The actual distribution of ^{228}Ra awaits further analysis at AWI. Once the concentrations of parent ^{228}Ra are available we will will interpret the ^{228}Th/^{228}Ra ratio as a measure of export production on a timescale of the half-life ^{228}Th (1.9 year), which averages out over a seasonal cycle in contrast to the usual method using ^{234}Th (half life 24 days). We will use the obtained estimates of ^{228}Th export rates to interpret ^{228}Th data collected in sediment traps during PS99, and to study remineralization and sinking of particles and associated trace metals in the Arctic. Additionally we will compare the data to ^{228}Th data and GEOTRACES trace metal data collected by established alternative techniques.

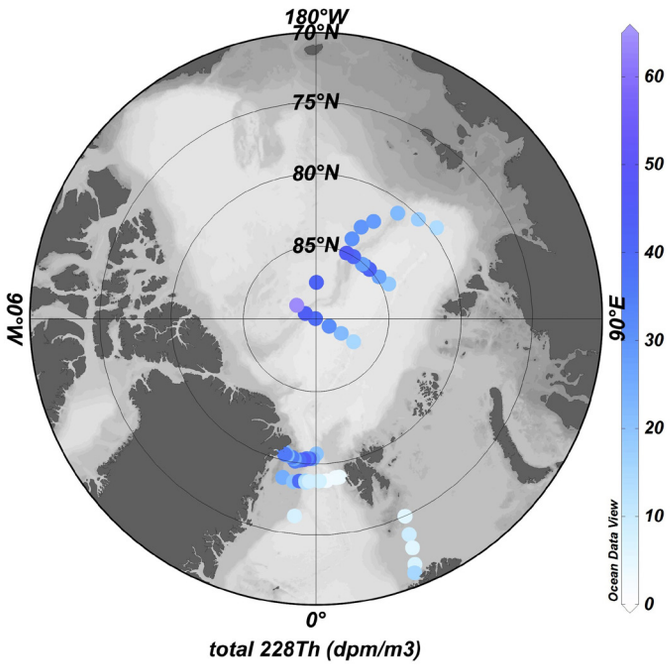

Fig. 6.7.1: Distribution of total ^{228}Th in surface water combining the data of expedition PS94 (ARK-XXVIII/3) and of the present cruise PS100 (ARK-XXX/2) up to station 120 showing the large contrast between the low concentrations in the inflowing Atlantic water and the high values in the East Greenland Current, likely derived from the Transpolar Drift.

W

The ^{228}Th distribution in the East Greenland Current showed a very strong vertical gradient at the halocline at a depth of about 50m (Sta 74). We expect that the distribution of parent ^{228}Ra, to be measured later, will have a similar distribution. The strong gradient can be used to constrain the vertical mixing rate across the halocline.

From the distribution of radium isotopes we hope to derive exchange rates of the shelf and slope with the open ocean at various depths. These exchange rates are needed in models describing the distribution of other tracers like ^{230}Th and ^{231}Pa. A long recount of the deep radium samples will be used to quantify ^{227}Ac. After correction for activity supported by ^{231}Pa, we will investigate whether there is a significant import or export of ^{227}Ac across Fram Strait.

Data management

See chapter 6. for details on data management.

References

Henderson PB, Morris PJ, Moore WS, Charette MA (2013) Methodological advances for measuring low-level radium isotopes in seawater. Journal of Radioanalytical and Nuclear Chemistry 296, 357-362.

Kadko D, Muench R (2005) Evaluation of shelf-basin interaction in the western Arctic by use of short-lived radium isotopes: The importance of mesoscale processes. Deep Sea Research Part II: Topical Studies in Oceanography 52, 3227.

Moore WS, Arnold R (1996) Measurement of ^{223}Ra and ^{224}Ra in coastal waters using a delayed coincidence counter. J. Geophys. Res. 101, 1321-1329.

Rutgers van der Loeff MM, Key RM, Scholten JC, Bauch D, Michel A (1995) ^{228}Ra as a tracer for shelf water in the Arctic Ocean. Deep-Sea Res. II 42, 1533-1553.

Rutgers van der Loeff MM, Cai P, Stimac I, Bauch D, Hanfland C, Roeske T, Bradley Moran S (2012) Shelf-basin exchange times of Arctic surface waters estimated from ^{228}Th/^{228}Ra disequilibrium. Journal of Geophysical Research - Oceans 117, C03024, doi:03010.01029/02011JC007478.

6.8 Anthropogenic radionuclides

Núria Casacuberta[1], Michiel Rutgers van der Loeff[2], Marcus Christl[1] [1]ETH/LIP, [2]AWI,
not on board: Christof Vockenhuber[1], Tim Kenna[3] [3]LDEO

Objectives

Artificial radionuclides have been widely used as oceanic tracers to study watermass circulation. Radioactive tracers (^{99}Tc, ^{90}Sr, ^{137}Cs and ^{129}I) dispersed from European nuclear fuel reprocessing plants located at Sellafield (formerly Windscale) in the UK and La Hague in France (Kershaw & Baxter, 1995) have proved particularly powerful to that aim. The discharged radioactive waste in coastal waters of northwest Europe has been used to track the water movement through the North Sea (Kershaw & Baxter, 1995), the Norwegian Coastal Current (Alfimov, Aldahan et al., 2004), the Arctic Ocean (Smith, Ellis et al., 1999; Smith, McLaughlin et al., 2011; Karcher, Smith et al., 2012) and the Nordic Seas (Alfimov, Aldahan et al. ,2004). The atmospheric weapon tests performed in the 1950's and 1960's have been another source of artificial radionuclides to the marine environment (Povinec, Aarkrog et al., 2005). Other than ^{137}Cs, ^{90}Sr, ^{99}Tc, ^{129}I, etc., in recent years, several studies have measured the anthropogenic occurrence of ^{236}U ($T_{1/2}$=23 My) in the ocean and pointed out its potential to become a new oceanographic tracer (Steier, Bichler et al., 2008; Christl, Lachner et al., 2012; Sakaguchi, Kadokura et al., 2012; Eigl, Srncik et al., 2013). Its conservative behavior in seawater and the fact that has it not yet reached steady state in the oceans, together with new developments in Accelerator Mass Spectrometry, proved that the ^{236}U/^{238}U atomic ratio can be used as a marker of water masses, particularly in the Arctic and Atlantic Oceans (Casacuberta, Christl et al., 2014). Atom ratios between different artificial radionuclides can be used to identify the sources of radionuclides in the (Kershaw and Baxter, 1995) marine environment (i.e. ^{240}Pu/^{239}Pu and ^{90}Sr/^{137}Cs) and track the water masses circulation (i.e. ^{129}I/^{137}Cs). For example, ^{129}I/^{137}Cs tracer measurements are used in simple mixing/advection models to estimate transit times from the North Sea to the Arctic Ocean. Similarly, and due to the different input functions of ^{129}I and ^{236}U from European reprocessing plants, the ^{129}I/^{236}U could become a potential tool in tagging the water masses in the North Atlantic and Arctic Oceans (Christl et al., 2012). The objective of our work during the PS100 cruise is to obtain a comprehensive dataset of artificial radionuclides in the Fram Strait to: i) constrain the sources of artificial radionuclides to the Fram Strait (i.e. global fallout, reprocessing plants, rivers); ii) use the ^{236}U/^{238}U atom ratio and ^{129}I/^{236}U to identify ocean currents and circulation patterns in this area (e.g. West Spitzbergen Current and East Greenland Current); iii) use the ^{236}U/^{238}U and ^{129}I/^{236}U to constrain the transit times of waters from the North Sea to the West Spitzbergen Current; and iv) use them as tracers of the water circulation in the Fram Strait.

Work at sea

A total number of 390 seawater samples (140 for ^{236}U and ^{129}I and 110 for Pu and Np isotopes) were taken for artificial radionuclide analysis during the PS100 cruise. Full depth profiles of different volumes were collected at 20 stations during the cruise track, covering the 79ºN transect from Svalbard to Greenland and part of the 80ºN section. 4 of these stations were located in the Norske Trough, following the section between the East Greenland Current and the 79N glacier. All samples were collected from a 24 bottles rosette coupled to a three Conductivity Temperature Depth (CTD) system.

For the analysis of ^{129}I, a subsample of 200 – 500 mL was taken and processed on board, following the method by Michel et al (2012). Briefly, Woodward iodine was added to the pre-calibrated sample and all iodine species were oxidized with $Ca(ClO)_2$ to iodate and subsequently reduced with NH_3OHCl and $NaHSO_3$ to iodide. After 45 minutes, pH was raised to 5-6 and

Iodine was extracted with a BioRad ® 1x8 anion exchange resin. Iodine was finally eluted with concentrated potassium nitrate solution (2.25 M) and precipitated as AgI. Precipitates were kept in filters for its final AMS measurement at ETH AMS Tandy (Zürich).

For the analysis of ^{236}U, 3 to 5 L samples were pre-processed on board. Samples were acidified and spiked with 3 pg of ^{233}U immediately after its collection. After 24 hours equilibration, uranium isotopes were pre-concentrated with Fe(OH)3 and kept in 250 mL bottles for its subsequent chemical analysis and measurement at ETH Zürich.

5 L samples were taken for Pu and Np isotopes analysis for Timothy Kenna (LDEO). Samples were stored in plastic cubitainers for its further delivery to US and its final analysis.

Expected results

The Fram Strait is the largest gateway to the Arctic Ocean and the only gateway allowing deep water exchange. Atlantic water flows northward in the West Spitsbergen Current while polar water and sea ice is transported southward in the East Greenland Current. Therefore, we expect our results will help constraining the inputs and outputs of artificial radionuclides to the Arctic and Atlantic oceans. This dataset will complement the already existing datasets of ^{236}U and ^{129}I of the past recent years, both in the Arctic and North Atlantic oceans taken in different GEOTRACES cruises. The quasi-synoptic view of distribution and fate of radionuclides will help constraining the main input sources of anthropogenic radionuclides to the marine environment (i.e. European reprocessing plants and global fallout) and identify other potential sources (e.g. Siberian rivers). Artificial radionuclides results will be coupled together with other anthropogenic tracers such as CFC's, SF_6, etc..

Results obtained from the concentration and atomic ratios of ^{129}I, Pu, Np isotopes and $^{236}U/^{238}U$ in the Fram Strait will be used as tracers of water circulation. We expect to find enhanced concentrations of these artificial radionuclides in the West Spitzbergen Current, carrying the signal of reprocessing plant-derived radionuclides. In contrast, we expect to find much diminished concentrations of artificial radionuclides in the East Greenland current, due to its longer transit time in the Arctic Ocean and dilution with water masses carrying a more reduced signal of artificial radionuclides (e.g. Pacific Waters). In addition, we also expect to be able to trace the recirculation of Atlantic Waters in the Fram Strait. To this aim, the $^{129}I/^{236}U$ atom ratio will be used in combination to $^{236}U/^{238}U$ ratio.

Pu and Np isotopes will be used as tracers for understanding sources, pathways, dynamics and the fate of pollutants and particles in the Fram Strait. Due to the well-defined spatial and temporal inputs of Pu, the long half-lives of ^{240}Pu and ^{239}Pu and its unique chemical properties, Pu can be used as tracer for various physical and biogeochemical ocean processes, including circulation, sedimentation and biological productivity, and hence a means of assessing the impacts of global climate change.

Data management

See chapter 6. for details on data management.

References

Alfimov V, A Aldahan, G Possnert, A Kekli and M Meili (2004) Concentrations of ^{129}I along a transect from the North Atlantic to the Baltic Sea. Nuclear Instruments and Methods in Physics Research Section B: Beam Interactions with Materials and Atoms 223–224(0): 446-450.

Alfimov V, A Aldahan, G Possnert and P Winsor (2004) Anthropogenic iodine-129 in seawater along a transect from the Norwegian coastal current to the North Pole. Marine Pollution Bulletin 49(11–12): 1097-1104.

Casacuberta N, M Christl, J Lachner, M R van der Loeff, P Masque and H A Synal (2014) A first transect of U-236 in the North Atlantic Ocean. Geochimica Et Cosmochimica Acta 133: 34-46.

Christl M, J Lachner, C Vockenhuber, O. Lechtenfeld, I Stimac, M Rutgers van der Loeff and H-A Synal (2012) A depth profile of uranium-236 in the Atlantic Ocean. Geochimica et Cosmochimica Acta 77(0): 98-107.

Eigl, R, M Srncik, P Steier and G Wallner (2013) $^{236}U/^{238}U$ and $^{240}Pu/^{239}Pu$ isotopic ratios in small (2 L) sea and river water samples. Journal of Environmental Radioactivity 116(0): 54-58.

Karcher M, J N Smith, F Kauker, R Gerdes and W M Smethie (2012) Recent changes in Arctic Ocean circulation revealed by iodine-129 observations and modeling. Journal of Geophysical Research: Oceans 117(C8): C08007.

Kershaw P and A Baxter (1995) The transfer of reprocessing wastes from north-west Europe to the Arctic. Deep Sea Research Part II: Topical Studies in Oceanography 42(6): 1413-1448.

Povinec P P, A Aarkrog, K O Buesseler, R Delfanti, K Hirose, G H Hong, T Ito, H D. Livingston, H Nies, V E Noshkin, S Shima and O. Togawa (2005) ^{90}Sr, ^{137}Cs and $^{239,240}Pu$ concentration surface water time series in the Pacific and Indian Oceans – WOMARS results. Journal of Environmental Radioactivity 81(1): 63-87.

Sakaguchi A, A Kadokura, P Steier, Y Takahashi, K Shizuma, M Hoshi, T Nakakuki and M Yamamoto (2012) Uranium-236 as a new oceanic tracer: A first depth profile in the Japan Sea and comparison with caesium-137. Earth and Planetary Science Letters 333–334(0): 165-170.

Smith J N, K M Ellis and T Boyd (1999) Circulation features in the central Arctic Ocean revealed by nuclear fuel reprocessing tracers from Scientific Ice Expeditions 1995 and 1996. Journal of Geophysical Research: Oceans 104(C12): 29663-29677.

Smith J N, F A McLaughlin, W M Smethie, S B Moran and K Lepore (2011) Iodine-129, ^{137}Cs, and CFC-11 tracer transit time distributions in the Arctic Ocean. Journal of Geophysical Research: Oceans 116(C4): C04024.

Steier P, M Bichler, KL Fifield, R Golser, W Kutschera, A Priller, F Quinto, S Richter, M Srncik, P Terrasi, L Wacker, A Wallner, G Wallner, K M Wilcken and EM Wild (2008) Natural and anthropogenic ^{236}U in environmental samples. Nuclear Instruments and Methods in Physics Research Section B: Beam Interactions with Materials and Atoms 266(10): 2246-2250.

7. STRUCTURAL VIBRATION

Keith Soal[1], Rosca de Waal[1], [1]Stellenbosch U
not on board: A. Bekker[1], J. Bienert[2] [2]TH Ingolstadt

Grant-No. AWI-PS100_05

Objectives

The aim of this project is the characterization of ship dynamic responses due to complex ice-structure and fluid-structure interactions, using operational modal analysis (OMA). This will enable investigations into structural health monitoring of the vessel, as well as fatigue life estimations. This data will also be used to estimate global ice and wave loads on the vessel hull and shaft line using a novel inverse force estimation method.

The main scientific questions include:

1. How do the various fluid-structure and ice-structure interactions occurring during real operation affect the dynamic response of the vessel hull and shaft line?
1. Is it possible to accurately estimate the ice loads on the ship hull from rigid body and elastic motion using a novel inverse technique?
2. Are these data driven structural dynamic models able to improve the fatigue life estimation and design optimization of ships through finite element model (FEM) updating?
3. Are vibration sensors able to accurately monitor the structural health of the vessel based on modal migration?
4. How do the different hull designs of *Polarstern* and the *S.A. Agulhas II* (South African polar supply and research vessel) compare in terms of their dynamic response?
5. What are the effects of ice impacts and cavitation on the dynamic performance of the shaft line?
6. Is it possible to estimate the propeller loads and fatigue life from shaft line measurements?

Work at sea

The cable network required for this research was installed over two and a half weeks during ship yard time in Bremerhaven in 2016. The sensors and data acquisition systems for the hull and shaft line were then installed while in the harbor in Tromsø. The system was then configured and tested during the first few days at sea. During the voyage the team monitored both recording systems and synchronized the recording times to the DShip system. Data was continually extracted and pre-processed. This provided insight into the data quality and often required sensors to be checked or fixed. During the voyage certain sensors required further electrical grounding and one cable required re-soldering. Due to a malfunction in the Lord MicroStrain wireless data transmission system it was required to stop the port side shaft

line during several short periods in order to test and rectify these faults. Various parameters were downloaded and monitored on the DShip system during the voyage. Technical drawing specifications were obtained from the chief engineer and stability information was collected from the captain throughout the voyage. During ice navigation ice observations were conducted from the bridge. These observations were recorded in an excel sheet and provide estimates of the ice concentration, thickness and floe size. At AWI's request measurements were conducted on a sensitive equipment mounting in the bow thruster room during ice and open water navigation. Measurements were also conducted for the University of Bremen on an infra-red camera mounting on the crow's nest during ice navigation. Modal analyses was also conducted on a spare propeller blade.

Preliminary results

Preliminary results are presented in six sections namely hull vibration measurements, shaft line measurements, ice observations, AWI sensitive equipment measurement, Bremen University infra-red camera measurements and propeller blade operational modal analyses.

Hull vibration measurements

Vibration measurements were conducted continuously throughout the voyage at 23 locations as shown in Fig. 7.1. Post processing revealed high data quality, and the measurement system ran without any major problems throughout the voyage, collecting an extremely valuable full scale data set. A visualization of a measured signal in the frequency domain is presented in a spectrogram in Fig. 7.2. Here it can be seen that discrete peaks occur at 2.89 Hz, 5.19 Hz and 7.01 Hz which are identified from an eigenvector analyses as vertical bending modes of the vessel, see Fig. 7.3. The vessels main engine's running at 620 rpm can also be seen at 10.3 Hz. These modes will be used together with a larger modal set, in order to investigate the dynamic response of the vessel to different ice and open water conditions. The modal model will then be used to estimate ice forces using a novel inverse technique. Investigations will also be conducted into the possibility of using vibration data for structural health monitoring on the *Polarstern.*

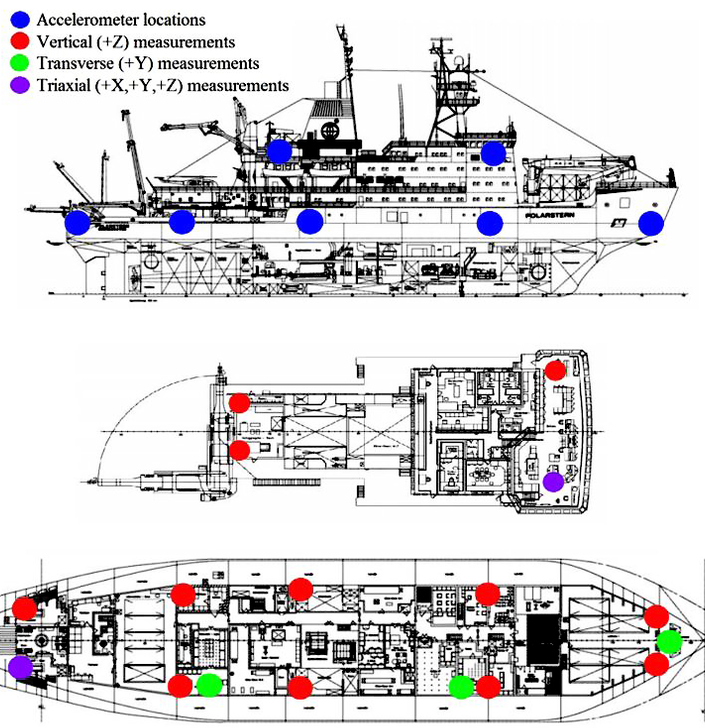

Fig. 7.1: Hull vibration measurement locations

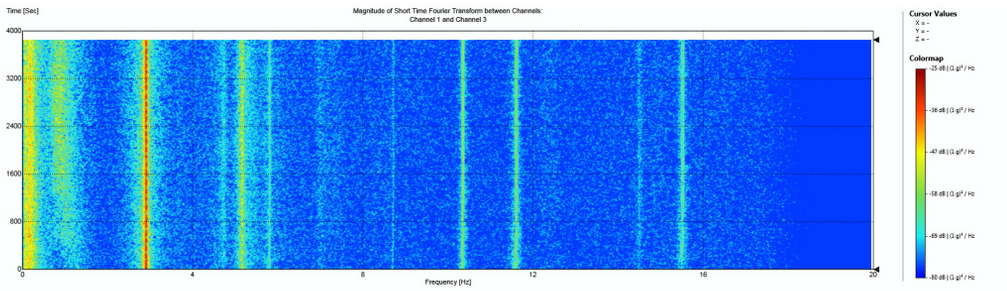

Fig. 7.2: Spectrogram of accelerometer measurements in the bow during 14 knots in open water

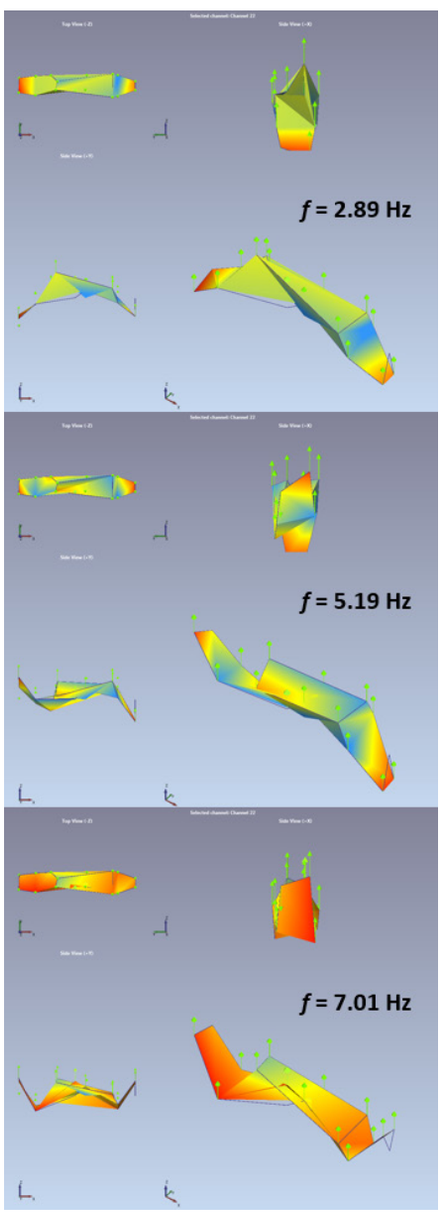

Fig. 7.3: Vertical bending modes of the Polarstern during 14 knots in open water.

Shaft line measurements

Torque and thrust were measured using strain gauges on the shaft line and a wireless transmission system, as presented in Fig. 7.4. Vibration was measured using accelerometers mounted on the main bearings and rpm was measured using a proximity sensor. The results of two operating conditions are presented, namely ice impacts (Fig. 7.5) and cavitation (Fig. 7.6). From these two cases it is evident that there is a much greater effect on torque during ice impacts compared to cavitation. Cavitation exerts a greater force along the axis of the shaft and therefore a much greater thrust force is experienced compared to the torsional force. Initial results show interesting differences between the *S.A. Agulhas II* and the *Polarstern*. The reasons for these differences in terms of design, operation and ice conditions will form part of further investigations. This information will be used to solve an inverse method problem of determining propeller blade loads from shaft line measurements.

Ice observations

Ice observations were conducted from the bridge during ice navigation in Fram Strait as well as off the Greenland coastline. Observers performed 10 minute averaged visual estimations of ice concentration, ice thickness and floe size. Other parameters included snow thickness, brash ice, number of rams and a subjective vibration estimate. The measurement stick with 50 cm markings used to estimate ice thickness is presented in Fig. 7.7. The results of ice concentration, thickness and floe size are presented in Fig. 7.8. Preliminary findings include a maximum thickness of 3 m, an average thickness of 96 cm, an average concentration of 35 % and an average floe size of 231 m.

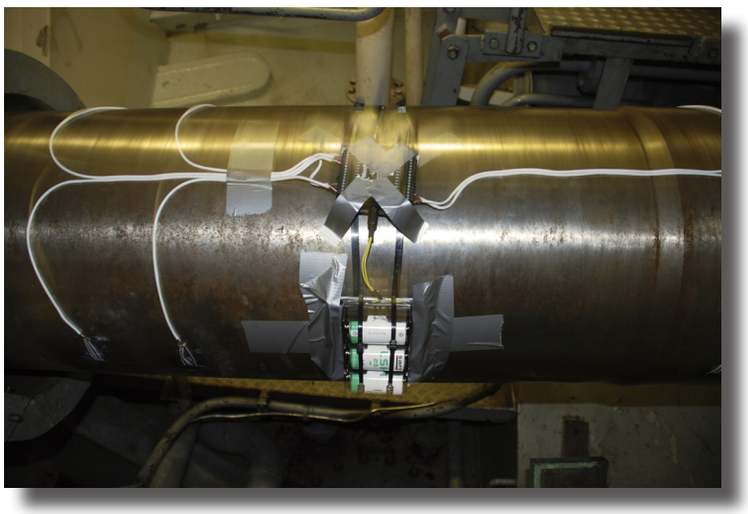

Fig. 7.4: Torque and thrust measurement setup on the shaft line

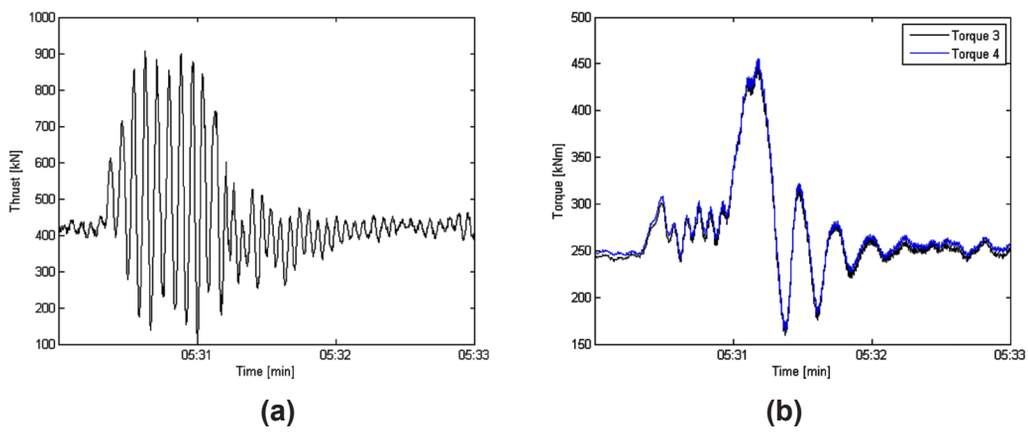

Fig. 7.5: Measurements during ice navigation for (a) thrust and (b) torque

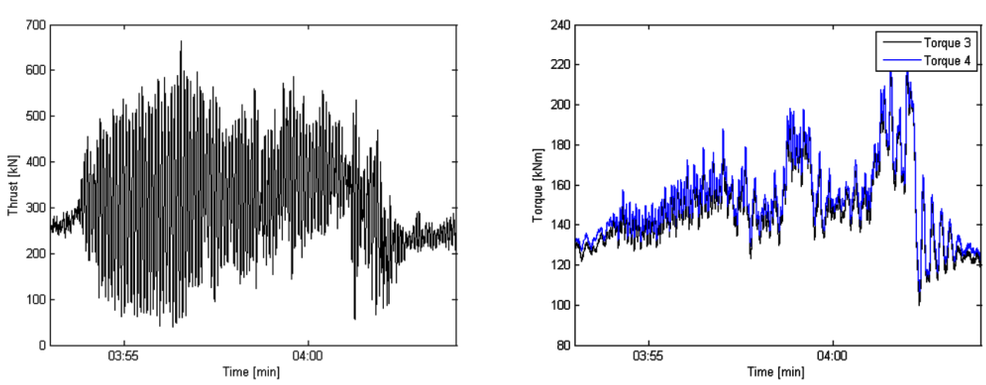

Fig. 7.6. Measurements during cavitation for (a) thrust and (b) torque

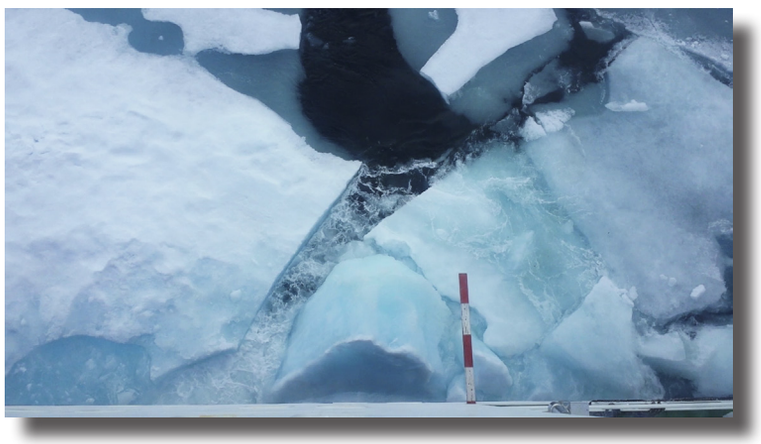

Fig. 7.7. View of the ice field from the bridge with the thickness measuring stick

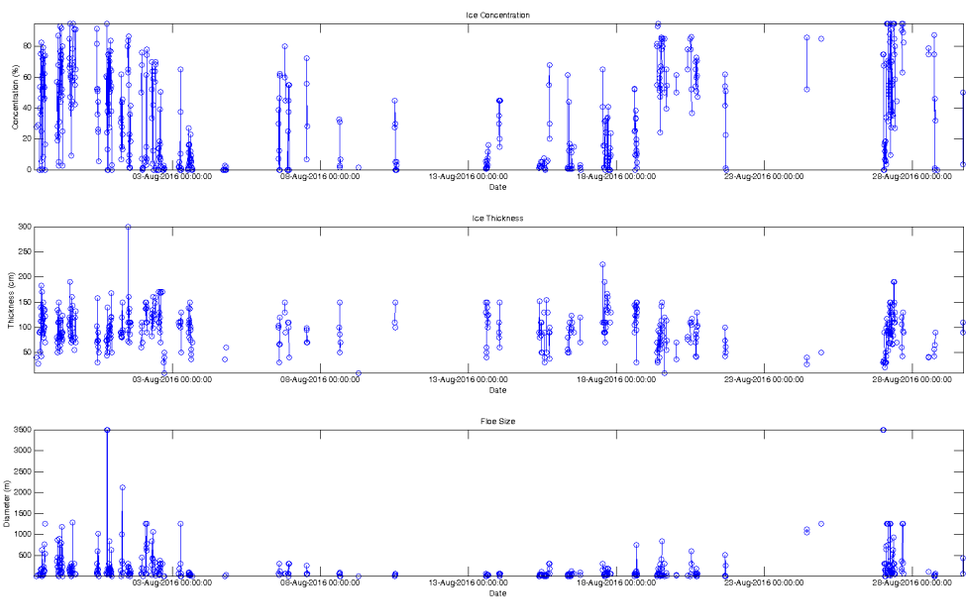

Fig. 7.8. Ice observation parameters

AWI sensitive equipment measurement

Measurements were conducted for AWI on a sensitive equipment mount in the bow thruster room as shown in Fig. 7.9. Measurements were conducted during ice and open water navigation on the frame structure both before and after the current vibration isolator. The frequency content of vibration in the +x, +y and +z directions are shown in Fig. 7.10 a), while the difference across the vibration isolator is shown in Fig. 7.10 b). It can be seen that the current isolator works well in damping out vibration energy in the bandwidth 50 Hz – 2 KHz. Lower frequencies can however be amplified and the requirements of specific sensitive equipment should be considered before mounting in this location. Further details are available in a report submitted to AWI.

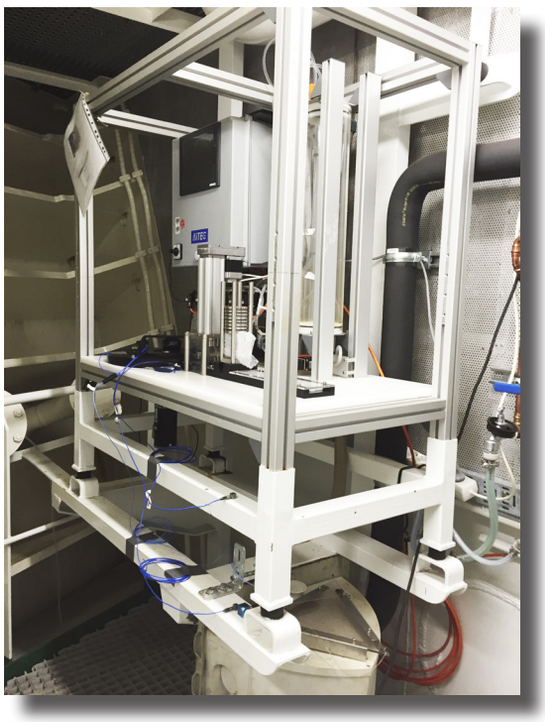

Fig. 7.9. AWI sensitive equipment mounting

Bremen University infra-red camera measurements

Vibration measurements were conducted in three directions on an infra-red camera mounting which is located on the crow's nest of the *Polarstern*. Measurements were conducted during ice navigation and the results are presented in a report to Uni Bremen.

Propeller blade operational modal analyses

Operational modal analyses was conducted on a spare propeller blade. The blade was randomly excited using a large hammer with a piece of rubber strapped to the impact surface. Modes were clearly identified using a frequency domain decomposition technique in the ARTeMIS software. The first six modes are presented in Fig. 7.11. This provides valuable information about the energy signature entering the vessel through the propeller.

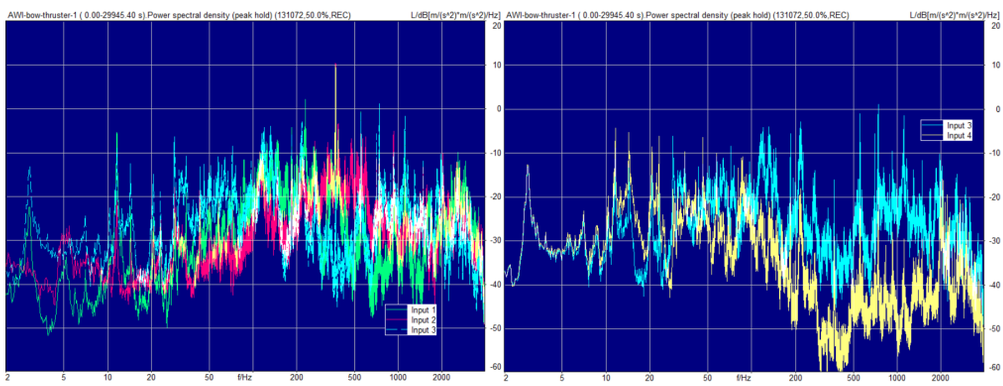

(a) **(b)**

Fig. 7.10. Power spectral density of AWI sensitive accelerometer measurements with (a) before isolator and (b) before and after isolator in the z direction

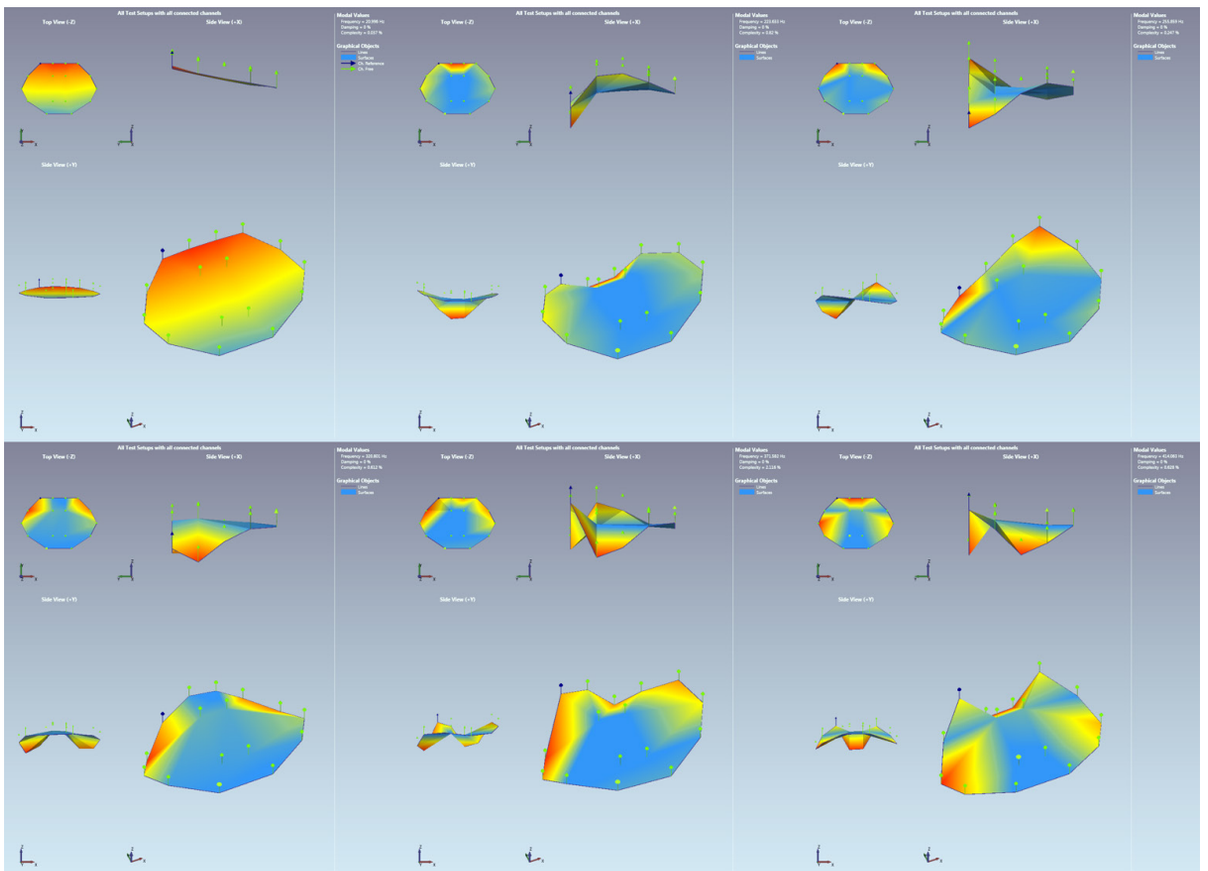

Fig. 7.11: Propeller blade mode shapes

Data management

The results from the data processing will be published in peer-reviewed articles and journals for access to the wider scientific community. There are also plans to publish parts of the, very large, raw data set in order to provide a benchmark full scale case study as a platform to test improvements to existing algorithms as well as new structural dynamic algorithms. Discussions are also underway in order to make the raw data available for planning purposes of the new *Polarstern*.

Acknowledgements

We are extremely grateful to AWI and the *Polarstern* crew for the fantastic support in making this research vision a reality. The professionalism and willingness to help shown by captain Schwarze and his officers, chief engineer Hinnerk Heuck and his team as well as Thomas Liebe, Ralf Krocker and Dietmar Kircher and his team have enabled the successful measurement of a valuable full scale data set.

8. GNSS OBSERVATIONS IN NORTH-EAST GREENLAND TO DETERMINE VERTICAL AND HORIZONTAL DEFORMATIONS OF THE EARTH'S CRUST

Mirko Scheinert[1] (not on board), Benjamin Ebermann[1], Andrei Kraemer[1]

[1]TU Dresden

Grant-No. AWI-PS100_06

Objectives

In Greenland, there still exists the only continental ice sheet outside Antarctica. It plays an important role for the global climate. Although it contains only 10 % of the global fresh-water storage in comparison to the Antarctic ice sheet, it reacts in a very sensitive way to changes in the environmental and climate conditions due to its location at high- and sub-polar latitudes. Therefore, the Greenland ice sheet has been subject to intensive geophysical and glaciological investigations for almost one century.

Changes of the ice sheet are visible indirectly at deformations of the surface of the Earth. Ice mass changes can be regarded as changing surface loads, which cause – due to the rheological properties of the upper layers of the Earth – long-term visco-elastic and immediate elastic reactions. Hence, in the observable vertical deformation of the Earth's crust we can find the integral effect of all ice-mass changes during glacial history and in present times.

North-East Greenland is characterized by a high variability of the ice edge with regard to its location and mass change as well as of a visco-elastic signal due to glacial history, that – according to model predictions – reaches maximum values for entire Greenland. Additionally, deformations of tectonic origin cannot be excluded, which will be tested analysing the horizontal components.

Satellite-based positioning by means of GNSS allows a precise geodetic determination of coordinates and, with repeated observations, the determination of changes of the horizontal as well as of the vertical components with an accuracy in the sub-centimetre level. In order to ensure a high accuracy of repeated measurements, a stable base for the GNSS marker has to be chosen. Therefore, the stations are to be set-up at ice-free bedrock locations.

This project is a continuation of research work done during *Polarstern* cruises PS72 (ARK-XXIII/1+2 (2008)) and PS74 (ARK-XXIV/3 (2009)).

The main goal of the geodetic work was the re-observation of GNSS stations at up to 10 ice-free locations in the coastal area of East Greenland between 78° and 81°N. These were installed and firstly observed during *Polarstern* PS72 (ARK-XXIII/1 and ARKXXIII/2) cruises in 2008. Some of these stations could be observed for the second time in 2009 during cruise PS74 (ARK-XXIV/3).

Work at sea and land

Polarstern with its two helicopters served as basis for the realization of the work. To reach the locations on land, *Polarstern* had to sail to positions close enough to Greenland's coast. The

geodetic flight program was adapted to the ship's route such that no additional ship time was necessary.

The first activities took place during biological station work close to the Greenland coastline. In that region, four GNSS stations were set up on old positions of 2008 that were within long-range flying distance of the helicopter.

In addition, a station was set up at the Nioghalvfjerdsbræ (see Fig. 8.1 right), at a location which is in the center of the ice stream and where the glacier is already floating. The analysis of these GNSS data will allow to infer the glacier's velocity which amounts to approximately 2 to 3 m/day as well as the vertical motion due to the ocean tides. The location was chosen in such a way that it has a distance of at least 10 km to the northern and southern coast. Thus, the ground GNSS data can be used to validate models of the glacier velocity and of the ocean tides.

The second operation period started on the way to the Nioghalvfjerdsbræ. There, another five stations could be reoccupied. At the end of this part, all stations, including the stations that were installed from the biological work area were successfully recovered.

Altogether, 10 GNSS stations were set up and a successful re-observation of the 2008 campaign took place. A geodetic GNSS station was built up by a special marker fixed to the rock, which served to take up the GNSS antenna and which worked as a forced centering for the antenna. The power supply was realized by means of solar modules and sealed batteries, specially adapted for usage with solar power. GNSS receiver, batteries and a charging controller were stored in a Zarges aluminum box, which protected the equipment from the influence of the weather. Fig. 8.1 and 8.2 show examples of the set-up of a GNSS station. The receivers collect data for a longer period (at least for three 24h-Sessions, starting at 00:00 UTC) with a data rate of 15s in order to meet the goal of an accuracy of the determined coordinates of some millimeters. A list of the GNSS stations is given in Table 8.1; the locations are also shown in the overview map (Fig. 8.3).

Fig. 8.1: Typical set-up of a GNSS station. Left: View at the final set-up of station CENT (Centrumsø). Right: At the glacier station NIOG (Nioghalvfjerdsbræ) the antenna is mounted on top of an iron rod fixed to the glacier by additional three guys. The solar panel is directly attached at top of the Zarges aluminium box.

Fig. 8.2: Set-up details of a GNSS station. Left: The GNSS antenna (directly fixed to the rock by a special bolt). Right: View into the Zarges aluminium box with charging controller (centre), GNSS receiver (black case) and a sealed battery (upper right).

Tab. 8.1: List of GNSS Stations with approximate coordinates and time of their observation

ID	Longitude	Latitude	Ellips. H [m]	Geographical Region	Start date	Stop date	24h Session
FRAN	18° 37' 38" W	78° 43' 42" N	337	Franske Øer S	05.08.16	14.08.16	8
BILD	23° 30' 12" W	78° 06' 59" N	900	Bildsøe Nunatakker (961m)	15.08.16	19.08.16	3
LAMW	22° 18' 22" W	79° 13' 35" N	189	Lambert Land W, Nunatak 172m	18.08.16	24.08.16	5
HOVG	18° 13' 50" W	79° 42' 01" N	581	Hovgård Ø (Kap Anna Bistrup)	03.08.16	20.08.16	16
BLAF	22° 38' 58" W	79° 31' 58" N	572	Blåsø (Kronprins Christian Land S, Blåsø Fjeld)	19.08.16	24.08.16	4
CRIW	24° 18' 49" W	80° 05' 33" N	344	Kronprins Christian Land SW	20.08.16	25.08.16	4
HOLM	16° 25' 53" W	80° 16' 23" N	410	Holm Land E	03.08.16	20.08.16	16
CENT	21° 43' 25" W	80° 11' 29" N	92	Centrumsø (Kronprins Christian Land CS)	21.08.16	25.08.16	3
NIOG	19° 59' 44" W	79° 36' 09" N	75	Nioghalvfjerdsbræ	04.08.16	24.08.16	19

Preliminary (expected) results

The GNSS observations will be processed at the home institution (so-called post-processing using the Bernese GNSS Software). In the analyses latest standards have to be incorporated used in geodesy (e.g. consistent and precise realization of the reference frame). From the analysis of the repeated GNSS observations we will come up with coordinate change rates (especially for the vertical deformation), that serve as an independent source of information

for the validation and improvement of models on the glacial history and on the recent ice mass balance of North-East Greenland. While testing the significance of horizontal deformations we will contribute to an improved analysis of the tectonic regime in the working area.

Data management

The geodetic GNSS data will be archived in a similar database like the SCAR GNSS Database that is maintained at TU Dresden. The long-term preservation of the data will be maintained also through the close cooperation within the SCAR Scientific Programme SERCE (Solid Earth Responses and Influences on Cryosphere Evolution).

A common structure of the data holdings is ensured through the application of the same scientific software package utilized to analysegeodetic GNSS measurements at TU Dresden (i.e., the Bernese GNSS Software). Further products and resulting models will be archived in the PANGAEA database at AWI.

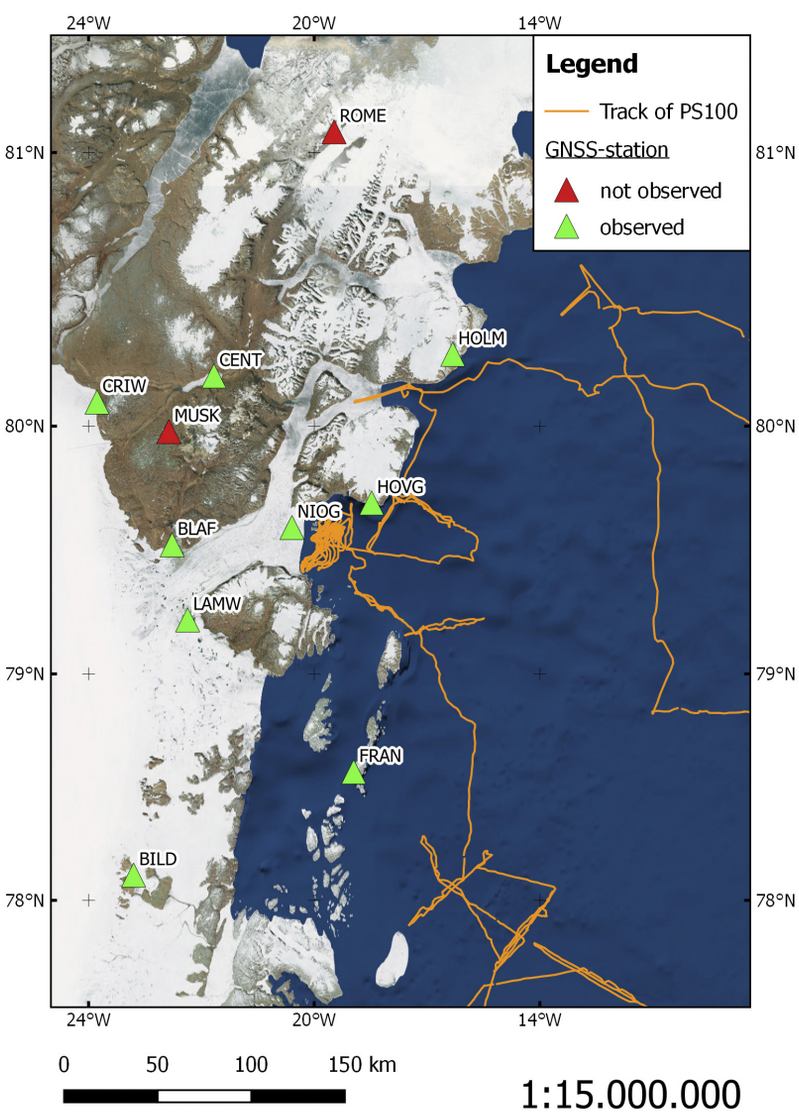

Fig. 8.3: Overview map showing the locations of the observed GNSS stations (Map: ArcGIS World_Imagery; mapping software: QGIS).

Acknowledgements

The geodetic program could be so successfully realized due to the great support by numerous colleagues in the preparation and realization of the expedition as well as by the crew of *Polarstern*. Especially we like to thank: T. Kanzow (chief scientist), L. Vaupel and J. Brauer (helicopter pilots) and S. Schwarze (Master of *Polarstern*).

9. AMICA - ARCTIC MARGINAL ICE ZONE COMMUNITY ASSESSMENT: BIODIVERSITY, PRODUCTIVITY & TROPHIC INTERACTIONS IN THE MARGINAL ICE ZONE OF FRAM STRAIT UNDER GLOBAL CHANGE

Holger Auel[1], Charlotte Havermans[1], Rita Melo Franco Santos[1,2], Natalie Prinz[1], Rita Jacinto[3], Joana Boavida[3]

[1]Uni HB,
[2]AWI,
[3]CCMAR-UAlg

Grant No. AWI-PS100_07

Objectives

In the framework of AMICA, biodiversity, productivity and trophic interactions within the Arctic marginal ice zone of western Fram Strait are quantified in order to assess potential impacts of global climate change on marine ecosystems in the Arctic. During recent years, episodes of unexpectedly high water temperatures and an increased inflow of Atlantic water masses via Fram Strait already led to a decline in sea-ice cover and changes in pelagic communities. The relative importance of phytoplankton *vs*. ice algae for primary production and for the nutrition of marine animals is quantified, and the fate of organic matter during its passage through the food web is traced. Because of the complex current regime at the East Greenland shelf (East Greenland Current, Return Atlantic Current), advection of organic matter and organisms into and out of the study area had to be taken into account, too.

The Arctic Ocean is the area most rapidly and intensely affected by global warming and climate change. Models predict a rise in air temperature by 3 to 6°C over the coming 50 years. The temperature increase will be similar throughout the year, but with stronger effects during the summer season, when it will result in a longer and more intense melting period of the sea ice. Multiyear sea ice has declined by ca. 15 % per decade over the last thirty years. It is expected that the geographical extent of permanent multiyear ice coverage will further decline, while areas with seasonal ice cover and the marginal ice zone will increase.

Field observations in Fram Strait, where sea ice comes into contact with relatively warm Atlantic water masses, show that melting may proceed rather rapidly. The ablation of the ice underside can reach 10-20 cm day^{-1}. Since most of the sea-ice organisms live in the lowermost centimetres of the ice, such a rapid melting results in the loss of most of the sea-ice community and, hence, a cessation of ice algal primary production.

Studies around Svalbard demonstrated that the marginal ice zone is a very dynamic habitat. During the spring break-up of the pack ice, the ice edge receded northward at a rate of 11 km day^{-1}. An early bloom of *Phaeocystis* in Fram Strait resulted in high new production of ca. 1 g C m^{-2} day^{-1} over a 35 day period. In polar systems, the ratio of new, i.e. nitrate-based, to total primary production is high, resulting in a high potential of these regions for influencing global carbon and nutrient cycles.

Ice-covered polar seas differ from most other oceanic regions due to the fact, that phytoplankton is not the only primary producer. Ice algae, mainly pennate diatoms, greatly contribute to total primary production and may present up to two-thirds of total primary production in ice-covered areas. On average ice algae contribute 57 % of the entire primary production in the central Arctic and 3 % in surrounding regions.

The loss of suitable sea-ice habitats and of the nutritional basis will lead to deleterious effects for endemic sympagic species such as under-ice amphipods and polar cod. On the other hand, seasonal pack-ice areas and the marginal ice zone are highly productive areas. Higher phytoplankton and total primary production in the Arctic may lead to increased zooplankton production and a better food supply for pelagic fish. However, these changes of the Arctic ecosystem are not certain. An early break-up of the ice could initiate a diatom bloom already in March prior to the ascent of copepods in April. This mismatch between the early spring bloom and copepod grazers could result in a pelagic food web dominated by protozooplankton and reduced amounts of organic matter available for higher trophic levels or export from the euphotic zone, despite the increased primary productivity.

At times and locations where sea ice melts, ice algae and sympagic fauna are released into the water column and present an additional food source for pelagic organisms. However, it is generally believed that strong pulses of released organic matter from melting sea ice supersede the ingestion and remineralization capabilities of epipelagic communities and are exported to deeper water layers and to benthic communities. Especially in areas where large amounts of sea ice melt regularly, for instance in Fram Strait, the sedimentation of ice organisms can present an important food source for the deep-sea fauna and contribute to the downward carbon flux.

In contrast to low-latitude ecosystems, polar seas host high biomasses of relatively large zooplankton organisms, which form an important direct link to top predators, such as seabirds and marine mammals, due to the low abundance or near-absence of small pelagic planktivorous fish in polar marine ecosystems. The long-standing paradox of high Arctic mesozooplankton biomass despite low phytoplankton production can be explained with the additional input of ice algae production, advection of Atlantic water masses and the import of organic matter from the vast Arctic shelves into the central Arctic deep-sea basins. Moreover, physiological adaptations in dominant Arctic zooplankton species, such as diapause, reduce the nutritional demands of the plankton community. Slow growth and long life-spans of Arctic zooplankton species result in rather large individual size despite limited food availability.

Mesozooplankton biomass in the Arctic Ocean and adjacent seas is strongly dominated by calanoid copepods. The three congeners *Calanus finmarchicus*, *C. glacialis* and *C. hyperboreus* together with *Metridia longa* represent two-thirds to three-quarters of total mesozooplankton biomass in the Arctic Ocean during summer. Zooplankton composition is influenced by the inflow of Atlantic water masses with boreal-Atlantic sister species gradually replacing native polar species. *C. finmarchicus* is the smallest and less lipid rich of the genus, being associated with the warmer Atlantic waters of the West Spitsbergen Current. In contrast, *C. glacialis* is abundant in the polar East Greenland Current and extremely rich in lipids. The largest congener *C. hyperboreous* mainly occurs in deeper parts of the Greenland Sea and Arctic Ocean.

Amphipods of the hyperiid genus *Themisto* play an important role in the entire Arctic Ocean: due to their high biomass they represent both an important predator on mesozooplankton and a major food source for Arctic marine vertebrates such as polar cod, seals and seabirds. *T. libellula* is associated with colder polar waters, whereas *T. abyssorum* is linked to waters of Atlantic origin. A previous biomarker study has shown different ecological niches for these two species with *T. libellula* being closely connected to the ice-algal production and feeding mainly on herbivorous copepods, whilst *T. abyssorum* is rather omnivorous, feeding also on

carnivorous prey (Auel et al. 2002). However, little is known on the ecology of the different species throughout the Arctic Ocean, particularly with regard to the distribution of the two species. These are hypothesized to become increasingly overlapping with the increased inflow of Atlantic water masses, and the more boreal-Atlantic *T. abyssorum* could potentially replace the native polar species *T. libellula*. In order to evaluate the consequences of these distributional shifts, we need to gain more information on the ecology and biology of these two species, and to find out to which extent the species are linked to the different water masses in the study area and/or to particular food resources (e.g. ice-algae).

The objectives of AMICA are to quantify the relative contributions of ice algal *vs*. phytoplankton primary production in the Arctic marginal ice zone and to trace the fate of organic matter throughout the marine food web. The empirical data obtained during PS100 allow assessing potential impacts of a declining sea-ice cover on Arctic marine ecosystems. The summer situation in Fram Strait where sea ice gets into contact with warm Atlantic waters and rapidly melts can act as a model system for future conditions in high-Arctic regions under scenarios of global climate change.

The specific aims were to ...

- Quantify abundance, biomass, biodiversity and production of ecologically important components and key species of the marine communities within the Arctic marginal ice zone including phytoplankton, ice algae, zooplankton (copepods, hyperiid amphipods, chaetognaths, gelatinous zooplankton), seabirds and marine mammals (seals, cetaceans);

- Characterize microbial and phytoplankton biodiversity with molecular tools via metabarcoding and metagenomic approaches to be applied to seawater communities from contrasting conditions and to sediment samples (environmental DNA and RNA analyses) and determine how microbial and phytoplankton communities varied over time and climatic conditions for the past 1,500 years as estimated by dated sediments (in collaboration with NEGIS researchers);

- Quantify import and export of organic matter and organisms (phyto- and zooplankton) into and out of the study area through advection by combining field data on phyto- and zooplankton biomass in different water layers with hydrographic data on water mass exchange and advection in Fram Strait;

- Study trophic interactions, grazing and predator-prey relationships in order to trace the pathways of organic matter through the marine food web in the Arctic marginal ice zone. For this purpose, classic approaches (feeding experiments, morphological gut content analysis) will be combined with state-of-the-art trophic biomarker studies (fatty acid biomarkers, stable isotopes) and molecular diet analyses.

- Investigate how the assimilation of energy and the allocation of dietary components vary in different *Calanus* species in relation to the type of food provided. Experiments elucidate the metabolic pathway of fatty acids from diet enriched with ^{13}C into copepods by means of compound specific stable isotope analysis.

- Establish species-specific tolerance thresholds for dominant pelagic species with regard to increasing water temperatures in polar *vs*. boreal-Atlantic sister species;

- Establish comparative gene expression responses and transcriptional regulation of polar *vs*. boreal-Atlantic key zooplankton species under varying thermal regimes. These data will be integrated with physiological responses to temperature to gain insight into

phenotypic differentiation in Arctic and boreal-Atlantic species that may be crucial for adaptation under climate change scenarios.

- Describe the regulatory cascades and control mechanisms involved in thermal tolerance and adaptation of dominant mesozooplankton species;
- Gain insights into the general ecology and biology of *Themisto abyssorum* and *T. libellula* by means of life history analyses and behavioural observations;
- Study the genetic structure of pelagic amphipods throughout the sampling region, and in a later stage, between the sampling region and other localities in the Arctic and sub-Arctic, in order to clarify their adaptation and spreading potential and interspecific evolutionary relationships.
- Provide the database for food web models of ice-covered Arctic seas with the ultimate goal to develop a predictive capacity for potential impacts of global climate change on Arctic marine ecosystems.

Work at sea

The AMICA station grid consisted of a closed box in the marginal ice zone of western/central Fram Strait between 79 and 80.5°N and from 12 to 0°W. The East Greenland Current transports zooplankton and sea ice from the central Arctic Ocean into this area, where the sea ice melts. The exact position of the station grid had to be adjusted and shifted northwards during the cruise in order to respond to the actual sea-ice situation derived from satellite images. Due to the opposing meridional warm- and cold-water currents in Fram Strait, i.e. West Spitsbergen Current *vs*. East Greenland Current, transects across Fram Strait allowed for sampling of polar, Arctic, sub-Arctic & boreal-Atlantic species in close proximity.

At in total 36 stations stratified mesozooplankton samples were collected with a HydroBios Multinet Midi (mouth opening 0.25 m^2) equipped with five nets of 150 µm mesh size. Sampling usually included the whole water column down to the seafloor or to a maximum depth of 2,000 m. Where required, two successive hauls were conducted at the same station (with maximum 8 separate depth intervals) in order to combine deep sampling with a higher resolution of the upper water column. Standard depth intervals included seafloor (or 2,000 m) to 1,500 m, 1,500 m to 1,000 m, 1,000 m to 500 m, 500 m to 200 m, 200 m to 100 m, 100 m to 50 m, and 50 m to the surface. Additional material for experimental work on board was collected from the surface layer (usually 50 m to 0 m) by vertical Bongo net hauls (mesh size 200 and 500 µm) with a large non-filtering cod end.

Rarer and more mobile macrozooplankton species, such as hyperiid amphipods, which can avoid slower nets and, thus, are usually underestimated in vertical hauls, were caught by double oblique hauls with a towed Bongo net (mesh size 500 µm, towing speed 2 knots), where possible depending on the sea-ice situation, bottom depth and visibility.

Along the northern and southern margin of the planktological sampling grid, stations were generally spaced at 1 or 1.5° longitude distance, equivalent to 10 to 17 nm distance, in order to provide a high spatial resolution over the continental rise and when crossing the East Greenland Current. Along the western and eastern margins, the spatial resolution was lower, reflecting more homogenuous environmental conditions on the East Greenland shelf and over deep Fram Strait, respectively. Additional planktological stations were located in the Norske Trough and in front of the 79°N glacier.

Zooplankton samples were sorted alive in a temperature-controlled laboratory container immediately after the catch in order to collect frozen and ethanol-preserved samples for trophic biomarker studies, ecophysiological and genetic analyses. Specimens of key copepod and amphipod species were incubated for several days on board at increasing temperatures of 0°C, 2°C, 4°C, and 8°C and their metabolic activity measured with optode respirometry in order to establish their response to increasing water temperatures and to identify ecophysiological thresholds and tipping points in polar *vs*. boreal-Atlantic sister species.

Since polar species are usually far bigger and more lipid-rich than their Atlantic counterparts, a shift in the community composition towards more warm-water species will negatively affect food quality for predators such as fish or seabirds. Plankton studies were supplemented by sea-ice sampling to collect ice algae and by five helicopter flights to assess the habitat use and potential stock size of seals and other marine mammals in the study area.

Additional molecular genetic analyses of gene expression (transcriptomics) in the home lab will show which genes are most important for temperature acclimation in zooplankton species and whether gene expression differs between polar and Atlantic congeners. For that purpose, 175 individuals each per station and ontogenetic stage (adult females or copepodids C5) were gently picked and randomly assigned to seven groups of 25 individuals. One of these, representing natural *in-situ* conditions, was immediately frozen in liquid nitrogen and stored at −80°C. The remaining six groups were placed in flasks (200 ml) filled with filtered seawater and placed in a temperature-controlled laboratory container at 0°C. After 48 to 160 h of acclimation at 0º C, a sample of 25 individuals (T0) was flash-frozen in liquid nitrogen and stored at −80 °C and all but one of the groups (control) were transferred to an incubator set at 2°C, in order to study the copepods' response to increasing temperatures. The incubation temperature was increased by 2°C per day until reaching 8ºC. Each day, a sample of 25 individuals was picked, flash-frozen in liquid nitrogen and stored at −80°C.

Pelagic amphipods were kept alive in aquaria for feeding experiments and behavioural observations on board. Behavioural observations included measurements of swimming speeds of both *T. libellula* and *T. abyssorum* for individuals of different sizes. Sinking speeds of dead individuals were measured for different size classes of both species with video recordings and time measurements and will be compared with similar size classes of other types of organisms such as chaetognaths and copepods. Video recordings captured feeding interactions between *Themisto* and potential prey items such as soft-bodied zooplankton as well as phytoplankton aggregates. Ethanol-preserved amphipod samples were taken for various purposes, including taxonomic, life history, phylogeographic and molecular diet analyses. RNAlater samples will be used for gene expression analyses and frozen samples for biomarker studies and dry weight calculations in the home laboratory.

Natural phytoplankton communities were sampled from contrasting hydrographic regimes, boreal-Atlantic and Arctic waters in Fram Strait, using a large volume rosette water sampler with 22 bottles of 24 l volume each, attached to the CTD probe. Samples were usually collected from the depth of the chlorophyll maximum, which was located between 15 and 50 m depth at most of the stations. Within 30 to 60 min after collection, triplicate samples were filtered (5 and 2 µm pore-etched polycarbonate filters; 1-18 l per triplicate), snap-frozen in liquid nitrogen to prevent RNA degradation and changes in gene expression patterns and kept at -80ºC for storage and transportation.

Sediments from 5 sites on the northeast Greenland shelf (300 to 550 m depth) were collected and stored as follows. Two sediment cores (3.8 and 9.5 m long) were recovered from Norske Trough using a gravity corer and triplicate samples (approximately 5 mg) were collected at each 30 cm depth. Samples were either snap-frozen in liquid nitrogen followed by storage at -80ºC or placed directly at -80ºC. Three giant box corer samples of approximately 40 cm depth

were collected in Norske Trough and close to the 79°N glacier. A sterile (washed with 96 % ethanol) corer tube of 12 cm diameter was used to sub-sample from the box corer. Cores were sectioned into 1 or 1.5 cm segments with a sterile scalpel blade, placed into sterile plastic petri dishes and Aluminium foil, and either snap-frozen in liquid nitrogen followed by storage at -80ºC or placed directly at -80ºC. All samples will be processed at the Center of Marine Sciences (CCMAR), Portugal, in collaboration with NEGIS researchers in order to investigate how microbial and phytoplankton communities varied over time and climatic conditions over the past 1,500 years.

Additional incubation experiments focussed on the energy budget of boreal-Atlantic *vs*. polar *Calanus* spp. and how dietary components such as fatty acids are allocated and incorporated into the consumer's body tissues. Therefore, three different species of prey items were cultured on board, i.e. *Rhodomonas salina*, *Oxyrrhis marina*, and *Thalassiosira weissflogii*. The former was used to feed *O. marina*, and the two latter were used to feed *Calanus* copepods. Batch cultures were created on a daily basis throughout the cruise. F/2 medium enriched with δ^{13}C-labelled sodium bicarbonate at a concentration of 12 mg l^{-1} was used to culture the algae. Cultures were kept at 11°C, *T. weissflogii* and *R. salina* under continuous light and *O. marina* under constant dim light. Before being fed to copepods, sub-samples of the *T. weissflogii* and *O. marina* cultures were filtered to determine their C/N content and fatty acid composition. For the experiments, copepods were divided between six incubation beakers so that each prey treatment was observed in three replicates. Copepods were kept under dim light and at their ambient temperature. A total of six experiments was performed. Starvation experiments were conducted in filtered seawater for 14 and 12 days with *C. finmarchicus* copepodids C5 and *C. hyperboreus* females, respectively. Feeding experiments with δ^{13}C-labelled prey lasted 14 days and were performed with *C. finmarchicus* C5 and females of both *C. glacialis* and *C. hyperboreus*. With assimilation, δ^{13}C accumulates in the zooplankton consumers and can be followed by compound-specific stable isotope analysis (CSIA), which will be conducted after the expedition in the laboratories at AWI. In addition, grazing, egg and faecal pellet production experiments were conducted with *C. hyperboreus* females by means of short-term incubations (<24 hrs).

Preliminary (expected) results

First preliminary results of the PS100 cruise show that ice algae, which are released into the water column, when sea ice melts, sink relatively quickly to great depths of more than 1,000 m. On their way down, they are grazed upon by copepods and amphipods.

Boreal-Atlantic species such as *Calanus finmarchicus* and *Themisto abyssorum* and inhabitants of the deep Arctic basins and Greenland Sea such as *Calanus hyperboreus* are advected far westwards onto the East Greenland Shelf by the inflow of Atlantic waters into Norske Trough and Westwind Trough.

During helicopter flights ringed seals, hooded seals, narwhals and polar bears were encountered inside the study area. In addition, fin whales were present close to the ice edge at the eastern margin of the study area.

A huge number of frozen samples was collected from all dominant components of the Arctic food web. The collection includes 170 phytoplankton samples from CTD/rosette water sampler casts at 43 stations encompassing a transect across Fram Strait from the West Spitsbergen Current to the East Greenland Shelf, Norske Trough and Westwind Trough, more than 800 zooplankton samples for trophic biomarker analyses (fatty acids and stable isotopes) including the full range of all dominant zooplankton species encountered during the cruise (e.g. copepods, amphipods, euphausiids, chaetognaths, pteropods, decapods, mysids, ctenophores, jellyfish), approx. 3,200 individual mesozooplankton samples from 8 species (*Calanus glacialis*, *C.*

hyperboreus, *C. finmarchicus*, *Metridia longa*, *Themisto libellula*, *Themisto abyssorum*, *Thysanoessa longicaudata*, and Ostracoda) and 13 sampling sites for gene expression analysis (transcriptomics) from the temperature-change experiments, and nearly 200 sediment samples from 5 stations to study palaeo-plankton communities by means of their environmental DNA remains and link potential past distributional shifts to the palaeo-climate.

With the samples collected during PS100 we expect to obtain high-quality reference transcriptome assemblies of each species and thus perform a large-scale analysis of transcriptional response to thermal stress. We will characterize genes and processes involved in thermal adaptation as well as regulatory controls, signal transduction pathways and stress response networks, for all the taxa. We will also identify molecular markers for physiological stressors, namely thermal stressors. From these data, we will be able to identify proteins and pathways involved in temperature responses.

Life history and population dynamic analyses of dominant zooplankton species from polar *vs*. boreal-Atlantic origin will gain more information on life-history traits such as temperature tolerance and recruitment periods. Comparative studies on sinking speeds of dead specimens will allow us to improve our understanding of the contribution of *Themisto* biomass to the downward carbon flux.

Data management

Results from the PS100 cruise will be published in peer-reviewed journals by the participating scientists in co-operation with other colleagues. Parts of the data set will also contribute to a doctoral thesis at the University of Bremen. Zooplankton samples will be archived and stored at the BreMarE Centre of the University of Bremen. Phytoplankton and sediment samples for molecular analyses will be stored at the CCMAR facilities under the coordination of Dr. Ester Serrão (eserrao@ualg.pt).

Geo-referenced data sets such as zooplankton abundance and biomass will be archived and made publicly available through the PANGAEA database during the publication process. By doing so, every data set, as a supplement to publications or separately, can be identified, published, cited and shared as a digital object identifier (DOI).

Genetic data obtained throughout the project will be submitted to the GenBank database. DNA and RNA sequence data will be deposited in the National Center for Biotechnology Information (NCBI) Sequence Read Archive (SRA). Transcriptomic data referred to in scientific publications will be made available as supplementary electronic file to the respective publications.

References

Auel H, Harjes M, da Rocha R, Stübing D, Hagen W (2002) Lipid biomarkers indicate different ecological niches and trophic relationships of the Arctic hyperiid amphipods *Themisto abyssorum* and *T. libellula*. Polar Biology, 25, 374-383.

10. BASAL MELT RATES OF THE FLOATING PART OF 79°N GLACIER

Benjamin Ebermann[2], Andrei Kraemer[2] [1]AWI,
not on board: Angelika Humbert[1], Daniel Steinhage[1] [2]TU Dresden

Grant No. AWI-PS100_08

Objectives

The 79°N Glacier is one of three outlet glaciers of the only large ice stream in Greenland, the NEGIS (North-East Greenland Ice Stream). In contrast to other glaciers in Greenland, which are typically tidewater glaciers, the 79°N Glacier forms a floating tongue and is rather comparable to an ice shelf. As the NEGIS drains about 8 % of the ice sheet, the question, whether its contribution to sea level change is increasing, is coming more into focus. The floating tongue is pinned by ice rises along the ice front, which keeps its lateral extent at the moment stable, however, the ice flow velocities at its grounding line are slightly increasing (Joughin, pers. comm.) and the upstream ice surface elevation has started to decrease in the past few years (Helm et al., 2014). Warm water masses were also already detected to drain underneath the floating tongue and hence the question arises if the warm water increases the basal melt of the floating tongue, causing grounding line retreat and weakening of the tongue itself.

We therefore aim to measure the seasonal variation of basal melt rates of the 79°N Glacier at two locations on its floating tongue. The melt rates at the ice-ocean transition are measured using a phase sensitive radar (Corr et al., 2002; Jenkins et al., 2006), that detects the change of the distance between internal layers of the glacier. This method can separate the ice thickness change due to stretching of the glacier from the thickness change due to basal melt. As the basal melt over a short period of time is too small to be detected by the amplitude of the radar signal, the phase of the radar signal is used for this purpose. The radar is a multi-frequency radar, that sends a burst of radar signals with defined repetition times and gives hence a change of the phase and hence the basal melt rate over time. With this method we can thus detect the penetration of warm water masses underneath the tongue that cause the change of the melt rates.

Work at sea and land

By using the helicopter, a group of two persons plus ranger was flown to the glacier to install the two autonomous radar stations. On *Polarstern,* a platform was built that holds the two antennas and the pRES case including the radar-measurement unit. To fix this platform at the field site, five flags were set up to get a stable configuration (Fig. 10.1). The first radar system was set up on 22.08.2016 near the grounding line on the southern site. On the next day, the second radar system was built on the northern site. The coordinates are:

Station	Latitude	Longitude	Alignment to magn. N
pRES-South	79° 19‘ 25“ N	22° 14‘ 04“ W	30°
pRES-North	79° 23‘ 58“ N	22° 24‘ 14“ W	70°

Fig. 10.1: Typical set-up of a pRES station. Left: final setup of the pRES station north. Right: view of the pRES station north from the helicopter.

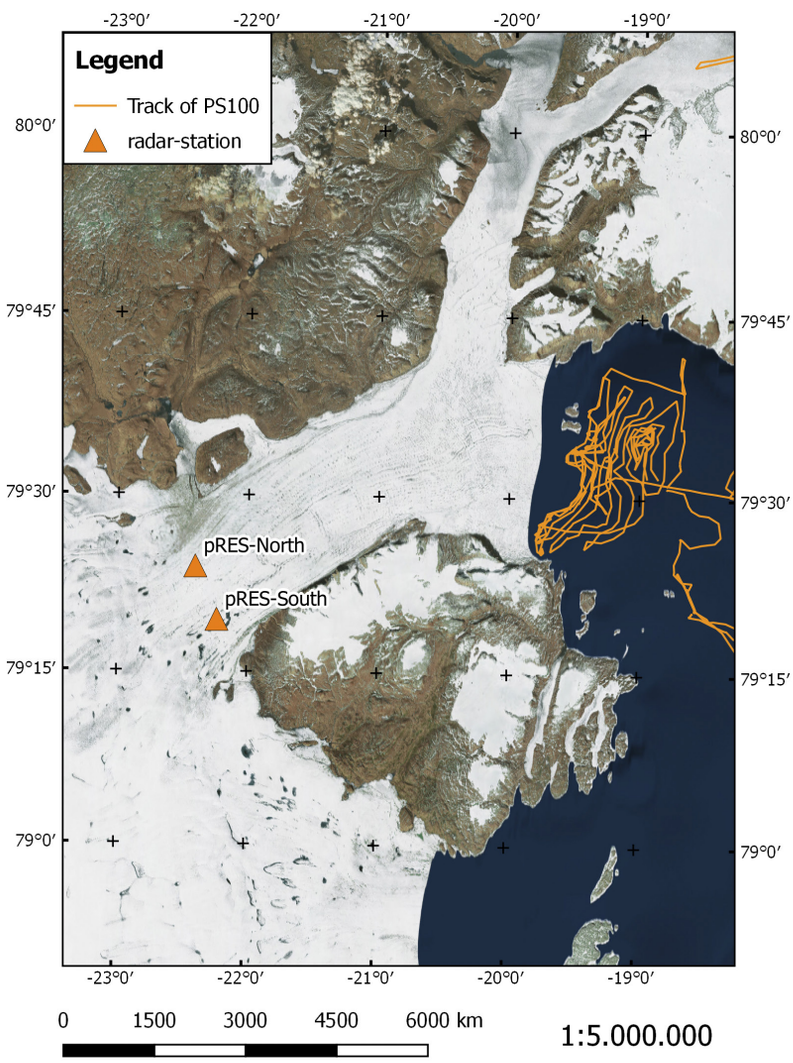

Fig. 10.2: Overview map showing the two locations of the pRES stations (Map: ArcGIS World_Imagery; mapping software: QGIS)

To check if the stations are working and to change some configurations, there was a third flight on 25.08.2016. The parameters of the config.ini files are listed below.

pRES South:

AlwaysAttended=0
CheckEthernet=1
maxDepthToGraph=500
N_ADC_SAMPLES=40000
NData=0
Triples=70,10,200,210,10,300,310:10:390
WATCHDOG_TASK_SECS=3600
NSubBursts=20
Average=0
RepSecs=3600
IntervalMode=0
MAX_DATA_FILE_LENGTH=1000000
LOGON=1
nAttenuators=1
Attenuator1=25,0,0,0
Attenuator2=0,0,0,0
SleepMode=0
GPSon=0
Housekeeping=1
SyncGPS=0
Iridium=0
; End of configuration file

pRES North:

AlwaysAttended=0
CheckEthernet=1
maxDepthToGraph=500
N_ADC_SAMPLES=40000
NData=0
Triples=70,10,200,210,10,300,310:10:390
WATCHDOG_TASK_SECS=3600
NSubBursts=20
Average=0
RepSecs=3600
IntervalMode=0
MAX_DATA_FILE_LENGTH=1000000
LOGON=1

nAttenuators=1
Attenuator1=31,0,0,0
AFGain=-6,0,0,0
SleepMode=0
GPSon=0
Housekeeping=1
SyncGPS=0
Iridium=0

Preliminary (expected) results

Time series of basal melt rates at two locations after recovery of the stations in 2017.

Data management

All data will be uploaded to the PANGAEA database. Unrestricted access to the data will be granted after about three years, pending analysis and publication.

References

Corr HFJ, Jenkins A, Nicholls KW, Doake CSM (2002) Precise measurement of changes in ice-shelf thickness by phase-sensitive radar to determine basal melt rates. Geophys. Res. Lett., 2, (8), p. 1232.

Helm V, Humbert A, Miller H (2014) Elevation and elevation change of Greenland and Antarctica derived from CryoSat-2. The Cryosphere, 8, 1539–1559, 2014, doi:10.5194/tc-8-1539-2014

Jenkins A, Corr HFJ, Nicholls KW, Stwart CL, Doake CSM (2006) Interactions between ice and ocean observed with phase-sensitive radar near an Antarctic ice-shelf grounding line. J. Glaciol., 52, (178), pp. 325–346

11. SEISMOLOGY

Vera Schlindwein[1], Henning Kirk[1] [1]AWI,
F. Krüger[2] (not on board) [2]Uni Potsdam

Grant-No. AWI-PS100_09

Objectives

Seismicity and lithosphere structure of the ultraslow spreading Knipovich Ridge

Ocean basins are formed by seafloor spreading at active mid-ocean ridges. Mantle material is upwelling under the ridges and melts to produce magma, which erupts onto the sea floor and crystallizes at depth to produce new oceanic crust. Crustal generation and plate separation rate keep pace over a wide range of spreading rates and produce oceanic crust with a uniform thickness of about 7 km. Yet models predict that at spreading rates below about 20 mm/y, the mantle loses heat by conduction and only small amounts of melt are produced at large depths (Bown & White, 1994). This melt is distributed very unevenly along the axis of ultraslow-spreading ridges: Isolated volcanoes at distances of about 100 km are separated by long ridge sections that show little or no magmatism and mantle rocks may be exposed directly at the seafloor (Michael et al*.,* 2003). Underneath these volcanic centres, the lithosphere is postulated to be thinner, such that melt can flow along the lithosphere-asthenosphere boundary along the segment towards the volcanoes and rise through a thinned lithosphere. For this geological model (e.g. Standish et al*.,* 2008), we found first geophysical evidence during a short-term deployment of ocean bottom seismometers (OBS) around Logachev Seamount on Knipovich Ridge (Fig. 11.1): The maximum depth of earthquakes marking the thickness of the elastic lithosphere rises from about 20 km depth to less than 8 km depth underneath Logachev Seamount (Schlindwein et al*.,* 2013). At the Southwest Indian Ridge, a long-term deployment of OBS in 2012 (Schlindwein, 2014) allowed to define in detail the topography of the lithosphere-asthenosphere boundary along a short ridge section (Schlindwein & Schmid, 2016).

In order to better understand how melts travel at segment scale along the axis of ultraslow spreading ridges and rise through the thick lithosphere, we aim to instrument for the first time an entire segment of an ultraslow spreading ridge with an about 180 km long network of ocean bottom seismometers (OBS) from the DEPAS instrument pool and record the earthquake activity of the ridge. From the seismicity pattern we can derive the thermal structure of the ridge and identify regions of contrasting deformation modes. Mantle rocks altered to serpentinite, for example, show little seismicity, whereas basalt dominated ridge areas break in numerous earthquakes (Schlindwein & Schmid, 2016). Earthquakes furthermore trace active faults that potentially play a significant role in the oblique spreading of Knipovich Ridge. Around Logachev Seamount, our OBS network will be denser to acquire a dataset that is suitable for seismic tomography to image the internal structure and plumbing system of a volcanic centre.

The OBS will remain for about one year at the seafloor and will be collected during a dedicated cruise with *Maria S. Merian* in 2017. At that time, we will additionally acquire refraction seismic profiles across Logachev Seamount (Fig. 11.1) for a high-resolution image of its structure and seismic velocities at depth. Bathymetry mapping in the off-axis direction of Logachev

Seamount will then complement our data to look for expressions of phases of tectonic and magmatic activity of Logachev Seamount in former times.

Icequake recording near the grounding line of 79°N glacier

An additional objective of our seismological field work is to record icequakes at the 79°N glacier as part of the multidisciplinary study GRIFF this and the upcoming season. Icequakes have recently received much attention as an increase in cryogenic seismicity could be observed over the last decade that may reflect changes in glacial dynamics (Müller pers. comm. 2010, Ekström et al*.,* 2006). Glacial earthquakes recorded by the global seismological network document a retreat of the grounding line of Greenland's temperate tidewater glaciers (Nettles & Ekström 2010). However, the monitoring potential of icequakes is still poorly understood, partly because every glacier has its own seismological fingerprint and the source processes of individual types of icequakes are difficult to determine. Classic seismological location routines rely on identifiable onsets of compressional and shear waves emitted by shear failure of a brittle material but the source processes of icequakes are much more complicated. They include as varied processes as the overturning of icebergs, fracturing at the grounding line due to bending or stick-slip motion at the glacier base. Water plays a significant role in modifying signal shapes (Hammer et al*.,* 2015). The signals may last from a fraction of a second to many minutes and their frequency content ranges from 100 Hz to 100 s period. Additional observations from multidisciplinary studies like camera images, tide gauges, GPS measurements etc. are often necessary to get an idea of the source processes of icequakes.

The multidisciplinary study GRIFF offers the opportunity to get a first impression of the seismicity associated with the 79°N glacier with contemporaneous measurements of tidal cycles and flow speeds. Its ice shelf looses mass through melting rather than calving and glacial earthquakes have not been detected at this glacier. We therefore expect tidally modulated bending processes at the grounding line comparable to Ekström Isen in Antarctica (Hammer et al*.,* 2015) or tidally triggered stick-slip motion events as on Whillans Ice Stream in Antarctica (Wiens et al*.,* 2008).

Work at sea

Seismicity and lithosphere structure of the ultraslow spreading Knipovich Ridge

After testing of the releasers at about 2,000 m water depth, the OBS were assembled on deck. The network was installed in two rounds, the first 10 instruments at the northern and southern end of the network during the transit to Fram Strait and the 13 central stations of the network about 6 weeks later on the way back to Tromsø (Fig. 11.1). Areas with flat topography were chosen based on swath bathmetry and the instruments were deployed in free-fall mode. Table 11.1 summarizes deployment locations and instrumentation details. Further six OBS stations marked P1-P6 (Fig. 11.1) will be deployed by our projects partners from the Institute of Geophysics of the Polish Academy of Science. Their instruments help to obtain a dense station cover of Logachev Seamount and the adjacent along-axis region. They will record seismicity approximately for the period October 2016 - May 2017.

Gravity acceleration was continuously measured by the ship's gravity meter throughout the cruise. Reference measurements were performed in Tromsø port prior to departure and after arrival to tie the relative measurements to a location with known absolute earth acceleration. The gravity data will be used to calculate relative variations in crustal thickness along Knipovich Ridge.

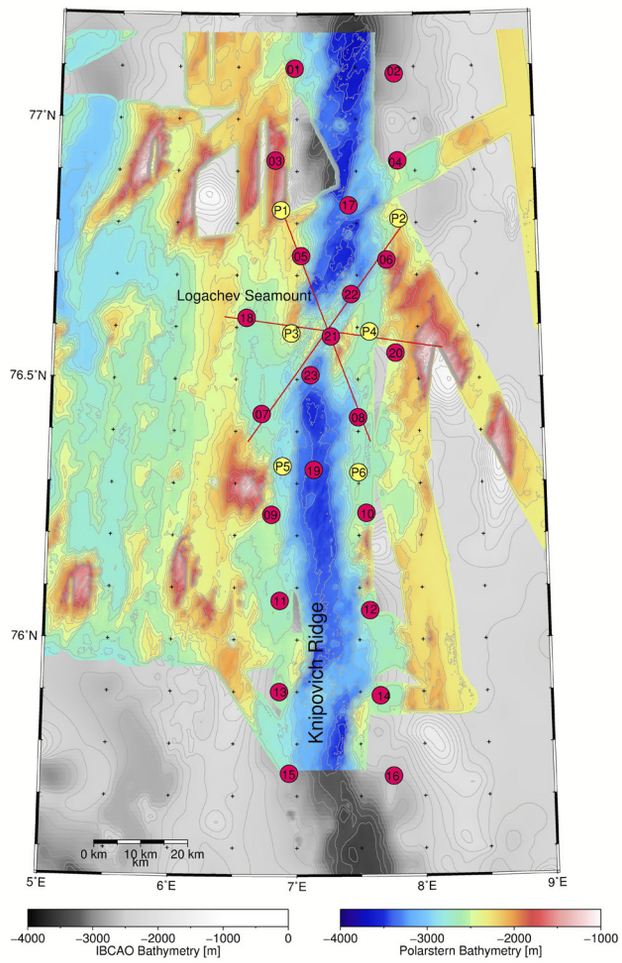

Fig. 11.1: Location of ocean bottom seismometers along Knipovich Ridge. Red dots are OBS deployed during this cruise, yellow dots OBS to be deployed by a partner project. Lines show refraction seismic profiles that will be acquired upon station retrieval.

Tab. 11.1: Ocean bottom seismometer deployment sites and recording parameters

OBS No	Latitude	Longitude	Depth [m]	Deployment Time	Sample rate	Autorelease Time	Recording Stop time
01	77°05.9'N	6°58.8'E	2604	21.7.16 05:36	50 Hz	13.7.18 15:00	10.7.17 06:00
02	77°05.2'N	7°49.9'E	2811	21.7.16 04:24	50 Hz	13.7.18 20:00	10.7.17 06:00
03	76°55.2'N	6°49.2'E	1804	21.7.16 01:38	50 Hz	13.7.18 10:00	10.7.17 06:00
04	76°55.2'N	7°51.0'E	2454	21.7.16 03:18	50 Hz	13.7.18 05:00	10.7.17 06:00
05	76°44.2'N	7°02.1'E	2376	03.9.16 02:49	50 Hz	12.7.18 09:00	24.8.17 06:00
06	76°43.8'N	7°44.9'E	2524	03.9.16 03:53	50 Hz	12.7.18 19:00	24.8.17 06:00
07	76°26.0'N	6°42.6'E	2686	03.9.16 09:22	50 Hz	11.7.18 07:00	24.8.17 06:00

OBS No	Latitude	Longitude	Depth [m]	Deployment Time	Sample rate	Autorelease Time	Recording Stop time
08	76°25.6'N	7°30.0'E	2663	03.9.16 10:39	50 Hz	11.7.18 03:00	24.8.17 06:00
09	76°14.4'N	6°47.7'E	2562	03.9.16 13:41	50 Hz	10.7.18 12:00	24.8.17 06:00
10	76°14.6'N	7°33.6'E	2581	03.9.16 12:31	50 Hz	10.7.18 17:00	24.8.17 06:00
11	76°04.5'N	6°51.8'E	2615	20.7.16 21:19	50 Hz	10.7.18 07:00	10.7.17 06:00
12	76°03.4'N	7°35.0'E	2614	20.7.16 20:10	50 Hz	10.7.18 02:00	10.7.17 06:00
13	75°54.0'N	6°51.6'E	2633	20.7.16 17:52	50 Hz	09.7.18 16:00	10.7.17 06:00
14	75°53.6'N	7°39.6'E	2597	20.7.16 19:05	50 Hz	09.7.18 21:00	10.7.17 06:00
15	75°44.6'N	6°56.3'E	2660	20.7.16 16:48	50 Hz	09.7.18 11:00	10.7.17 06:00
16	75°44.3'N	7°45.3'E	2694	20.7.16 15:25	50 Hz	09.7.18 06:00	10.7.17 06:00
17	76°50.1'N	7°26.1'E	3244	03.9.16 01:56	50 Hz	13.7.18 00:00	24.8.17 06:00
18	76°37.1'N	6°35.0'E	2577	03.9.16 07:21	100 Hz	12.7.18 04:00	-
19	76°19.6'N	7°08.2'E	3402	03.9.16 11:36	50 Hz	10.7.18 22:00	24.8.17 06:00
20	76°33.0'N	7°48.8'E	2502	03.9.16 05:25	100 Hz	11.7.18 13:00	-
21	76°35.0°N	7°16.9'E	2700	03.9.16 06:18	100 Hz	11.7.18 18:00	-
22	76°39.8'N	7°27.1'E	3208	03.9.16 04:30	100 Hz	12.7.18 14:00	-
23	76°30.5'N	7°06.7'E	3345	03.9.16 08:32	100 Hz	11.7.18 23:00	-

Icequake recording near the grounding line of 79°N glacier

We deployed a trial seismic array consisting of two Güralp CMG-3ESP and one Trillium broadband three-component seismometer (reconfigured OBS) near the southern end of the grounding line on a small exposure of bedrock west of Lambert Land (Fig. 11.2). The array has an approximate aperture of 500 m and continuously recorded seismicity during 6 days with a sampling rate of 100 Hz (see Tab. 11.2). The records give a first impression of the seismicity of the glacier and help to design a network geometry adapted to the signal types to be studied during the field season of 2017 when a longer deployment of more stations will be possible.

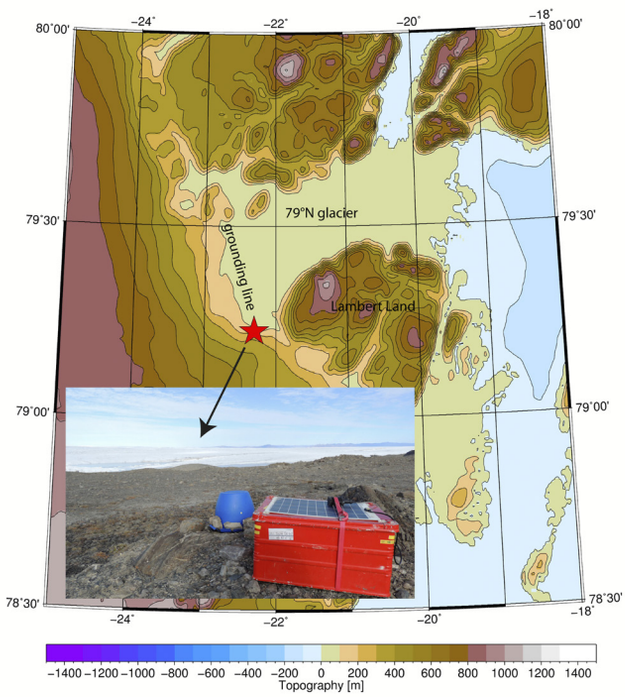

Fig. 11.2: Position of the land seismic network (red star) near the grounding line of the 79°N glacier west of Lambert Land. The seismometer is placed on bedrock and covered by a blue bucket. The red box contains battery, GPS and recording unit.

Tab. 11.2: Land seismic network deployment sites

Station	Action	Date	Time (UTC)	Latitude/ Longitude	Altitude/ Orientation wrt magnetic north
79N01	deployment	18.08.2016	11:09	79° 13.89' N	90 m
	recovery	24.08.2016	13:35	22° 17.82' W	-75°
79N02	deployment	18.08.2016	10:17	79° 14.35' N	27 m
	recovery	24.08.2016	11:15	22° 16.72' W	-20°
79N03	deployment	18.08.2016	16:24	79° 14.11' N	32 m
Trillium, OBS	recovery	24.08.2016	11:25	22° 16.31' W	unknown

Preliminary (expected) results

Seismicity and lithosphere structure of the ultraslow spreading Knipovich Ridge

The seismic data recorded by the Knipovich Ridge seismic network can only be accessed upon retrieval of the OBS stations in October 2017. We expect to record about 6,000-10,000 local earthquakes in the magnitude range 0-4 and about 50 teleseismic earthquakes above magnitude 6 that can be used for determining the seismicity and lithospheric structure of this area.

Icequake recording near the grounding line of 79°N glacier

The three seismic stations recorded without failures throughout the deployment period. The raw data have been converted into a Seiscomp miniseed archive of day-files and screened to check data quality. Figs. 11.3 and 11.4 show 13 hours of recording of the vertical channel of station 79N01 in different frequency ranges. Above 5 Hz, cryogenic seismicity dominates the character of the seismograms. Periods with frequent seismic events can be distinguished from calmer periods. At lower frequencies, regional events and teleseismic events above magnitude Mw≈6 could clearly be detected by all stations, indicating a good ground coupling although station 79N02 was installed on a loose boulder rather than bedrock. Fig. 11.5 shows an impulsive cryogenic event recorded throughout the network at high quality. It arrives from west at the westernmost station 79N01. Heavily crevassed potential source areas are located at 79°18.4'N 22°36.3'W, 79°14.5'N 22°29.0'W and 79°13.5'N 22°24.3'W near the seismic network. Two seismic phases can be identified, the second potentially representing a multiple reflection on the glacier surface or bottom. Different high frequency event types with longer duration (up to one minute) could be detected, but long period events were not obvious upon preliminary inspection of the data.

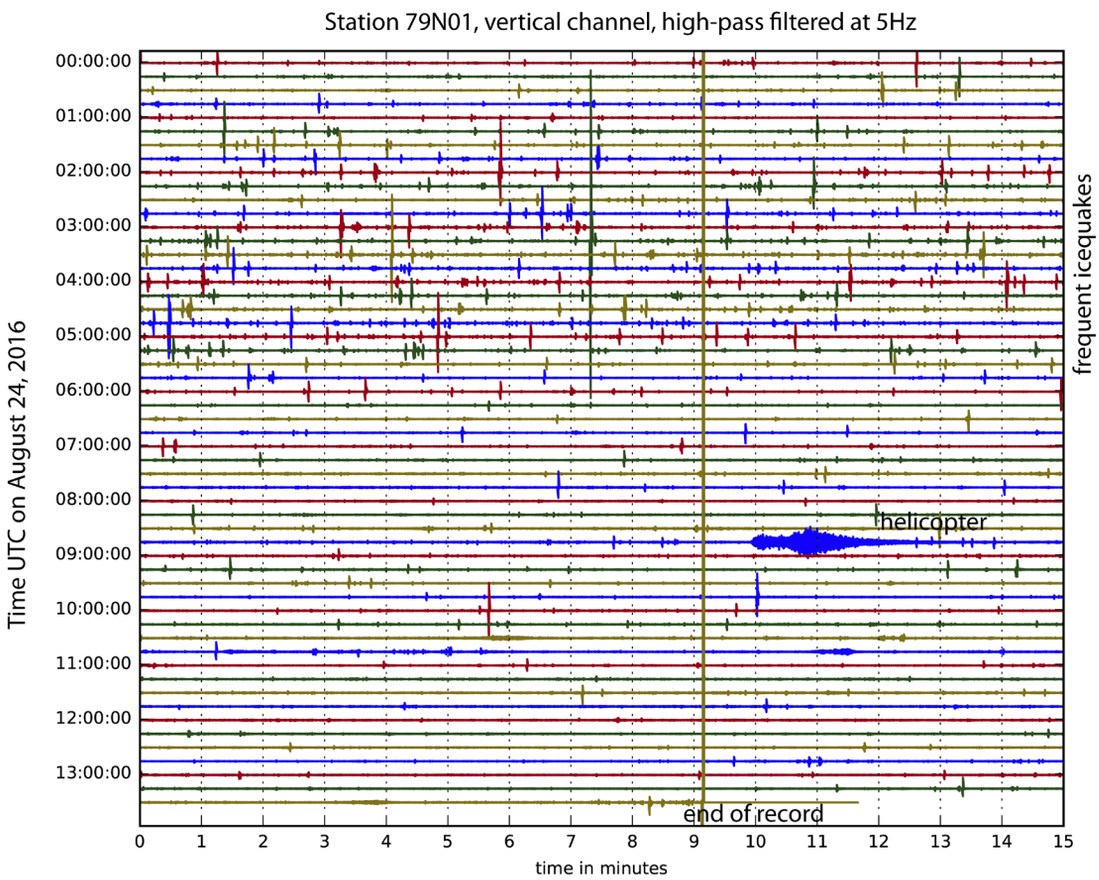

Fig. 11.3: Record example of the vertical channel of station 79N01 showing high-frequency signals

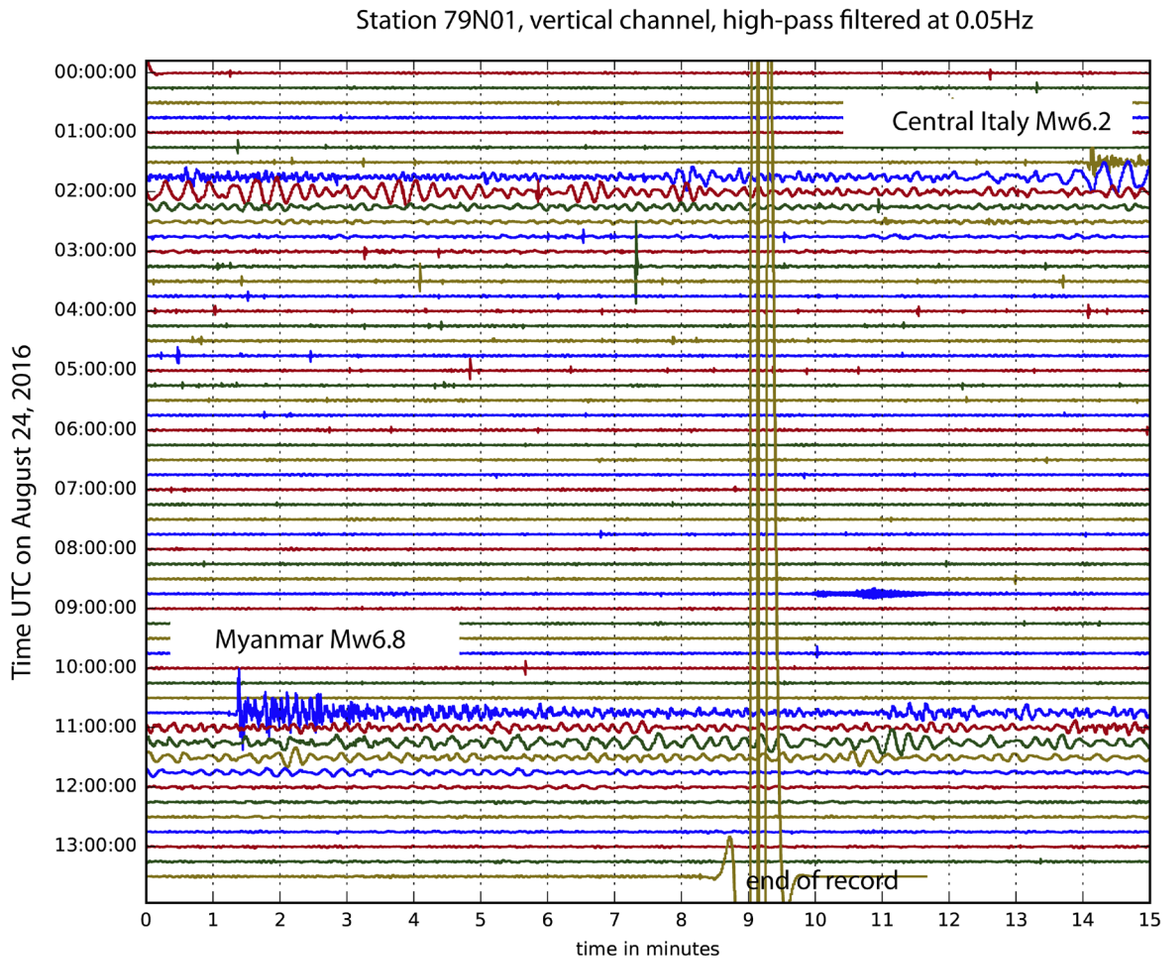

Fig. 11.4: Record example of the vertical channel of station 79N01 showing low-frequency phases of large teleseismic earthquakes

Data management

Our seismic data will be archived in a common data repository for all data acquired with the OBSs of the DEPAS instrument pool. As data processing of this large data set is very time consuming, we will make the data publicly available through the GEOFON seismic data request system after 5 years of restricted access.

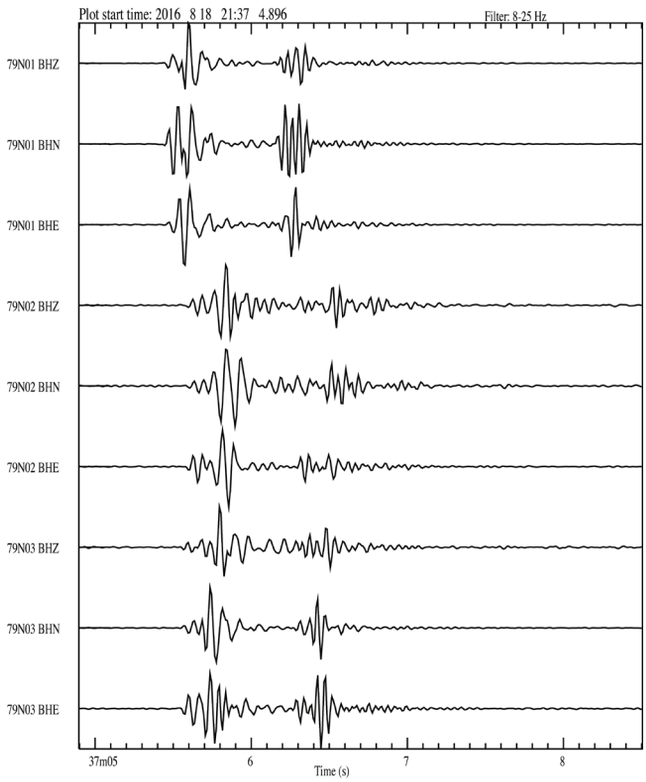

Fig. 11.5: Example of an impulsive high-frequency icequake recorded with high quality by all three stations of the array on all three channels

References

Bown JW, White RS (1994) Variation with spreading rate of oceanic crustal thickness and geochemistry. Earth Planet. Sci. Lett., 121, 435-449.

Ekström G, Nettles M, Tsai VC (2006) Seasonality and increasing frequency of Greenland glacial earthquakes. Science, 311, 1756-1758.

Hammer C, Ohrnberger M, Schlindwein V (2015) Pattern of cryospheric seismic events observed at Ekström Ice Shelf, Antarctica. Geophys. Res. Lett., 42, doi:10.1002/2015GL064029.

Michael PJ et al. (2003) Magmatic and amagmatic seafloor generation at the ultraslow-spreading Gakkel ridge, Arctic Ocean. Nature, 423, 956-961.

Nettles M, Ekström G (2010) Glacial earthquakes in Greenland and Antarctica. Annu. Rev. Earth Planet. Sci., 38, 467-491.

Schlindwein V, Demuth A, Geissler WH, Jokat W (2013) Seismic gap beneath Logachev Seamount: Indicator for melt focusing at an ultraslow mid-ocean ridge? Geophys. Res. Lett., 40, doi:10.1002/grl.50329.

Schlindwein V (2014) The Expedition of the Research Vessel “Polarstern” to the Antarctic in 2013 ANT-XXIX/8. Rep. Polar Marine Res., 672, 14-22.

Schlindwein V, Schmid F (2016) Mid-ocean ridge seismicity reveals extreme types of ocean lithosphere. Nature, 535, 276-279.

Standish JJ, Dick HJB, Michael PJ, Melson WG, O'Hearn T (2008) MORB generation beneath the ultraslow spreading Southwest Indian Ridge 9–25°E: Major element chemistry and the importance of process versus source. Geochem. Geophys. Geosyst., 9, doi:10.1029/2008gc001959.

Wiens DA, Anandakrishnan S, Winberry JP, King MA (2008) Simultaneous teleseismic and geodetic observations of the stick–slip motion of an Antarctic ice stream. Nature, 453, 770-775.

APPENDIX

A.1 PARTICIPATING INSTITUTIONS

A.2 CRUISE PARTICIPANTS

A.3 SHIP'S CREW

A.4 STATION LIST

A.1 TEILNEHMENDEINSTITUTE/PARTICIPATINGINSTITUTIONS

	Address
AWI	Alfred-Wegener-Institut Helmholtz-Zentrum für Polar- und Meeresforschung Postfach 120161 27515 Bremerhaven Germany
CCMAR-UAlg	Centre of Marine Sciences (CCMAR) Universidade do Algarve 8005-139 Faro Portugal
DUR	Durham University Department of Geography Science Laboratories South Rd Durham DH1 3LE, UK
DWD	Deutscher Wetterdienst Geschäftsbereich Wettervorhersage Seeschifffahrtsberatung Bernhard Nocht Str. 76 20359 Hamburg Germany
ETH/LIP	ETH-Zurich Laboratory of Ion Beam Physics Otto-Stern-Weg 5 8093 Zurich Switzerland
GEOMAR	Helmholtz-Zentrum für Ozeanforschung (GEOMAR) Wischhofstr. 1-3 24148 Kiel Germany
HeliService	HeliService International GmbH Am Luneort 15 27572 Bremerhaven Germany

	Address
MIO	CNRS/Mediterranean Institute of Oceanography Chemin de la Batterie des Lions 13007 MARSEILLE France
MIT	Massachusetts Institute of Technology 77 Massachusetts Avenue Cambridge, MA 02139-4307, USA
NIOZ	Royal Netherlands Institute for Sea Research ‘t Horntje Texel, The Netherlands
RUG	Rijks Universiteit Groningen Centre for Energy and Environmental Sciences Nijenborgh 4 9747 AG Groningen, The Netherlands
Squarewavemarine	Squarewavemarine.com PO Box 2511 Sidney, BC V8L 4B9, Canada
Stellenbosch U	Stellenbosch University Department of Mechanical Engineering Sound and Vibration Research Group Stellenbosch, 7559, South Africa
TU Dresden	Technische Universität Dresden Institut für Planetare Geodäsie 01062 Dresden, Germany
UGOT	University of Gothenburg Department of Chemistry & Molecular Biology Medicinaregatan 9 c 40530 Göteborg Sweden

	Address
UHB-IUP	University of Bremen Institute of Environmental Physics (IUP) – Oceanography Otto-Hahn-Allee 28359 Bremen, Germany
Uni HB	Universität Bremen Marine Zoologie (FB 02) Postfach 330 440 D-28334 Bremen Germany
University of Delaware	University of Delaware 111 Robinson Hall Newark, DE 19716 USA
WHOI	Woods Hole Oceanographic Institution 266 Woods Hole Road Woods Hole, MA 02543-1050 USA

A.2 FAHRTTEILNEHMER / CRUISE PARTICIPANTS

Name/ Last name	Vorname/ First name	Institut/ Institute	Beruf/ Profession	Fachbereich/ Discipline
Auel	Holger	Uni HB	Scientist	Biology
Boavida	Joana	CCMAR-UAlg	Scientist	Biology
Brauer	Jens	HeliService	Pilot	
Callard	Sarah Louise	DUR	Scientist	Geology
Casacuberta	Nuria	ETH/LIP	Scientist	Geochemistry
De Waal	Rosca	Stellenbosch U	Student	Engineering
Ebermann	Benjamin	TU Dresden	Scientist	Geodesy
Engicht	Carina	AWI	Technician	Oceanography
Evers	Florian	GEOMAR	Technician	Geochemistry
Gerken	Jan Günter	UHB-IUP	Student	Tracer Oceanography
Graeve	Martin	AWI	Scientist	Geochemistry
Grob	Henrik	AWI	Student	Geology
Havermans	Charlotte	Uni HB	Scientist	Biology
Heim	Thomas	HeliService	Technician	
Heimbürger	Lars-Eric	MIO	Scientist	Geochemistry
Herzberg	Nicola	GEOMAR	Student	Geochemistry
Huhn	Oliver	UHB-IUP	Scientist	Tracer Oceanography
Jacinto	Rita	CCMAR-UAlg	Student	Biology
Jones	Elisabeth	RUG/NIOZ	Scientist	Geochemistry
Kanzow	Torsten	AWI	Chief Scientist	Oceanography
Kappelsberger	Maria	AWI	Student	Geology
Kirk	Henning	AWI	Technician	Seismology
Köhler	Dennis	AWI	Technician	Geochemistry
Köhn	Eike	GEOMAR	Student	Oceanography
Kraemer	Andrei	TU Dresden	Student	Geodesy
Krisch	Stephan	GEOMAR	Student	Geochemistry
Lloyd	Jerry	DUR	Scientist	Geology
Lodeiro Fernandez	Pablo	GEOMAR	Scientist	Geochemistry
Ludwichowski	Kai-Uwe	AWI	Technician	Geochemistry
Melo Franco Santos	Rita	Uni HB/AWI	Student	Biology
Meulenbroek	Kirsten	GEOMAR	Student	Geochemistry
Miller	Max	DWD	Meteorologist	
Monsees	Matthias	AWI	Technician	Oceanography
Ó Cofaigh	Colm	DUR	Scientist	Geology

Name/ Last name	**Vorname/ First name**	**Institut/ Institute**	**Beruf/ Profession**	**Fachbereich/ Discipline**
Poole	Jonathan	Square-wavemarine	Technician	Oceanography
Prinz	Natalie	Uni HB	Student	Biology
Roberts	David	DUR	Scientist	Geology
Rutgers van der Loeff	Michiel	AWI	Scientist	Geochemistry
Santos Fernandez	Victor	HeliService	Technician	
Schaffer	Janin	AWI	Student	Oceanography
Schlindwein	Vera	AWI	Scientist	Seismology
Soal	Keith	Stellenbosch U	Student	Engineering
Sonnabend	Hartmut	DWD	Technician	
Tsubouchi	Takamasa	AWI	Scientist	Oceanography
Ulfsbo	Adam	UGOT	Scientist	Geochemistry
Valk	Ole	AWI	Student	Geochemistry
Vaupel	Lars	HeliService	Chief pilot	
von Appen	Wilken-Jon	AWI	Scientist	Oceanography
Wegehaupt	Timm	UHB-IUP	Student	Tracer Oceanography
Wilson	Nat	MIT-WHOI	Student	Oceanography
Yong	Jaw Chuen	GEOMAR	Student	Geochemistry
Wegehaupt	Timm	UHB-IUP	Student	Tracer Oceanography

A.3 SCHIFFSBESATZUNG / SHIP'S CREW

No.	Name	Rank
1	Schwarze, Stefan	Master
2	Grundmann, Uwe	1. Offc.
3	Heuck, Hinnerk	Ch. Eng.
4	Janik, Michael	2. Offc.
5	Hering, Igor	2. Offc.
6	Fallei, Holger	3. Offc.
7	Pohl, Klaus	Doctor
8	Fröb, Martin	R. Offc.
9	Grafe, Jens	2. Eng.
10	Krinfeld, Oleksandr	2. Eng.
11	Holst, Wolfgang	2. Eng.
12	Redmer, Jens	Elec. Eng.
13	Christian, Boris	ELO
14	Hüttebräucker, Olaf	ELO
15	Markert, Winfried	ELO
16	Pliet, Johannes	Sys-man
17	Himmel,Frank	Boatsw.
18	Loidl, Reiner	Carpenter
19	Reise, Lutz	A.B.
20	Hagemann, Manfred	A.B.
21	Winkler, Michael	A.B.
22	Scheel, Sebastian	A.B.
23	Bäcker, Andreas	A.B.
24	Brück, Sebastian	A.B.
25	Wende, Uwe	A.B.
26	Völker, Frank Rainer	A.B.
27	Wittek, Sönke,	A.B./Tr.
28	Schulz, Fabian	A.B./Tr.
29	Preußner, Jörg	Storek.
30	Teichert, Uwe	Mot-man
31	Rhau, Lars-Peter	Mot-man
32	Lamm, Gerd	Mot-man
33	Schünemann, Mario	Mot-man
34	Kittmann, Markus	Mot-man
35	Redmer, Klaus-Peter	Cook
36	Silinski, Frank	Cooksmate
37	Martens, Michael	Cooksmate
38	Czyborra, Bärbel	1. Stwdess
39	Wöckener, Martina	Stwdess/N.
40	Dibenau, Torsten	2. Stwdess
41	Silinski, Carmen	2. Steward
42	Grigull, Elke	2. Stwdess
43	Arendt, Rene	2. Steward
44	Sun, Yong Shen	2. Stwdess
45	Yu, Kwok Yuen	Laundrym.

A.4 STATIONSLISTE / STATION LIST

Station	Date	Time	Gear	Action	Position Lat	Position Lon	Water depth [m]
PS100/001-1	2016-07-19	7:57:00	REL	on ground/ max depth	70° 59.59' N	15° 28.96' E	1971.2
PS100/002-1	2016-07-20	8:05:00	CTD/L	on ground/ max depth	75° 06.89' N	08° 36.05' E	2672.3
PS100/002-2	2016-07-20	9:51:00	CTD/UC	on ground/ max depth	75° 06.89' N	08° 36.16' E	2666.3
PS100/002-3	2016-07-20	9:59:00	MN	on ground/ max depth	75° 06.89' N	08° 36.23' E	2666.7
PS100/002-4	2016-07-20	10:57:00	BONGO	on ground/ max depth	75° 06.75' N	08° 32.46' E	2668.9
PS100/003-1	2016-07-20	15:26:59	OBS	on ground/ max depth	75° 44.34' N	07° 45.32' E	2681
PS100/004-1	2016-07-20	16:47:59	OBS	on ground/ max depth	75° 44.60' N	06° 56.24' E	2660.1
PS100/005-1	2016-07-20	17:50:59	OBS	on ground/ max depth	75° 54.01' N	06° 51.56' E	2637.1
PS100/006-1	2016-07-20	19:05:59	OBS	on ground/ max depth	75° 53.56' N	07° 39.59' E	2601
PS100/007-1	2016-07-20	20:10:59	OBS	on ground/ max depth	76° 03.41' N	07° 34.98' E	2612.7
PS100/008-1	2016-07-20	21:18:59	OBS	on ground/ max depth	76° 04.49' N	06° 51.78' E	2598.1
PS100/009-1	2016-07-21	1:37:59	OBS	on ground/ max depth	76° 55.24' N	06° 49.13' E	1858.6
PS100/010-1	2016-07-21	3:17:59	OBS	on ground/ max depth	76° 55.20' N	07° 50.96' E	2457.2
PS100/011-1	2016-07-21	4:23:59	OBS	on ground/ max depth	77° 05.23' N	07° 49.87' E	2889.6
PS100/012-1	2016-07-21	5:36:59	OBS	on ground/ max depth	77° 05.86' N	06° 58.79' E	2602.3
PS100/013-1	2016-07-21	9:36:00	CTD/UC	on ground/ max depth	77° 29.94' N	09° 16.62' E	1964.6
PS100/013-2	2016-07-21	12:49:00	CTD/L	on ground/ max depth	77° 29.86' N	09° 16.80' E	1969.1
PS100/013-3	2016-07-21	14:19:00	CTD/UC	on ground/ max depth	77° 29.83' N	09° 17.09' E	1966.8
PS100/013-3	2016-07-21	15:27:00	CTD/UC	on ground/ max depth	77° 29.63' N	09° 17.28' E	1967.9
PS100/014-1	2016-07-22	17:23:00	MOR	on ground/ max depth	78° 50.12' N	08° 40.28' E	228
PS100/015-1	2016-07-22	19:15:00	CTD/UC	on ground/ max depth	79° 00.07' N	08° 19.70' E	793.2
PS100/015-2	2016-07-22	20:17:00	CTD/L	on ground/ max depth	78° 59.96' N	08° 19.68' E	784
PS100/015-3	2016-07-22	22:01:00	ISP	on ground/ max depth	78° 59.98' N	08° 19.80' E	786.8
PS100/015-4	2016-07-23	2:31:00	MN	on ground/ max depth	79° 00.15' N	08° 19.71' E	792.8
PS100/015-5	2016-07-23	3:22:00	CTD/L	on ground/ max depth	79° 00.26' N	08° 19.69' E	797.1

Station	Date	Time	Gear	Action	Position Lat	Position Lon	Water depth [m]
PS100/016-1	2016-07-23	6:57:00	MOR	on ground/ max depth	79° 00.02' N	08° 19.84' E	785.2
PS100/017-1	2016-07-23	8:44:01	MOR	on ground/ max depth	79° 00.03' N	07° 59.95' E	1075.3
PS100/018-1	2016-07-23	13:44:00	MOR	on ground/ max depth	79° 00.01' N	07° 00.03' E	1218.5
PS100/019-1	2016-07-23	17:53:01	MOR	on ground/ max depth	79° 00.02' N	05° 40.12' E	2100.4
PS100/019-2	2016-07-23	19:00:00	CTD/L	on ground/ max depth	78° 59.43' N	05° 40.06' E	2148.9
PS100/020-1	2016-07-23	21:39:00	CTD/L	on ground/ max depth	79° 00.01' N	06° 30.01' E	1402.3
PS100/021-1	2016-07-24	0:25:00	CTD/UC	on ground/ max depth	79° 00.02' N	07° 29.90' E	1223.9
PS100/021-2	2016-07-24	2:06:00	CTD/L	on ground/ max depth	79° 00.04' N	07° 30.12' E	1223.7
PS100/022-1	2016-07-24	4:28:00	CTD/L	on ground/ max depth	79° 00.03' N	07° 59.83' E	1077.9
PS100/023-1	2016-07-24	9:00:00	MOR	on ground/ max depth	79° 00.01' N	08° 32.51' E	345.9
PS100/024-1	2016-07-24	10:19:00	MOR	on ground/ max depth	78° 49.66' N	08° 19.20' E	787
PS100/025-1	2016-07-24	11:32:00	MOR	on ground/ max depth	78° 50.06' N	08° 20.24' E	0
PS100/026-1	2016-07-24	13:40:00	MOR	on ground/ max depth	78° 49.98' N	08° 01.87' E	996.5
PS100/027-1	2016-07-24	16:08:00	CTD/L	on ground/ max depth	78° 59.62' N	08° 32.80' E	319.7
PS100/027-2	2016-07-24	16:42:00	MN	on ground/ max depth	78° 59.61' N	08° 32.70' E	324.6
PS100/028-1	2016-07-24	19:20:00	CTD/UC	on ground/ max depth	78° 59.16' N	06° 59.66' E	1200.2
PS100/028-2	2016-07-24	20:38:00	CTD/L	on ground/ max depth	78° 59.16' N	06° 59.66' E	1204.5
PS100/028-3	2016-07-24	22:19:00	ISP	on ground/ max depth	78° 59.19' N	06° 59.66' E	1198.4
PS100/028-4	2016-07-25	2:51:00	CTD/L	on ground/ max depth	78° 59.22' N	06° 59.58' E	1199.7
PS100/028-5	2016-07-25	4:05:00	MN	on ground/ max depth	78° 59.22' N	06° 59.45' E	1199.4
PS100/029-1	2016-07-25	6:03:00	MOR	on ground/ max depth	78° 49.68' N	07° 03.26' E	1398.5
PS100/030-1	2016-07-25	9:02:00	MOR	on ground/ max depth	78° 49.90' N	06° 00.96' E	2418
PS100/031-1	2016-07-25	11:22:00	MOR	on ground/ max depth	78° 44.89' N	05° 30.46' E	2419.1
PS100/032-1	2016-07-25	14:54:00	MOR	on ground/ max depth	78° 50.46' N	04° 39.00' E	2725.7
PS100/033-1	2016-07-25	18:15:00	CTD/UC	on ground/ max depth	78° 49.16' N	04° 59.84' E	2688
PS100/033-2	2016-07-25	20:29:00	CTD/L	on ground/ max depth	78° 49.10' N	04° 60.00' E	2685.3

Station	Date	Time	Gear	Action	Position Lat	Position Lon	Water depth [m]
PS100/034-1	2016-07-25	23:43:00	CTD/L	on ground/ max depth	78° 55.15' N	05° 20.29' E	2580.7
PS100/035-1	2016-07-26	3:12:00	CTD/L	on ground/ max depth	78° 49.71' N	04° 15.06' E	2405.2
PS100/036-1	2016-07-26	6:00:00	MOR	on ground/ max depth	78° 50.16' N	05° 00.33' E	2701.2
PS100/037-1	2016-07-26	15:57:00	CTD/UC	on ground/ max depth	78° 50.00' N	03° 30.15' E	2301
PS100/037-2	2016-07-26	17:54:00	CTD/L	on ground/ max depth	78° 50.01' N	03° 30.38' E	2300.8
PS100/037-3	2016-07-26	20:18:00	ISP	on ground/ max depth	78° 50.01' N	03° 30.12' E	2300.1
PS100/037-4	2016-07-27	0:55:00	CTD/L	on ground/ max depth	78° 50.03' N	03° 30.02' E	2301
PS100/038-1	2016-07-27	4:05:00	CTD/L	on ground/ max depth	78° 50.41' N	02° 14.83' E	2495
PS100/039-1	2016-07-27	8:47:00	CTD/L	on ground/ max depth	78° 50.06' N	00° 00.01' W	2599.4
PS100/039-2	2016-07-27	13:48:00	MOR	on ground/ max depth	78° 50.01' N	00° 00.09' E	2596.5
PS100/040-1	2016-07-27	14:49:00	MOR	on ground/ max depth	78° 51.34' N	00° 48.33' W	2640.8
PS100/041-1	2016-07-27	16:14:00	MOR	on ground/ max depth	78° 50.07' N	00° 47.89' W	2619.2
PS100/042-1	2016-07-27	19:01:00	CTD/UC	on ground/ max depth	78° 50.02' N	00° 53.96' W	2600.7
PS100/042-2	2016-07-27	21:21:00	CTD/L	on ground/ max depth	78° 50.11' N	00° 53.36' W	2609.9
PS100/043-1	2016-07-28	2:31:00	CTD/L	on ground/ max depth	79° 10.01' N	00° 01.87' E	2683.8
PS100/044-1	2016-07-28	6:50:00	CTD/UC	on ground/ max depth	78° 49.83' N	01° 05.67' E	2474.9
PS100/044-2	2016-07-28	9:04:00	CTD/L	on ground/ max depth	78° 49.79' N	01° 05.87' E	2476.7
PS100/044-3	2016-07-28	11:46:00	ISP	on ground/ max depth	78° 49.80' N	01° 05.54' E	2473.1
PS100/044-4	2016-07-28	16:32:00	CTD/L	on ground/ max depth	78° 49.63' N	01° 05.32' E	2468.6
PS100/044-5	2016-07-28	18:53:00	IFISH	on ground/ max depth	79° 13.12' N	00° 27.97' E	2724.3
PS100/045-1	2016-07-28	23:25:00	MOR	on ground/ max depth	79° 30.00' N	00° 00.03' W	2778
PS100/046-1	2016-07-29	2:26:00	CTD/L	on ground/ max depth	79° 29.98' N	00° 04.88' E	2761.3
PS100/046-2	2016-07-29	5:31:00	MN	on ground/ max depth	79° 29.67' N	00° 04.49' E	2782.7
PS100/046-3	2016-07-29	7:09:00	MN	on ground/ max depth	79° 29.53' N	00° 03.93' E	2787.7
PS100/047-1	2016-07-29	18:14:00	MOR	on ground/ max depth	80° 09.75' N	00° 10.19' E	3034.1
PS100/048-1	2016-07-29	19:58:00	CTD/L	on ground/ max depth	80° 09.38' N	00° 17.25' E	3014.9

Station	Date	Time	Gear	Action	Position Lat	Position Lon	Water depth [m]
PS100/048-2	2016-07-29	22:18:00	MN	on ground/ max depth	80° 08.51' N	00° 18.98' E	3052.7
PS100/048-3	2016-07-30	0:07:00	BONGO	on ground/ max depth	80° 06.30' N	00° 18.68' E	3254.7
PS100/049-1	2016-07-30	6:03:00	CTD/L	on ground/ max depth	80° 30.11' N	00° 10.60' E	3187.9
PS100/049-2	2016-07-30	8:25:00	MN	on ground/ max depth	80° 28.96' N	00° 16.74' E	3131.3
PS100/049-3	2016-07-30	10:01:00	MN	on ground/ max depth	80° 27.65' N	00° 17.34' E	3123
PS100/050-1	2016-07-30	13:47:00	CTD/UC	on ground/ max depth	80° 42.83' N	00° 07.68' W	3203.6
PS100/051-1	2016-07-30	18:59:00	REL	on ground/ max depth	80° 47.78' N	00° 08.41' E	3084.1
PS100/052-1	2016-07-30	21:44:00	CTD/UC	on ground/ max depth	80° 45.67' N	00° 07.66' E	3158.9
PS100/052-2	2016-07-30	23:02:00	CTD/L	on ground/ max depth	80° 45.03' N	00° 05.19' E	3180.8
PS100/052-3	2016-07-31	2:00:00	ISP	on ground/ max depth	80° 44.56' N	00° 01.42' E	3191.1
PS100/052-4	2016-07-31	7:10:00	CTD/L	on ground/ max depth	80° 42.68' N	00° 09.13' E	3207.1
PS100/052-5	2016-07-31	7:59:00	CTD/UC	on ground/ max depth	80° 42.08' N	00° 09.97' E	3207.6
PS100/053-1	2016-07-31	12:34:00	MOR	on ground/ max depth	80° 51.18' N	00° 07.23' W	3139.5
PS100/053-2	2016-07-31	14:28:00	CTD/UC	on ground/ max depth	80° 51.19' N	00° 12.35' W	3170.5
PS100/054-1	2016-07-31	22:11:00	CTD/L	on ground/ max depth	80° 23.17' N	01° 28.67' W	4018.4
PS100/054-2	2016-07-31	23:54:00	MN	on ground/ max depth	80° 22.50' N	01° 31.03' W	4053.6
PS100/054-3	2016-08-01	1:28:00	MN	on ground/ max depth	80° 22.26' N	01° 34.58' W	4005.4
PS100/055-1	2016-08-01	6:40:00	CTD/L	on ground/ max depth	80° 22.41' N	02° 53.94' W	3355.7
PS100/055-2	2016-08-01	8:53:00	MN	on ground/ max depth	80° 21.77' N	02° 49.01' W	3425.6
PS100/056-1	2016-08-01	13:26:00	CTD/UC	on ground/ max depth	80° 19.55' N	04° 00.56' W	2543.8
PS100/056-2	2016-08-01	15:49:00	CTD/L	on ground/ max depth	80° 19.85' N	04° 01.47' W	2533.2
PS100/056-3	2016-08-01	17:35:00	MN	on ground/ max depth	80° 20.13' N	03° 58.90' W	2573
PS100/056-4	2016-08-01	19:10:00	MN	on ground/ max depth	80° 19.89' N	03° 55.31' W	2620.9
PS100/056-5	2016-08-01	20:45:00	CTD/L	on ground/ max depth	80° 19.22' N	03° 52.40' W	2621.9
PS100/057-1	2016-08-01	23:17:00	CTD/L	on ground/ max depth	80° 18.22' N	04° 30.87' W	2052.8
PS100/058-1	2016-08-02	2:20:00	CTD/L	on ground/ max depth	80° 16.19' N	04° 59.40' W	1468.5

Station	Date	Time	Gear	Action	Position Lat	Position Lon	Water depth [m]
PS100/058-2	2016-08-02	4:15:00	MN	on ground/ max depth	80° 16.90' N	04° 58.47' W	1525.4
PS100/059-1	2016-08-02	7:12:00	CTD/L	on ground/ max depth	80° 16.09' N	05° 29.43' W	906.4
PS100/060-1	2016-08-02	9:36:00	CTD/L	on ground/ max depth	80° 14.81' N	06° 01.10' W	361.5
PS100/060-2	2016-08-02	10:18:00	MN	on ground/ max depth	80° 14.71' N	06° 01.26' W	362.7
PS100/061-1	2016-08-02	13:14:00	CTD/L	on ground/ max depth	80° 12.27' N	06° 59.67' W	287
PS100/061-2	2016-08-02	13:48:00	MN	on ground/ max depth	80° 12.53' N	06° 58.23' W	282.4
PS100/062-1	2016-08-02	16:15:00	CTD/L	on ground/ max depth	80° 08.85' N	07° 57.20' W	310.5
PS100/062-2	2016-08-02	16:56:00	MN	on ground/ max depth	80° 08.56' N	07° 55.16' W	320.8
PS100/063-1	2016-08-02	18:40:00	CTD/L	on ground/ max depth	80° 00.76' N	08° 23.68' W	144.4
PS100/064-1	2016-08-02	19:47:00	CTD/L	on ground/ max depth	80° 03.36' N	08° 20.90' W	204.2
PS100/065-1	2016-08-02	21:14:00	CTD/L	on ground/ max depth	80° 08.58' N	08° 15.10' W	327.8
PS100/066-1	2016-08-02	22:38:00	CTD/L	on ground/ max depth	80° 12.99' N	08° 11.48' W	289.2
PS100/067-1	2016-08-03	0:39:00	CTD/L	on ground/ max depth	80° 18.19' N	08° 04.26' W	269.9
PS100/068-1	2016-08-03	2:23:00	CTD/L	on ground/ max depth	80° 23.01' N	07° 58.47' W	248.2
PS100/069-1	2016-08-03	4:02:00	CTD/L	on ground/ max depth	80° 27.75' N	07° 53.30' W	240
PS100/070-1	2016-08-03	5:52:00	CTD/L	on ground/ max depth	80° 31.72' N	07° 49.33' W	269.6
PS100/071-1	2016-08-03	7:00:00	ICE	on ground/ max depth	80° 32.78' N	07° 51.41' W	256.1
PS100/072-1	2016-08-03	9:38:00	CTD/L	on ground/ max depth	80° 38.28' N	07° 44.65' W	101.7
PS100/073-1	2016-08-03	15:08:00	MOR	on ground/ max depth	80° 11.49' N	08° 08.96' W	306.8
PS100/074-1	2016-08-03	15:53:00	CTD/UC	on ground/ max depth	80° 13.11' N	08° 08.66' W	283.3
PS100/074-2	2016-08-03	17:15:00	ISP	on ground/ max depth	80° 13.00' N	08° 08.88' W	285
PS100/075-1	2016-08-03	21:54:00	CTD/L	on ground/ max depth	80° 15.05' N	09° 00.41' W	302.2
PS100/075-2	2016-08-03	22:34:00	MN	on ground/ max depth	80° 15.02' N	09° 01.38' W	302.9
PS100/076-1	2016-08-04	0:20:00	CTD/L	on ground/ max depth	80° 20.48' N	10° 00.19' W	325
PS100/076-2	2016-08-04	1:01:00	MN	on ground/ max depth	80° 20.50' N	10° 00.34' W	324.5
PS100/076-3	2016-08-04	1:39:00	BONGO	on ground/ max depth	80° 21.13' N	10° 01.53' W	326.9

Station	Date	Time	Gear	Action	Position Lat	Position Lon	Water depth [m]
PS100/077-1	2016-08-04	3:22:00	CTD/L	on ground/ max depth	80° 25.91' N	10° 59.30' W	295.2
PS100/077-2	2016-08-04	4:08:00	MN	on ground/ max depth	80° 25.89' N	10° 58.90' W	300.7
PS100/078-1	2016-08-04	5:46:00	CTD/L	on ground/ max depth	80° 25.81' N	12° 00.42' W	268
PS100/078-2	2016-08-04	6:23:00	MN	on ground/ max depth	80° 25.82' N	12° 00.17' W	278.4
PS100/078-3	2016-08-04	6:46:00	BONGO	on ground/ max depth	80° 25.74' N	12° 00.39' W	278.8
PS100/078-3	2016-08-04	6:57:00	BONGO	on ground/ max depth	80° 25.71' N	12° 00.50' W	269
PS100/078-3	2016-08-04	7:07:00	BONGO	on ground/ max depth	80° 25.74' N	12° 00.45' W	268.9
PS100/078-3	2016-08-04	7:16:00	BONGO	on ground/ max depth	80° 25.76' N	12° 00.37' W	269.3
PS100/078-4	2016-08-04	7:57:00	MST	on ground/ max depth	80° 25.75' N	12° 01.65' W	263.4
PS100/078-4	2016-08-04	8:07:00	MST	on ground/ max depth	80° 25.72' N	12° 02.29' W	267.8
PS100/078-4	2016-08-04	8:17:00	MST	on ground/ max depth	80° 25.69' N	12° 03.01' W	261.1
PS100/078-4	2016-08-04	8:27:00	MST	on ground/ max depth	80° 25.67' N	12° 03.82' W	259
PS100/078-4	2016-08-04	8:40:00	MST	on ground/ max depth	80° 25.63' N	12° 04.75' W	260.5
PS100/078-4	2016-08-04	8:52:00	MST	on ground/ max depth	80° 25.58' N	12° 05.65' W	262.3
PS100/078-4	2016-08-04	9:37:00	MST	on ground/ max depth	80° 25.55' N	12° 08.42' W	268
PS100/078-4	2016-08-04	10:43:00	MST	on ground/ max depth	80° 25.41' N	12° 11.86' W	265.5
PS100/078-4	2016-08-04	10:54:00	MST	on ground/ max depth	80° 25.40' N	12° 12.57' W	263.1
PS100/078-4	2016-08-04	11:04:00	MST	on ground/ max depth	80° 25.43' N	12° 13.22' W	264.7
PS100/078-4	2016-08-04	11:16:00	MST	on ground/ max depth	80° 25.44' N	12° 13.87' W	264.2
PS100/078-4	2016-08-04	11:27:00	MST	on ground/ max depth	80° 25.44' N	12° 14.48' W	265.5
PS100/078-4	2016-08-04	11:38:00	MST	on ground/ max depth	80° 25.47' N	12° 15.00' W	266.7
PS100/078-4	2016-08-04	11:50:00	MST	on ground/ max depth	80° 25.49' N	12° 15.49' W	268.1
PS100/078-4	2016-08-04	12:00:00	MST	on ground/ max depth	80° 25.52' N	12° 15.92' W	264.1
PS100/078-4	2016-08-04	12:12:00	MST	on ground/ max depth	80° 25.53' N	12° 16.63' W	269.7
PS100/078-4	2016-08-04	12:24:00	MST	on ground/ max depth	80° 25.56' N	12° 17.33' W	268.6
PS100/078-4	2016-08-04	12:35:00	MST	on ground/ max depth	80° 25.62' N	12° 17.80' W	266.2

Station	Date	Time	Gear	Action	Position Lat	Position Lon	Water depth [m]
PS100/078-4	2016-08-04	12:47:00	MST	on ground/ max depth	80° 25.69' N	12° 18.19' W	263.5
PS100/078-4	2016-08-04	12:59:00	MST	on ground/ max depth	80° 25.76' N	12° 18.56' W	265.1
PS100/078-4	2016-08-04	13:10:00	MST	on ground/ max depth	80° 25.83' N	12° 18.83' W	268
PS100/078-4	2016-08-04	13:22:00	MST	on ground/ max depth	80° 25.91' N	12° 19.07' W	268.3
PS100/078-4	2016-08-04	13:33:00	MST	on ground/ max depth	80° 26.00' N	12° 19.22' W	269.7
PS100/079-1	2016-08-04	15:50:00	CTD/L	on ground/ max depth	80° 26.86' N	12° 50.77' W	280.5
PS100/079-2	2016-08-04	16:24:00	MN	on ground/ max depth	80° 26.99' N	12° 49.43' W	280.5
PS100/080-1	2016-08-04	18:14:00	CTD/L	on ground/ max depth	80° 36.00' N	13° 36.20' W	134.4
PS100/081-1	2016-08-04	19:29:00	CTD/L	on ground/ max depth	80° 31.34' N	13° 23.77' W	274.6
PS100/082-1	2016-08-04	22:41:00	CTD/UC	on ground/ max depth	80° 26.90' N	13° 11.65' W	289.8
PS100/082-2	2016-08-04	23:20:00	CTD/L	on ground/ max depth	80° 26.91' N	13° 11.31' W	289.1
PS100/083-1	2016-08-05	1:55:00	CTD/L	on ground/ max depth	80° 22.28' N	12° 57.05' W	260.4
PS100/084-1	2016-08-05	3:38:00	CTD/L	on ground/ max depth	80° 17.93' N	12° 45.80' W	167.9
PS100/085-1	2016-08-05	5:21:00	CTD/L	on ground/ max depth	80° 13.93' N	12° 36.87' W	97.4
PS100/086-1	2016-08-05	7:29:00	CTD/L	on ground/ max depth	80° 01.55' N	12° 00.08' W	123.3
PS100/086-2	2016-08-05	7:55:00	MN	on ground/ max depth	80° 01.53' N	12° 00.18' W	119.8
PS100/087-1	2016-08-05	9:48:00	CTD/L	on ground/ max depth	79° 47.70' N	11° 53.67' W	200.4
PS100/087-2	2016-08-05	10:23:00	MN	on ground/ max depth	79° 47.80' N	11° 53.72' W	204.9
PS100/087-3	2016-08-05	10:55:00	BONGO	on ground/ max depth	79° 47.41' N	11° 53.16' W	194.4
PS100/088-1	2016-08-05	13:18:00	CTD/L	on ground/ max depth	79° 28.06' N	11° 59.41' W	296
PS100/088-2	2016-08-05	13:57:00	MN	on ground/ max depth	79° 27.98' N	11° 59.71' W	301.8
PS100/089-1	2016-08-05	16:44:00	CTD/L	on ground/ max depth	79° 08.20' N	11° 52.82' W	216.9
PS100/089-2	2016-08-05	17:18:00	MN	on ground/ max depth	79° 08.22' N	11° 51.81' W	216.9
PS100/089-3	2016-08-05	17:38:00	BONGO	on ground/ max depth	79° 08.35' N	11° 51.13' W	216.9
PS100/089-3	2016-08-05	17:50:00	BONGO	on ground/ max depth	79° 08.42' N	11° 50.63' W	215
PS100/089-3	2016-08-05	18:01:00	BONGO	on ground/ max depth	79° 08.43' N	11° 50.27' W	214.5

Station	Date	Time	Gear	Action	Position Lat	Position Lon	Water depth [m]
PS100/089-3	2016-08-05	18:11:00	BONGO	on ground/ max depth	79° 08.40' N	11° 50.05' W	229
PS100/089-3	2016-08-05	18:20:00	BONGO	on ground/ max depth	79° 08.35' N	11° 49.88' W	228.2
PS100/090-1	2016-08-05	21:28:00	CTD/UC	on ground/ max depth	78° 49.85' N	11° 59.71' W	201.6
PS100/090-2	2016-08-05	22:05:00	CTD/L	on ground/ max depth	78° 49.86' N	11° 59.99' W	203.5
PS100/090-3	2016-08-05	22:36:00	MN	on ground/ max depth	78° 49.85' N	12° 00.24' W	193.5
PS100/091-1	2016-08-06	0:59:00	CTD/L	on ground/ max depth	78° 50.08' N	11° 00.10' W	325.5
PS100/091-2	2016-08-06	1:46:00	MN	on ground/ max depth	78° 50.16' N	10° 59.10' W	328.5
PS100/091-3	2016-08-06	2:14:00	MN	on ground/ max depth	78° 50.35' N	10° 58.32' W	334.4
PS100/091-3	2016-08-06	2:25:00	MN	on ground/ max depth	78° 50.44' N	10° 58.20' W	335.4
PS100/091-3	2016-08-06	2:35:00	MN	on ground/ max depth	78° 50.52' N	10° 58.13' W	339.3
PS100/091-3	2016-08-06	2:45:00	MN	on ground/ max depth	78° 50.58' N	10° 57.99' W	312.8
PS100/092-1	2016-08-06	4:59:00	CTD/L	on ground/ max depth	78° 50.38' N	09° 58.99' W	261.5
PS100/092-2	2016-08-06	5:38:00	MN	on ground/ max depth	78° 50.40' N	09° 57.99' W	246.3
PS100/093-1	2016-08-06	7:40:00	CTD/L	on ground/ max depth	78° 48.20' N	08° 56.35' W	192.4
PS100/093-2	2016-08-06	8:15:00	MN	on ground/ max depth	78° 47.63' N	08° 54.40' W	198.6
PS100/094-1	2016-08-06	10:05:00	CTD/UC	on ground/ max depth	78° 40.67' N	07° 56.90' W	169.7
PS100/094-2	2016-08-06	10:35:00	CTD/L	on ground/ max depth	78° 40.68' N	07° 56.60' W	172.5
PS100/094-3	2016-08-06	11:02:00	MN	on ground/ max depth	78° 40.70' N	07° 56.50' W	174.3
PS100/095-1	2016-08-06	13:42:00	CTD/L	on ground/ max depth	78° 40.79' N	07° 00.31' W	220.9
PS100/095-2	2016-08-06	14:18:00	MN	on ground/ max depth	78° 40.91' N	07° 00.95' W	198
PS100/095-3	2016-08-06	14:54:00	BONGO	on ground/ max depth	78° 41.09' N	07° 01.79' W	216.9
PS100/096-1	2016-08-06	18:13:00	CTD/L	on ground/ max depth	78° 45.90' N	05° 59.35' W	325.3
PS100/096-2	2016-08-06	18:52:00	MN	on ground/ max depth	78° 45.86' N	05° 58.99' W	325
PS100/097-1	2016-08-06	21:41:00	CTD/L	on ground/ max depth	78° 48.77' N	05° 00.41' W	971.5
PS100/097-2	2016-08-06	23:02:00	MN	on ground/ max depth	78° 48.05' N	05° 04.21' W	885.1
PS100/097-3	2016-08-06	23:45:00	BONGO	on ground/ max depth	78° 47.71' N	05° 06.43' W	839.3

Station	Date	Time	Gear	Action	Position Lat	Position Lon	Water depth [m]
PS100/097-3	2016-08-06	23:54:00	BONGO	on ground/ max depth	78° 47.63' N	05° 06.88' W	828.1
PS100/097-3	2016-08-07	0:04:00	BONGO	on ground/ max depth	78° 47.54' N	05° 07.38' W	814.3
PS100/097-3	2016-08-07	0:14:00	BONGO	on ground/ max depth	78° 47.49' N	05° 07.83' W	805.4
PS100/097-3	2016-08-07	0:23:00	BONGO	on ground/ max depth	78° 47.46' N	05° 08.31' W	794.8
PS100/097-3	2016-08-07	0:32:00	BONGO	on ground/ max depth	78° 47.42' N	05° 08.80' W	786.3
PS100/098-1	2016-08-07	3:56:00	CTD/L	on ground/ max depth	78° 50.67' N	04° 01.29' W	1890.3
PS100/098-2	2016-08-07	5:11:00	MN	on ground/ max depth	78° 50.86' N	04° 02.45' W	1875.4
PS100/098-3	2016-08-07	6:44:00	MN	on ground/ max depth	78° 51.14' N	04° 04.44' W	1854.5
PS100/099-1	2016-08-07	9:49:01	MOR	on ground/ max depth	78° 48.77' N	04° 34.45' W	1380.6
PS100/100-1	2016-08-07	11:30:00	MOR	on ground/ max depth	78° 44.24' N	04° 02.84' W	1761.9
PS100/101-1	2016-08-07	15:27:00	CTD/UC	on ground/ max depth	78° 48.26' N	03° 30.59' W	2222.1
PS100/101-2	2016-08-07	17:37:00	CTD/L	on ground/ max depth	78° 46.60' N	03° 33.01' W	2164.6
PS100/101-3	2016-08-07	19:54:00	ISP	on ground/ max depth	78° 44.56' N	03° 33.96' W	2115.3
PS100/101-4	2016-08-08	0:34:00	CTD/L	on ground/ max depth	78° 40.65' N	03° 40.08' W	2010.2
PS100/102-1	2016-08-08	4:00:00	CTD/UC	on ground/ max depth	78° 51.22' N	02° 34.01' W	2576.7
PS100/102-2	2016-08-08	6:16:00	CTD/L	on ground/ max depth	78° 51.34' N	02° 35.96' W	2566.6
PS100/102-3	2016-08-08	7:56:00	MN	on ground/ max depth	78° 50.74' N	02° 38.68' W	2562.2
PS100/102-4	2016-08-08	10:08:00	MN	on ground/ max depth	78° 50.28' N	02° 45.73' W	2542.9
PS100/102-5	2016-08-08	12:17:00	BONGO	on ground/ max depth	78° 50.91' N	02° 47.91' W	2534.5
PS100/103-1	2016-08-08	14:17:01	MOR	on ground/ max depth	78° 49.59' N	01° 58.75' W	2670.8
PS100/103-2	2016-08-08	17:14:00	CTD/UC	on ground/ max depth	78° 49.32' N	02° 02.51' W	2667.7
PS100/103-3	2016-08-08	19:39:00	CTD/L	on ground/ max depth	78° 48.16' N	02° 13.18' W	2652.1
PS100/103-4	2016-08-08	22:30:00	ISP	on ground/ max depth	78° 47.59' N	02° 28.36' W	2606.6
PS100/103-5	2016-08-09	3:16:00	CTD/L	on ground/ max depth	78° 47.79' N	02° 31.35' W	2603.3
PS100/104-1	2016-08-09	6:20:00	MOR	on ground/ max depth	78° 34.79' N	01° 00.19' W	2803.9
PS100/105-1	2016-08-09	8:39:00	CTD/L	on ground/ max depth	78° 30.06' N	00° 00.11' W	2738.1

Station	Date	Time	Gear	Action	Position Lat	Position Lon	Water depth [m]
PS100/106-1	2016-08-09	13:54:01	MOR	on ground/ max depth	78° 10.21' N	00° 00.04' E	3012.9
PS100/106-2	2016-08-09	14:44:00	CTD/L	on ground/ max depth	78° 09.68' N	00° 02.34' W	3015.7
PS100/107-1	2016-08-10	6:48:00	BUOY	on ground/ max depth	76° 43.27' N	06° 20.17' W	1266.8
PS100/108-1	2016-08-10	10:14:00	HS_PS	profile start	76° 45.37' N	07° 27.04' W	311.9
PS100/108-1	2016-08-10	17:12:59	HS_PS	profile end	77° 07.66' N	10° 34.51' W	493.8
PS100/109-1	2016-08-10	20:30:00	CTD/L	on ground/ max depth	76° 53.51' N	08° 55.79' W	372.2
PS100/110-1	2016-08-10	22:15:00	CTD/L	on ground/ max depth	76° 49.99' N	08° 39.92' W	365.7
PS100/111-1	2016-08-10	23:27:00	CTD/L	on ground/ max depth	76° 46.59' N	08° 24.34' W	358.1
PS100/112-1	2016-08-11	0:41:00	CTD/L	on ground/ max depth	76° 43.11' N	08° 09.07' W	340.3
PS100/113-1	2016-08-11	2:21:00	CTD/L	on ground/ max depth	76° 37.89' N	07° 45.21' W	322
PS100/114-1	2016-08-11	3:29:00	CTD/L	on ground/ max depth	76° 36.25' N	07° 37.89' W	333.3
PS100/115-1	2016-08-11	4:29:00	CTD/L	on ground/ max depth	76° 34.44' N	07° 29.64' W	535.2
PS100/116-1	2016-08-11	5:55:00	CTD/L	on ground/ max depth	76° 32.79' N	07° 22.52' W	771.9
PS100/117-1	2016-08-11	7:11:00	CTD/L	on ground/ max depth	76° 30.85' N	07° 14.23' W	1003.2
PS100/118-1	2016-08-11	9:07:00	CTD/L	on ground/ max depth	76° 29.25' N	07° 07.00' W	1192.6
PS100/119-1	2016-08-11	10:51:00	CTD/L	on ground/ max depth	76° 25.71' N	06° 51.43' W	1604
PS100/120-1	2016-08-11	13:39:00	CTD/L	on ground/ max depth	76° 18.14' N	06° 18.71' W	2319
PS100/121-1	2016-08-11	17:48:00	MST	on ground/ max depth	76° 32.72' N	07° 22.45' W	774.5
PS100/121-1	2016-08-11	19:17:00	MST	on ground/ max depth	76° 32.42' N	07° 23.50' W	770.5
PS100/121-1	2016-08-11	19:46:00	MST	on ground/ max depth	76° 32.29' N	07° 23.65' W	777.3
PS100/121-1	2016-08-11	19:59:00	MST	on ground/ max depth	76° 32.24' N	07° 23.68' W	780.5
PS100/121-1	2016-08-11	20:13:00	MST	on ground/ max depth	76° 32.20' N	07° 23.64' W	784.5
PS100/121-1	2016-08-11	20:30:00	MST	on ground/ max depth	76° 32.15' N	07° 23.56' W	786.8
PS100/121-1	2016-08-11	20:48:00	MST	on ground/ max depth	76° 32.08' N	07° 23.37' W	793.1
PS100/121-1	2016-08-11	21:03:00	MST	on ground/ max depth	76° 32.01' N	07° 23.26' W	798.8
PS100/122-1	2016-08-11	22:49:00	MST	on ground/ max depth	76° 36.00' N	07° 37.86' W	333.2

Station	Date	Time	Gear	Action	Position Lat	Position Lon	Water depth [m]
PS100/122-1	2016-08-11	23:08:00	MST	on ground/ max depth	76° 35.97' N	07° 37.47' W	336.4
PS100/122-1	2016-08-11	23:29:00	MST	on ground/ max depth	76° 35.91' N	07° 37.22' W	334.1
PS100/122-1	2016-08-11	23:44:00	MST	on ground/ max depth	76° 35.88' N	07° 36.97' W	339.1
PS100/122-1	2016-08-11	23:58:00	MST	on ground/ max depth	76° 35.85' N	07° 36.70' W	338
PS100/122-1	2016-08-12	0:11:00	MST	on ground/ max depth	76° 35.81' N	07° 36.49' W	337.9
PS100/123-1	2016-08-12	1:20:00	MST	on ground/ max depth	76° 37.72' N	07° 45.34' W	328.2
PS100/123-1	2016-08-12	1:33:00	MST	on ground/ max depth	76° 37.62' N	07° 45.20' W	324.2
PS100/123-1	2016-08-12	1:46:00	MST	on ground/ max depth	76° 37.51' N	07° 44.98' W	324.2
PS100/123-1	2016-08-12	1:58:00	MST	on ground/ max depth	76° 37.39' N	07° 44.82' W	320
PS100/123-1	2016-08-12	2:11:00	MST	on ground/ max depth	76° 37.27' N	07° 44.60' W	325.6
PS100/123-1	2016-08-12	2:26:00	MST	on ground/ max depth	76° 37.16' N	07° 44.48' W	327.3
PS100/123-1	2016-08-12	2:39:00	MST	on ground/ max depth	76° 37.11' N	07° 44.36' W	329.4
PS100/123-1	2016-08-12	2:52:00	MST	on ground/ max depth	76° 37.06' N	07° 44.27' W	328.9
PS100/124-1	2016-08-12	4:11:00	CTD/L	on ground/ max depth	76° 40.52' N	07° 57.41' W	336.4
PS100/125-1	2016-08-12	5:22:00	MST	on ground/ max depth	76° 43.17' N	08° 09.12' W	341
PS100/125-1	2016-08-12	5:34:00	MST	on ground/ max depth	76° 43.26' N	08° 09.11' W	340.3
PS100/125-1	2016-08-12	5:47:00	MST	on ground/ max depth	76° 43.35' N	08° 09.09' W	339.8
PS100/125-1	2016-08-12	5:58:00	MST	on ground/ max depth	76° 43.42' N	08° 09.04' W	338.3
PS100/125-1	2016-08-12	6:09:00	MST	on ground/ max depth	76° 43.49' N	08° 09.00' W	338.5
PS100/125-1	2016-08-12	6:21:00	MST	on ground/ max depth	76° 43.56' N	08° 08.97' W	339.3
PS100/126-1	2016-08-12	8:46:00	GC	on ground/ max depth	76° 44.71' N	07° 13.10' W	310.7
PS100/127-1	2016-08-12	9:52:00	GC	on ground/ max depth	76° 45.57' N	07° 28.31' W	311.6
PS100/128-1	2016-08-12	12:20:00	GC	on ground/ max depth	76° 51.07' N	08° 13.15' W	345
PS100/129-1	2016-08-12	13:32:00	GC	on ground/ max depth	76° 54.13' N	08° 38.67' W	353.4
PS100/130-1	2016-08-12	18:53:00	CTD/L	on ground/ max depth	76° 28.03' N	09° 41.30' W	264.5
PS100/131-1	2016-08-12	20:11:00	CTD/L	on ground/ max depth	76° 32.03' N	09° 28.18' W	285.2

Station	Date	Time	Gear	Action	Position Lat	Position Lon	Water depth [m]
PS100/132-1	2016-08-12	21:20:00	CTD/L	on ground/ max depth	76° 36.07' N	09° 15.47' W	278.4
PS100/133-1	2016-08-12	22:31:00	CTD/L	on ground/ max depth	76° 40.05' N	09° 02.93' W	296.4
PS100/134-1	2016-08-12	23:40:00	CTD/L	on ground/ max depth	76° 43.90' N	08° 49.44' W	339
PS100/135-1	2016-08-13	1:00:00	CTD/UC	on ground/ max depth	76° 48.09' N	08° 36.88' W	350.9
PS100/135-2	2016-08-13	1:37:00	CTD/L	on ground/ max depth	76° 48.08' N	08° 37.03' W	354.3
PS100/135-3	2016-08-13	2:23:00	MN	on ground/ max depth	76° 48.18' N	08° 37.31' W	354.6
PS100/136-1	2016-08-13	3:50:00	CTD/L	on ground/ max depth	76° 52.10' N	08° 23.94' W	358.3
PS100/137-1	2016-08-13	5:16:00	CTD/L	on ground/ max depth	76° 56.41' N	08° 11.64' W	353.2
PS100/138-1	2016-08-13	6:52:00	CTD/L	on ground/ max depth	77° 00.41' N	07° 58.28' W	302.5
PS100/139-1	2016-08-13	8:11:00	CTD/L	on ground/ max depth	77° 03.99' N	07° 43.74' W	289.3
PS100/140-1	2016-08-13	9:29:00	CTD/L	on ground/ max depth	77° 08.09' N	07° 31.42' W	283.8
PS100/141-1	2016-08-13	10:52:00	CTD/L	on ground/ max depth	77° 11.95' N	07° 18.24' W	273
PS100/142-1	2016-08-13	15:44:00	MOR	on ground/ max depth	76° 48.09' N	08° 36.93' W	352.6
PS100/143-1	2016-08-13	19:16:00	GC	on ground/ max depth	77° 05.30' N	10° 14.22' W	458.5
PS100/144-1	2016-08-13	20:19:00	GC	on ground/ max depth	77° 07.51' N	10° 34.24' W	492.6
PS100/144-2	2016-08-13	21:05:00	BC	on ground/ max depth	77° 07.58' N	10° 34.13' W	494.1
PS100/145-1	2016-08-13	23:33:00	HS_PS	profile start	77° 18.52' N	11° 12.36' W	465
PS100/145-1	2016-08-14	7:38:59	HS_PS	profile end	77° 48.19' N	14° 37.13' W	430.8
PS100/146-1	2016-08-14	13:17:00	GC	on ground/ max depth	77° 31.37' N	12° 20.14' W	505.5
PS100/146-2	2016-08-14	14:15:00	GC	on ground/ max depth	77° 31.39' N	12° 20.15' W	505.1
PS100/147-1	2016-08-14	16:48:00	GC	on ground/ max depth	77° 36.71' N	13° 04.70' W	380.7
PS100/148-1	2016-08-14	18:13:00	GC	on ground/ max depth	77° 39.51' N	13° 27.13' W	381.1
PS100/148-2	2016-08-14	18:43:00	GC	on ground/ max depth	77° 39.51' N	13° 27.11' W	380.9
PS100/149-1	2016-08-14	19:42:00	GC	on ground/ max depth	77° 40.64' N	13° 35.45' W	369.3
PS100/150-1	2016-08-15	0:43:00	CTD/L	on ground/ max depth	77° 36.06' N	15° 44.37' W	334.1
PS100/151-1	2016-08-15	2:18:00	CTD/L	on ground/ max depth	77° 31.96' N	15° 58.46' W	317.5

Station	Date	Time	Gear	Action	Position Lat	Position Lon	Water depth [m]
PS100/152-1	2016-08-15	3:46:00	CTD/L	on ground/ max depth	77° 28.01' N	16° 12.69' W	281
PS100/153-1	2016-08-15	5:14:00	CTD/L	on ground/ max depth	77° 24.19' N	16° 27.22' W	136.2
PS100/154-1	2016-08-15	6:40:01	MOR	on ground/ max depth	77° 23.43' N	16° 17.41' W	181
PS100/155-1	2016-08-15	8:17:00	MOR	on ground/ max depth	77° 25.53' N	16° 02.50' W	281.7
PS100/155-1	2016-08-15	8:28:00	MOR	on ground/ max depth	77° 25.54' N	16° 02.64' W	280.8
PS100/156-1	2016-08-15	9:28:00	MOR	on ground/ max depth	77° 27.93' N	15° 46.72' W	306.9
PS100/157-1	2016-08-15	12:22:00	MOR	on ground/ max depth	77° 42.85' N	15° 26.46' W	372.9
PS100/158-1	2016-08-15	16:24:00	MOR	on ground/ max depth	77° 57.93' N	14° 29.94' W	403.5
PS100/159-1	2016-08-15	17:40:00	CTD/L	on ground/ max depth	77° 56.03' N	14° 34.28' W	443.5
PS100/159-2	2016-08-15	18:43:00	MST	on ground/ max depth	77° 55.91' N	14° 33.52' W	441.5
PS100/159-2	2016-08-15	19:00:00	MST	on ground/ max depth	77° 56.01' N	14° 33.22' W	442.4
PS100/159-2	2016-08-15	19:15:00	MST	on ground/ max depth	77° 56.03' N	14° 32.63' W	439.4
PS100/159-2	2016-08-15	19:34:00	MST	on ground/ max depth	77° 56.02' N	14° 32.61' W	439.5
PS100/159-2	2016-08-15	19:49:00	MST	on ground/ max depth	77° 56.09' N	14° 32.31' W	441
PS100/159-2	2016-08-15	20:03:00	MST	on ground/ max depth	77° 56.16' N	14° 31.81' W	446.1
PS100/159-2	2016-08-15	20:19:00	MST	on ground/ max depth	77° 56.14' N	14° 31.68' W	436.1
PS100/159-2	2016-08-15	20:33:00	MST	on ground/ max depth	77° 56.10' N	14° 31.60' W	436.8
PS100/159-2	2016-08-15	20:48:00	MST	on ground/ max depth	77° 56.05' N	14° 31.58' W	440.9
PS100/159-2	2016-08-15	21:07:00	MST	on ground/ max depth	77° 56.00' N	14° 31.31' W	439.9
PS100/159-2	2016-08-15	21:21:00	MST	on ground/ max depth	77° 55.93' N	14° 31.11' W	437.7
PS100/159-2	2016-08-15	21:36:00	MST	on ground/ max depth	77° 55.88' N	14° 30.80' W	436.9
PS100/159-2	2016-08-15	21:50:00	MST	on ground/ max depth	77° 55.87' N	14° 30.31' W	436.2
PS100/159-2	2016-08-15	22:07:00	MST	on ground/ max depth	77° 55.79' N	14° 29.97' W	435.5
PS100/159-2	2016-08-15	22:21:00	MST	on ground/ max depth	77° 55.80' N	14° 29.28' W	434.3
PS100/159-2	2016-08-15	22:36:00	MST	on ground/ max depth	77° 55.75' N	14° 28.71' W	431.4
PS100/159-2	2016-08-15	22:50:00	MST	on ground/ max depth	77° 55.73' N	14° 27.87' W	428.1

Station	Date	Time	Gear	Action	Position Lat	Position Lon	Water depth [m]
PS100/159-2	2016-08-15	23:05:00	MST	on ground/ max depth	77° 55.71' N	14° 27.15' W	427.3
PS100/159-2	2016-08-15	23:27:00	MST	on ground/ max depth	77° 55.69' N	14° 26.24' W	423.1
PS100/159-2	2016-08-15	23:41:00	MST	on ground/ max depth	77° 55.73' N	14° 25.54' W	422
PS100/159-2	2016-08-15	23:58:00	MST	on ground/ max depth	77° 55.72' N	14° 24.75' W	419.5
PS100/159-2	2016-08-16	0:12:00	MST	on ground/ max depth	77° 55.64' N	14° 24.36' W	420.2
PS100/159-2	2016-08-16	0:27:00	MST	on ground/ max depth	77° 55.61' N	14° 23.83' W	442.1
PS100/159-2	2016-08-16	0:42:00	MST	on ground/ max depth	77° 55.63' N	14° 23.24' W	418.9
PS100/159-2	2016-08-16	0:57:00	MST	on ground/ max depth	77° 55.63' N	14° 22.83' W	431.6
PS100/159-2	2016-08-16	1:12:00	MST	on ground/ max depth	77° 55.64' N	14° 22.38' W	405.7
PS100/159-2	2016-08-16	1:26:00	MST	on ground/ max depth	77° 55.66' N	14° 21.95' W	417.1
PS100/159-2	2016-08-16	1:39:00	MST	on ground/ max depth	77° 55.67' N	14° 21.57' W	419.6
PS100/159-2	2016-08-16	1:54:00	MST	on ground/ max depth	77° 55.66' N	14° 21.16' W	415.7
PS100/159-2	2016-08-16	2:09:00	MST	on ground/ max depth	77° 55.64' N	14° 20.90' W	415.6
PS100/159-2	2016-08-16	2:24:00	MST	on ground/ max depth	77° 55.62' N	14° 20.63' W	414
PS100/160-1	2016-08-16	3:29:00	CTD/L	on ground/ max depth	77° 57.97' N	14° 26.96' W	406.3
PS100/161-1	2016-08-16	4:49:00	CTD/L	on ground/ max depth	78° 00.26' N	14° 20.15' W	230.2
PS100/162-1	2016-08-16	5:53:00	CTD/L	on ground/ max depth	78° 02.73' N	14° 12.87' W	134.6
PS100/163-1	2016-08-16	6:52:00	MOR	on ground/ max depth	77° 59.91' N	14° 18.44' W	239.7
PS100/164-1	2016-08-16	8:28:00	MOR	on ground/ max depth	77° 55.58' N	14° 38.65' W	459.2
PS100/164-1	2016-08-16	8:36:00	MOR	on ground/ max depth	77° 55.61' N	14° 38.54' W	454.4
PS100/165-1	2016-08-16	10:18:00	CTD/UC	on ground/ max depth	77° 52.00' N	14° 48.06' W	465.7
PS100/165-2	2016-08-16	11:11:00	CTD/L	on ground/ max depth	77° 52.05' N	14° 46.48' W	459
PS100/165-3	2016-08-16	12:37:00	ISP	on ground/ max depth	77° 52.15' N	14° 47.49' W	462.5
PS100/166-1	2016-08-16	17:11:00	CTD/L	on ground/ max depth	77° 47.94' N	15° 02.26' W	396.1
PS100/167-1	2016-08-16	18:31:00	CTD/L	on ground/ max depth	77° 43.99' N	15° 16.86' W	367.7
PS100/168-1	2016-08-16	19:56:00	CTD/L	on ground/ max depth	77° 40.04' N	15° 31.03' W	356

Station	Date	Time	Gear	Action	Position Lat	Position Lon	Water depth [m]
PS100/169-1	2016-08-16	22:12:00	HS_PS	profile start	77° 48.91' N	14° 50.26' W	136.1
PS100/169-1	2016-08-17	5:25:59	HS_PS	profile end	78° 17.50' N	17° 06.04' W	518.3
PS100/170-1	2016-08-17	5:48:00	CTD/L	on ground/ max depth	78° 17.56' N	17° 05.57' W	522.3
PS100/170-2	2016-08-17	6:51:00	MN	on ground/ max depth	78° 17.53' N	17° 04.51' W	519
PS100/171-1	2016-08-17	9:28:00	BC	on ground/ max depth	78° 08.43' N	16° 50.05' W	542.3
PS100/171-2	2016-08-17	10:23:00	GC	on ground/ max depth	78° 08.49' N	16° 49.60' W	545.4
PS100/172-1	2016-08-17	11:30:00	GC	on ground/ max depth	78° 05.99' N	16° 45.53' W	522
PS100/173-1	2016-08-17	13:42:00	GC	on ground/ max depth	78° 00.57' N	16° 10.22' W	505.2
PS100/174-1	2016-08-17	17:44:00	GC	on ground/ max depth	77° 43.36' N	15° 22.51' W	375
PS100/175-1	2016-08-17	18:51:00	GC	on ground/ max depth	77° 44.27' N	15° 20.17' W	375.8
PS100/176-1	2016-08-17	22:11:00	GC	on ground/ max depth	77° 56.01' N	14° 33.92' W	529.9
PS100/177-1	2016-08-17	23:27:00	GC	on ground/ max depth	77° 58.91' N	14° 23.07' W	398.7
PS100/178-1	2016-08-18	4:52:00	CTD/L	on ground/ max depth	78° 09.07' N	15° 54.94' W	413.6
PS100/179-1	2016-08-18	6:11:00	CTD/L	on ground/ max depth	78° 10.88' N	15° 43.68' W	360.8
PS100/180-1	2016-08-18	7:22:00	CTD/L	on ground/ max depth	78° 12.59' N	15° 33.67' W	265
PS100/180-2	2016-08-18	8:12:00	MOR	on ground/ max depth	78° 12.45' N	15° 33.68' W	265.8
PS100/181-1	2016-08-18	10:02:00	MOR	on ground/ max depth	78° 10.59' N	15° 43.26' W	350.9
PS100/182-1	2016-08-18	11:09:01	MOR	on ground/ max depth	78° 09.02' N	15° 54.00' W	416
PS100/182-2	2016-08-18	11:20:00	HS_PS	profile start	78° 08.99' N	15° 53.97' W	416.5
PS100/182-2	2016-08-18	15:02:59	HS_PS	profile end	77° 55.66' N	17° 05.24' W	374.5
PS100/183-1	2016-08-18	15:32:00	MOR	on ground/ max depth	77° 55.62' N	17° 05.22' W	364.6
PS100/183-2	2016-08-18	16:14:00	CTD/L	on ground/ max depth	77° 55.94' N	17° 07.21' W	360.4
PS100/184-1	2016-08-18	20:02:00	GC	on ground/ max depth	78° 01.15' N	16° 36.17' W	493
PS100/185-1	2016-08-18	22:02:00	GC	on ground/ max depth	78° 05.53' N	16° 11.93' W	476.3
PS100/186-1	2016-08-19	11:15:00	CTD/L	on ground/ max depth	79° 09.70' N	17° 30.12' W	144.4
PS100/187-1	2016-08-19	12:32:00	CTD/L	on ground/ max depth	79° 10.10' N	17° 25.18' W	231.3
PS100/188-1	2016-08-19	13:56:00	CTD/L	on ground/ max depth	79° 10.39' N	17° 18.42' W	367.2

Station	Date	Time	Gear	Action	Position Lat	Position Lon	Water depth [m]
PS100/189-1	2016-08-19	15:50:00	CTD/UC	on ground/ max depth	79° 11.73' N	17° 06.30' W	398
PS100/189-2	2016-08-19	16:58:00	CTD/L	on ground/ max depth	79° 11.93' N	17° 05.50' W	397
PS100/189-3	2016-08-19	18:30:00	ISP	on ground/ max depth	79° 11.97' N	17° 04.90' W	385
PS100/190-1	2016-08-19	23:01:00	CTD/L	on ground/ max depth	79° 11.07' N	16° 56.56' W	395.3
PS100/191-1	2016-08-20	0:19:00	CTD/L	on ground/ max depth	79° 11.50' N	16° 48.34' W	383.2
PS100/192-1	2016-08-20	2:05:00	CTD/L	on ground/ max depth	79° 11.92' N	16° 36.79' W	368.1
PS100/192-2	2016-08-20	2:38:59	CTD/L	on ground/ max depth	79° 12.03' N	16° 36.58' W	367.2
PS100/193-1	2016-08-20	6:49:00	CTD/L	on ground/ max depth	79° 12.23' N	16° 21.77' W	322
PS100/194-1	2016-08-20	9:03:00	CTD/L	on ground/ max depth	79° 12.28' N	16° 15.84' W	311.5
PS100/195-1	2016-08-20	10:22:00	CTD/L	on ground/ max depth	79° 12.48' N	16° 05.42' W	297.2
PS100/196-1	2016-08-20	11:40:00	CTD/L	on ground/ max depth	79° 13.33' N	15° 54.83' W	237.9
PS100/197-1	2016-08-20	12:44:00	CTD/L	on ground/ max depth	79° 14.06' N	15° 44.76' W	81.4
PS100/198-1	2016-08-20	16:40:00	BC	on ground/ max depth	79° 11.32' N	17° 06.95' W	391.8
PS100/198-2	2016-08-20	17:29:00	GC	on ground/ max depth	79° 11.47' N	17° 06.42' W	397.8
PS100/199-1	2016-08-20	18:44:00	GC	on ground/ max depth	79° 10.40' N	17° 14.00' W	400.1
PS100/200-1	2016-08-21	0:16:00	CTD/L	on ground/ max depth	79° 20.42' N	18° 35.28' W	281.3
PS100/201-1	2016-08-21	1:31:00	CTD/L	on ground/ max depth	79° 18.99' N	18° 19.00' W	336.1
PS100/202-1	2016-08-21	2:40:00	CTD/UC	on ground/ max depth	79° 17.24' N	18° 05.87' W	362.3
PS100/202-2	2016-08-21	3:28:00	CTD/L	on ground/ max depth	79° 17.21' N	18° 05.19' W	362.4
PS100/202-3	2016-08-21	4:05:00	BONGO	on ground/ max depth	79° 17.08' N	18° 04.13' W	363.5
PS100/202-3	2016-08-21	4:16:00	BONGO	on ground/ max depth	79° 17.11' N	18° 03.93' W	356.1
PS100/202-3	2016-08-21	4:27:00	BONGO	on ground/ max depth	79° 17.07' N	18° 03.76' W	362
PS100/202-3	2016-08-21	4:37:00	BONGO	on ground/ max depth	79° 17.07' N	18° 03.62' W	362.2
PS100/202-3	2016-08-21	4:46:00	BONGO	on ground/ max depth	79° 17.13' N	18° 03.42' W	361.9
PS100/203-1	2016-08-21	5:53:00	CTD/L	on ground/ max depth	79° 16.68' N	17° 50.46' W	333.6

Station	Date	Time	Gear	Action	Position Lat	Position Lon	Water depth [m]
PS100/204-1	2016-08-21	7:14:00	CTD/L	on ground/ max depth	79° 14.49' N	17° 41.78' W	279.1
PS100/205-1	2016-08-21	8:23:00	CTD/L	on ground/ max depth	79° 13.15' N	17° 31.63' W	142.9
PS100/206-1	2016-08-21	10:43:00	MST	on ground/ max depth	79° 16.53' N	18° 02.80' W	371.8
PS100/206-1	2016-08-21	10:59:00	MST	on ground/ max depth	79° 16.47' N	18° 02.71' W	370.1
PS100/206-1	2016-08-21	11:18:00	MST	on ground/ max depth	79° 16.40' N	18° 02.21' W	372.5
PS100/206-1	2016-08-21	11:32:00	MST	on ground/ max depth	79° 16.30' N	18° 01.63' W	370.8
PS100/206-1	2016-08-21	11:44:00	MST	on ground/ max depth	79° 16.22' N	18° 01.20' W	370.3
PS100/206-1	2016-08-21	12:15:00	MST	on ground/ max depth	79° 16.12' N	18° 00.47' W	370
PS100/206-1	2016-08-21	12:27:00	MST	on ground/ max depth	79° 16.07' N	17° 60.00' W	368.5
PS100/206-1	2016-08-21	12:54:00	MST	on ground/ max depth	79° 16.10' N	17° 58.91' W	368.7
PS100/206-1	2016-08-21	13:08:00	MST	on ground/ max depth	79° 16.00' N	17° 58.53' W	369.4
PS100/206-1	2016-08-21	13:21:00	MST	on ground/ max depth	79° 15.98' N	17° 58.66' W	509.3
PS100/206-1	2016-08-21	13:33:00	MST	on ground/ max depth	79° 15.90' N	17° 58.38' W	371.8
PS100/207-1	2016-08-21	15:18:00	GC	on ground/ max depth	79° 19.75' N	18° 27.68' W	268.6
PS100/208-1	2016-08-21	16:25:00	GC	on ground/ max depth	79° 20.60' N	18° 33.47' W	304.8
PS100/209-1	2016-08-21	17:25:00	GC	on ground/ max depth	79° 20.78' N	18° 33.74' W	0
PS100/210-1	2016-08-21	18:18:00	GC	on ground/ max depth	79° 22.56' N	18° 37.39' W	187.2
PS100/211-1	2016-08-21	19:39:00	CTD/L	on ground/ max depth	79° 23.92' N	18° 43.45' W	102.4
PS100/212-1	2016-08-21	20:40:00	CTD/L	on ground/ max depth	79° 26.76' N	18° 40.80' W	301.5
PS100/213-1	2016-08-21	23:37:00	CTD/L	on ground/ max depth	79° 30.92' N	18° 47.34' W	345.4
PS100/214-1	2016-08-22	0:32:00	CTD/UC	on ground/ max depth	79° 32.97' N	18° 41.29' W	424.9
PS100/214-2	2016-08-22	1:22:00	CTD/L	on ground/ max depth	79° 32.96' N	18° 41.35' W	424.5
PS100/215-1	2016-08-22	2:49:00	CTD/L	on ground/ max depth	79° 35.94' N	18° 41.09' W	458.1
PS100/216-1	2016-08-22	4:06:00	CTD/L	on ground/ max depth	79° 38.97' N	18° 40.38' W	445
PS100/217-1	2016-08-22	5:29:00	CTD/L	on ground/ max depth	79° 41.81' N	18° 40.12' W	141.4
PS100/218-1	2016-08-22	6:12:00	HS_PS	profile start	79° 38.88' N	18° 40.58' W	444.7

Station	Date	Time	Gear	Action	Position Lat	Position Lon	Water depth [m]
PS100/218-1	2016-08-22	16:23:59	HS_PS	profile end	79° 25.35' N	19° 46.46' W	110.4
PS100/218-2	2016-08-22	12:13:00	TEST	on ground/ max depth	79° 33.91' N	19° 27.69' W	468.4
PS100/219-1	2016-08-22	17:03:00	CTD/L	on ground/ max depth	79° 25.27' N	19° 44.97' W	79
PS100/220-1	2016-08-22	17:55:00	CTD/L	on ground/ max depth	79° 26.87' N	19° 46.74' W	322.5
PS100/221-1	2016-08-22	19:15:00	CTD/L	on ground/ max depth	79° 27.81' N	19° 45.78' W	117.7
PS100/222-1	2016-08-22	20:06:00	CTD/L	on ground/ max depth	79° 28.61' N	19° 42.38' W	109.9
PS100/223-1	2016-08-22	21:09:00	CTD/L	on ground/ max depth	79° 28.90' N	19° 39.83' W	143.2
PS100/224-1	2016-08-22	21:49:00	CTD/L	on ground/ max depth	79° 29.10' N	19° 33.21' W	135.3
PS100/225-1	2016-08-22	23:00:00	CTD/L	on ground/ max depth	79° 29.72' N	19° 31.33' W	124.7
PS100/225-2	2016-08-22	23:43:00	CTD/L	on ground/ max depth	79° 30.30' N	19° 27.96' W	200.7
PS100/227-1	2016-08-23	0:54:00	CTD/L	on ground/ max depth	79° 31.22' N	19° 26.71' W	294.5
PS100/228-1	2016-08-23	1:40:00	CTD/L	on ground/ max depth	79° 32.08' N	19° 25.29' W	301.7
PS100/229-1	2016-08-23	3:02:00	CTD/L	on ground/ max depth	79° 32.92' N	19° 24.95' W	303.9
PS100/230-1	2016-08-23	4:04:00	CTD/L	on ground/ max depth	79° 33.16' N	19° 34.10' W	361.8
PS100/231-1	2016-08-23	5:18:00	CTD/L	on ground/ max depth	79° 33.64' N	19° 33.77' W	399.9
PS100/232-1	2016-08-23	6:22:00	CTD/L	on ground/ max depth	79° 34.13' N	19° 31.13' W	468.9
PS100/233-1	2016-08-23	8:25:00	CTD/L	on ground/ max depth	79° 34.34' N	19° 25.35' W	469.1
PS100/234-1	2016-08-23	9:45:00	CTD/L	on ground/ max depth	79° 36.94' N	19° 24.05' W	97.2
PS100/235-1	2016-08-23	10:40:00	CTD/L	on ground/ max depth	79° 37.63' N	19° 21.20' W	304.5
PS100/236-1	2016-08-23	11:40:00	CTD/L	on ground/ max depth	79° 39.06' N	19° 18.74' W	117.2
PS100/237-1	2016-08-23	12:38:00	CTD/L	on ground/ max depth	79° 40.24' N	19° 17.55' W	94.3
PS100/237-2	2016-08-23	12:50:00	HS_PS	profile start	79° 40.28' N	19° 17.57' W	95.6
PS100/237-2	2016-08-23	14:37:59	HS_PS	profile end	79° 34.13' N	19° 27.13' W	474.1
PS100/238-1	2016-08-23	15:34:00	MOR	on ground/ max depth	79° 34.13' N	19° 27.58' W	475
PS100/239-1	2016-08-23	16:36:00	MOR	on ground/ max depth	79° 31.16' N	19° 25.82' W	296.3
PS100/240-1	2016-08-23	19:06:00	MOR	on ground/ max depth	79° 26.40' N	19° 46.64' W	326.2
PS100/241-1	2016-08-23	21:31:00	CTD/UC	on ground/ max depth	79° 34.13' N	19° 31.08' W	468.9

Station	Date	Time	Gear	Action	Position Lat	Position Lon	Water depth [m]
PS100/241-2	2016-08-23	22:22:00	CTD/L	on ground/ max depth	79° 34.12' N	19° 31.08' W	471.3
PS100/241-3	2016-08-23	23:42:00	ISP	on ground/ max depth	79° 34.10' N	19° 31.21' W	469.4
PS100/241-4	2016-08-24	3:49:00	BONGO	on ground/ max depth	79° 34.15' N	19° 30.01' W	473
PS100/241-5	2016-08-24	4:10:00	HS_PS	profile start	79° 33.89' N	19° 31.80' W	477.7
PS100/241-5	2016-08-25	7:30:59	HS_PS	profile end	79° 27.32' N	19° 27.96' W	308.9
PS100/242-1	2016-08-25	7:57:00	GC	on ground/ max depth	79° 27.33' N	19° 32.91' W	300.3
PS100/243-1	2016-08-25	8:44:00	GC	on ground/ max depth	79° 27.81' N	19° 45.68' W	125.1
PS100/244-1	2016-08-25	10:22:00	GC	on ground/ max depth	79° 26.51' N	19° 47.52' W	325.6
PS100/245-1	2016-08-25	11:57:00	GC	on ground/ max depth	79° 32.81' N	19° 28.89' W	141.1
PS100/246-1	2016-08-25	12:37:01	ZODIAK	on ground/ max depth	79° 34.09' N	19° 30.32' W	471.1
PS100/246-1	2016-08-25	15:28:01	ZODIAK	on ground/ max depth	79° 32.70' N	19° 14.23' W	213.8
PS100/246-2	2016-08-25	12:50:00	GC	on ground/ max depth	79° 34.12' N	19° 30.25' W	470.7
PS100/246-3	2016-08-25	13:13:00	BONGO	on ground/ max depth	79° 34.12' N	19° 30.12' W	472.7
PS100/246-3	2016-08-25	13:21:00	BONGO	on ground/ max depth	79° 34.11' N	19° 30.06' W	472.1
PS100/246-3	2016-08-25	13:28:00	BONGO	on ground/ max depth	79° 34.10' N	19° 30.06' W	473.1
PS100/246-3	2016-08-25	13:38:00	BONGO	on ground/ max depth	79° 34.11' N	19° 30.08' W	472.7
PS100/246-3	2016-08-25	13:54:00	BONGO	on ground/ max depth	79° 34.10' N	19° 30.12' W	472.6
PS100/246-3	2016-08-25	14:10:00	BONGO	on ground/ max depth	79° 34.11' N	19° 30.07' W	473
PS100/246-3	2016-08-25	14:16:00	BONGO	on ground/ max depth	79° 34.12' N	19° 30.06' W	470
PS100/247-1	2016-08-25	15:14:00	GC	on ground/ max depth	79° 32.70' N	19° 14.22' W	194.7
PS100/248-1	2016-08-25	16:02:00	GC	on ground/ max depth	79° 33.40' N	19° 13.36' W	171.6
PS100/249-1	2016-08-25	17:09:00	GC	on ground/ max depth	79° 30.39' N	19° 19.17' W	308.3
PS100/249-2	2016-08-25	18:01:00	BC	on ground/ max depth	79° 30.42' N	19° 19.25' W	310.3
PS100/250-1	2016-08-25	18:54:00	CTD/L	on ground/ max depth	79° 28.85' N	19° 15.03' W	437.7
PS100/251-1	2016-08-25	20:13:01	CTD/L	on ground/ max depth	79° 30.91' N	19° 21.05' W	304.1
PS100/252-1	2016-08-25	21:21:00	CTD/L	on ground/ max depth	79° 33.01' N	19° 20.02' W	363.6

Station	Date	Time	Gear	Action	Position Lat	Position Lon	Water depth [m]
PS100/253-1	2016-08-25	22:37:00	CTD/L	on ground/ max depth	79° 35.00' N	19° 20.63' W	370.7
PS100/254-1	2016-08-25	23:58:00	CTD/L	on ground/ max depth	79° 36.18' N	19° 19.40' W	334
PS100/255-1	2016-08-26	1:05:00	CTD/L	on ground/ max depth	79° 38.61' N	19° 07.41' W	425.9
PS100/256-1	2016-08-26	2:26:00	MST	on ground/ max depth	79° 35.42' N	19° 20.74' W	336.7
PS100/256-1	2016-08-26	2:56:00	MST	on ground/ max depth	79° 35.23' N	19° 21.00' W	357.2
PS100/256-1	2016-08-26	3:10:00	MST	on ground/ max depth	79° 35.13' N	19° 21.40' W	372.9
PS100/256-1	2016-08-26	3:49:00	MST	on ground/ max depth	79° 35.91' N	19° 18.94' W	337.4
PS100/256-1	2016-08-26	4:18:00	MST	on ground/ max depth	79° 35.83' N	19° 19.81' W	320.8
PS100/256-1	2016-08-26	4:30:00	MST	on ground/ max depth	79° 35.80' N	19° 20.18' W	319.8
PS100/256-1	2016-08-26	4:43:00	MST	on ground/ max depth	79° 35.79' N	19° 20.54' W	320.5
PS100/256-1	2016-08-26	4:56:00	MST	on ground/ max depth	79° 35.78' N	19° 20.81' W	321.3
PS100/256-1	2016-08-26	5:09:00	MST	on ground/ max depth	79° 35.77' N	19° 20.99' W	323
PS100/257-1	2016-08-26	13:21:01	MOR	on ground/ max depth	79° 35.06' N	19° 20.56' W	358.7
PS100/257-2	2016-08-26	14:05:00	MST	on ground/ max depth	79° 35.29' N	19° 20.79' W	347.9
PS100/257-2	2016-08-26	14:32:00	MST	on ground/ max depth	79° 35.28' N	19° 20.98' W	357.9
PS100/257-2	2016-08-26	14:48:00	MST	on ground/ max depth	79° 35.27' N	19° 21.22' W	359.9
PS100/257-2	2016-08-26	15:03:00	MST	on ground/ max depth	79° 35.26' N	19° 21.36' W	359.4
PS100/257-2	2016-08-26	15:19:00	MST	on ground/ max depth	79° 35.25' N	19° 21.59' W	354.4
PS100/257-2	2016-08-26	16:10:00	MST	on ground/ max depth	79° 35.27' N	19° 21.02' W	377.6
PS100/257-2	2016-08-26	16:26:00	MST	on ground/ max depth	79° 35.18' N	19° 20.70' W	360.2
PS100/257-2	2016-08-26	16:41:00	MST	on ground/ max depth	79° 35.16' N	19° 20.49' W	355.7
PS100/257-2	2016-08-26	17:07:00	MST	on ground/ max depth	79° 35.20' N	19° 20.17' W	344.3
PS100/257-2	2016-08-26	17:58:00	MST	on ground/ max depth	79° 35.13' N	19° 19.86' W	353.6
PS100/257-2	2016-08-26	18:13:00	MST	on ground/ max depth	79° 35.11' N	19° 20.09' W	358
PS100/257-2	2016-08-26	18:28:00	MST	on ground/ max depth	79° 35.05' N	19° 20.16' W	370.8
PS100/258-1	2016-08-26	19:28:00	MST	on ground/ max depth	79° 32.10' N	19° 20.39' W	338.6

Station	Date	Time	Gear	Action	Position Lat	Position Lon	Water depth [m]
PS100/258-1	2016-08-26	19:41:00	MST	on ground/ max depth	79° 32.03' N	19° 20.49' W	338.1
PS100/258-1	2016-08-26	19:54:00	MST	on ground/ max depth	79° 31.93' N	19° 20.69' W	340.7
PS100/258-1	2016-08-26	20:08:00	MST	on ground/ max depth	79° 31.81' N	19° 20.97' W	335.8
PS100/258-1	2016-08-26	20:22:00	MST	on ground/ max depth	79° 31.67' N	19° 21.19' W	333.5
PS100/258-1	2016-08-26	20:37:00	MST	on ground/ max depth	79° 31.53' N	19° 21.36' W	330.1
PS100/258-1	2016-08-26	20:51:00	MST	on ground/ max depth	79° 31.39' N	19° 21.52' W	325.8
PS100/258-1	2016-08-26	21:05:00	MST	on ground/ max depth	79° 31.25' N	19° 21.67' W	323.6
PS100/258-1	2016-08-26	21:19:00	MST	on ground/ max depth	79° 31.11' N	19° 21.83' W	316.1
PS100/258-1	2016-08-26	21:32:00	MST	on ground/ max depth	79° 30.98' N	19° 21.95' W	297.3
PS100/258-2	2016-08-26	21:48:00	HS_PS	profile start	79° 31.02' N	19° 22.46' W	297
PS100/258-2	2016-08-27	8:06:59	HS_PS	profile end	79° 33.58' N	15° 54.33' W	146.7
PS100/259-1	2016-08-27	8:29:00	CTD/L	on ground/ max depth	79° 34.10' N	15° 54.48' W	138
PS100/260-1	2016-08-27	9:25:00	CTD/L	on ground/ max depth	79° 35.31' N	16° 09.01' W	181.1
PS100/261-1	2016-08-27	10:35:00	CTD/L	on ground/ max depth	79° 36.73' N	16° 23.90' W	285.6
PS100/262-1	2016-08-27	11:43:00	CTD/UC	on ground/ max depth	79° 38.30' N	16° 39.36' W	237
PS100/262-2	2016-08-27	12:23:00	CTD/L	on ground/ max depth	79° 38.36' N	16° 38.40' W	246.6
PS100/263-1	2016-08-27	13:51:00	CTD/L	on ground/ max depth	79° 40.12' N	16° 53.96' W	270.5
PS100/263-3	2016-08-27	14:59:00	MOR	on ground/ max depth	79° 40.15' N	16° 53.36' W	256.6
PS100/264-1	2016-08-27	15:53:00	CTD/L	on ground/ max depth	79° 40.58' N	17° 02.84' W	228.7
PS100/265-1	2016-08-27	18:16:00	CTD/L	on ground/ max depth	79° 42.07' N	17° 30.71' W	275.5
PS100/266-1	2016-08-27	18:51:00	CTD/L	on ground/ max depth	79° 42.43' N	17° 33.55' W	343.1
PS100/267-1	2016-08-27	20:14:00	CTD/L	on ground/ max depth	79° 43.21' N	17° 40.47' W	404.5
PS100/268-1	2016-08-27	21:02:00	CTD/L	on ground/ max depth	79° 43.45' N	17° 45.68' W	105.6
PS100/269-1	2016-08-27	23:51:00	GC	on ground/ max depth	79° 30.43' N	18° 18.11' W	469.6
PS100/270-1	2016-08-28	0:45:00	GC	on ground/ max depth	79° 29.83' N	18° 08.38' W	423.6
PS100/271-1	2016-08-28	4:40:00	MST	on ground/ max depth	79° 42.60' N	17° 33.02' W	334.8

Station	Date	Time	Gear	Action	Position Lat	Position Lon	Water depth [m]
PS100/271-1	2016-08-28	4:52:00	MST	on ground/ max depth	79° 42.57' N	17° 32.77' W	329.4
PS100/271-1	2016-08-28	5:06:00	MST	on ground/ max depth	79° 42.56' N	17° 32.50' W	329.9
PS100/271-1	2016-08-28	5:20:00	MST	on ground/ max depth	79° 42.55' N	17° 32.32' W	326.6
PS100/271-1	2016-08-28	5:32:00	MST	on ground/ max depth	79° 42.54' N	17° 32.24' W	326.3
PS100/271-1	2016-08-28	5:45:00	MST	on ground/ max depth	79° 42.53' N	17° 32.27' W	326.5
PS100/271-1	2016-08-28	6:06:00	MST	on ground/ max depth	79° 42.56' N	17° 32.12' W	326
PS100/271-1	2016-08-28	6:20:00	MST	on ground/ max depth	79° 42.50' N	17° 31.92' W	326
PS100/271-1	2016-08-28	6:32:00	MST	on ground/ max depth	79° 42.46' N	17° 31.55' W	321.1
PS100/272-1	2016-08-28	8:38:00	MOR	on ground/ max depth	79° 43.23' N	17° 40.40' W	404.1
PS100/273-1	2016-08-28	11:41:00	MOR	on ground/ max depth	79° 37.15' N	16° 32.61' W	287
PS100/273-2	2016-08-28	12:32:00	MST	on ground/ max depth	79° 36.35' N	16° 31.33' W	291.7
PS100/273-2	2016-08-28	12:43:00	MST	on ground/ max depth	79° 36.35' N	16° 30.93' W	290.4
PS100/273-2	2016-08-28	13:01:00	MST	on ground/ max depth	79° 36.33' N	16° 31.17' W	291.3
PS100/273-2	2016-08-28	13:13:00	MST	on ground/ max depth	79° 36.32' N	16° 30.87' W	296.3
PS100/273-2	2016-08-28	13:45:00	MST	on ground/ max depth	79° 36.39' N	16° 30.71' W	289.2
PS100/273-2	2016-08-28	13:58:00	MST	on ground/ max depth	79° 36.36' N	16° 30.78' W	289.4
PS100/273-2	2016-08-28	14:41:00	MST	on ground/ max depth	79° 36.20' N	16° 29.99' W	277.4
PS100/273-2	2016-08-28	14:54:00	MST	on ground/ max depth	79° 36.15' N	16° 29.85' W	268.1
PS100/273-3	2016-08-28	15:05:00	HS_PS	profile start	79° 36.13' N	16° 29.80' W	276.1
PS100/273-3	2016-08-29	0:09:59	HS_PS	profile end	80° 09.87' N	17° 23.16' W	150
PS100/274-1	2016-08-29	0:27:59	MOR	on ground/ max depth	80° 08.92' N	17° 24.56' W	155.1
PS100/274-2	2016-08-29	0:54:00	CTD/UC	on ground/ max depth	80° 08.96' N	17° 22.85' W	177.7
PS100/274-3	2016-08-29	1:25:00	CTD/L	on ground/ max depth	80° 08.99' N	17° 23.00' W	176.7
PS100/274-4	2016-08-29	1:42:00	HS_PS	profile start	80° 08.99' N	17° 22.57' W	174.8
PS100/274-4	2016-08-29	5:45:59	HS_PS	profile end	80° 09.65' N	17° 23.11' W	169.2
PS100/275-1	2016-08-29	5:59:00	GC	on ground/ max depth	80° 09.75' N	17° 24.05' W	166.7
PS100/276-1	2016-08-29	7:06:00	GC	on ground/ max depth	80° 08.50' N	17° 13.05' W	169.7

Station	Date	Time	Gear	Action	Position Lat	Position Lon	Water depth [m]
PS100/277-1	2016-08-30	8:43:00	CTD/L	on ground/ max depth	79° 35.95' N	06° 10.34' W	300.4
PS100/278-1	2016-08-30	10:50:00	CTD/L	on ground/ max depth	79° 36.24' N	05° 38.18' W	349.4
PS100/279-1	2016-08-30	12:52:00	CTD/L	on ground/ max depth	79° 35.54' N	05° 11.11' W	910.1
PS100/280-1	2016-08-30	14:59:00	CTD/UC	on ground/ max depth	79° 35.34' N	04° 46.31' W	1336
PS100/280-2	2016-08-30	16:24:00	CTD/L	on ground/ max depth	79° 34.65' N	04° 47.58' W	1320.9
PS100/281-1	2016-08-30	19:32:00	CTD/L	on ground/ max depth	79° 35.19' N	04° 09.30' W	1811.1
PS100/282-1	2016-08-30	21:46:00	CTD/L	on ground/ max depth	79° 36.14' N	03° 43.51' W	2083.2
PS100/283-1	2016-08-31	0:49:00	CTD/L	on ground/ max depth	79° 36.54' N	03° 19.83' W	2245.6
PS100/284-1	2016-08-31	17:26:00	MOR	on ground/ max depth	78° 48.40' N	04° 33.17' W	1394.2
PS100/285-1	2016-08-31	20:02:00	CTD/L	on ground/ max depth	78° 48.09' N	04° 58.16' W	988.1
PS100/285-2	2016-08-31	21:50:00	ISP	on ground/ max depth	78° 46.19' N	04° 57.65' W	968.8
PS100/285-3	2016-09-01	2:22:00	CTD/L	on ground/ max depth	78° 43.36' N	04° 54.03' W	916.1
PS100/286-1	2016-09-01	11:11:00	REL	on ground/ max depth	78° 58.47' N	02° 57.39' W	0
PS100/287-1	2016-09-01	12:55:00	MOR	on ground/ max depth	78° 57.08' N	02° 58.21' W	2470.9
PS100/288-1	2016-09-01	17:17:00	CTD/L	on ground/ max depth	78° 49.73' N	04° 11.30' W	1728
PS100/288-2	2016-09-01	19:08:00	CTD/L	on ground/ max depth	78° 48.36' N	04° 11.59' W	1699.9
PS100/289-1	2016-09-02	4:00:01	MOR	on ground/ max depth	78° 29.23' N	02° 27.31' W	2739.9
PS100/290-1	2016-09-02	10:53:00	CTD/UC	on ground/ max depth	77° 49.98' N	00° 00.14' W	3048.9
PS100/290-2	2016-09-02	12:35:00	CTD/L	on ground/ max depth	77° 49.98' N	00° 00.02' W	3074
PS100/291-1	2016-09-03	1:55:59	OBS	on ground/ max depth	76° 50.06' N	07° 26.01' E	3245.5
PS100/292-1	2016-09-03	2:49:59	OBS	on ground/ max depth	76° 44.21' N	07° 02.14' E	2378.7
PS100/293-1	2016-09-03	3:52:59	OBS	on ground/ max depth	76° 43.76' N	07° 44.80' E	2475.1
PS100/294-1	2016-09-03	4:30:59	OBS	on ground/ max depth	76° 39.81' N	07° 27.09' E	3201.4
PS100/295-1	2016-09-03	5:24:59	OBS	on ground/ max depth	76° 33.04' N	07° 48.79' E	2416.9
PS100/296-1	2016-09-03	6:17:59	OBS	on ground/ max depth	76° 34.97' N	07° 16.84' E	2700.8
PS100/297-1	2016-09-03	7:21:59	OBS	on ground/ max depth	76° 37.09' N	06° 34.97' E	2576.1

Station	Date	Time	Gear	Action	Position Lat	Position Lon	Water depth [m]
PS100/298-1	2016-09-03	8:32:59	OBS	on ground/ max depth	76° 30.51' N	07° 06.63' E	3347.9
PS100/299-1	2016-09-03	9:22:59	OBS	on ground/ max depth	76° 25.99' N	06° 42.65' E	2685.7
PS100/300-1	2016-09-03	10:38:59	OBS	on ground/ max depth	76° 25.62' N	07° 29.89' E	2663.2
PS100/301-1	2016-09-03	11:35:59	OBS	on ground/ max depth	76° 19.57' N	07° 08.21' E	3401.6
PS100/302-1	2016-09-03	12:31:59	OBS	on ground/ max depth	76° 14.60' N	07° 33.58' E	2584.3
PS100/303-1	2016-09-03	13:40:59	OBS	on ground/ max depth	76° 14.39' N	06° 47.69' E	2563.7
PS100/304-1	2016-09-03	15:19:00	CTD/L	on ground/ max depth	76° 11.91' N	06° 29.83' E	2413.2
PS100/304-2	2016-09-03	16:24:00	HS_PS	profile start	76° 12.73' N	06° 25.75' E	2314.7
PS100/304-2	2016-09-03	16:56:00	HS_PS	profile end	76° 09.91' N	06° 38.32' E	2591.9
PS100/304-2	2016-09-03	17:07:00	HS_PS	profile start	76° 09.91' N	06° 38.49' E	2588.3
PS100/304-2	2016-09-03	17:29:00	HS_PS	profile end	76° 11.81' N	06° 29.14' E	2397.5
PS100/304-2	2016-09-03	17:43:00	HS_PS	profile start	76° 11.84' N	06° 29.13' E	2384.6
PS100/304-2	2016-09-03	18:27:00	HS_PS	profile end	76° 09.92' N	06° 38.34' E	2589.4
PS100/304-2	2016-09-03	18:47:00	HS_PS	profile start	76° 09.11' N	06° 37.75' E	2591.1
PS100/304-2	2016-09-03	19:09:00	HS_PS	profile end	76° 11.80' N	06° 42.38' E	2551
PS100/304-2	2016-09-03	19:23:00	HS_PS	profile start	76° 11.76' N	06° 42.39' E	2547.7
PS100/304-2	2016-09-03	19:46:00	HS_PS	profile end	76° 09.10' N	06° 37.81' E	2586
PS100/304-2	2016-09-03	19:53:00	HS_PS	profile start	76° 08.54' N	06° 39.78' E	2571.7
PS100/304-2	2016-09-03	20:14:00	HS_PS	profile end	76° 06.58' N	06° 48.22' E	2632.1
PS100/304-2	2016-09-03	20:47:00	HS_PS	profile start	76° 09.67' N	06° 44.06' E	2545.4
PS100/304-2	2016-09-03	21:09:00	HS_PS	profile end	76° 07.65' N	06° 52.65' E	2723.8
PS100/304-2	2016-09-03	21:20:00	HS_PS	profile start	76° 07.65' N	06° 52.60' E	2726.4
PS100/304-2	2016-09-04	4:00:59	HS_PS	profile end	75° 42.14' N	08° 11.73' E	2130.5

List of acronyms:	
BC	Box Corer
BONGO	Bongo Net
BUOY	Ice Buoy Recovery
CTD/L	CTD/Large Volume Rosette
CTD/UC	CTD/Ultra Clean Rosette
GC	Gravity Corer
HS_PS	Hydrosweep
ICE	Ice Station
IFISH	Iron Fish Deployment
ISP	In-situ Pump
MN	Multi Net
MOR	Mooring
MST	Microstructure Profiler
OBS	Ocean Bottom Seismometer
REL	Releaser Test
TEST	Instrument Test
ZODIAK	Small Boat Deployment

Die **Berichte zur Polar- und Meeresforschung** (ISSN 1866-3192) werden beginnend mit dem Band 569 (2008) als Open-Access-Publikation herausgegeben. Ein Verzeichnis aller Bände einschließlich der Druckausgaben (ISSN 1618-3193, Band 377-568, von 2000 bis 2008) sowie der früheren **Berichte zur Polarforschung** (ISSN 0176-5027, Band 1-376, von 1981 bis 2000) befindet sich im electronic Publication Information Center **(ePIC)** des Alfred-Wegener-Instituts, Helmholtz-Zentrum für Polar- und Meeresforschung (AWI); see http://epic.awi.de. Durch Auswahl “Reports on Polar- and Marine Research“ (via “browse”/”type”) wird eine Liste der Publikationen, sortiert nach Bandnummer, innerhalb der absteigenden chronologischen Reihenfolge der Jahrgänge mit Verweis auf das jeweilige pdf-Symbol zum Herunterladen angezeigt.

The **Reports on Polar and Marine Research** (ISSN 1866-3192) are available as open access publications since 2008. A table of all volumes including the printed issues (ISSN 1618-3193, Vol. 377-568, from 2000 until 2008), as well as the earlier **Reports on Polar Research** (ISSN 0176-5027, Vol. 1-376, from 1981 until 2000) is provided by the electronic Publication Information Center **(ePIC)** of the Alfred Wegener Institute, Helmholtz Centre for Polar and Marine Research (AWI); see URL http://epic.awi.de. To generate a list of all Reports, use the URL http://epic.awi.de and select “browse”/ ”type” to browse ”Reports on Polar and Marine Research”. A chronological list in declining order will be presented, and pdf-icons displayed for downloading.

Zuletzt erschienene Ausgaben:

Recently published issues:

705 (2017) The Expedition PS100 of the Research Vessel POLARSTERN to the Fram Strait in 2016, edited by Torsten Kanzow

704 (2016) The Expeditions PS99.1 and PS99.2 of the Research Vessel POLARSTERN to the Fram Strait in 2016, edited by Thomas Soltwedel

703 (2016) The Expedition PS94 of the Research Vessel POLARSTERN to the central Arctic Ocean in 2015, edited by Ursula Schauer

702 (2016) The Expeditions PS95.1 and PS95.2 of the Research Vessel POLARSTERN to the Atlantic Ocean in 2015, edited by Rainer Knust and Karin Lochte

701 (2016) The Expedition PS97 of the Research Vessel POLARSTERN to the Drake Passage in 2016, edited by Frank Lamy

700 (2016) The Expedition PS96 of the Research Vessel POLARSTERN to the southern Weddell Sea in 2015/2016, edited by Michael Schröder

699 (2016) Die Tagebücher Alfred Wegeners zur Danmark-Expedition 1906/08, herausgegeben von Reinhard A. Krause

698 (2016) The Expedition SO246 of the Research Vessel SONNE to the Chatham Rise in 2016, edited by Karsten Gohl and Reinhard Werner

697 (2016) Studies of Polygons in Siberia and Svalbard**,** edited by Lutz Schirrmeister, Liudmila Pestryakova, Andrea Schneider and Sebastian Wetterich

696 (2016) The Expedition PS88 of the Research Vessel POLARSTERN to the Atlantic Ocean in 2014, edited by Rainer Knust and Frank Niessen

695 (2016) The Expedition PS93.1 of the Research Vessel POLARSTERN to the Arctic Ocean in 2015, edited by Ruediger Stein

ALFRED-WEGENER-INSTITUT
HELMHOLTZ-ZENTRUM FÜR POLAR-
UND MEERESFORSCHUNG

BREMERHAVEN

Am Handelshafen 12
27570 Bremerhaven
Telefon 0471 4831-0
Telefax 0471 4831-1149
www.awi.de

HELMHOLTZ
GEMEINSCHAFT